THE UNIVERSITY
of EDINBURGH

New Approaches to Stapled Peptides Targeting the p53-MDM2 Interaction

Alexander William Saunders

THE UNIVERSITY *of* EDINBURGH

Doctor of Philosophy

The University of Edinburgh

2015

Declaration

This thesis is submitted in part fulfilment of the requirements for the degree of Doctor of Philosophy at The University of Edinburgh. Unless otherwise stated, the work described in this thesis is original and has not been submitted previously in whole or in part for any degree or other qualification at this or any other university. In accordance with the dissertation regulations as specified by The University of Edinburgh, this thesis does not exceed 100,000 words in length.

Alex Saunders

Acknowledgements

I would first like to thank Alison Hulme for giving me the opportunity to work in her research group. The freedom and encouragement I was given to pursue ideas speaks volumes to her confidence in me as a chemist, for which I am extremely grateful. With her patience and mentorship, my knowledge and ability has grown and improved significantly.

Thank you to the Hulme Group members, past and present, who have made the day to day research easy and enjoyable with cake in the afternoons and relentless boozing on nights out: Helen, Sarah B., Kevin, Nico, Heather, Lore, Sarah T., Faye, Anne, Clinton, Fergus, Richard, Will, David, Chris and Alisia: Special thanks go to Helen and Kevin, who looked after me during my Masters project and the beginning of my Ph.D., Faye my long time chemistry pal, and Fergus and Richard, for interesting discussions about mechanisms, debates about techniques, and putting up with relentless questions about using equipment.

Thank you to the School of Chemistry support staff, in particular Juraj Bella and Lorna Murray (NMR); Alan Taylor and Logan Mackay (MS); John Knox, Tim Calder, Raymond Borthwick and Mark Forrest (Stores); Thank you also to Jeff Walton for teaching me how to make peptides, and Janice Bramham for helping find out how helical they are.

Thank you to my examiners Andrew Jamieson and Annamaria Lilienkampf for their time, advice and suggestions of improvement.

There are far too many people to thank here that have had a hand in keeping me going over the past 4 years, but I am thankful, and I will find you and tell you. However there are a few that cannot go unthanked.

Cairnan Duffy, whose friendship and ability to make me laugh has been vital to my sanity. See you in The Dagda.

The Stotts: Gerard, Sarah, Declan and Theo, who have been nothing but welcoming, generous and kind. Thank you for making me feel like one of the family.

The Saunders: Ma, Pa and Jack. You have always pushed me to try my hardest, no matter what it is I do. I would not be where I am without your love and encouragement, which I hope you know I am immeasurably thankful for. I love you all.

Finally, I would like to thank Holly, without whom this thesis would have near impossible to complete, and whose love and support has kept me going, without you I would be lost. I love you more every day.

"by convention sweet and by convention bitter,

by convention hot, by convention cold, by convention color;

but in reality atoms and void."

Democritus

"How long will this last, this delicious feeling of being alive, of having penetrated the veil which hides beauty and the wonders of celestial vistas? It doesn't matter, as there can be nothing but gratitude for even a glimpse of what exists for those who can become open to it."

Alexander Shulgin

Abstract

Recent approaches to constraining peptide sequences into more structurally-defined α-helical secondary structures, so-called peptide stapling, are discussed. Stapled peptides are a class of therapeutics that have been shown to more effectively target protein-protein interactions, which are harder to target using a classical small-molecule therapeutic approach. Stapling a peptide constrains it into a well-defined secondary structure. This more accurately mimics the protein-protein interaction making the peptide a more viable therapeutic.

Starting from the p53-MDM2 interaction, a protein-protein interaction with important implications in cell health, a known peptidyl inhibitor of this interaction was stapled and analysed for increased α-helicity. This was achieved by using monomers that utilise the copper (I) alkyne azide cycloaddition as a cross-linking methodology, which has been less well researched in the context of peptide stapling. The viability of a novel stapled peptomer inhibitor approach, accomplished using a new, optimised monomer synthesis, is investigated.

Additionally, the synthesis of a ligand series designed for use in the copper(I) alkyne azide cycloaddition is also discussed.

Lay Abstract

Proteins are large molecules which have a number of important functions within the body, such as keeping cells healthy. Proteins can regulate these functions in many ways, including interacting with other proteins. The p53 protein is very important in maintaining cell health, and is regulated by the MDM2 protein. In cancerous cells the levels of p53 and MDM2 are often different to those found in healthy cells, and so finding a way of restoring the balance could be an effective cancer treatment.

Molecules called peptides, which are built from the same building blocks that the body uses to make proteins, can be created to mimic the p53 protein. These man-made molecules can interact with the MDM2 protein, disrupting the interaction with p53, and potentially increasing the amount of p53 in cells.

The peptide molecules made in the laboratory however do not have the same 3D shape as the natural p53 protein, which is vital for effective interaction with the MDM2 protein. Also, because the peptide molecules are made from amino acid building blocks, the body can recognise the peptides and break them down. This thesis discusses ways of making peptide molecules that more effectively mimic the shape of the p53 protein, and are more stable to breakdown by the body; making these non-natural peptides more effective as possible cancer treatments.

Abbreviations

3,3-DEP	3,3-diethyloxypropyne
4-(BM)MB	4-(bromomethyl)methyl benzoate
5-CP	5-chloropent-1-yne
6Cl-W	6-chloro tryptophan
Ac	acetyl
Ac_3c	1-aminocyclopropane carboxylic acid
Aib	α-aminoisobutyric acid
Alg	allylglycine
Alloc	allyloxycarbonyl
AP	Active Peptide
Bak	BCL-2 homologous antagonist killer
BCL	B-cell lymphoma
BCL-x_L	B-cell lymphoma extra large
BH	BCL-2 homology
BID	BH3 interacting domain agonist
Boc	*tert*-butyloxycarbonyl
Cba	cyclobutylalanine
CD	circular dichroism
CETSA	Cellular Thermal Shift Assay
CuAAC	copper (I) alkyne azide cycloaddition
DCE	1,2-dichloroethane
DCM	dichloromethane
DIPEA	di-isopropylethylamine
DMF	*N*,*N*-dimethyl formamide
DMPU	*N*,*N*'-dimethylpropylene urea
DMSO	dimethyl sulfoxide
DNA	deoxyribose nucleic acid
EDA	ethylene diamine
ELISA	enzyme linked immunosorbent assay
eq	equivalents
ESI	electrospray ionisation
Fm	9-fluorenylmethyl
Fmoc	9-fluorenylmethyloxycarbonyl
HBS	hydrogen bond surrogate
hDM2	human double minute 2
hDMX	human double minute X
HFA	hexafluoroacetone
HMBC	heteronuclear multiple-bond correlation
HMPA	hexamethylphosphoramide
HSQC	heteronuclear single quantum coherence

IC_{50}	inhibitory concentration 50%
IR	infra-red
ITC	isothermal titration calorimetry
K_d	dissociation constant
K_i	inhibition constant
MDM2	Murine Double Minute 2
MDMX	Murine Double Minute X
MeCN	acetonitrile
MS	mass spectrometry
ND	not determined
NMR	nuclear magnetic resonance
nOe	nuclear Overhauser effect
OSu	*O*-Succinimide
PDB	Protein Data Bank
pDI	Peptide Dual Inhibitor
PMI	p53 MDM2/MDMX Inhibitor
PMP	4-phosphonomethylphenylalanine
PPI	protein-protein interaction
Pra	propargyl
PTHrP	parathyroid hormone related protein
RCM	ring-closing metathesis
RP-HPLC	reverse phase-high pressure liquid chromatography
rt	room temperature
SAHB	stabilised α-helix of Bcl-2 domains
Sar	sarcosine
SPPS	solid phase peptide synthesis
SPR	surface plasmon resonance
TBAI	tetrabutyl ammonium iodide
TBTA	tris(benzyltriazolylmethyl)amine
TEA	triethylamine
TFA	trifluoroacetic acid
TFAA	trifluoroacetic anhydride
Tfac	trifluoroacetyl
TFE	2,2,2-trifluoroethanol
THPTA	tris(hydroxypropyltriazolylmethyl)amine
TLC	thin layer chromatography
TMBA	tris(2-benzimidazolylmethyl)amine
TMS	trimethylsilyl
UV	ultra violet

Nomenclature

The nomenclature $X_{(i,i+Y)}X(\#)$ defines the stereochemistry (X = S or R) of the cross-linking monomers within a stapled peptide. The relative positions of the first and second cross-lining monomers within the peptide are denoted i and i+Y respectively, with Y-1 residues between the cross-linking monomers. When present, (#) defines the least number of atoms that form the linker. The notation reads from the N-terminus to the C-terminus of a peptide.

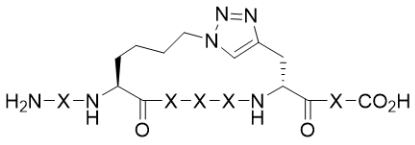

$S_{(i,i+4)}R(8)$

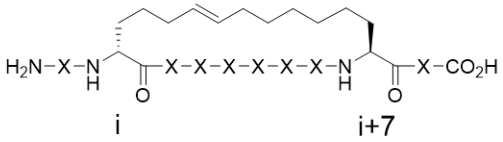

$R_{(i,i+7)}S(11)$

The nomenclature “u” or “c” after a peptide denotes whether the peptide is “uncyclised” or “cyclised” respectively.

The nomenclature “1,4-” or “4,1-” before a peptide denotes the orientation of the uncyclised azide and alkyne or cyclised triazole as read from the N-terminus of the peptide.

Contents

Chapter 1 - Designing Stapled Peptides

1 Targeting α-Helical Protein-Protein Interactions

Protein-protein interactions (PPIs) are responsible for almost all critical control points in intracellular processes. The α-helix protein secondary structural conformation is seen in approximately 40% of proteins,[1] but 62% of protein-protein interactions have an α-helical motif at the interface.[2] Given that it is estimated that on average proteins interact with up to 5 others, being able to target these PPIs individually and in isolation successfully would be of great therapeutic benefit. However, using a classical "small molecule" (M_W < 500 Da)[3] pharmaceutical approach to inhibit PPIs is usually not feasible. The approximate contact surface area of small molecule-protein interactions is 300-1000 Å, whereas the contact area of most protein-protein interactions is 1500-3000 Å, up to a factor of ten larger.[4,5] This diminished reach of small molecules also does not take into account that a large number of PPIs often lack the pockets and grooves that small molecules can bind to,[6] unlike enzymes, which have a well-defined binding site for a natural substrate (Figure 1).

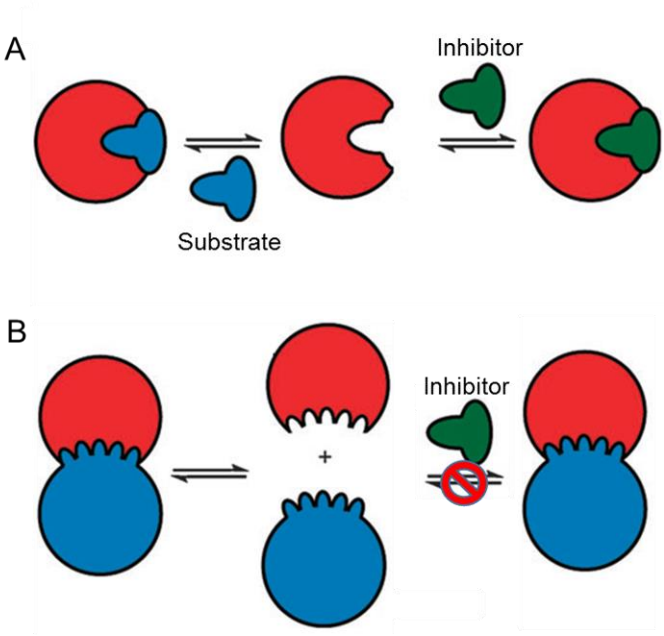

Figure 1- Representation of **A** Small Molecule Inhibition of an Enzyme **B** The Ineffective Inhibition of a Protein-Protein Interaction with a Small Molecule[7]

Ideally, the α-helical peptide sequence from an interacting protein could be used as a PPI inhibitor, however short sequence synthetic peptides do not have equivalently stable secondary structure when in solution and separated from the context of the protein.[8,9] They are also easily degraded by the peptidases, and thus not viable as therapeutics. However by replacing amino acids not critical to binding, spaced ~3.6 residues apart on the same face of the α-helix and linking them, the cyclised peptide can fold into a thermodynamically favourable α-helical conformation. As the link is constrains the sequence, it is said to be "stapled" (Figure 2).

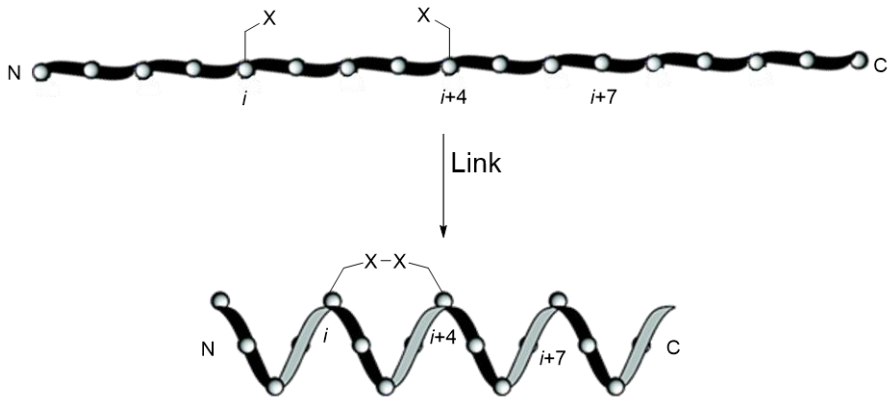

Figure 2- Representation of a Stapled Peptide

A stapled peptide is theoretically a better a protein-protein interaction inhibitor compared to a small molecule inhibitor or a non-cyclised peptide as it more closely mimics the surface area and shape of the native interaction. In addition to being thermodynamically stabilised, stapled peptides have increased resistance to proteolytic enzymes, as α-helical folded peptides are not recognised by proteases.[10] There is also evidence that stapled peptides have increased cell permeability, though there has been some debate as to how effective this is.[11–14] The mechanism of cellular penetration is not definitively known, but is thought to proceed through an energy dependent endocytotic mechanism.[15] Cyclised peptides are eventually broken down by peptidases into non-toxic amino acid metabolites, which is a favourable characteristic for a therapeutic.

The most commonly used method of determining whether a peptide, stapled or otherwise, has α-helical character is circular dichroism.[16,17] This uses circularly polarised light in the ultraviolet and visible region (180-250 nm) as this range spans most of the electronic transitions of the amide chromophore. However, the minima and maxima that are observed are significantly different depending on the secondary structure of the peptide. An α-helical peptide has characteristic minima at 220 nm and 208 nm, with a maximum peak at 193 nm (Figure 3).

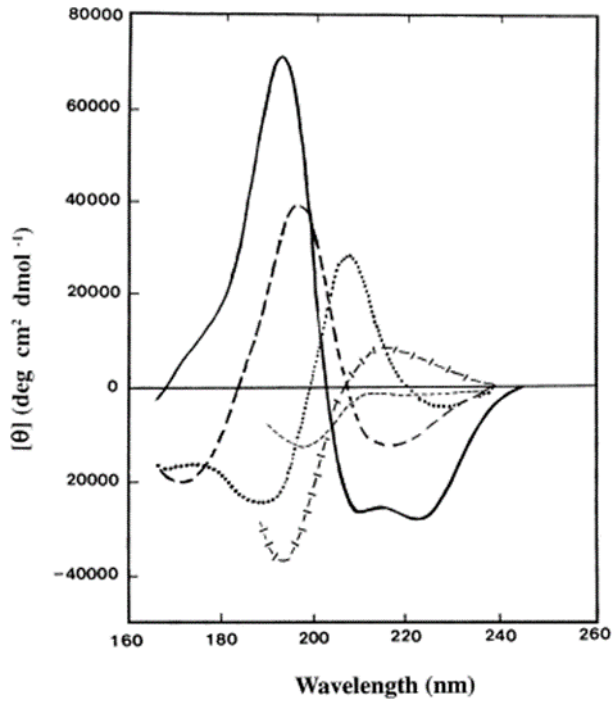

Figure 3- Circular Dichroism Spectra of Peptide Secondary Structure Characteristics Solid line, α-helix; long dashed line, anti-parallel β-sheet; dotted line, type I β-turn; cross dashed line, extended 3_{10}-helix or poly (Pro) II helix; short dashed line, irregular structure[17]

1.1 Methods of Stapling

There are many documented methods of constraining peptides into various secondary conformations, from using non-covalent interactions including salt bridging,[18–23] ion complexing,[24–29] π,π-interactions[30] and cation,π-interactions,[31,32] to using thiol chemistry to form disulphide bonds,[33,34] and thioether linked spacers.[35–37] There are examples of reversible oxime linkers[38] and photoactived azo-benzene[39] and

pyrazoline[40] linkers. Recently it has been shown that it is possible to form macrocyclic peptides using tryptophan residues.[41,42] With all these methods available, it is essential to consider certain key properties when looking to design a peptide stapling system. Analysis of some of the most thoroughly investigated stapling systems should emphasise these trends.

1.1.1 Side Chain Lactamisation

One of the simplest ways of forming a peptide staple is to use the inherent reactivity of the functional groups found on the side chains of amino acids. By using common proteinogenic residues such as lysine, aspartic acid and glutamic acid, a stable amide bond can be formed (Figure 4).[43] The cyclisation can be easily monitored by MS and IR.

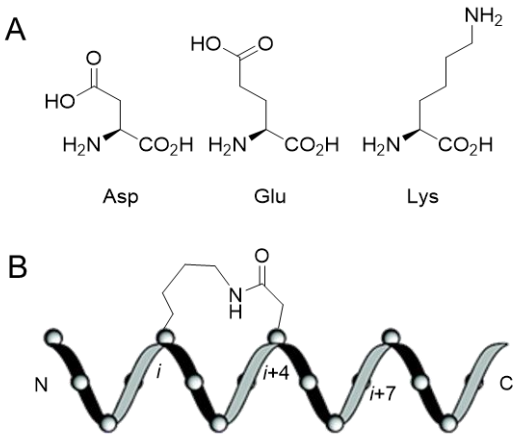

Figure 4- **A** Proteinogenic Residues used in (*i,i*+4) Lactamisation **B** Representation of Lactam Stapled Peptide

1.1.1.1 Lactam Linker Length/Regioisomerism

One restriction of using proteinogenic residues, however, is the linker can only encompass one helical turn effectively. Shepherd *et al*.[44] previously demonstrated that polymers of the lactamised pentapeptide motif Ac-[KARAD]$_n$-NH$_2$ had increased helicity as shown by circular dichroism spectra[16,17] (Figure 5), and resistance to proteolytic cleavage by trypsin when compared to the uncyclised counterparts.

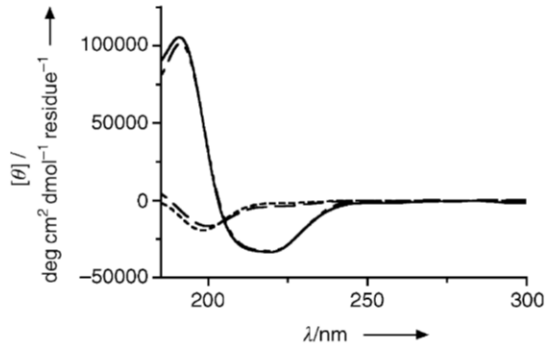

Ac-[KARAD]$_n$-NH$_2$		% Helicity	
n		u	c
2	**1**	3	99
3	**2**	7	88

Figure 5- CD Spectra of Lactamised Pentapeptide Polymers Ac-[KARAD]$_n$-NH$_2$ in 10 mM phosphate buffer[44]

Taking this concept further, Shepherd *et al.*[45] attempted to stabilise a single pentapeptide, the minimum number of residues to represent one helical turn (Figure 6), using a lactam bridge.

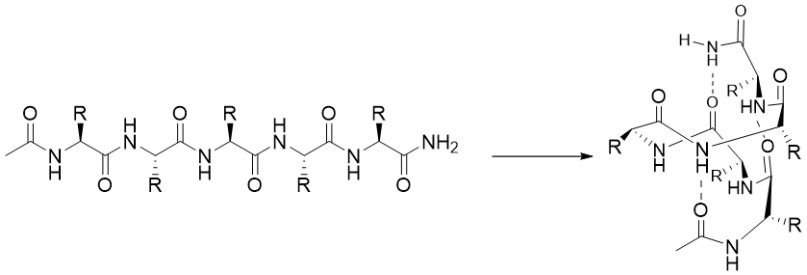

Figure 6- Pentapeptide Single Helical Turn

To investigate the optimal linker, ornithine was used in addition to the proteinogenic amino acids, allowing the linker length and lactam position to be probed. The macrocyclisation was achieved on resin using the Alloc/Allyl protecting groups (Figure 7), which are orthogonal to Fmoc solid-phase peptide synthesis (SPPS).[46–48] Using relatively high loading resins and prolonged reaction times resulted in oligomerisation. Switching to a lower loading resin improved the purity and yield of the monomeric cyclic products (Figure 8).

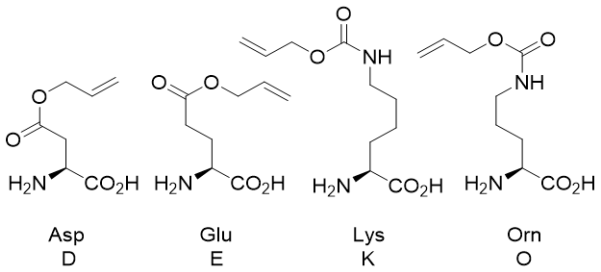

Figure 7- Allyl/Alloc Protected Residues

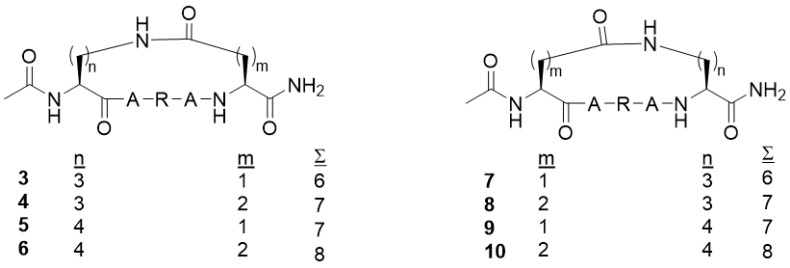

	n	m	Σ
3	3	1	6
4	3	2	7
5	4	1	7
6	4	2	8

	m	n	Σ
7	1	3	6
8	2	3	7
9	1	4	7
10	2	4	8

Figure 8- Regioisomeric Lactam Peptides Investigated by Shepherd *et al*.[45]

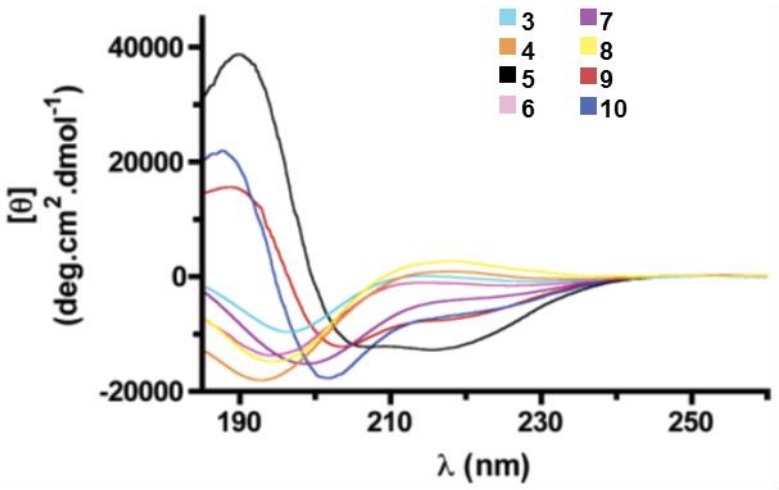

Figure 9- CD Spectra of Lactamised Pentapeptides **3**-**10**[45]

Table 1- % Helicity of Lactamised Pentapeptides

Sequence		Σ^a	% Helicity
Ac-KARAD-NH_2 [b]	**11**	-	4
Ac-KARAD-NH_2	**5**	7	100
Ac-DARAK-NH_2	**9**	7	60
Ac-KARAE-NH_2	**6**	8	8
Ac-EARAK-NH_2	**10**	8	58
Ac-OARAD-NH_2	**3**	6	0
Ac-DARAO-NH_2	**7**	6	37
Ac-OARAE-NH_2	**4**	7	0
Ac-EARAO-NH_2	**8**	7	0

a Σ *atoms in linker; b Uncyclised;*

The results in Figure 9 and Table 1 show that there is a clear preference for linker length (compare **5**, **6**, and **3**; compare **9**, **10** and **7**) and position of the lactam within the macrocycle. Increasing the linker by one atom knocks out most of the induced helicity (**5** vs **6**). Arguably this could be due to competitive hydrogen bonding to the lactam, which becomes possible because of the increased flexibility in the linker. This flexibility may explain the increase in helicity from **6** to **10**, as the position of the lactam has moved to an unfavourable position for this competitive bonding. Shifting the lactam closer to the N-terminus (**5** vs **9**) reduced the relative helicity. There is also complete elimination of helicity when the lactam linker length is kept the same, but the position of the lactam is more centralised (**5** vs **4**, **9** vs **8**).

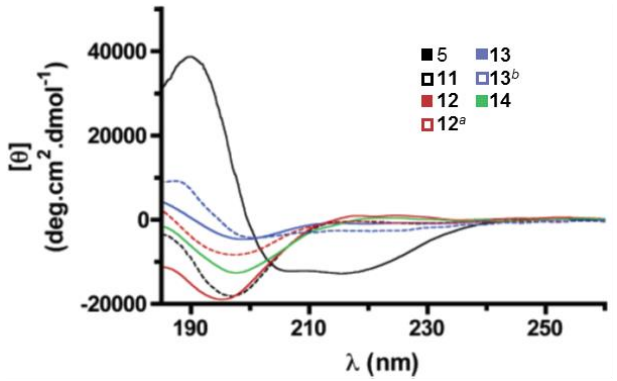

Figure 10- CD Spectra of Ac-KARAD-NH_2 **5** and Hydrogen Bond Knock Out Lactamised Pentapeptides **12**-**14**; *a* pH 2; *b* pH 10.

Table 2- % Helicity of Hydrogen Bond Knock Out Lactamised Pentapeptides

Sequence		Σ^a	% Helicity
Ac-KARAD-NH_2	**5**	7	100
Ac-KARAD-OH	**12**	7	0 (6)[b]
H-KARAD-NH_2	**13**	7	6 (20)[c]
H-KARAD-OH	**14**	7	8

a Σ atoms in linker; b pH 2; c pH 10;

In Table 2 and Figure 10 the effect of removing 1 (**12**, **13**) or 2 (**14**) of the peptidyl backbone hydrogen bonds from the optimally cyclised peptide **5** is shown. Even at controlled pH to remove respective terminal charges it is evident that at least 3 hydrogen bonds are required for α-helical induction and that cyclisation in and of itself is not enough to induce helicity (Figure 11).[45]

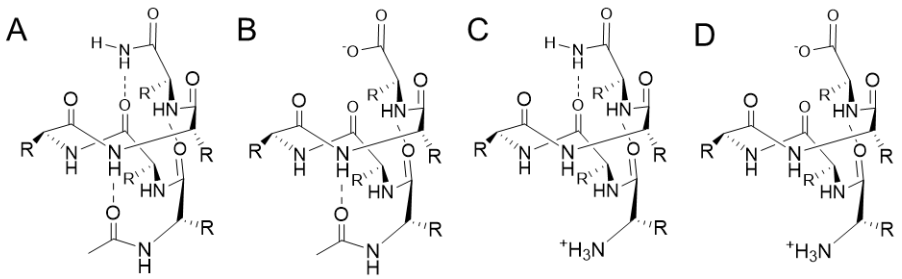

Figure 11- Pentapeptides with **A** 3 **B** and **C** 2 and **D** 1 Backbone Hydrogen Bond(s)

It has been shown that the side chains of amino acids can be inherently α-helix stabilising or destabilising. To investigate this, a series of hexapeptides of the form Ac-RKAXAD-NH_2 were synthesised, with the R residue retained to improve the aqueous solubility of the peptides (Table 3). It was demonstrated that helicity is highly dependent on sequence, and although these peptides are extremely short, possibly exaggerating deleterious effects, again it indicates a staple can only be of so much benefit.[45]

Table 3- % Helicity of Hexapeptides

Sequence		S/N/D[a]	% Helicity
Ac-RKAAAD-NH_2	**15**	S	91
Ac-RKALAD-NH_2	**16**	S	100
Ac-RKAMAD-NH_2	**17**	S	80
Ac-RKAQAD-NH_2	**18**	S	84
Ac-RKAFAD-NH_2	**19**	N	76
Ac-RKAGAD-NH_2	**20**	D	32
Ac-RKGGGD-NH_2	**21**	D	14

a S Stabilising; N Neutral; D Destabilising

1.2 Bio-Orthogonal Methods of Stapling

A potential problem in using unmodified amino acid side-chain residues to stabilise a peptide's secondary structure, via a staple, is the inevitable loss of efficacy that will occur when the staple is eventually cleaved by some physiological process. One way to circumvent this is to use a bio-orthogonal macrocyclisation technique to close the staple. This strategy has the advantage that the staple can be formed without the need for protecting groups, simplifying synthesis, and the product will typically be biologically inert.

1.2.1 Ring Closing Metathesis

Ring-Closing Metathesis (RCM) is a catalytic carbon-carbon bond forming technique which involves the scission and consequent combination of two olefin groups via some late transition metal alkylidene (Figure 12).[49–51] The direct formation of carbon-carbon bonds in this way is not observed in nature, and the hydrocarbon link formed is biologically stable. The reaction can also easily be monitored by mass spectrometry due to the loss of ethylene. RCM has been shown to be synthetically useful in that the ruthenium catalyst centre has a high functional group tolerance, and so does not interfere with solid phase synthesis of peptides.

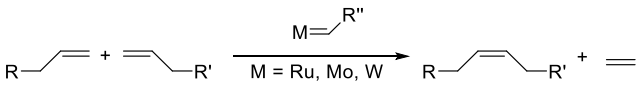

Figure 12- Schematic Representation of RCM

1.2.1.1 Constriction of Peptides into Recognisable Secondary Structure

One of the first investigations into the macrocyclisation of peptides via RCM was performed by Miller *et al*.[52,53] They were able to demonstrate that the Grubbs catalysts gave complete macrocyclisation of olefin groups in the presence of free and allylated amide NH groups. Originally looking at RCM as a way of forming conformationally restricted amino acids similar to proline,[52] Miller *et al*. turned their attention to the formation of a disulphide β-turn mimetic, as a RCM surrogate of a β-turn would not be susceptible to conditions that would cleave a disulphide bond. Following the replacement of cysteine residues in the tetrapeptide Boc-Cys-Pro-Aib-Cys-NHMe **22**, a known β-turn mimetic[54], with racemic allylglycine (Alg) residues to form a statistical distribution of 4 diastereomeric tetrapeptides (**23u**), the resultant peptides were then subjected to standard RCM conditions (Figure 13).

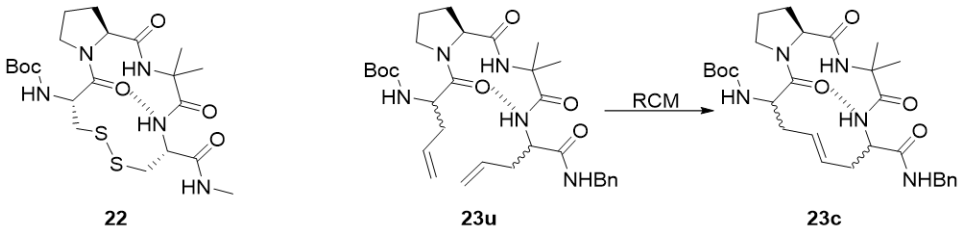

Figure 13- RCM Analogue of β-Turn Tetrapeptide Boc-Cys-Pro-Aib-Cys-NHMe

Interestingly, only the (*S*,*S*,*S*) diastereomer of **23c**, was seen to form the macrocycle within the mixture of diastereomeric peptides. The experiment was repeated with the isolated (*S*,*S*,*S*) and (*R*,*S*,*R*) diastereomers of **23u** only and again only the (*S*,*S*,*S*) diastereomer cyclised, with the (*R*,*S*,*R*) recovered unreacted. It is thought that an internal hydrogen bond affords some pre-organisation of the macrocycle, facilitating closure of the "natural" diastereomeric analogue, whilst destabilising the other analogues via some trans-annular effect.

Continuing from this preliminary work, Miller *et al*.[53] investigated how important the conformationally restricting non-natural amino acid aminoisobutyric acid (Aib)[55,56] was to the mimicking of a β-turn. The Glutaredoxin active site contains an (*i*,*i*+3) disulphide β-turn motif[57] similar to the model tetrapeptide. This new pentapeptide (Boc-*S*-Alg-Pro-Tyr(OCbz(Br))-*S*-Alg-Gly-OMe **24**, Figure 14) was synthesised in an similar manner to the model. The presence of β-turn hydrogen bonding was confirmed by IR and NMR spectroscopy. It was noted that the unprotected tyrosine pentapeptide macrocycle **25c** was also synthesised with similar success, showing the free phenol does not interfere with the efficiency of the catalyst.[53]

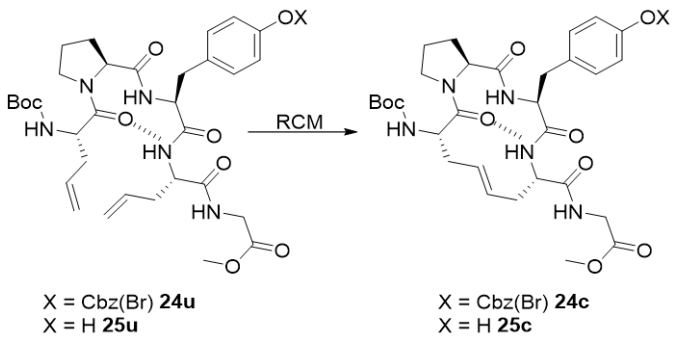

Figure 14- RCM of Boc-*S*-Alg-Pro-Tyr(OX)-*S*-Alg-Gly-OMe

Going further, the Pro-Aib motif was also removed in the original tetrapeptide, as proline residues are themselves conformationally constraining. The monomers were replaced with two leucine residues, leaving the tetrapeptide Boc-*S*-Alg-Leu-Leu-*S*-Alg-NHBn (**26**, Figure 15) without any inherent secondary structure.[53] Again the macrocyclisation was achieved with the secondary structure confirmed by IR and NMR. This demonstrated that the use of RCM as a peptide macrocyclisation technique does not require any pre-organisation.

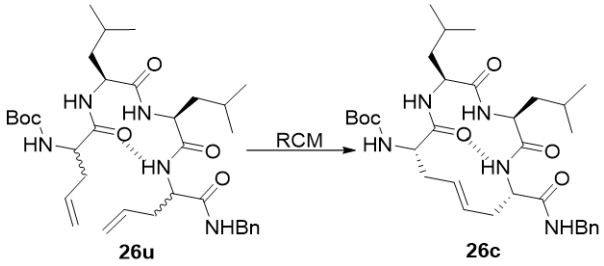

Figure 15- RCM of Boc-*S*-Alg-Leu-Leu-*S*-Alg-NHBn

A crucial experiment performed was the macrocyclisation of peptides whilst on a solid support. Following standard Fmoc-SPPS (solid-phase peptide synthesis) procedures the resin was swollen in DCM, the optimum solvent for efficient catalyst activity, and the reaction repeated. After deprotection and cleavage from the resin, the stapled peptides was detected with the acyclic starting material. This established the utility of RCM in the macrocyclisation of peptides on solid supports.[53]

1.2.1.2 **RCM Inducing Helicity**

The first application of this methodology to the helical constriction of peptides was demonstrated by Blackwell *et al*.[58,59] Using a known helical hydrophobic peptide[60,61] to exclude any intermolecular solvent effects and promote the catalytic activity of the ruthenium alkylidene catalyst, Boc-Val-Ala-Leu-Aib-Val-Ala-Leu-OMe was selected as a peptidyl scaffold to attempt the first RCM helical peptide staple. Replacing the alanine residues in the (*i*,*i*+4) positions of the sequence with *O*-allyl serine and *O*-allyl homoserine, selected for the availability and ease of derivatisation of the starting materials, allowed the investigators to probe the linker length (Figure 16-A).

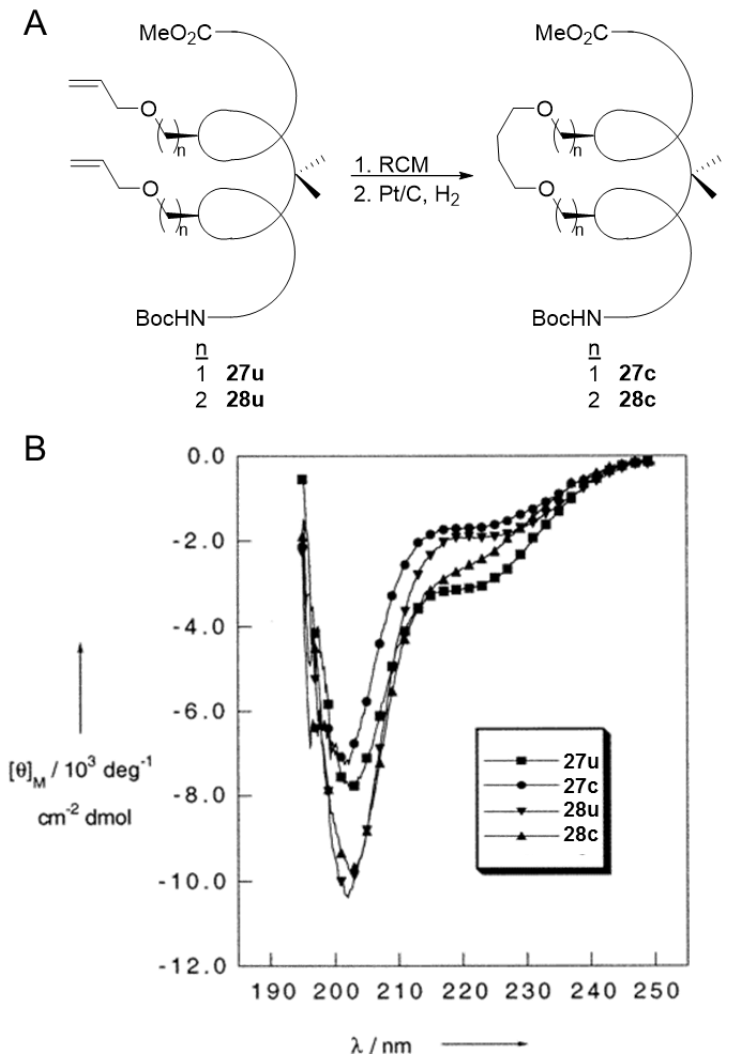

Figure 16- A Stapling of a Helical Peptides **27** and **28 B** CD Spectra of peptides **27u**, **27c**, **28u** and **28c**.

After synthesis of the peptides and subsequent RCM, the olefin was subjected to hydrogenation to remove any effect due to *E*/*Z* isomerism of the C=C double bond. Comparing the CD spectra of the cyclised (**27c** and **28c**) and uncyclised (**27u** and **28u**) peptides, it was shown that there was little to no change in the degree of helicity exhibited by the peptides (Figure 16-B). This however could be due to the fact that the peptides contain an Aib residue in the centre of the sequence, and the fact that the CD spectra were ran in 100% trifluoroethanol (TFE), a known kosmotropic solvent.[62–64] This solvent could both contribute to the pre-organisation of the heptapeptide into its most helical conformation thereby disguising any additional helix-inducing effects from the linker. Additional NMR experiments[59] provided evidence that the cyclised

peptides fold into a 3_{10}-helical conformation. A 3_{10}-helix has 3 residues per helical turn, and so has a thinner and more extended secondary structure in comparison to an α-helix (Figure 17).[65] This suggests that although there is a high helix propensity and the linkers are replacing residues on the same helical face, the linker formed may be too lax, stabilising the extended 3_{10}-conformation. This work highlights the need for linker optimisation even within a known helical peptide.

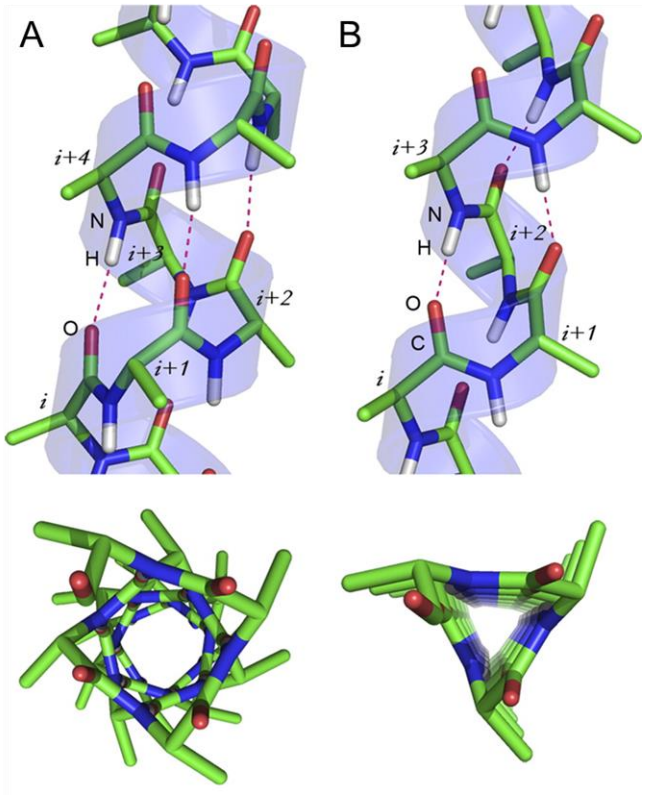

Figure 17- Comparison of Backbone Hydrogen Bonding and Side Chain Orientation in **A** α-helix **B** 3_{10} Helix[65]

1.2.1.3 **RCM Inducing α-Helicity**

One of the seminal investigations to take the design and optimisation of an all hydrocarbon staple into consideration was described by Schafmeister *et al.*[66] It was posited that not only the linker length, but the diastereomeric configuration of the staple could either increase or decrease the overall helicity. To add to the total stability imparted by the staple the synthesised monomers were methylated at the α-carbon of

the amino acids,[67] analogous to the Aib residue. These monomers (Figure 18-A) were incorporated into a peptide based on the C-peptide sequence of RNAse-A, Ac-EWAETAAAKFLAAHA-NH_2,[68] a 15-mer peptide shown to have partial helicity in water due to side-chain salt bridge interactions.[18,19] Comparison to the native sequence allowed any increases or decreases in helicity to be determined. During SPPS, residues were replaced at both (*i*,*i*+4) and (*i*,*i*+7) positions (one or two helical turns) within the helices (Figure 18-B,C).

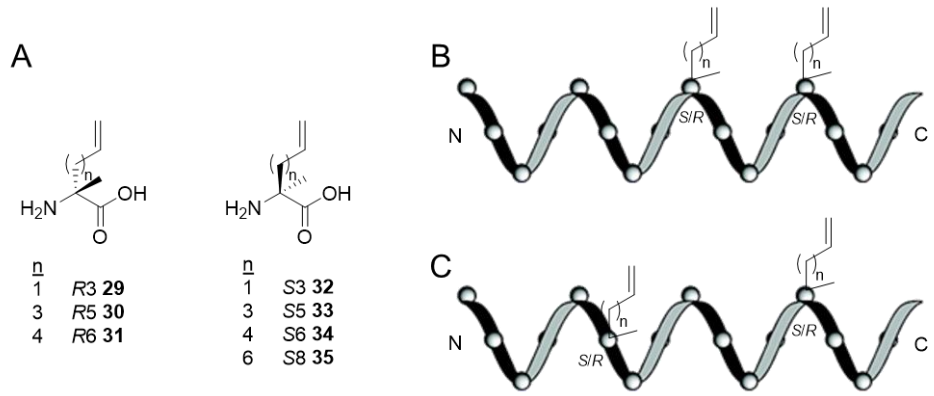

Figure 18- A α,α-Disubstituted RCM Monomers Used **B** Representation of $X_{(i,i+4)}X$ Stapling Position **C** Representation of $X_{(i,i+7)}X$ Stapling Position in RNAse-A Analogues

When subjected to metathesis conditions, $R_{(i,i+4)}S$ linkers of any length did not undergo reaction. Only $R_{(i,i+4)}R$ and $S_{(i,i+4)}S$ linkers longer than 7 carbon atoms in length were metathesized to any appreciable extent (Table 4, **38**, **39** and **41**, **42** respectively). A similar trend with regard to an optimum linker length was noted in the (*i*,*i*+7) staples, with monomers only forming staples with at least 9 carbon atoms in the linker, (**44-47**). This was thought to be due to the pre-organisation of the helices on solid support in DCE. If the sequence has already folded into a restricted conformation, only side chains of adequate length would be able to undergo cross-metathesis and form the staple (Figure 19).

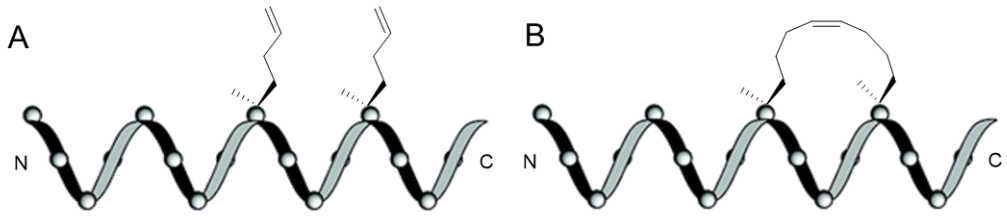

Figure 19- Representation of **A** Ineffective $S_{(i,i+4)}S(6)$ Staple (**40**) and **B** Effective $S_{(i,i+4)}S(8)$ RCM Staple (**42**)

Table 4- Analysis of % Helicity Before and After RCM

Ac-EWAE$\mathbf{X_1}$AA$\mathbf{X_2}$KFL$\mathbf{X_3}$AHA-NH_2					Yield (%)[a]	% Helicity	
X_1	X_2	X_3	Σ^b			u	c
T	A	A	-	**36**	-	41	-
T	*R*3 **29**	*R*5 **30**	6	**37**	0	-	-
T	*R*3 **29**	*R*6 **31**	7	**38**	17	ND	ND
T	*R*5 **30**	*R*5 **30**	8	**39**	>98	37	39
T	*S*3 **32**	*S*5 **33**	6	**40**	0	ND	ND
T	*S*3 **32**	*S*6 **34**	7	**41**	68	49	48
T	*S*5 **33**	*S*5 **33**	8	**42**	>98	40	39
*R*5 **30**	A	*S*5 **33**	8	**43**	0	ND	ND
*R*5 **30**	A	*S*6 **34**	9	**44**	51	54	33
*R*6 **31**	A	*S*6 **34**	10	**45**	77	59	47
*R*5 **30**	A	*S*8 **35**	11	**46**	>98	59	85
*R*6 **31**	A	*S*8 **35**	12*c*[c]	**47a**	>98[d]	53	71
*R*6 **31**	A	*S*8 **35**	12*t*[c]	**47b**	>98[d]	53	60

a RCM Cyclisation; b Σ atoms in linker; c cis / trans; d total yield; ND: Not Determined;

Peptides that underwent macrocyclisation by RCM to ~50% or greater conversion (**39**, **41**, **42**, **44**-**47**) were analysed in the cyclised and uncyclised forms by CD for α-helicity with the native peptide sequence (**36**) used as a control. The inclusion of α,α-disubstituted amino acids tended to increase helicity[56,69] with respect to the native sequence. In the (*i*,*i*+4) sequences, cross-linking appeared to have no effect on helicity with respect to the unmetathesised counterparts. However in the (*i*,*i*+7) series (**44**-**47**) there was a range of stabilising and deleterious effects observed. Again, this seemed

to follow the trend of linker length, with helicity increasing with increasing linker length, reaching a maximum at 11 carbon atoms (26% with respect to the uncyclised analogue, 44% compared to the native sequence, Table 4- **46**) and subsequently decreasing. Importantly, the C9 and C10 linkers were found to destabilise helicity with respect to the uncyclised versions (-21% and -12% compared to the uncyclised sequences respectively, Table 4- **44** and **45**). The C12 cross-linked peptide displayed cis/trans isomerism possibly due to the increased ring size, with the two isomers having different retention times when purified by RP-HPLC. Interestingly the *cis* isomer showing a greater increase in helicity than the *trans* isomer (18% and 7% respectively, Table 4- **47a** and **47b**). It was reported that hydrogenation of the olefin linkers showed no marked change in α-helicity when compared to the unsaturated precursors. It was also determined by sedimentation equilibrium that any helical induction was not due to aggregation of the peptides.

The $R_{(i,i+7)}S$ stapled peptides were tested for increased stability against proteases. As the sequence between the monomers contained a lysine residue, trypsin was used in an *in vitro* assay. The increased helicity afforded by the monomers alone was enough to decrease the rate of peptidyl degradation approximately 5-fold. Cyclisation and hydrogenation decreased the rate of cleavage even further. Again, this was shown to be related to the trend of the effectiveness of the linker inducing helicity in the peptide, with the C11 linker peptide (**46**) exhibiting the slowest rate of trypsin digestion which showed an approximately 9-fold reduction in cleavage with respect to the uncyclised analogue and a 41-fold reduction when compared to the native sequence (**36**). These experiments were the first to offer evidence of the utility of RCM as an effective α-helical peptide stabilisation technique.

1.2.1.4 **RCM Inducing α-Helicity in Biologically Relevant Peptides**

The increased metabolic stability of stapled peptides is one of the qualities that make them appealing as drug candidates for protein-protein interactions. This theoretical pharmaceutical activity was first examined by Walensky *et al.*[70] The BCL-2 protein family are crucial in cell apoptotic pathways.[71–73] The family is defined as containing

a number of BCL-2 homology (BH) domains, with the α-helical BH3 domain critical to apoptosis upon protein-protein binding.[74–77] The peptide sequence from BID, a BH3-only BCL-2 protein, was used as the template for inserting the α,α-disubstituted alkene monomers (Figure 18) for macrocyclisation of the stabilised α-helices of BCL-2 domains, (SAHBs, Table 5).

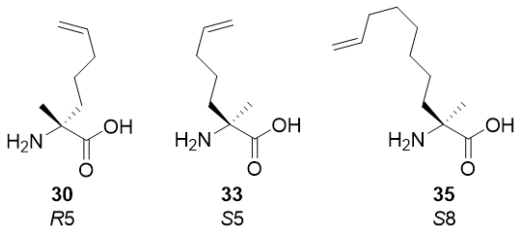

Figure 20- Olefin Monomers Incorporated into Stapled Peptides by Walensky *et al*.[70]

Table 5- BID-BH3 and Stabilised α-Helix of BCL-2 Domains (SAHB) Sequences[70]

Name	Sequence		% Helicity
BID-BH3	Ac-EDIIRNIARHLAQVGDSN$_L$DRSIW-NH_2	**48**	15.7
SAHB$_A$	Ac-EDIIRNIARHLA**X$_1$**VGD**X$_1$**N$_L$DRSIW-NH_2	**49**	87.5
SAHB$_A$ (G/E)	Ac-EDIIRNIARHLA**X$_1$**VED**X$_1$**N$_L$DRSIW-NH_2	**50**	77.8
SAHB$_B$	Ac-EDIIRNI**X$_1$**RHL**X$_1$**QVGDSN$_L$DRSIW-NH_2	**51**	85.5
SAHB$_C$	Ac-EDIIRNIA**X$_1$**HLA**X$_1$**VGDSN$_L$DRSIW-NH_2	**52**	59.7
SAHB$_D$	Ac-EDIIRNIAR**X$_2$**LAQVGD**X$_3$**N$_L$DRSIW-NH_2	**53**	35.6

***X$_1$* 33**; ***X$_2$* 30**; ***X$_3$* 35**; *N$_L$ Norleucine;*

Circular dichroism of the 23-mer native sequence **48** in aqueous potassium phosphate solution showed little to no intrinsic helicity (~16%). Inclusion and metathesis of the monomers at (*i*,*i*+4) and (*i*,*i*+7) positions highlighted in Table 5 (**49**-**53**) all increased helicity with respect to the native sequence (Figure 21). Interestingly, all the (*i*,*i*+4) staples increased the helicity to a greater extent than the (*i*,*i*+7) stapled peptide **53**, the opposite result from the antecedent work from Schafmeister *et al*.[66] suggesting that optimum linker length is highly dependent on the peptide being stapled.

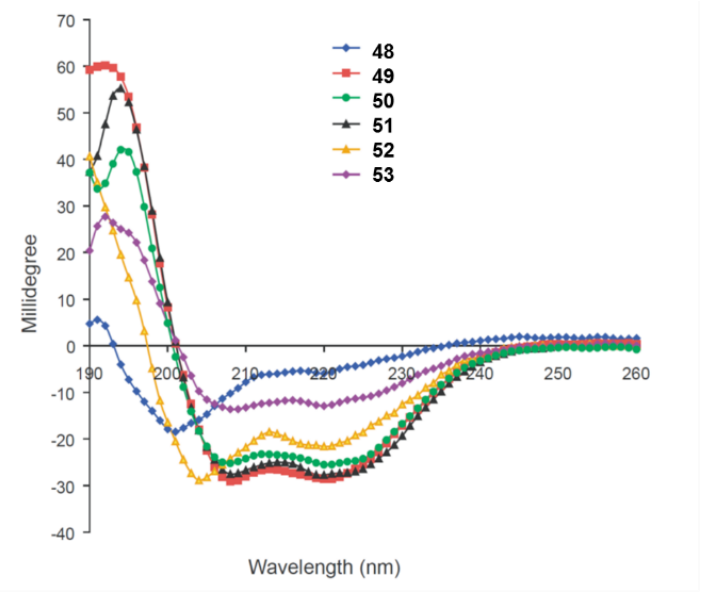

Figure 21- CD Spectra of BID-BH3 **48** and SAHBs **49** - **53**[70]

The SAHB with the highest helical content, $SAHB_A$ (**49**), was tested for proteolytic stability against trypsin (Figure 22-A) and serum (*in vitro*). In all the experiments, $SAHB_A$ showed a greater stability against digestion than the native BID-BH3 peptide **48**. To confirm that $SABH_A$ was interacting in an analogous way to the native BID-BH3 sequence, ^{15}N-^{1}H HSQC NMR experiments were performed on a ^{15}N enriched BCL isoform. The similarity of the spectra verified that $SABH_A$ was binding in the same hydrophobic pocket as the native peptide. In fact, following a fluorescence polarisation binding assay it was determined that $SABH_A$ showed a greater than 6-fold increase in binding affinity to the isoform than the native sequence (Figure 22-B). The fluorescently labelled peptides were also used to monitor the transit of the molecules through the cell membrane, which is a challenge for peptides with charged residues. It is thought the hydrophobic nature of the staple may impart increased lipophilicity.

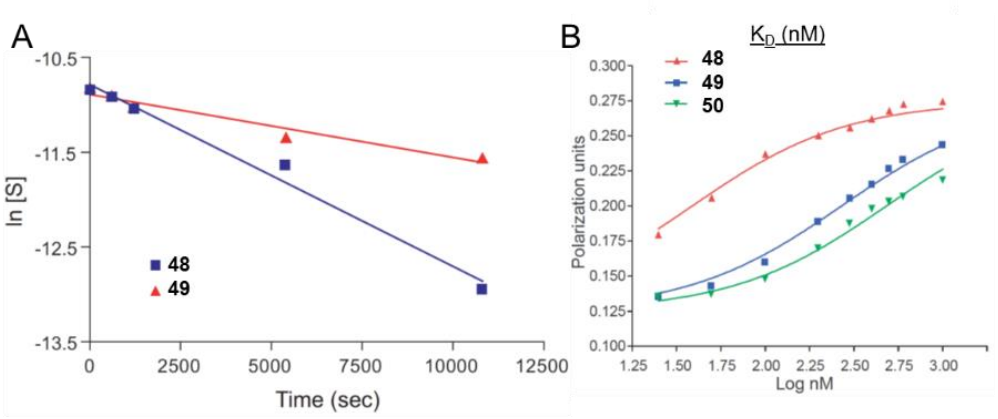

Figure 22- A Rate of BID-BH3 and $SAHB_A$ Digestion by Trypsin **B** Fluorescence Polarisation Binding Assay[70]

Notably, $SAHB_A$ was able to activate the apoptosis pathway, both *in vitro* across a number of leukaemia cell lines (Figure 23) and *in vivo* in mice. Importantly, $SAHB_A$ displayed no toxicity in normal tissue. This investigation provided the first evidence that stapled peptides could be used as therapeutics for protein-protein interactions.

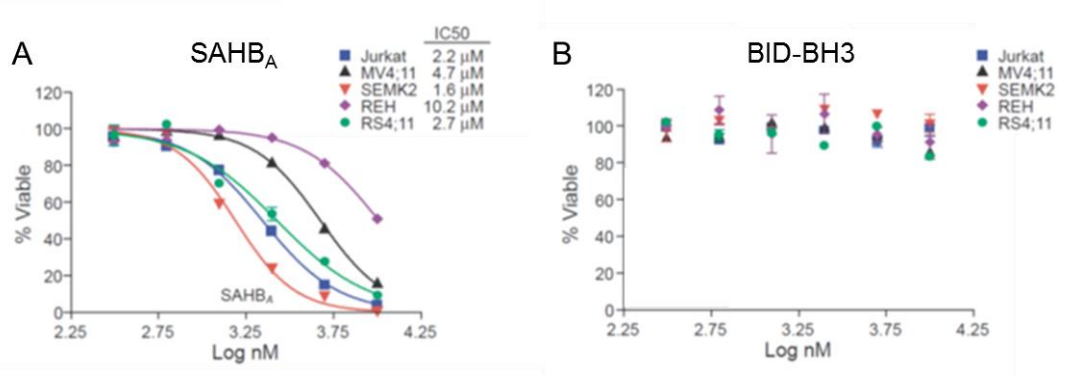

Figure 23- Therapeutic Potential of $SAHB_A$ Peptide - **A** $SAHB_A$ Against Leukaemia Cell Lines **B** Native BID-BH3 Against Leukaemia Cell Lines[70]

1.2.1.5 RCM Linker Length and Thermodynamic Benefits

From the results of the previously discussed studies, it appears that the effectiveness of an (*i*,*i*+4) over an (*i*,*i*+7) staple cannot be predicted. To explore this, Kutchukian *et al.*[78] used knowledge-based potentials in Monte Carlo folding *in silico* calculations[79–

[81] and compared the experimental data from Schafmeister *et al*.[66] and Walensky *et al*.[70] (Table 6).

Table 6- Peptides Analysied *in silico* by Kutchukian *et al*.

Sequence	
Ac-EWAETAAAKFLAAHA-NH_2	**36**
Ac-EWAETAA**X_1**KFL**X_1**AHA-NH_2	**42**
Ac-EWAE**X_2**AAAKFL**X_3**AHA-NH_2	**46**
Ac-EDIIRNIARHLAQVGDSN$_L$DRSIW-NH_2	**48**
Ac-EDIIRNIARHLA**X_1**VGD**X_1**N$_L$DRSIW-NH_2	**49**
Ac-EDIIRNIAR**X_2**LAQVGD**X_3**N$_L$DRSIW-NH_2	**53**
X_1 33 *;* ***X_2 30*** *;* ***X_3 35*** *;*	

According to polymer theory, the stability that comes from covalently linking polypeptides is from the reduction in entropy, making the unfolded state less favourable. If this were true however, a longer linker encompassing a greater number of residues would be more stabilising.[82–85] Following the simulations and analysis, the models were found to be in agreement with the experimental data of the relative stability of the stapled peptides. The helical contribution imparted to the individual residues in the RNAse A peptide[66] (**36**) was found to be increased around both the (*i*,*i*+4) and (*i*,*i*+7) staples (**42** and **46**) with this propensity decreasing the greater the distance from the cross-linked residues. In the BID-BH3 peptide **48**,[70] the (*i*,*i*+4) staple (**49**) increased the relative helicity of all the residues, especially those within three residues of the staple. However the (*i*,*i*+7) staple (**53**) was shown to impart helicity towards the N-terminus effectively, but it was discovered that it helped stabilise a partially folded state that may not be present in the native protein (Figure 24).

Figure 24- Representative Structures of the **A** Native (**48**) **B** (*i,i*+4) Stapled (**49**) and **C** (*i,i*+7) Stapled (**53**) BID-BH3 Peptides[78]

In both the macrocyclised peptides there was some degree of α-helix stabilisation, with evidence that the wild type sequence can access conformations disallowed in the stapled analogues, highlighting the entropic stabilisation given. However, it was found that: (i)- the enthalpic gains from the internal hydrogen bonding networks formed, and (ii)- the disfavourable increase in backbone torsion of the denatured peptide were greater contributors to the overall free energy gained by the most stabilised peptides than any entropic factor.

1.2.1.6 **RCM (*i,i*+4) Staple Stereochemistry**

As with linker length, the relative stereochemistry of the amino acids containing the non-natural side chains can have an effect on the overall helicity and stability imparted to the peptide. This was investigated by Kim *et al.*[86] Using the α,α-disubstituted pentene monomers (**30**, **33**, Figure 25) and incorporating them into the RNAse-A sequence **36**, Ac-EWAETAAAKFLAAHA-NH_2,[66] altering the position of the (*i,i*+4) staple to the 4th and 8th residues (Table 7) it was found that the $S_{(i,i+4)}S$ (**54**) and $R_{(i,i+4)}R$ (**55**) cross-linked peptides had vast differences. Although there was no significant change in the rate or yield of the macrocyclisation step the CD spectra showed that the $S_{(i,i+4)}S$ was more helical than the $R_{(i,i+4)}R$ stapled peptide and the native (72%, 40% and 29% respectively, Figure 26-A,B). The $S_{(i,i+4)}S$ also displayed a greater uptake into HeLa cells than the $R_{(i,i+4)}R$ diastereomer, however both showed greater uptake when compared to the native sequence (Figure 26-C).

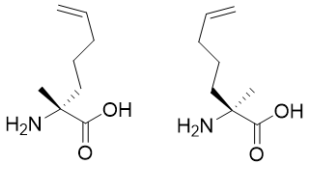

Figure 25- Olefinic Monomers Incorporated by Kim *et al*.[86]

Table 7- % Helicity of RNAse-A and Stapled Analogues

Sequence		% Helicity	
		u	c
Ac-EWAETAAAKFLAAHA-NH_2	**36**	29	-
Ac-EWA**X$_1$**TAA**X$_1$**KFLAAHA-NH_2	**54**	36	72
Ac-EWA**X$_2$**TAA**X$_2$**KFLAAHA-NH_2	**55**	24	40

X$_1$ 33; ***X$_2$ 30***;

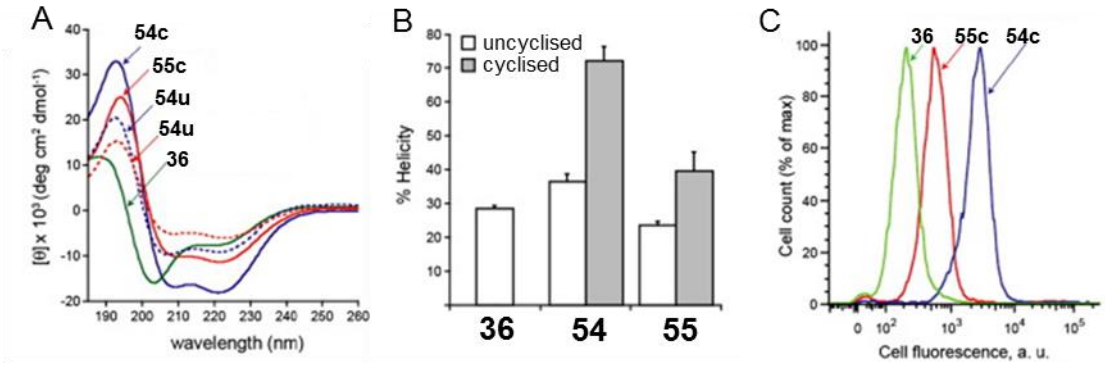

Figure 26- Comparison of Native, $S_{(i,i+4)}S$ and $R_{(i,i+4)}R$ RNAse-A Peptides - **A** Measured α-Helicity **B** Difference in % Helicity **C** Flow cytometry profiles showing cellular uptake of **36**, **54c** and **55c** into HeLa cells[86]

To see if the relative diminished stability of the *R*,*R* conformation was a common trend in (*i*,*i*+4) stapled peptides, the *R*,*R* staple was also incorporated into the BID-BH3 sequence **48**, Ac-EDIIRNIARHLA**X**VGD**X**N$_L$DRSIW-NH_2.[70] Again, compared to the $S_{(i,i+4)}S$ stapled peptide (SAHB$_A$, **49**) the $R_{(i,i+4)}R$ analogue imparted less helicity and cell permeability to the sequence (Figure 27-A,B). These results emphasise that stapled peptides, while able to mimic protein secondary structure successfully, cannot always negate the fact that D-amino acids are inherently α-helix destabilising.[87,88]

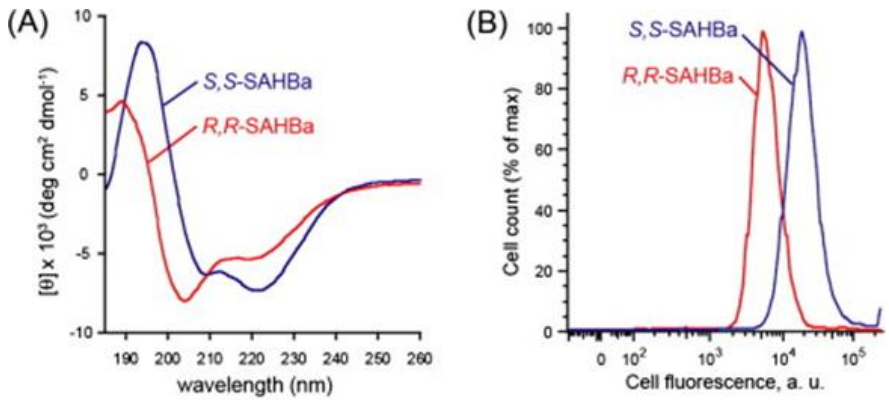

Figure 27- Comparison of $S_{(i,i+4)}S$ and $R_{(i,i+4)}R$ BID-BH3 Peptides - **A** Measured α-Helicity **B** Flow cytometry profile of stapled peptide cellular uptake into HeLa cells[86]

1.2.1.7 Necessity for α,α-Disubstituted RCM Monomers

With the information that D-amino acids are generally α-helix destabilising it could be argued that although the aminoisobutyric acid (Aib)[55,56,69] type α,α-disubstituted monomers increase the rigidity of the peptide backbone, they could have a minor destabilising effect. Alanine residues themselves have been shown to substantially contribute to helix propensity,[89–91] and so disubstitution at the C_α may not be a prerequisite to stabilising α-helical folding. Yeo *et al*.[92] explored this by replacing the pentenyl methyl disubstituted glycine monomers with the monosubstituted counterparts[93,94] (Figure 28- **56**) in the BID-BH3 sequence[70] (Table 8).

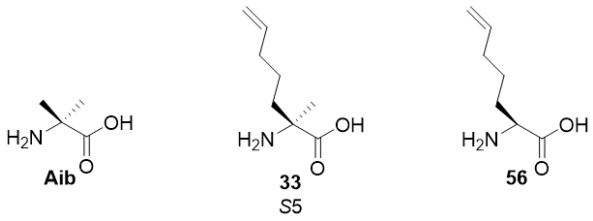

Figure 28- Monomers Incorporated by Yeo *et al*.[92]

Table 8- Effect of Monosubstitution in BID-BH3 Stapled Sequence

Sequence		% Helicity
Ac-EDIIRNIARHLAQVGDSN_LDRSIW-NH_2	**48**	12
Ac-EDIIRNIARHLA**X_1**VGD**X_1**N_LDRSIW-NH_2	**57**	31
Ac-EDIIRNIARHLA**X_2**VGD**X_2**N_LDRSIW-NH_2	**49**	80
Ac-EDIIRNIARHLA**X_3**VGD**X_3**N_LDRSIW-NH_2	**58**	73

X_1 *Aib;* ***X_2*** ***33****;* ***X_3*** ***56****;* *N_L Norleucine;*

The new monomer peptide **58** was compared to the wild type sequence, Aib analogue **57**, and the disubstituted monomer analogue **49**. It was found that both the monosubstituted and disubstituted sequences behaved similarly in terms of overall helicity, proteolytic stability and binding affinity when assessed against the Aib substituted and native sequences (Figure 29). This data infers that α-methylated monomers are not a requirement for an effective peptide staple.

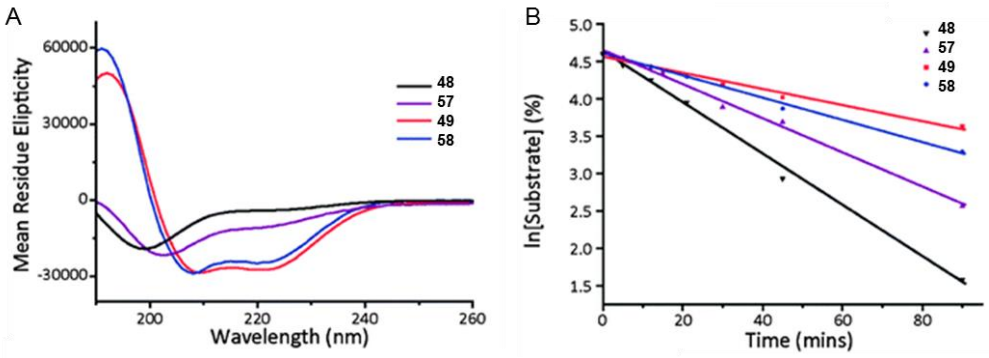

Figure 29- Comparison of Wild Type **48** and Substituted Analogues **49**, **57** and **58** of BID-BH3 **A** α-Helicity **B** Peptide digestion by trypsin in PBS buffer at 25 °C[92]

1.2.1.8 **RCM Staple Regioisomerism**

With the hypothesis that an $S_{(i,i+4)}S$ 8 atom linker is one of the most effective RCM cross-linkers, Pham *et al.*[95] considered the consequence of the position of the olefin within the staple using the monomers shown below (Figure 30-A). Using the RNAse-A sequence[66,86] as a template, the monomers were inserted and the peptides cyclised (Figure 30-B,C,D).

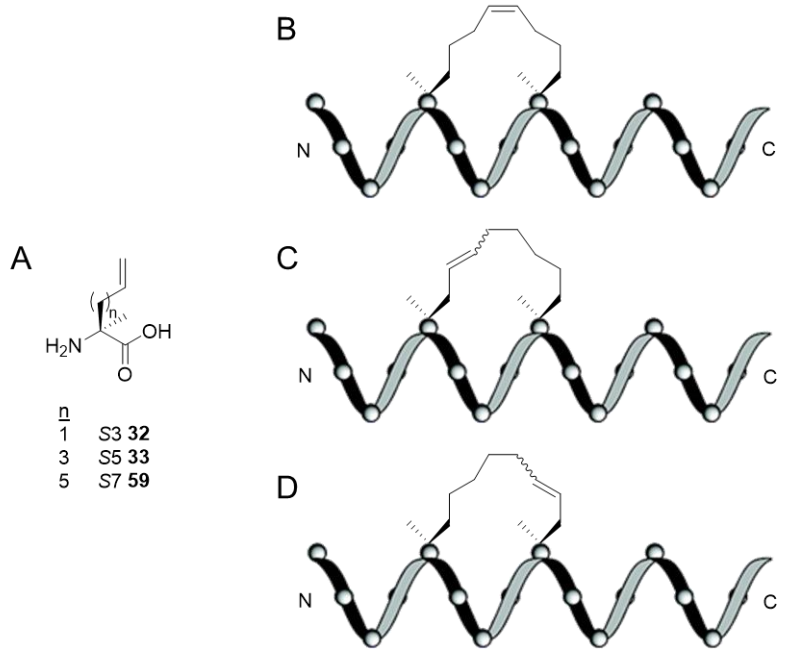

Figure 30- Investigating the Importance of Symmetry in RCM Staples - **A** Olefin Monomers Incorporated into **B** Symmetrical Δ-4 Stapled **C** Unsymmetrical Δ-2 and **D** Unsymmetrical Δ-6 Stapled RNAse-A Peptides[95]

It was found that cross-linking of the unsymmetrical oct-2-ene staples did not proceed at room temperature, unlike the Δ-4 symmetrical staple (Table 9). Heating at 60 °C afforded the Δ-2 analogue **60** in high yield, however even with heating, the Δ-6 macrocyclic peptide did not form and in fact decomposed. The difference in efficiency of the metathesis step is thought to be due to either coordination of the ruthenium centre to carbonyl groups in the peptide backbone[96] (Figure 31) or the allylglycine monomer **32** being too hindered for efficient catalysis.

Table 9- Peptides Investigating Staple Symmetry from Pham *et al*.[95]

Sequence		Yield %[a]	% Helicity
Ac-EWAETAAAKFLAAHA-NH_2	**36**	N/A	30
Ac-EWA$\mathbf{X_1}$TAA$\mathbf{X_3}$KFLAAHA-NH_2	**60**	>95[b]	49
Ac-EWA$\mathbf{X_2}$TAA$\mathbf{X_2}$KFLAAHA-NH_2	**54**	90	77
Ac-EWA$\mathbf{X_3}$TAA$\mathbf{X_1}$KFLAAHA-NH_2	**61**	-	-

a 2 h, RT; b 2 h, 60 °C; ***X₁ 32****;* ***X₂ 33****;* ***X₃ 59****;*

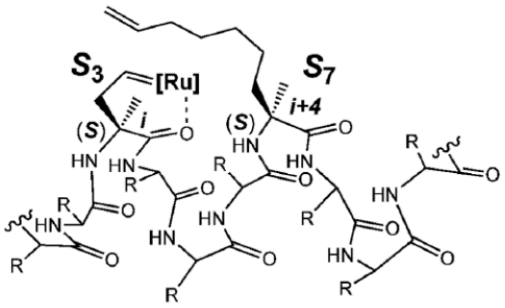

Figure 31- Coordination of Ru-Alkylidene to Carbonyl in Δ-2 RNAse-A Peptide[95]

The peptides that cyclised were analysed using CD (Figure 32). The Δ-2 unsymmetrical staple **60** showed a greater helicity that the native sequence **36**, but was much less helical than the symmetrical Δ-4 peptide **54**. This could indicate that the torsional strain caused by the unsymmetrical staple may be unfavourable to α-helix induction. These results show that the position of the olefin within the staple is a variable to consider.

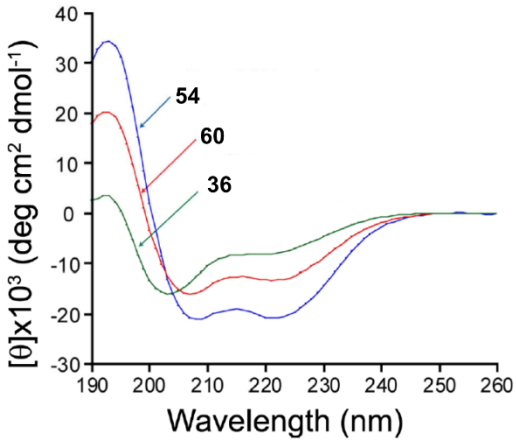

Figure 32- CD Spectra of RNAse-A **36** and Stapled Analogues Δ-4 **54** and Δ-2 **60**[95]

1.2.1.9 RCM Linker Length Over One Helical Turn

For some protein-protein interacting peptides, it may necessary to use a short staple to constrain the sequence to avoid replacing critical residues, or minimise unwanted staple-protein interactions. Kim *et al*.[97] have explored the feasibility of an (*i*,*i*+3) cross-

linker, as side-chains at these positions are still on the same face of the helix, and has approximately the same helical pitch as the established (*i*,*i*+4) linker (0.83 and 1.11 residues respectively). Using the RNAse-A sequence and the α,α-disubstituted pentenyl monomers (**30** and **33**, Figure 33),[66] the different enantiomeric pairings were screened for cyclisation efficiency (Table 10). It was apparent that the $R_{(i,i+3)}S$ (**63**) combination was preferred, with yields comparable to the more typical $S_{(i,i+4)}S$ linker (**54**) (Figure 34). The position of the staple in the sequence was altered (**66**-**69**) however similar results were seen suggesting that this tendency is not due to monomer placement within the peptide. Shortening the (*i*,*i*+3) linker length to 6 carbons (not shown) was found to be less stabilising than the 8 atom equivalent.[98]

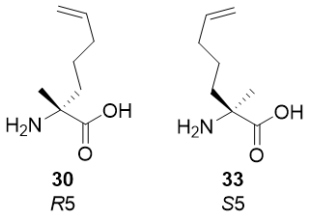

30 *R*5 **33** *S*5

Figure 33- Monomers Used by Kim *et al*.[97]

Table 10- Yields of (*i*,*i*+3) Peptides and $S_{(i,i+4)}S$ Counterparts

Ac-EWA**X$_1$**TA**X$_2$**AK**X$_3$**LAAHA-NH$_2$				
X_1	X_2	X_3		% Conversion
*R*5 **30**	*R*5 **30**	F	**62**	46
*R*5 **30**	*S*5 **33**	F	**63**	94
*S*5 **33**	*R*5 **30**	F	**64**	12
*S*5 **33**	*S*5 **33**	F	**65**	9
E	*R*5 **30**	*R*5 **30**	**66**	40
E	*R*5 **30**	*S*5 **33**	**67**	91
E	*S*5 **33**	*R*5 **30**	**68**	27
E	*S*5 **33**	*S*5 **33**	**69**	14
Ac-EWA**X^1**TAA**X^1**KFLAAHA-NH$_2$ (**54**)				86
Ac-EWAET**X^1**AAK**X^1**LAAHA-NH$_2$ (**70**)				82
***X^1* 33**;				

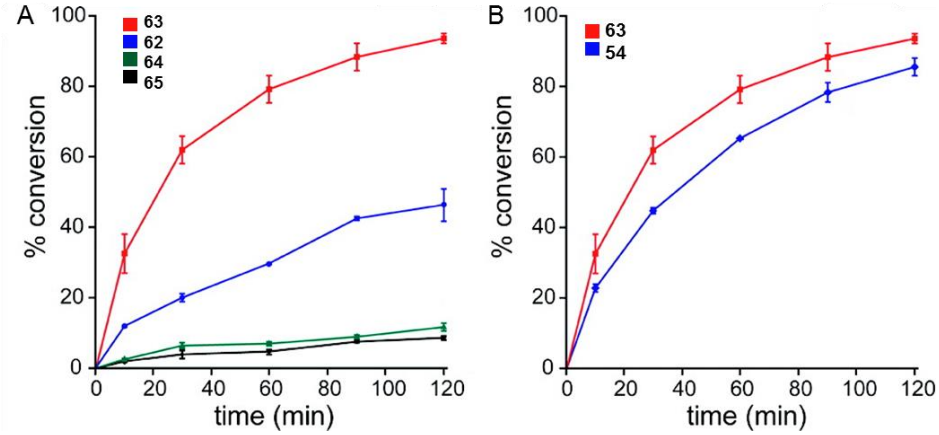

Figure 34- Comparison of RCM Macrocylisation Yield of (*i,i*+3) Staple - **A** Enantiomer Pairing **B** RCM Macrocylisation Yield of $R_{(i,i+3)}S$ **63** and $S_{(i,i+4)}S$ **54**[97]

Molecular dynamic simulations were concordant with the experimental data, suggesting that the $R_{(i,i+3)}S$ crosslink was the most stable, with the other pairs higher in energy (14-37 kcal/mol) due to unfavourable interactions between the α-methyl group and the staple (Figure 35).

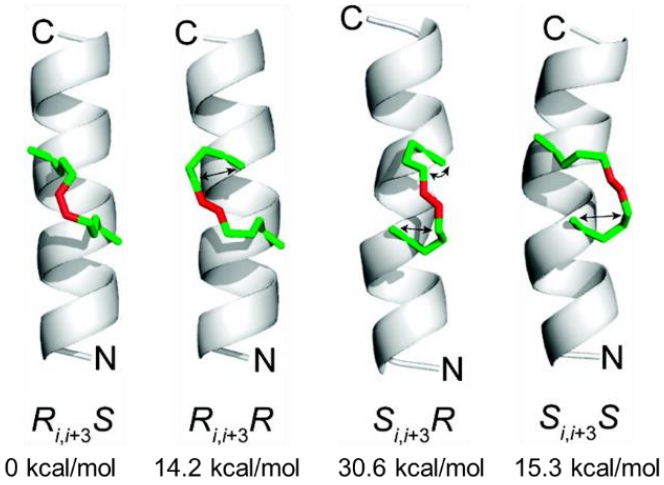

Figure 35- Representation of (*i,i*+3) Staples, Highlighting Unfavourable *syn*-Pentane Interactions (Arrows)[97]

The two $R_{(i,i+3)}S$ peptides **63** and **67**, along with the $S_{(i,i+4)}S$ analogues **54** and **70**, were analysed for induced helicity and increased stability (Figure 36-A). All the macrocylic peptides showed increased helicity over the unmodified sequence **36**, with crosslinked

sequences **54** and **63** exhibiting greater helical induction. Interestingly, in the trypsin digestion assays, the less helical stapled peptides **67** and **70** were the most stable, with no noticeable degradation at an substrate:enzyme ratio of 80:1 or 20:1. Only at a 2:1 ratio was there evidence of cleavage of the peptide **70**, with peptide **67** remaining undigested. The incredible stability of these peptides can be attributed to the location of the cleavage site within the sequence; the amino acid recognised by trypsin, in this case lysine, is contained between the alkenyl monomers. This may be explained by the fact that the greatest helicity imparted to the residues encompassed by the staple,[78] and proteases cannot recognise folded structures.[99] There is also evidence that α,α-disubstituted amino acids are not recognised by trypsin, and can halt peptidolysis when surrounding the enzymatically recognised residue.[100] The most helical peptides were tested for increased cellular uptake (Figure 36-B). Surprisingly, it was found that cyclic peptide **63** was only moderately more penetrant than the uncyclised native **36**.

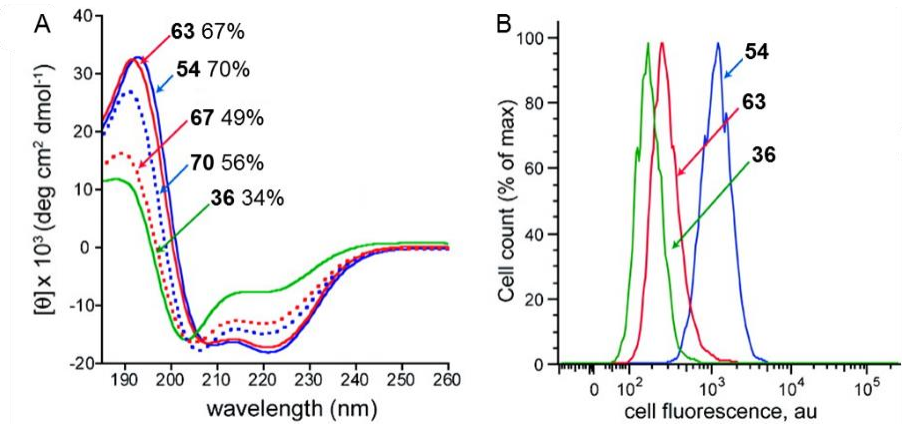

Figure 36- Analysis of RNAse-A Analogues - **A** CD Spectra **B** Flow cytometry profile showing cellular uptake of **36**, **54** and **63** into HeLa cells[97]

1.2.1.10 **Stereoselectivity of Bis-RCM Staples**

The orthogonal stereochemical preferences of the (*i*,*i*+3) and (*i*,*i*+4) linkers can also be utilised to design multi-stapled peptides which have been shown to have increased proteolytic stability.[101] This was demonstrated by Kim *et al*.[97] by incorporating the residues **30** and **33** (Figure 37) into two new peptides **71** and **72** based on the RNAse-A sequence **36** (Table 11). By relying on the most favourable $S_{(i,i+4)}S$ and unfavourable

$S_{(i,i+3)}S$ (Figure 38-A) and $S_{(i,i+3)}R$ (Figure 38-B) interactions, both the doubly stapled peptides formed selectively. This was further illustrated by synthesising the polyalanine 13-mer **73**. Following the reaction by LC-MS it was evident that as a result of the disadvantageous central $S_{(i,i+3)}S$ pairing, the bis-stapled product of **73** formed cleanly.

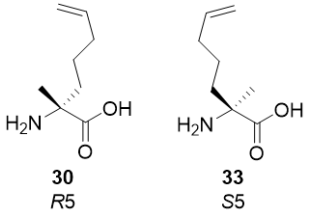

Figure 37- Monomers used by Kim *et al*. in Bis-Stapled Peptides

Table 11- Bis-Stapled Peptides from Kim *et al*.

Sequence	
Ac-EWAETAAAKFLAAHA-NH_2	**36**
Ac-EW$\mathbf{X_1}$ETA$\mathbf{X_1}$AK$\mathbf{X_1}$LAA$\mathbf{X_1}$A-NH_2	**71**
Ac-EWA$\mathbf{X_1}$TAA$\mathbf{X_1}$KF$\mathbf{X_2}$AA$\mathbf{X_1}$A-NH_2	**72**
Ac-$\mathbf{X_1}$AAA$\mathbf{X_1}$AA$\mathbf{X_1}$AAA$\mathbf{X_1}$A-NH_2	**73**
X_1 33; X_2 30;	

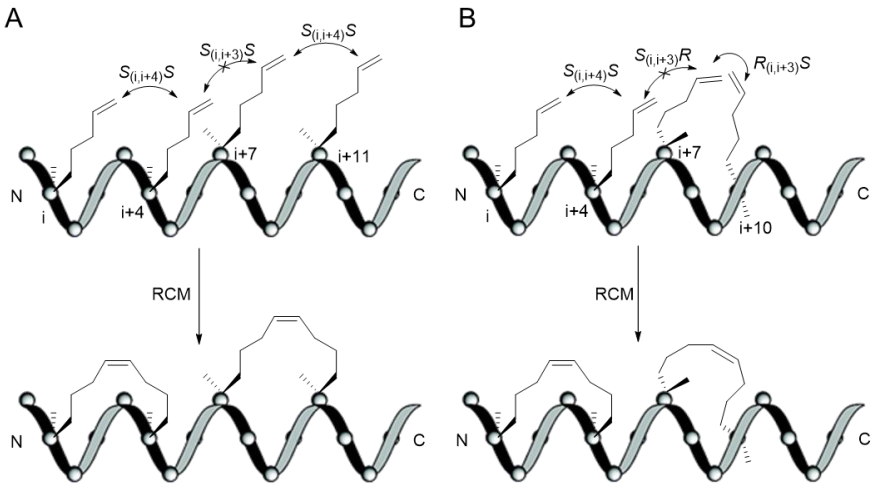

Figure 38- Respresentations of Disadvantageous **A** $S_{(i,i+3)}S$ and **B** $S_{(i,i+3)}R$ Interactions Utilised for Selective Staple Formation in **71** and **72**[97]

Building upon this and previous work on the RNAse-A peptide (**36**),[66,86] Hilinski *et al*.[102] used the information that an (*i*,*i*+4) staple would favour an 8 atom linker with the *S*,*S* configuration of monomers and an (*i*,*i*+7) staple would favour an 11 atom linker with *R*,*S* configuration (Figure 39-B). Identifying that a bis-pentenyl glycine monomer (Figure 39-A, **74**) would have the required pro-*S* and pro-*R* side chains for both staples, and would maintain the α,α-disubstitution that aids this stereoselection via detrimental steric interactions,[78] this "stitched" peptide (Figure 39-B) should theoretically have the same stability equivalent to a bis-stapled peptide while encompassing a greater number of residues within the macrocycles.

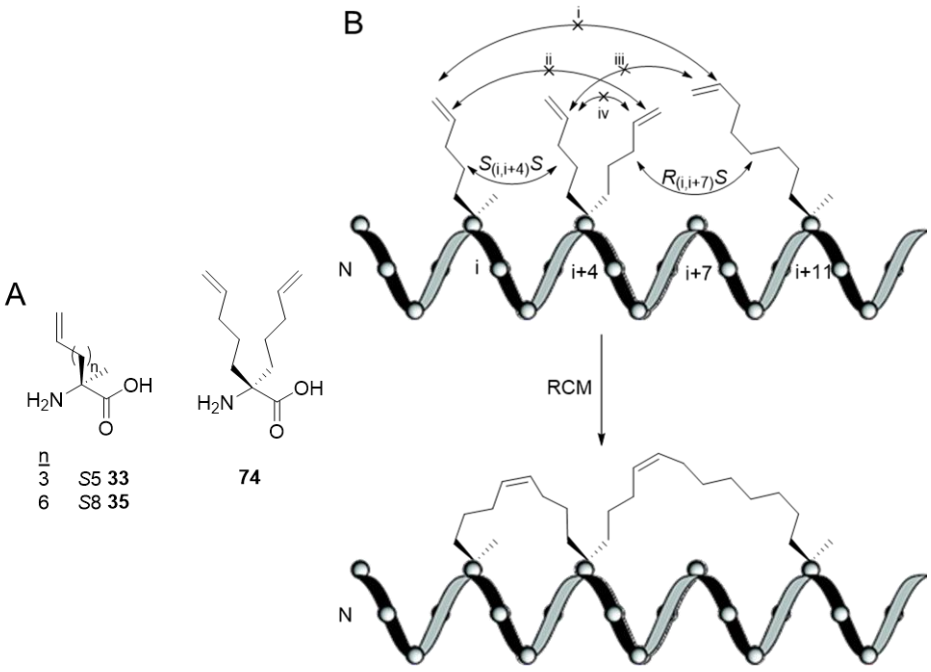

Figure 39- **A** Monomers Incorporated into Stitched Peptides **B** Representation of Favoured ($S_{(i,i+4)}S$ and $R_{(i,i+7)}S$) and Unfavourable (i, ii iii, iv) Interactions for cyclisation in RCM Stitched Peptides[102]

This new methodology was applied to a polyarginine (R12) sequence, one of the most potent cell penetrating peptides known,[103] but which is intrinsically disordered due to the cationic side-chain repulsions.[104,105] The stitched polyarginine sequence, Ac-(**33**)RRR(**74**)RRRRRR(**35**)-NH_2, showed a vast increase in helical secondary structure compared to the $R_{(i,i+7)}S$(11) stapled (R-Stp) and the unmetathesised stitched

peptide (59%, 23% and 15% respectively, Figure 40-A), suggesting that macrostabilisation plays a greater role than the minor rigidifying effects from α,α-disubstituted amino acids. Performing a computational solvation analysis, it was found that the stitched peptide has less water molecules associated with each residue when compared to the native R12 and R-Stp sequences, which is in agreement with the theory that macrocyclisation increases hydrophobicity and prevents disruption of secondary structure by co-ordinating water at amide hydrogen bonding sites.[106–108] Comparing the cellular uptake of the R12, R-Stp and R-Stc, again it was found that the hydrocarbon crosslinked peptides had a greater penetrance than the polyarginine 12-mer sequence (Figure 40-B). Interestingly, while the stitched peptide has fewer cationic residues it displayed the greatest uptake, indicating the benefits of increased hydrophobicity and pre-organisation. Finally, the peptides were tested for stability in a trypsin digestion assay. Trypsin recognises charged basic residues, so thus not surprisingly at 25 °C and a substrate:enzyme ratio of 800:1, the R12 sequence was metabolised completely in 5 minutes. Under the same conditions, the R-Stp and R-Stc sequences were relatively undamaged (41% and 94%, Figure 40-C). Even after 1 h the R-Stc sequence was still greater than 50% intact, underlining the increased proteolytic resistance that can be imparted when peptides are constricted into an α-helical secondary structure.[99]

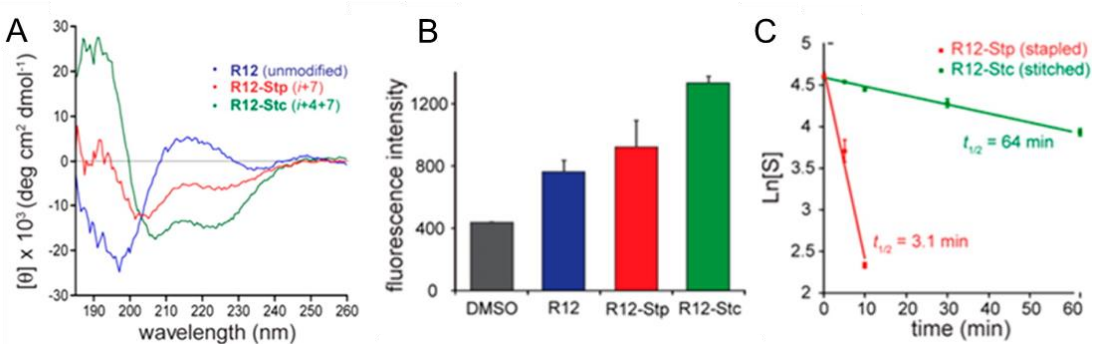

Figure 40- Comparison of poly-R Peptides **A** α-Helicity **B** Epifluorescent microscopy analysis of cellular uptake into HeLa cells **C** Stability of R-Stp and R-Stc toward trypsin at 25 °C [102]

1.2.1.11 **Non Side-Chain Side-Chain RCM for α-Helical Induction**

There is evidence that helix induction requires the pre-organisation of only three amino acid residues, and that overcoming this energy is the main thermodynamic barrier.[8,109,110] Building upon previous work,[111–113] Chapman *et al*.[114] used RCM to mimic the chain of 13 atoms that are characteristic of α-helical secondary structure (Figure 41-A). Using the control peptide, Ac-GEAAAAEA-OMe (**75**), which had no inherent secondary structure, A3 was replaced by an *N*-allylated analogue, synthesised by alkylating the 2-nitrosulfonamide of alanine *tert*-butyl ester,[115,116] and the *N*-acylated glycine was substituted for 4-pentenoic acid (**76u**).

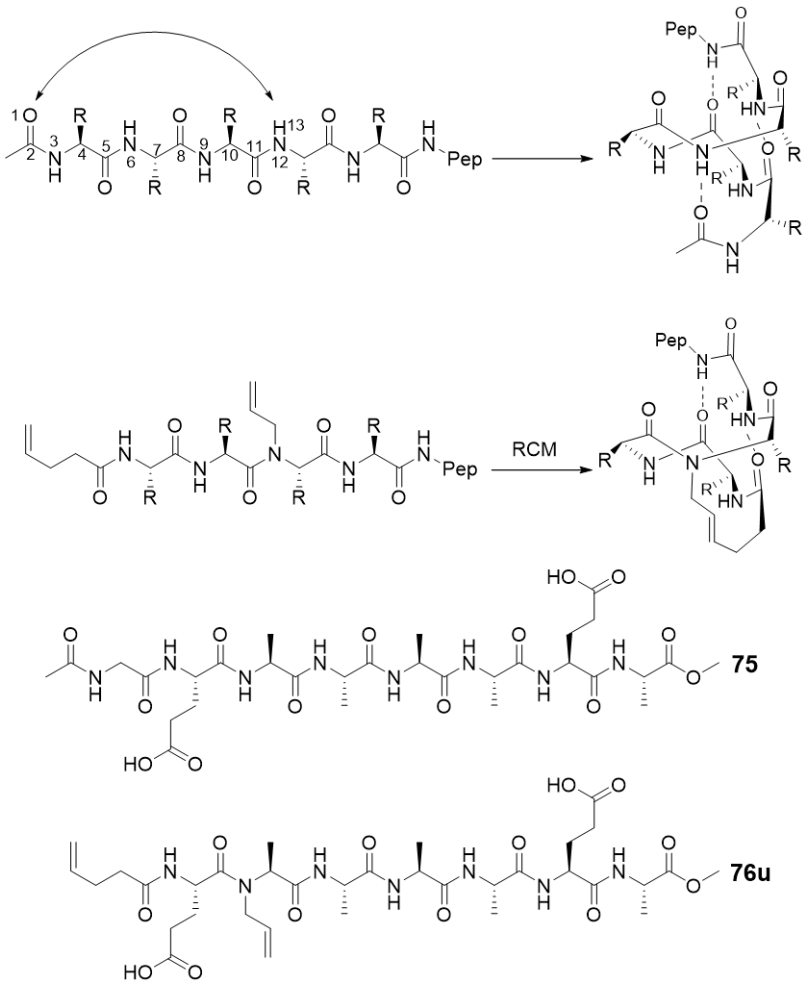

Figure 41- Representation of **A** 13 Atom Chain in α-Helix Hydrogen Bonding **B** RCM Hydrogen Bond Surrogate **C** Peptide **75** and HBS Analogue **76u**

It was shown that, following metathesis, the all carbon hydrogen-bond surrogate (HBS, **76c**) installed could induce a helix in the peptide sequence, as shown by the characteristic minima at 220 nm and 202 nm (Figure 42-$A_{(i)}$). Addition of trifluoroethanol[62–64] did not result in an increase of helicity (Figure 42-$A_{(ii)}$). Calculating the relative percent helicity,[117] and correcting for small peptides,[118] it was discovered that the HBS peptide was determined to be 100% helical. Comparatively, the native sequence showed no relative helicity (Figure 42-$A_{(iii)}$), in any amount of trifluoroethanol (Figure 42-B).

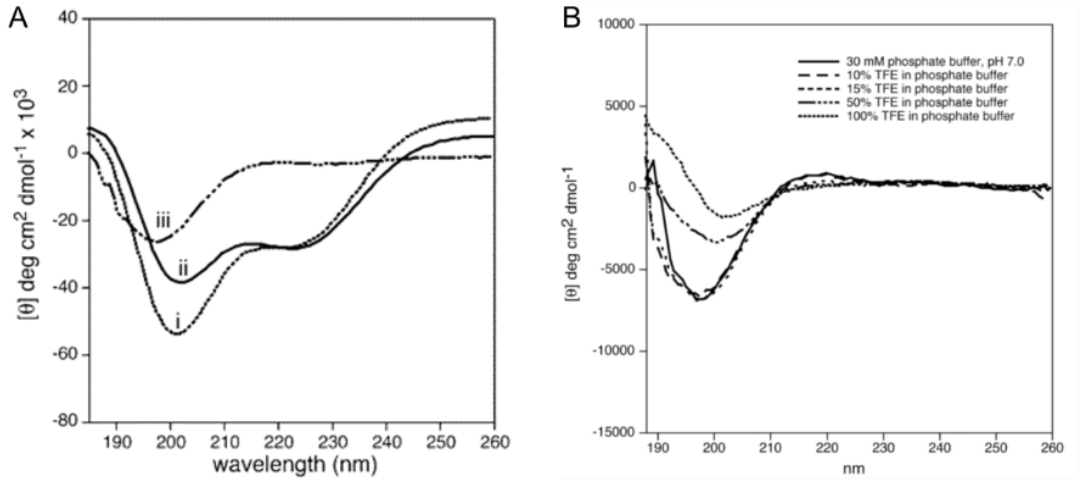

Figure 42- CD Spectra of **$A_{(i)}$ 76c** in 30 mM Phosphate Buffer **$A_{(ii)}$ 76c** in 20% TFE in 30 mM Phosphate Buffer **$A_{(iii)}$ 75** in 30 mM Phosphate Buffer **B 75** in 0%, 10%, 15%, 50% and 100% TFE in 30 mM Phoshate Buffer[114]

The HBS method, after optimisation for solid phase sythesis,[119] has been shown to induce helicity in a number of biologically relevant peptides.[120,121] One of the benefits of this approach is that it can be used to synthesise α-helices for protein-protein interactions that have residues on opposite faces of the peptide required for activity.[122]

1.2.2 Copper(I) Alkyne-Azide Cycloaddition (CuAAC)

The copper(I) alkyne-azide cycloaddition, unlike its non-catalysed precedent,[123–125] regioselectively forms 1,4-disubstituted 1,2,3-triazole products (Figure 43).[126,127] This transformation has been used ubiquitously in synthesis. The facile, robust nature of the

reaction facilitates the rapid creation of combinatorial libraries, and the use of copper makes triazolyl bioconjugation more appealing as it is cheaper and less toxic than ruthenium.[128]

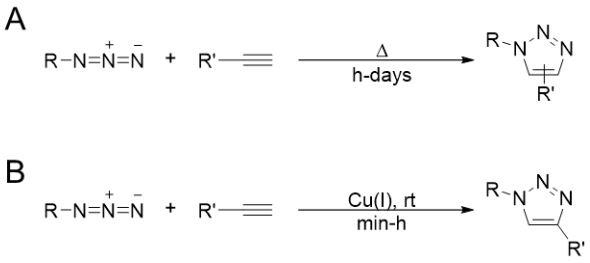

Figure 43- Schematic Representations of **A** Alkyne Azide Cycloaddition **B** CuAAC

The heterocycle, which is inert to the proteasome and synthesised from biologically silent functional groups, can be considered an amide isostere (Figure 44) and has been used as such. These properties make the CuAAC reaction appealing as a stapling technique.

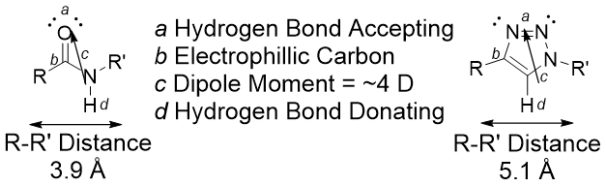

Figure 44- Comparison of Amide and Triazole

1.2.2.1 **CuAAC (*i*,*i*+4) Staple**

The first example of α-helical induction using CuAAC was from Cantel *et al.*[129] Based on prior studies that showed that alkyne and azide bearing peptides can be cyclised on resin with high tolerance of peptidyl functional groups and in high yields,[130] Cantel *et al*. looked at Parathyroid Hormone related Protein (PTHrP), a protein associated with tumour malignancy which has a bioactive α-helical section.[131] The Ac-PTHrP-(11-19)NH_2 sequence, Ac-KGKSIQDLR-NH_2 (Figure 45-A **77u**), a truncated peptide which had been derived from a longer sequence that already shown increased secondary structure stabilisation following the (*i*,*i*+4) lactamisation of K13 and D17

(Figure 45-A, **77c**),[132–134] was used as a model substrate. The lactamising residues were replaced with alkyne and azide equivalents (Figure 45-B) to allow direct comparison.

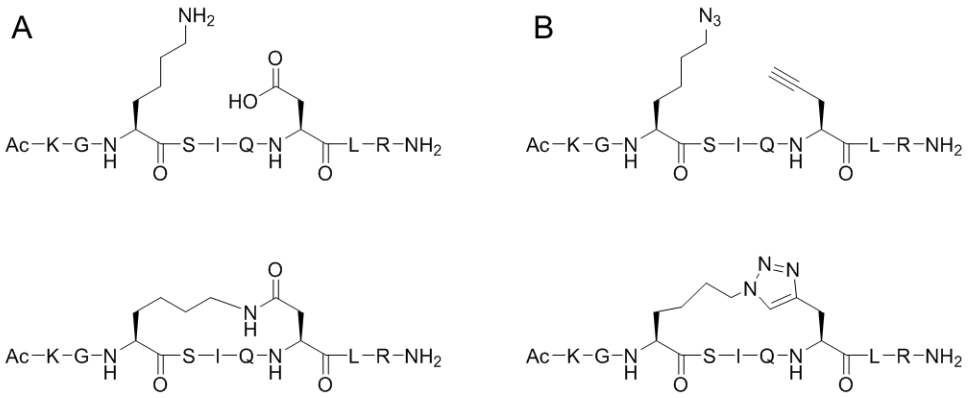

Figure 45- A Ac-PTHrP-(11-19)-NH_2 **77u/c B** CuAAC Analogue **78u/c**

The azide was installed in the peptide by diazo transfer on a lysine residue by triflic azide.[135–138] Attempted cyclisation on resin however gave poor yields, or a mixture of product and cyclodimer.[139–141] The peptide **78u** was instead cleaved from the resin and, following purification by RP-HPLC, cyclised in solution using supra-stoichiometric amounts of copper to yield the cyclised monomer. The cyclised peptides were analysed by CD for α-helicity. The lactamyl (**77c**, Figure 46-A) and triazolyl (**78c**, Figure 46-B) peptides showed no secondary structure in 100% water (Figure 46-A,B-Solid) but showed greater than 50% relative helicity (Figure 46-A,B-Dashed) in 50:50 hexafluoroacetone (HFA):water.[142] NMR nOe experiments also saw an increase in cross-peaks following solvent substitution, confirming organisation of the peptide.

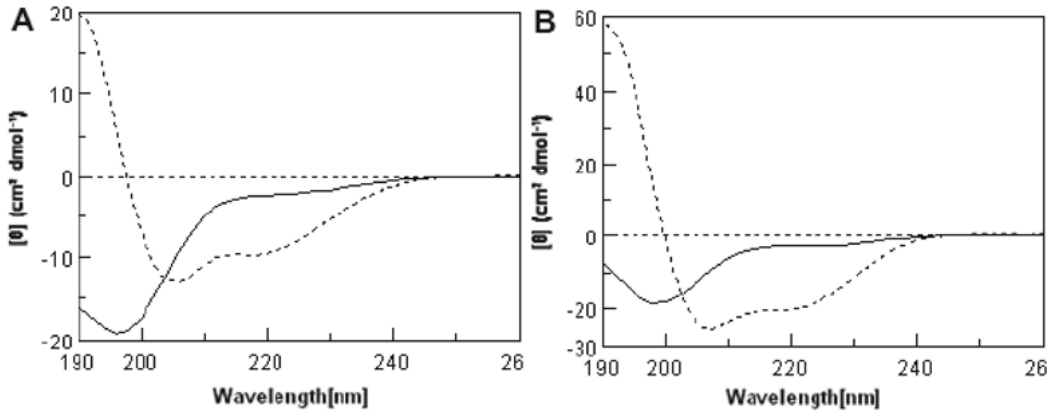

Figure 46- CD Spectra of **A 77c** and **B 78c** in 100% Water (Solid) and 50:50 Water:HFA (Dashed)[129]

1.2.2.2 Linker Length and Regioisomerism in (*i*,*i*+4) CuAAC Staple

Continuing the investigation into the utility of the CuAAC as a stapling method Scrima *et al*.,[143] using the same Ac-PTHrP-(11-19)NH_2 model **77u**, replaced the lysine and aspartic acid residues for alkynyl and azido non-natural amino acids with various side chain lengths (Figure 47).[144] The order of each of the monomers was varied to account for the regioisomers that exist due to the asymmetry of the triazole.[145]

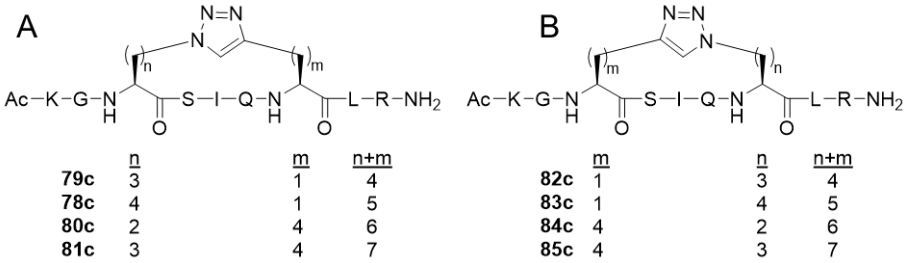

	n	m	n+m
79c	3	1	4
78c	4	1	5
80c	2	4	6
81c	3	4	7

	m	n	n+m
82c	1	3	4
83c	1	4	5
84c	4	2	6
85c	4	3	7

Figure 47- A 1,4- and **B** 4,1- Regioisomeric Triazolyl Peptides of Ac-PTHrP-(11-19)NH_2 **77u**

The circular dichroism spectra of these peptides were run in both water and water:HFA (50:50) for direct comparison to the previous study.[129] Analysis of the spectra showed that the triazolyl cyclic peptides showed little secondary structure in water. In water:HFA all the peptides showed a high helical propensity. Molecular dynamic simulations from NMR experiments showed that peptides with staples where n+m = 4

(**79c** and **82c**) constricted the peptides into non-canonical secondary structures. Staples where n+m = 7 (**81c** and **85c**) did not constrict the peptides effectively enough, allowing a flexibility within the backbone that allowed irregular conformations. Peptides that had staples containing either n+m = 4 or 5 seemed to be the most effective, however it was shown that in the peptides where n+m = 5 (**78c** and **83c**) the position of the triazole can affect the structure, whereas this effect was not observed when n+m = 6 (**80c** and **84c**). This suggests that a linker where n+m = 6 may be more broadly applicable.[143]

Expanding on their previous investigation, Scrima *et al.*[146] continued analysis of a number of the triazolyl peptides previously synthesised[143,144] (Figure 48). To verify that the α-helicity of the triazolyl peptides was not due to the water:HFA solvent, NMR experiments were performed in DMSO:water (80:20), a biomimetic solvent mixture which exhibits high viscosity and so restricts the flexibility of the peptide, allowing observation of the most common conformers.[147–149]

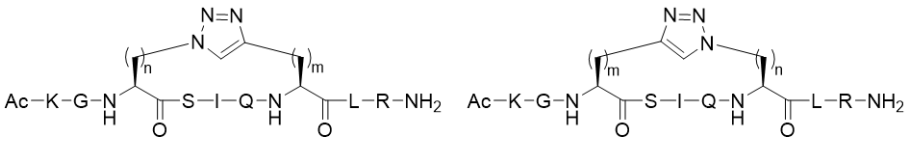

	n	m	n+m
79c	3	1	4
86c	2	4	6
87c	3	4	7

	m	n	n+m
82c	1	3	4
88c	4	2	6
89c	4	3	7

Figure 48- Triazolyl Regioisomeric Peptides Analysed in DMSO:H_2O by Scrimia *et al.*

Interestingly, although in good agreement with the previous results, cyclopeptides that contained a 4,1-orientated triazole (**82c**, **88c** and **89c**), regardless of linker length, displayed non-helical or non-regular conformations. In contrast, 1,4-orientated triazolyl peptides where n+m = 6 or 7 (**86c** and **87c**) allowed helical secondary structure. Study of the calculated structures showed that the nitrogen lone pairs of the triazole interacted with the serine or glutamine side chain residues either advantageously or deleteriously to α-helical induction, stressing the need to consider the chemistry of the heterocycle when using CuAAC in stapling.[146]

1.2.2.3 Stereochemistry of Alkynyl and Azido Monomers/Bis Stapling

In a comprehensive study, Kawamoto *et al*.[150] selected the BCL9/β-catenin protein-protein interaction as a model system for triazole stapling. Controlling a number of cell cycle and apoptosis regulating genes, the upregulation of β-catenin is associated with tumorigenesis in a number of human cancer types.[151,152] It is known to form a complex with a number of proteins, including B-cell lymphoma 9 (BCL9). The unique binding site for the α-helical section of BCL9,[153] a necessary interaction for β-catenin mediated transcriptional activation, makes the interaction attractive as a therapeutic stapled peptide target. Using an optimised minimum binding 24-mer sequence Ac-LSQEQLEHRERSLQTLRDIQRMLF-NH_2 **90**,[154] avoiding the replacement of positively charged residues to enhance cell permeability,[155] solvent exposed residues E360 and Q364 located on the same helical face in the middle of the peptide (Figure 49) were swapped for alkynyl[93,94] and azido[135–138] monomers of different lengths and chirality (Figure 50). The % helicity and binding of the uncyclised and cyclised peptides were measured by circular dichroism and competitive fluorescence polarisation assay respectively (Table 12).

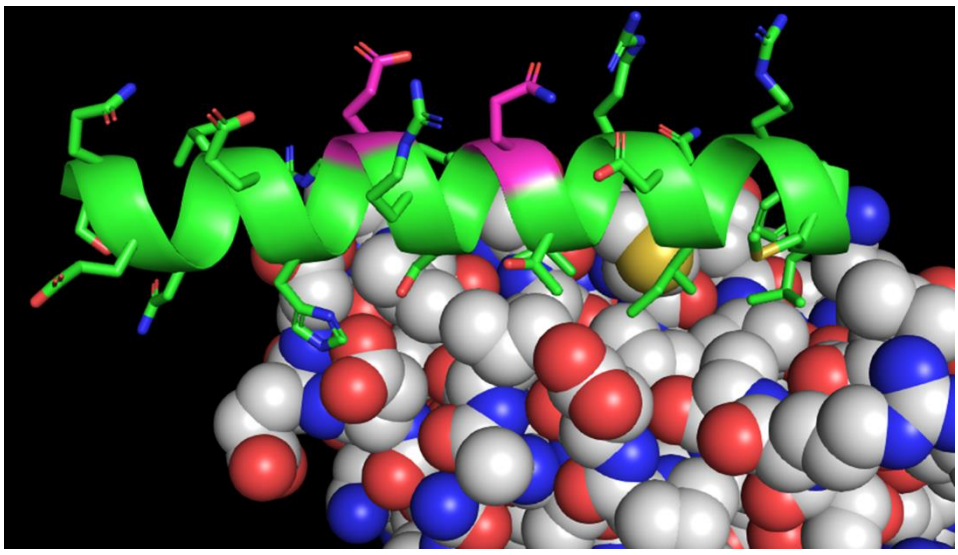

Figure 49- BCL9 based peptide **90** (green) bound to β-Catenin with solvent exposed residues E360 and Q364 (magenta). PDB code 2GL7, reproduced using PyMol.

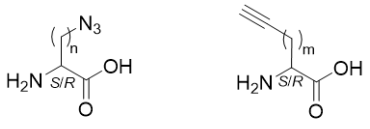

n		m	
3	**91**	1	**93**
4	**92**	2	**94**

Figure 50- Monomers Incorporated in BCL9 Triazolyl Stapled Peptides

Table 12- % Helicity and K_i of BCL9 Peptides **90** and **95** and Analogues **96**-**103**

Ac-LSQEQLEHR**X$_1$**RSL**X$_2$**TLRDIQR**X$_3$**LF-NH$_2$					% Helicity		K_i ± SD (μM)	
X_1	X_2	X_3[a]	n+m		u	c	u	c
E	Q	M	-	**90**	44	-	0.60 ± 0.14	-
E	Q	L	-	**95**	47	-	0.94 ± 0.17	-
*S***92**	*S***93**	M	5	**96**	44	66	1.4 ± 0.2	0.33 ± 0.6
*S***92**	*R***93**	M	5	**97**	45	90	4.9 ± 0.9	0.13 ± 0.05
*S***91**	*S***93**	M	4	**98**	42	26	2.4 ± 0.2	NB
*S***92**	*S***94**	M	6	**99**	49	48	1.4 ± 0.1	3.0 ± 0.3
*S***91**	*S***94**	L	5	**100**	50	30	1.9 ± 0.4	30 ± 5[b]
*S***93**	*S***92**	L	5	**101**	49	ND[c]	3.6 ± 1.0	0.77 ± 0.18
*S***93**	*R***92**	L	5	**102**	32	57	11.0 ± 1.0	1.17 ± 0.51
*R***93**	*S***92**	L	5	**103**	34	67	2.2 ± 0.2	4.3 ± 0.4

a L replaced M due to oxidation; b extrapolated; c peptide insoluble; ND: Not Determined; NB: No Binding;

The native sequences and uncyclised peptides (**90**, **95**, **96u**-**103u**) showed moderate relative helicity and binding affinity to β-catenin, however following cyclisation clear distinctions became obvious. As previously found,[143,146] in cyclised peptides with a linker length n+m = 4 (**98c**) there was a significant drop in % helicity and a total loss of affinity. Interestingly, when the linker length is n+m = 6 (**99**), cyclisation did not result in increased relative helicity or binding with respect to the uncyclised sequence which is in contradiction to previous studies. Moving the triazole one atom to a more central position within the staple (**100c**) reduced the solubility, binding affinity and removed the helicity of the sequence noticeably. This once more suggests that the dipole of the triazole can affect the stability of stapled peptides.[146]

The effect of monomer chirality can be seen in peptides **96**, **97**, and **101**-**103**. Linear peptides with D-amino acids (**97u**, **102u** and **103u**) tended to have lower relative

helicities than the native sequences (**90** and **95**). A vast increase in helicity is observed in peptide **97c** from the inversion of stereochemistry in the propargyl monomer **93** (Figure 51), thought to be due less distortion of the peptide backbone. Again, the regioisomerism of the triazole affects the properties of the peptides, with the 4,1-triazolyl peptides **101**-**103** showing less favourable characteristics than the 1,4-triazole counterparts. It could be argued that the most effective combination of 1,4-regioisomer with the $S_{(i,i+4)}R$ enantiomeric pairing (**97c**) is mirrored in the 4,1-regiosomer with $R_{(i,i+4)}S$ pairing (**103c**), which is more helical than the diastereomeric peptide **102c**, though the pairing is less favourable overall.[150]

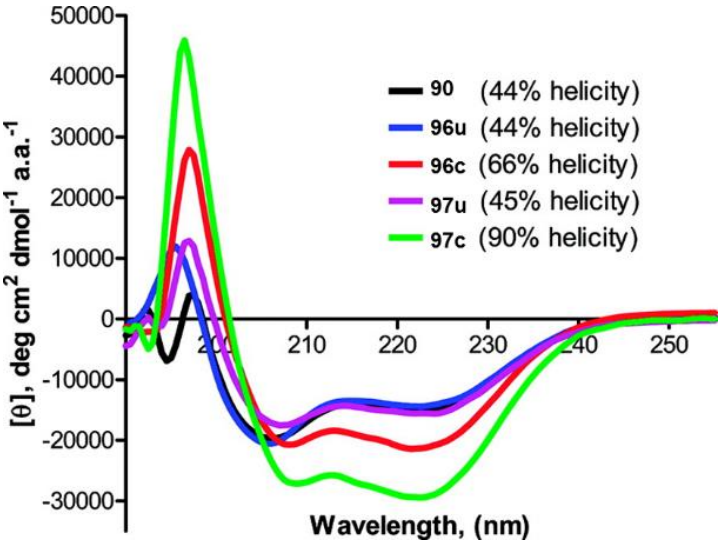

Figure 51- % Helicity of Diastereomeric CuAAC Peptides

As the native peptides **90** and **95** encompass 6 helical turns, the effect of different stapling positions was considered. Using the optimal linker pairing of S**92**$_{(i,i+4)}R$**93** exhibited in peptide **97c** (Table 12) and maintaining the greatest number of positively charged residues, new (*i*,*i*+4) staples were installed and the possibility of a bis triazolyl stapled peptide was also investigated (Table 13). By reversing the functionality of the side chain, it was postulated that the double staple would preferentially form over the disfavoured mixed staple (Figure 52).

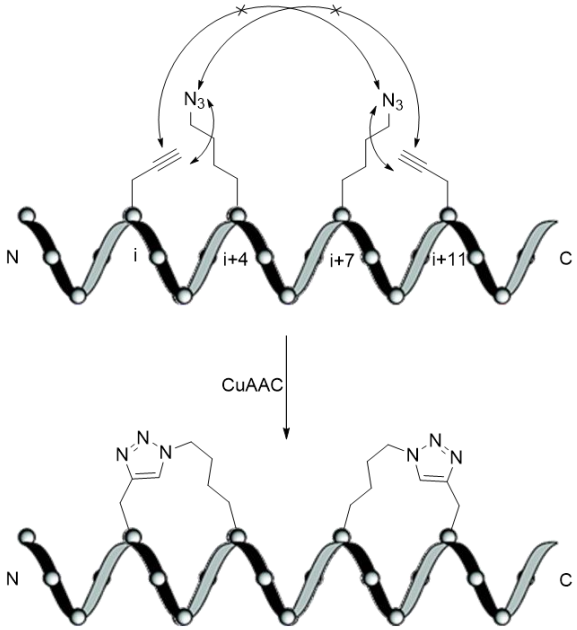

Figure 52- Representation of Regioselectivity Expected in Bis-Triazolyl Stapled Analogues of BCL9

Table 13- % Helicity and K_i of Mono- and Bis-Stapled BCL9 Analogues

Ac-LSQEQ**X$_1$**EHR**X$_2$**RSL**X$_3$**TLR**X$_4$**IQRLLF-NH$_2$					% Helicity		K_i ± SD (μM)	
X_1	X_2	X_3	X_4		u	c	u	c
*S***92**	*R***93**	Q	L	**104**	21	60	1.97 ± 0.2	0.41 ± 0.05
L	E	*S***92**	*R***93**	**105**	31	81	2.01 ± 0.1	0.26 ± 0.04
L	E	*S***93**	*R***92**	**106**	16	42	6.66 ± 0.4	0.56 ± 0.05
*S***92**	*R***93**	*S***93**	*R***92**	**107**	12	95	13.2 ± 0.9	0.41 ± 0.07
*S***93**	*R***92**	*S***92**	*R***93**	**108**	20	96	14.5 ± 1.1	0.61 ± 0.01
Ac-LS**X$_1$**EQL**X$_2$**HRERSL**X$_3$**TLR**X$_4$**IQRLLF-NH$_2$								
X_1	X_2	X_3	X_4					
*S***92**	*R***93**	*S***92**	*R***93**	**109**	ND[a]	99	3.6 ± 0.1	0.19 ± 0.03

a peptide insoluble; ND: Not Determined

Moving the staple closer to the C terminus (**105**) was shown to increase relative helicity more than moving the staple toward the N terminus (**104**), though both exhibited similar binding affinity to β-catenin. This is thought to be due to the encompassing of threonine, a known α-helix destabilising residue.[156] As the regioisomer **106** was also tolerated, the bis triazolyl peptides **107c** and **108c** were synthesised. Both displayed increased relative helicity and binding affinity, but a peptide containing two staples with the most stabilising monomer pairing *S***92**$_{(i,i+4)}$*R***93**,

removing the unfavourable 4,1-regioisomer, separated by a helical turn (**109c**) showed even greater helical induction. Notably, while the double stapled peptides showed greater helical induction, the binding affinity for β-catenin did not vary vastly in comparison to some of the mono stapled sequences. This highlights the point that although there is a correlation between affinity and α-helicity, the maximum affinity is dependent on the sequence and when reached, additional stapling will only increase the efficacy of the peptide.[150]

1.3 Considerations of Design

After looking at the previous examples, it becomes apparent that although ultimately the efficiency of each staple is highly dependent on the sequence, certain properties need to be considered:

1. Length of the linker – too short and the linker may not form or constrict the peptide into undesired conformations. Too long and the peptide becomes too flexible and the staple is redundant. An optimum linker length would constain the peptide, but allow for some flexibility to allow for the dynamic nature of PPIs.
2. Linker position – The linker should be positioned such that it will be located near the greatest number of residues critical for binding. Ideally it should be close to helix destabilising residues also, ensuring maximum helical induction of these residues.
3. Number of Staples – For short peptides (< 13 residues) a single optimised staple should be sufficient. For longer sequences a multiple stapling strategy should be considered.
4. Regioisomerism – There will be a preferred regioisomer or directionality to the staple.
5. Stereoisomerism – The optimal chiral pairing of the linking monomers will vary with the linker being used.
6. Chemistry – The physicochemical properties of the stapling system may interfere with the induced helicity.

Chapter 2- The p53 MDM2 Interaction as a Therapeutic Target

2 The p53 MDM2 Interaction

The p53 protein is key in regulating cell health and viability by a number of processes including senescence, DNA repair, cell cycle arrest, cell metabolism, apoptosis, or autophagy.[157] This myriad of essential effects has resulted in p53 being described as "guardian of the genome".[158] Unsurprisingly, loss of p53 activity is responsible for 50% of human cancers. This is usually due to its tumour suppression being hindered by regulating proteins such as MDM2 and MDMX. MDM2 is an E3 ubiquitin ligase and has p53 as a transcription factor, and so forms a negative feedback loop.[159] While MDMX does not have any E3 ligase activity, in forming a heterodimer with MDM2, ubiquitinylation of p53 is triggered and the complex is removed from the cell nucleus.[160,161] A number of tumour cells either under-express p53 or over-express MDM2 and/or MDMX and it has been shown that re-activation of p53 can halt tumour growth. Therefore, inhibiting MDM2 and MDMX provides a non-genotoxic pathway for cancer therapy (Figure 53).

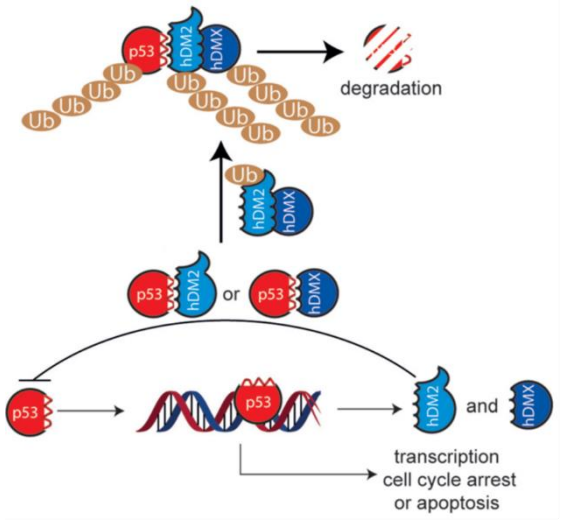

Figure 53- Summary of the Autoregulatory Loop of p53, MDM2 and MDMX[162]

Both MDM2 and MDMX bind to p53 at the N-terminal transcription activation domain (residues 1-44, Figure 54). While p53 has a number of intrinsically disordered domains,[163] the transactivational domain of p53 adopts an α-helical structure when

binding to the MDM-homologues. To reactivate p53 activity, an inhibitor must be able to block both the hydrophobic pockets of MDM2 and MDMX. A number of peptide sequences of different length, derived from the p53 transactivation domain, have been used as a control to measure inhibition of MDM2 and MDMX. These peptides typically use sequences from within the L14 to C31 residues. However, all the sequences contain the three residues that are critical for binding to the hydrophobic pockets of both MDM2 and MDMX: F19, W23 and L26 (Figure 55).[164,165]

Figure 54- Functional Domains of p53- 1-44: Transactivation domain, activates downstream target genes; 58-101: Proline rich domain, mediates p53 response to DNA damage through apoptosis; 102-292: DNA-binding domain; 325-356: Oligomerization domain, responsible for p53 dimer and tetramer formation; Nuclear localization signals (NLS) and nuclear export signals (NES) have also been identified.[166]

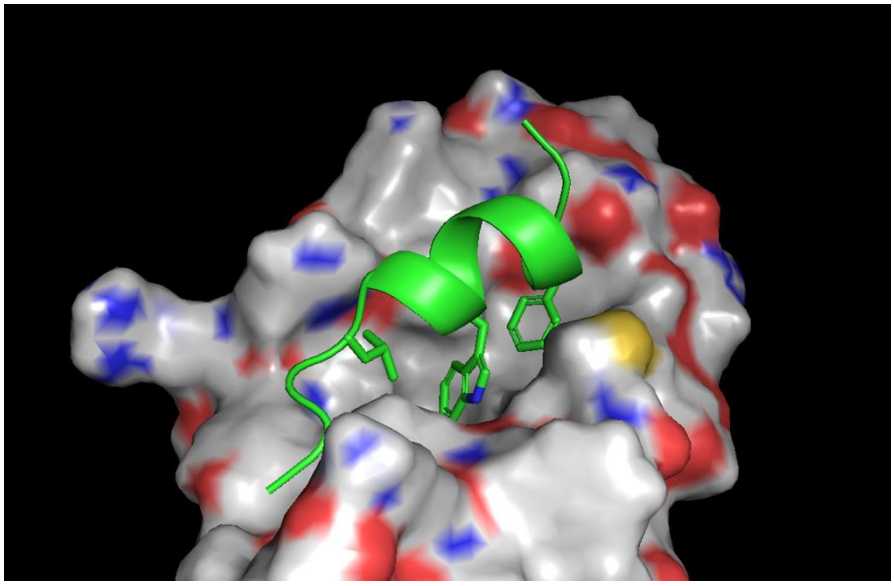

Figure 55- Crystal Structure of p53 α-Helical Transactivation Domain (green) bound to MDM2, with Critical Residues F19, W23 and L26 shown. PDB code 1YCR, reproduced using PyMol.

2.1 Small Molecule Inhibitors of the p53 Binding Site

A number of small molecule drugs have been discovered that inhibit the p53-MDM2 interaction. The first were the Nutlin family of *cis*-imidizoline inhibitors (Figure 56), discovered from a small molecule library.[167] The compounds were able to displace p53 from MDM2 within an IC_{50} range of 100-300 nM. As with most pharmaceuticals, the chirality of the *cis*-imidazoline has important consequences for binding, with one enantiomer (Nutlin-3a, **112a**) exhibiting 151-fold greater binding to MDM2 (Figure 57).

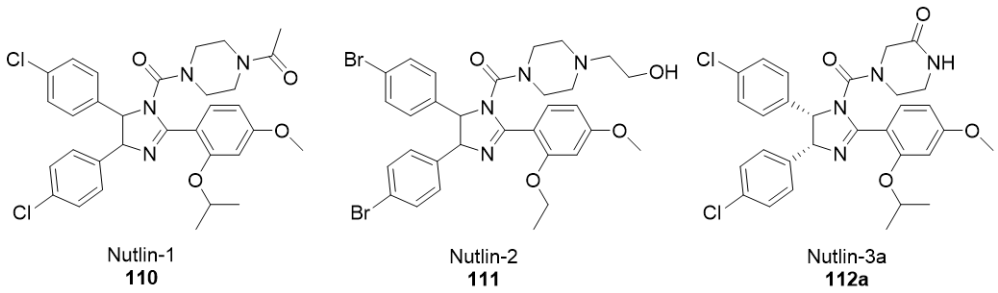

Figure 56- Structure of Nutlin Inhibitors

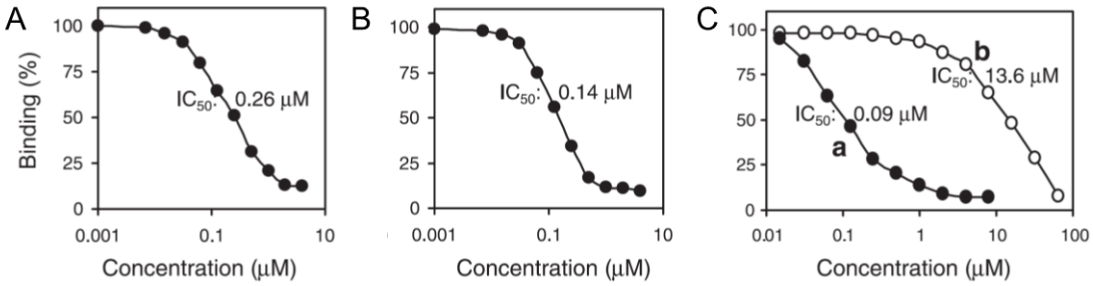

Figure 57- MDM2 IC_{50} values for **A** Nutlin-1 **B** Nutlin-2 **C** Nutlin-3a and Nutlin-3b[167]

The halophenyl groups on the Nutlin inhibitors are projected into the hydrophobic binding pocket of MDM2 in a similar way to the native p53 peptide (Figure 58).[167]

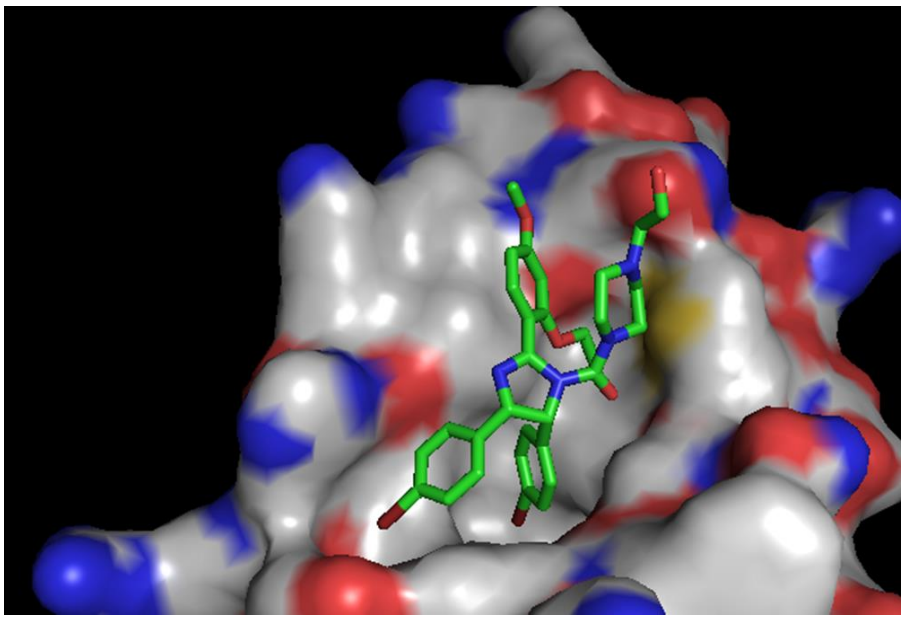

Figure 58- Nutlin-2 bound to MDM2.[168] PDB code 1RV1, reproduced using PyMol.

2.2 Peptidomimetic Inhibitors of the p53 Binding Site

Although small molecules can interact with the hydrophobic pocket of MDM2, they cannot accurately mimic the larger surface area of a true protein-protein interaction. Peptidomimetics are larger molecules that more accurately simulate the larger surface area of a PPI.

2.2.1 Oligoaryl Peptidomimetics

The first report of oligoaryl peptidomimetics came from Orner *et al*.[169] The premise was that *ortho*-side chains on a terphenyl scaffold would accurately mimic the residue side chains of an α-helix (Figure 59). This approach allows a great variety of function to be installed into the side-chains, in part due to the facile nature of the synthesis by sequential cross-coupling reactions.

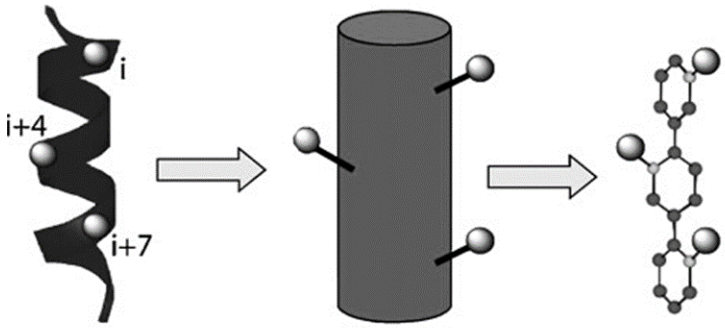

Figure 59- Comparison of α-helix and Terphenyl Peptidomimetics[170]

Employing this strategy to target the p53-hDM2 interaction was first attempted by Yin *et al*.[171] Using a selection of hydrophobic *ortho*-substituted phenyl groups a library of terphenyl inhibitors was synthesised. The most effective inhibitor was found to be **113** (Figure 60), thought to be partly due to the 2-methylnaphthalene side-chain which more accurately mimics the conformation of the critical residue W23 in the p53 N-terminal binding domain.

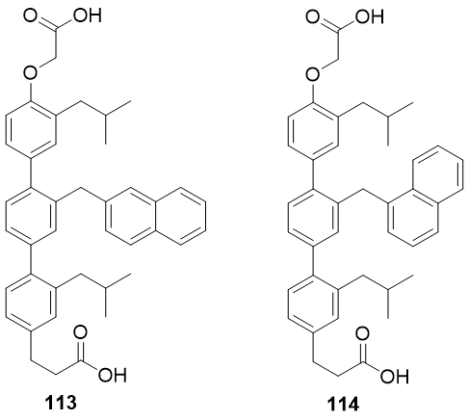

Figure 60- Terphenyl Inhibitors of p53-hDM2

It was shown that these scaffolds can be engineered to selectively bind to protein targets. By changing the orientation of the methylnaphthalene side chain slightly (**114**), the binding to hDM2 is diminished 100-fold. The inhibitors were tested against two other apoptosis regulating proteins with hydrophobic binding pockets, Bcl-2 and Bcl-x_L which both bind the α-helical BH3 domain of the Bak protein.[76,77,172] Again, this

small alteration to the orientation of the naphthalene group increased the selectivity of **114** for Bcl-x_L and Bcl-2 by 22- and 124-fold respectively (Table 14).[171]

Table 14- Inhibitory Concentrations of Terphenyl Scaffolds **113** and **114**

K_i (μM)	hDM2	Bcl-x_L	Bcl-2
113	0.182	2.50	15.0
114	25.7	0.114	0.121

Problems with the terphenyl scaffold are the inherent hydrophobicity and the lack of flexibility within the "backbone". To address this, Plante *et al*.[173] synthesised peptidomimetics based upon on an oligobenzamide backbone (Figure 61). This modification adds an amount of conformational flexibility, increases solubility of the scaffold and still makes synthesis from commercially available starting materials simple.

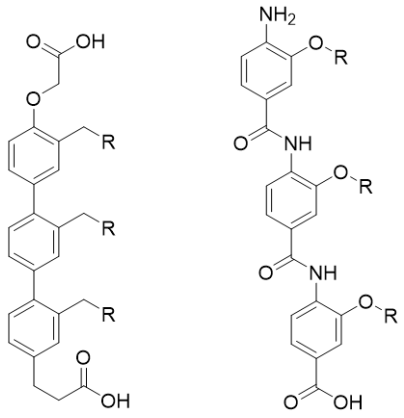

Figure 61- Comparison of Terphenyl and Oligoamide Peptidomimetics

A small library of these new oligobenzamide inhibitors were synthesised and tested for activity against hDM2.[174] Not surprisingly the oligobenzamide inhibitor **115** (Figure 62), which is analogous to the best terphenyl inhibitor **113,** proved the most effective. This was also the case with the *N*-alkylated[175] oligobenzamide **116**, however all of these inhibitors had a similar IC_{50} value to the $^{15\text{-}31}$p53 peptide sequence (Table 15). This suggest that the oligobenzamides would be ineffective therapeutic hDM2 inhibitors.

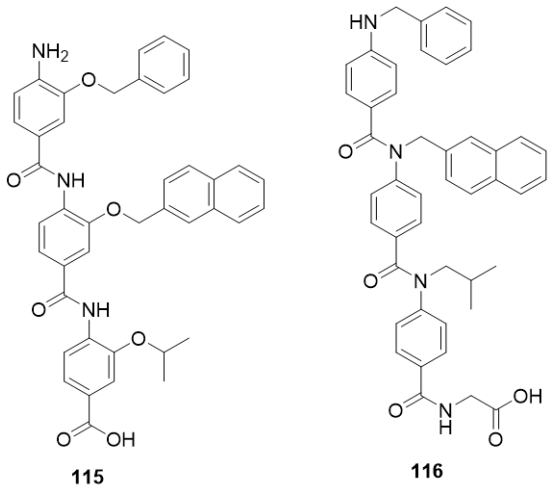

Figure 62- Oligobenzamide Inhibitors of hDM2

Table 15- IC_{50} Values for Oligobenzamides **115**[174] and **116**[175]

	$^{15\text{-}31}$p53	**115**	**116**
IC_{50} (μM)	1.2 ± 0.04	1.0 ± 0.11	2.8 ± 0.8

2.2.2 Peptoids

Peptoids are oligoamides that consist of *N*-substituted glycine monomers (Figure 63). Using amino acids means the peptoid closely mimics a peptide. Additionally, by moving the side-chain from the α-carbon to the nitrogen, the peptoid has increased cell permeability[176] and resistance to proteolysis[177] when compared to the equivalent amino acid sequence.

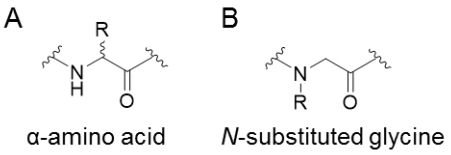

Figure 63- Monomers Present in **A** Peptides **B** Peptoids

Using this strategy, Hara *et al*.[178] attempted to synthesise a peptoid inhibitor of hDM2. It has previously been observed that although the backbone is devoid of chirality,

peptoid oligomers can fold into well-defined secondary structures. In addition it has been shown that incorporation of chiral side chains can induce helicity.[179,180] The peptoidyl helices are more tightly wound compared to an α-helical peptide, having only 3 residues per helical turn as opposed to 3.6. When comparing this to the wild type p53 peptide sequence, the critical ^{19}F and ^{23}W residues are in the (*i*,*i*+4) positions with respect to each other, which would not be on the same face of the peptoid helix. This sequence incongruity was remedied by reducing the number of residues by one between these positions within the peptoids. The angle at which the side chains of the *N*-substituted glycine monomers protrude from the peptoidyl helix is slightly different also. To accommodate for this, an extra methylene group was added to the side chains of the residues corresponding to the binding residues ^{19}F and ^{23}W, which when compared to the native p53 sequence *in silico*, appeared to reproduce the necessary binding conformation (Figure 64).

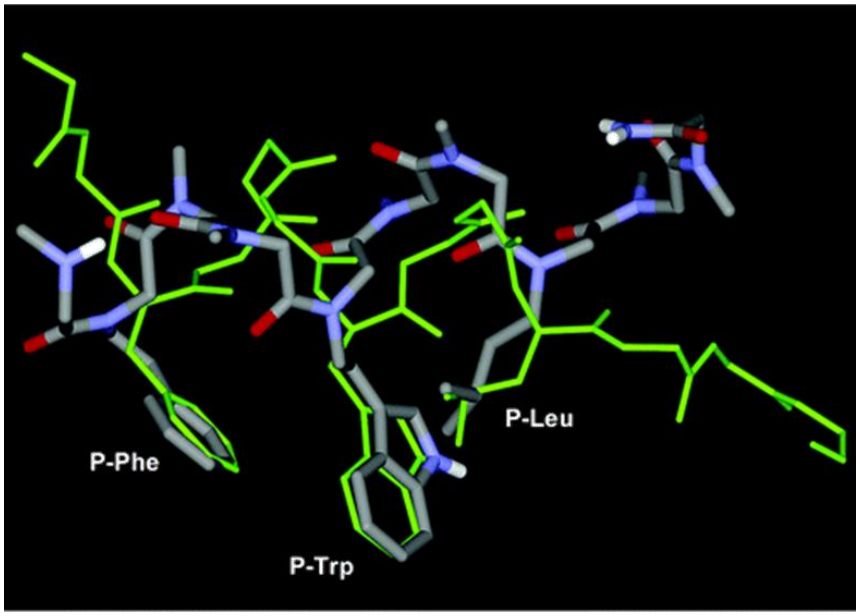

Figure 64- Energy Minimised Conformation of a Peptoid with WTp53 Sequence Overlaid (Green). Only Critical Binding Residues are Highlighted.[178]

During the optimisation of the peptoid **117** (Figure 65) the equivalent critical residues were replaced in a "sarcosine (*N*-methyl glycine) scan", analogous to an alanine scan in peptides, to confirm that the peptoid was binding to hDM2 in a similar way to the

wild type p53 sequence. Systematic removal of the residues with critical side chains saw an increase in the IC_{50} value of the peptoid (**118**-**120** vs **117**, Table 16).

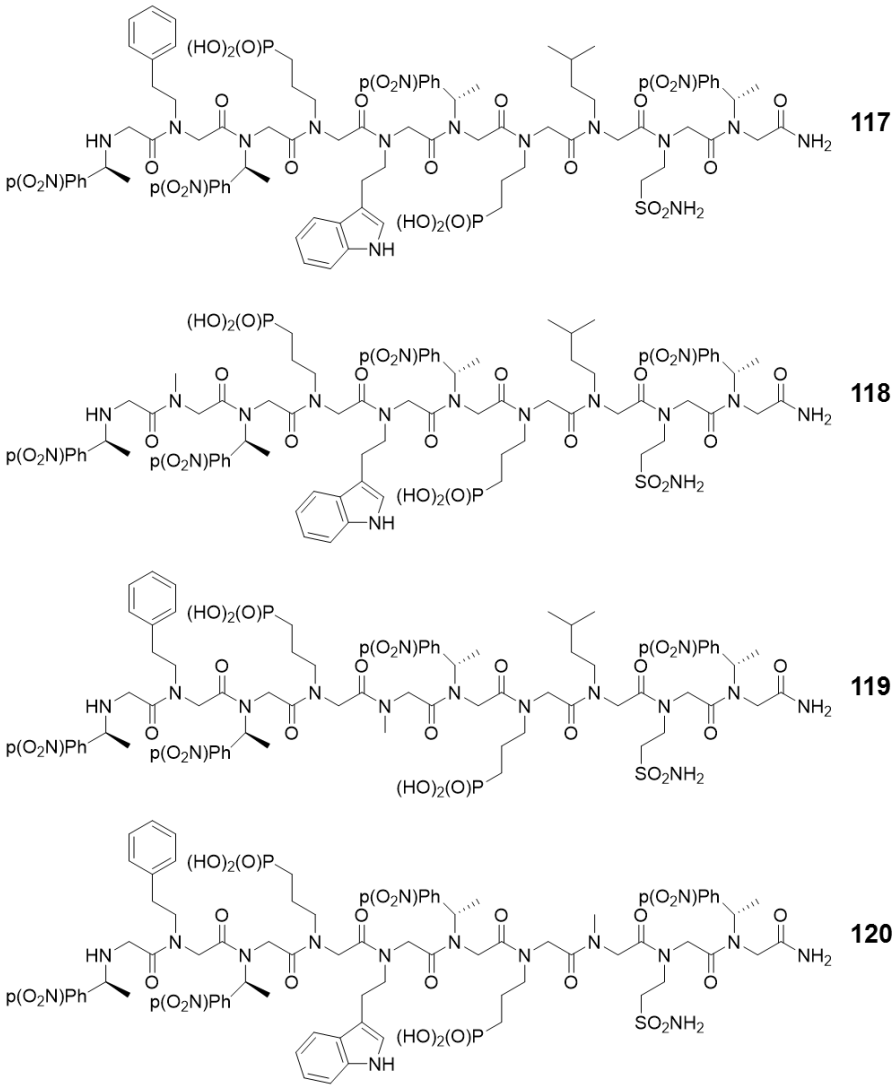

Figure 65- Structure of Lead (**117**) and Sarcosine Scan Peptoids from Hara *et al*.[178]

Table 16- IC_{50} Values of Peptoids **117**-**120** to hDM2

Sequence	**117**	**118**	**119**	**120**
IC_{50} (μM)	17.8	59.8	28.3	25.3

Interestingly, although removing chirality in the side chains (Figure 66) induced a loss of helicity (determined by circular dichroism), the IC_{50} value of the sequence was

similar to the chiral sequence (**121** vs **117**, Table 17). This suggests that the peptoids can fold into non-helical conformations that are still efficacious, or possibly that the peptoids folds into a helical conformer upon binding to hDM2.[178] The addition of a 6-chloro group on the tryptophan residue has been shown to increase binding to MDM2 and MDMX (discussed in 2.3.1.1).[181,182] Incorporation of this modification into the peptoids **122** and **123** saw a further decrease in IC_{50}.

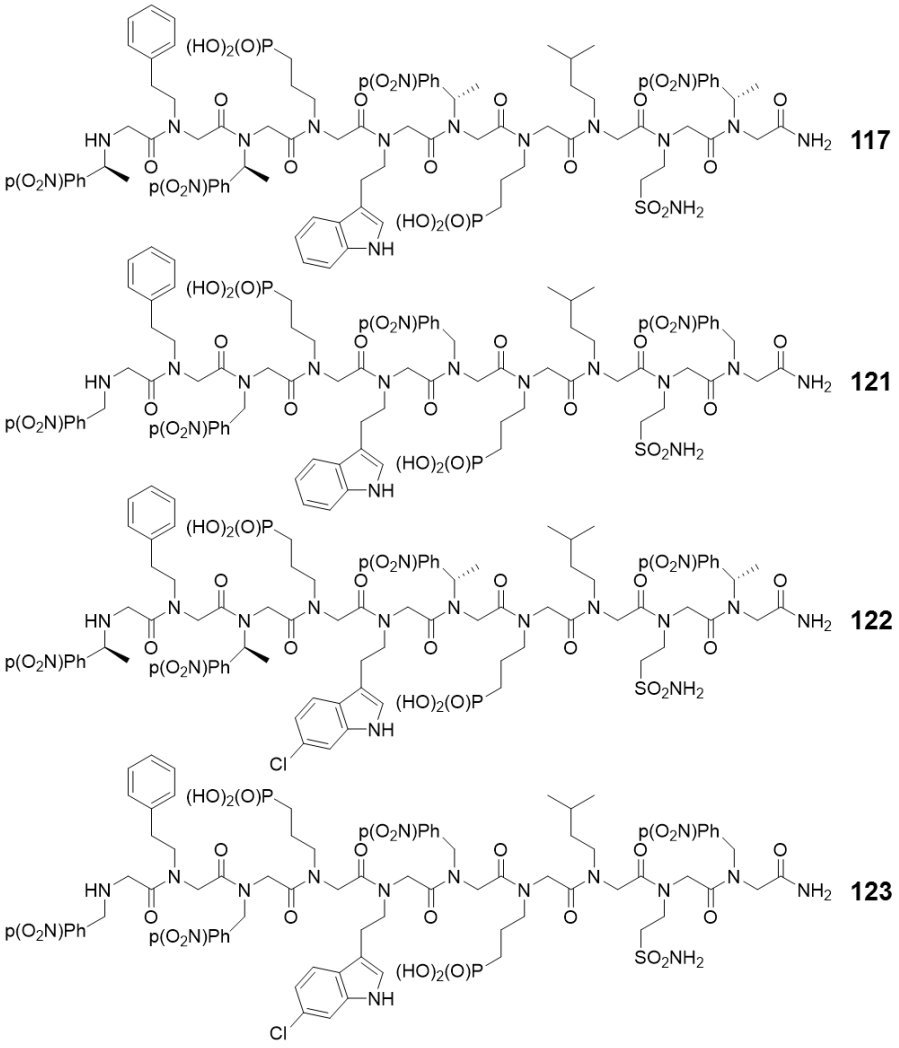

Figure 66- Chiral and Achiral Peptoid Inhibitors of MDM2 from Hara *et al*.[178]

Table 17- IC_{50} Values of Peptoids **117** and **121**-**123** to hDM2

Sequence	**117**	**121**	**122**	**123**
IC_{50} (μM)	17.8	18.2	9.9	6.6

2.3 Peptide Inhibitors of the p53 Binding Site

One way to inhibit a protein-protein interaction would be to synthesise the peptide sequence responsible for binding. The advantages of using peptides as inhibitors of PPIs include the more accurate mimicry of the protein inhibitor, as well as the greater surface contact and the conformational flexibility afforded from a larger molecule. Additionally, from a therapeutic standpoint, the peptides would be digested into non-toxic metabolites.

2.3.1 Phage Display Peptides

A number of peptide inhibitors of the p53 MDM2 interaction have been discovered by phage display. Phage display is a technique that encodes a peptide or protein of interest to the surface of a bacteriophage, a virus that infects bacteria. The genetic information that encodes this protein is contained within the phage. A library of these phages are used to target a specific protein that has been immobilised (Figure 67). A phage that displays a peptide that interacts with the immobilised target will also become immobilised upon binding, those phages that do not bind are washed away. The bound phages are then eluted from the immobilised protein, and are used to infect bacteria to amplify binding peptides or proteins. After repeating these steps a number of times (panning) phages will be enriched with high affinity binding partners, which can be identified after sequencing.

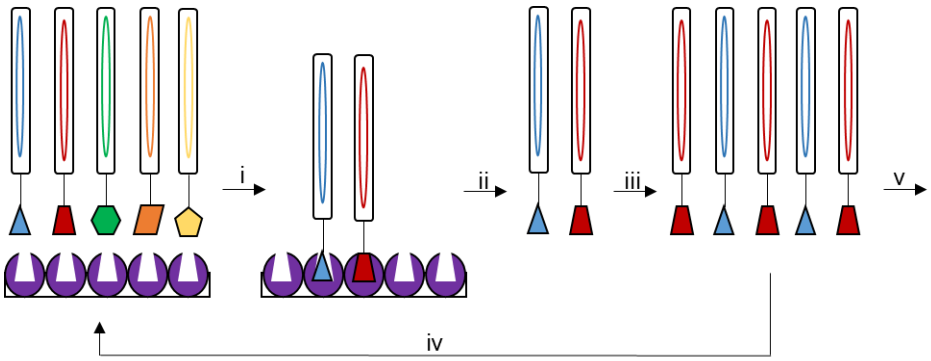

Figure 67- Phage Display: Bacteriophages are exposed to a bound target (purple). The active phages bind to the target and the rest are washed away (i); The active phages are eluted from the bound target (ii); The phages are amplified (iii); The steps are repeated (iv) or the phages are analysed (v).

2.3.1.1 **Active Peptide - AP**

Following a screening of a phage display library and discovery of a high affinity 12-mer peptide Ac-MPRFMDYWEGLN-NH_2 **124**,[183] Garcia-Echeverria *et al.*[181] synthesised truncated versions, between 6-11 residues, to discover the minimum sequence length for hDM2 inhibition. It was found that all of the 6- and 7-mer peptides were poor inhibitors of hDM2, however an 8-mer peptide **125** (Figure 68) was found to have comparable binding to the $^{16\text{-}27}$p53 native sequence, and so was used a lead for further optimisation.

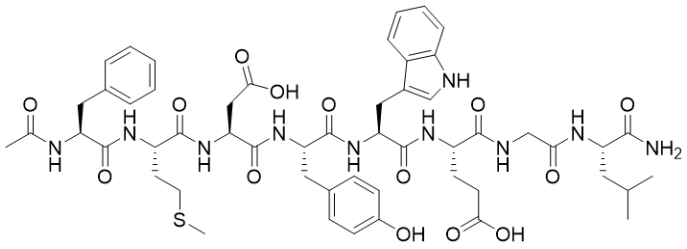

Figure 68- 8-mer Lead Peptide **125**

Replacing residues D3 and G7, which are on the opposite helical face to the critical binding residues, with helix-favouring α,α-disubstituted residues α-aminoisobutyric acid (Aib) and 1-amino-cyclopropane carboxylic acid (Ac_3c)[69] (Figure 69) increased the affinity of the 8-mer **125** for hDM2 4-fold, and constricted the peptide into a more

helical binding conformer (**126**, Table 18) as observed by NMR. After exploring a model of peptide **126** bound to hDM2, it was found that, although replacement of the tyrosine and tryptophan residues would be deleterious to binding,[184] they could be modified to improve the affinity of the peptide. It was observed that the phenolic OH of the tyrosine residue was close to the side chain of K94 in hDM2. Swapping the tyrosine residue for a similar 4-phosphonomethylphenylalanine (Pmp) would allow a salt bridge interaction to be established. This substitution produced a 7-fold increase in binding affinity of the peptide (**126** vs **127**).[181]

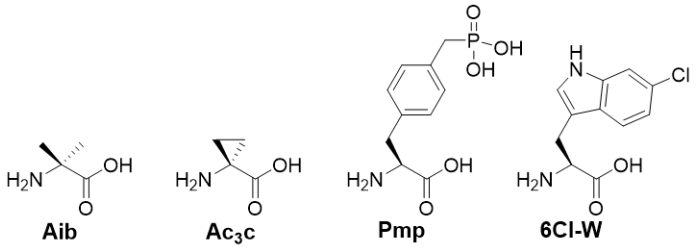

Figure 69- Monomers used in the AP Peptide

Table 18- Peptide Library from Garcia-Echeverria *et al*.[181]

Sequence					IC_{50} (nM)
Ac-QETFSDLWKLLP-NH_2				$^{16-27}$p53	8673 ± 164
Ac-MPRFMDYWEGLN-NH_2				**124**	313 ± 10
Ac-FM**$X_1X_2X_3$**E**X_4**L-NH_2					
X_1	X_2	X_3	X_4		
E	Y	W	G	**125**	8949 ± 588
Aib	Y	W	Ac_3c	**126**	2210 ± 346
Aib	Pmp	W	Ac_3c	**127**	314 ± 88 (313[a])
Aib	Pmp	6Me-W	Ac_3c	**128**	10 ± 1 (25[a])
Aib	Pmp	5Me-W	Ac_3c	**129**	235[a]
Aib	Pmp	6F-W	Ac_3c	**130**	14 ± 1
Aib	Pmp	6Cl-W	Ac_3c	**131**	5 ± 1 (0.74[b])
Aib	Pmp	D-6Cl-W	Ac_3c	**132**	138 000 ± 27000
Aib	F	6Cl-W	Ac_3c	**133**	1.5[b]

a Data From Separate Assay; b Data from Sakurai et al.;

It was also observed from the binding model and parallel computational studies[185] that there was a small gap in the tryptophan hydrophobic pocket (Figure 70). Altering the tryptophan residue, by substitution at the 6-position of the indole resulted in peptides with significantly increased binding to hDM2 (Figure 71), with the 6-Cl substitution giving rise to the lowest IC_{50} value (**131**). Substitution at the 5-position did not result in as great a change in the binding affinity (**127** vs **129**).[181] Continuing the study, Chene *et al*.[186] demonstrated that AP was active *in vitro*, though only in cells expressing p53. Administration of the peptide to cells overexpressing hDM2 resulted in apoptosis, and so AP **131** was shown to be the first inhibitor of the p53 hDM2 interaction in cells. Interestingly, following resolution of the crystal structure of peptide **131** by Sakurai *et al*.,[187] it was discovered that the Pmp residue does not form a salt bridge with K94 in hDM2, but in fact projects into the solvent, forming hydrogen bonds with surface-bound water molecules. Replacing the Pmp residue with a Phe resulted in only a 2-fold decrease in binding affinity (**131** vs **133**), confirming the hydrogen bonding has little effect on the affinity of the peptide, and that hydrophobic contact is the most important stabilising factor.[187]

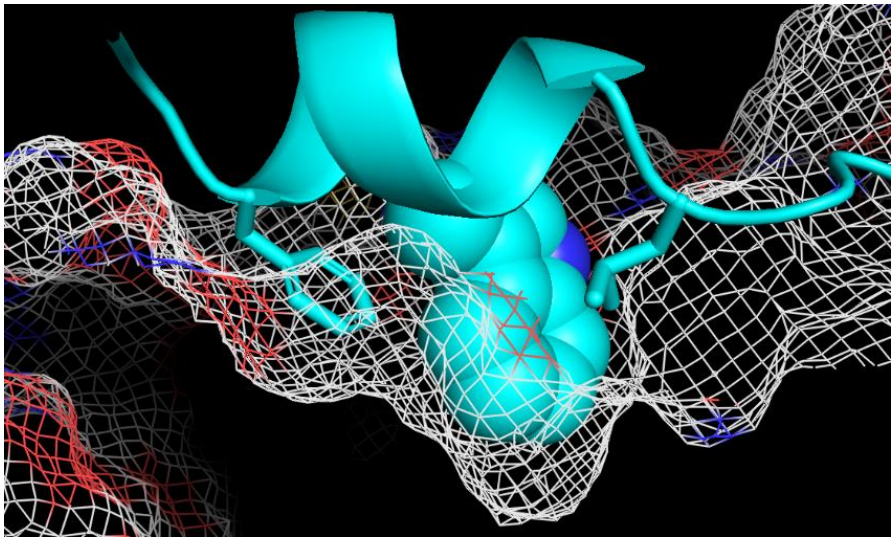

Figure 70- p53 Peptide bound to MDM2, showing the hydrophobic space available below W23. PDB code 1YCR, reproduced using PyMol.

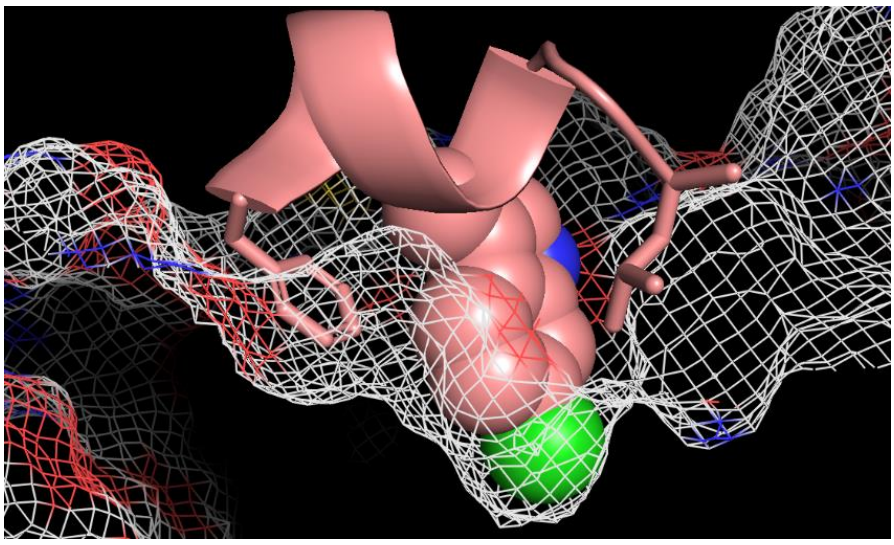

Figure 71- AP Peptide **131** bound to hDM2. PDB code 2GV2, reproduced using PyMol.

2.3.1.2 **Peptide Dual Inhibitor - pDI**

One of the first peptidyl inhibitors to target the homologous MDMX protein in addition to MDM2 using phage display was from Hu *et al*.[188] As MDMX only shares 50% homology in the p53 N-terminal binding domain with MDM2, a number of small molecule inhibitors, including the Nutlins, and terphenyl type peptidomimetics are ineffective at inhibiting MDMX.[189–191] There is evidence that suggests that MDMX inactivates p53 by sequestering the protein, as opposed to acting as a E3 ligase, although the heterodimerisation of MDM2 and MDMX has been shown to accelerate ubiquitination of p53.[192,193] After phage panning, it became evident that the immobilised MDM-homologues had a preference for the sequence LTFEHYWAQLTS, termed pDI (**134**, Table 19**)**. In an ELSIA assay, pDI showed IC_{50} values of 10 and 100 nM for MDM2 and MDMX respectively (Table 19). These inhibitory concentrations are 60- and 300- fold lower than values given for $^{16\text{-}27}$p53 and Nutlin-3a (**112a**) inhibition of MDM2 and 275-fold lower for $^{16\text{-}27}$p53 to MDMX. Replacing the key hydrophobic residues F, W and L for alanine (p3A, **135**) resulted in a complete loss of inhibition of both proteins. The ~10-fold difference in IC_{50} values between MDM2 and MDMX for $^{16\text{-}27}$p53 and **134** further validates the proposed mechanism of MDMX inhibition of p53 by sequestration.

Table 19- Comparison of pDI Peptide to Known Inhibitors of MDM2 and MDMX

Sequence		IC_{50} (μM)	
		MDM2	MDMX
NH_2-QETFSDLWKLLP-CO_2H	p53[a]	3.00	27.50
Nutlin 3a	**112a**	0.60	-
NH_2-LTFEHYWAQLTS-CO_2H	pDI **134**	0.01	0.10
NH_2-LTAEHYAAQATS-CO_2H	p3A **135**	-	-

a $^{16\text{-}27}p53$;

Using pDI as a starting point, Phan *et al*.[194] attempted to design a peptide with improved binding properties. Replacing the tyrosine residue for tryptophan, another hydrophobic aromatic amino acid, improved the binding to MDMX approximately 2-fold (pDI6W, XX, Table 20). From the crystal structures of pDI and pDI6W bound to both MDM2 and MDMX, it was observed that a large number of co-ordinated water molecules were conserved, with both the phenolic hydroxyl and indolic amine groups contributing to hydrogen bonding at the 6th residue position. It is argued that a greater contributor to the increased binding was the additional number of hydrophobic van der Waals interactions from the tryptophan residue (Y6 vs W6). This is in agreement with the attenuation or removal of activity of the peptide with more polar residues asparagine or serine (**137**, **138**). The replacement of L1 for glutamic acid to increase solubility (L1E, **139**) resulted in an additional 2-fold decrease in binding from pDI6W. Replacement of the alanine residue with a serine (A8S, **140**), to form an intrapeptide hydrogen bond, lead to a decrease in IC_{50} value in comparison to both pDI and pDI6W. Inhibition of the MDM-homologues also increased upon the substitution of the C-terminal threonine for leucine (T11L, **141**), to increase hydrophobic interactions. Incorporation of all these advantageous mutations, (L1E, Y6W, A8S, T11L) culminated in peptide pDIQ (peptide dual inhibitor quadruple mutant, **142**), which exhibits a 55- and 5-fold decrease in IC_{50} of MDM2 and MDMX with respect to $p53^{17\text{-}29}$ and pDI respectively.[194]

Table 20- Peptide Library of Mutations from Phan *et al*.[194]

Sequence		IC_{50} (nM)	
		MDM2	MDMX
NH_2-ETFSDLWKLLPE-CO_2H	p53[a]	2000	6000
NH_2-LTFEHYWAQLTS-CO_2H	pDI **134**	44	550
NH_2-LTFEHWWAQLTS-CO_2H	pDI6W **136**	36	250
NH_2-LTFEHNWAQLTS-CO_2H	**137**	400	4000
NH_2-LTFEHSWAQLTS-CO_2H	**138**	-	-
NH_2-ETFEHWWAQLTS-CO_2H	**139**	20	200
NH_2-LTFEHWWSQLTS-CO_2H	**140**	24	180
NH_2-LTFEHWWAQLLS-CO_2H	**141**	20	140
NH_2-ETFEHWWSQLLS-CO_2H	pDIQ **142**	8	110

a $^{17\text{-}28}$*p53;*

2.3.1.3 **p53-MDM2/MDMX Inhibitor – PMI**

Around the same time as pDI **134**, the peptide sequence TSFAEYWNLLSP, termed p53-MDM2/MDMX Inhibitor (PMI **143**) was discovered by phage display by Pagzier *et al*.[195] The sequence was compared against two p53 peptides, $^{17\text{-}28}$p53 and the extended $^{15\text{-}29}$p53 sequence SQETFSDLWKLLPEN using isothermal titration calorimetry (ITC). It was found that PMI bound to MDM2 and MDMX with K_d values of 3.3 and 8.9 nM respectively (Table 21). This corresponds to an approximately 20-fold increase when compared to $^{15\text{-}29}$p53 binding to MDM2 and MDMX. When compared to the $^{17\text{-}28}$p53 sequence, which consists of the same number of residues, PMI displayed 89- and 43-fold greater binding affinity for MDM2 and MDMX respectively.

Table 21- Comparison of PMI to p53 Sequences

Sequence		K_d (nM)	
		MDM2	MDMX
NH_2-SQETFSDLWKLLPEN-CO_2H	p53[a]	61.3	202
NH_2-ETFSDLWKLLPE-CO_2H	p53[b]	295	386
NH_2-TSFAEYWNLLSP-CO_2H	PMI **134**	3.3	8.9

a $^{15\text{-}29}$*p53; b* $^{17\text{-}28}$*p53;*

The increase in binding affinity of PMI compared to the p53 peptides is thought to come from an increased number of α-helix stabilising hydrogen bonds. It has previously been demonstrated that the P27S mutation of p53 increases the helicity of the sequence and, consequently, the binding affinity for MDM2 50-fold.[196,197] This substitution correlates to S11 in PMI. In addition, the SXXE sequence is typical of an N-terminal expanded capping box, a common helical motif in peptides and proteins.[198–201] This arrangement is present in PMI (S2-E5, Figure 72) but absent in the wild type sequence.

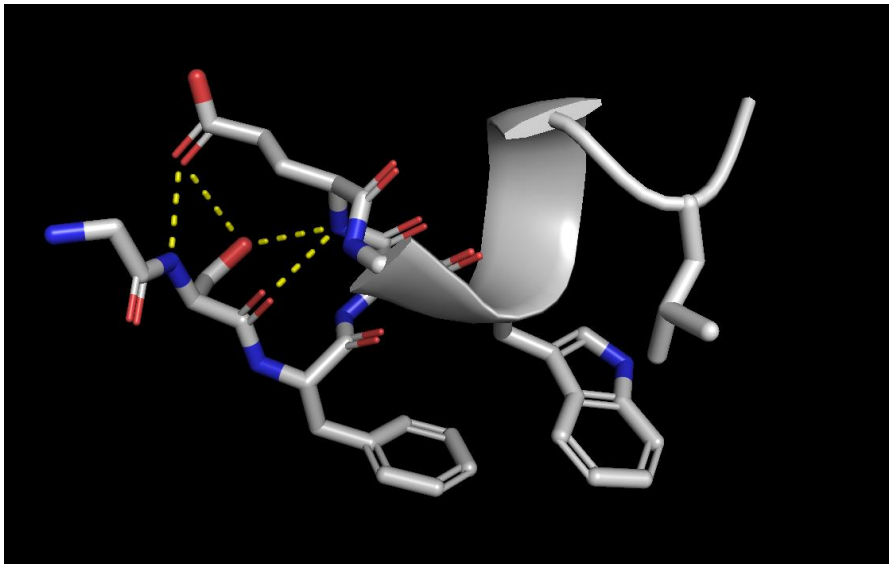

Figure 72- SXXE N-Terminal Capping Box Motif in PMI. PDB code 3EQS, reproduced using PyMol.

The PMI peptide binding to MDM2 and MDMX was verified by a surface plasmon resonance (SPR) competition assay. In addition to the p53 peptides, the binding of

PMI was compared to Nutlin-3 and pDI. Again, PMI exhibited the greatest binding affinity for both MDM2 and MDMX (Table 22).

Table 22- Comparison of PMI to Known Inhibitors of MDM2

Sequence		K_d (nM)	
		MDM2	MDMX
NH_2-SQETFSDLWKLLPEN-CO_2H	p53[a]	140 ± 5	270 ± 9
NH_2-ETFSDLWKLLPE-CO_2H	p53[b]	452 ± 11	646 ± 26
Nutlin 3[c]	**112**	263 ± 60	-
NH_2-LTFEHYWAQLTS-CO_2H	pDI **134**	19.6 ± 1.4	77.0 ± 8.7
NH_2-TSFAEYWNLLSP-CO_2H	PMI **143**	3.36 ± 0.75	4.15 ± 1.47

a $^{15\text{-}29}$p53; b $^{17\text{-}28}$p53; c racemate;

To try to understand and increase the affinity further, Li *et al.*[202] conducted alanine scans on the PMI peptide and the equivalent $^{17\text{-}28}$p53 sequence (Table 23).

Table 23- Alanine Scan of $^{17\text{-}28}$p53 Sequence

Sequence		K_d (M)		ΔΔG (kcal/mol)[a]	
		MDM2	MDMX	MDM2	MDMX
NH_2-ETFSDLWKLLPE-CO_2H	p53[b]	$4.4 \pm 0.4 \times 10^{-7}$	$6.4 \pm 0.5 \times 10^{-7}$	0.00	0.00
NH_2-**A**TFSDLWKLLPE-CO_2H	E17A	$5.6 \pm 0.2 \times 10^{-7}$	$6.8 \pm 0.1 \times 10^{-7}$	0.14	0.03
NH_2-E**A**FSDLWKLLPE-CO_2H	T18A	$1.2 \pm 0.1 \times 10^{-6}$	$2.3 \pm 0.1 \times 10^{-6}$	0.58	0.75
NH_2-ET**A**SDLWKLLPE-CO_2H	F19A	-	-	-	-
NH_2-ETF**A**DLWKLLPE-CO_2H	S20A	$2.1 \pm 0.1 \times 10^{-7}$	$3.1 \pm 0.1 \times 10^{-7}$	-0.43	-0.43
NH_2-ETFS**A**LWKLLPE-CO_2H	D21A	$8.3 \pm 0.2 \times 10^{-7}$	$1.1 \pm 0.1 \times 10^{-6}$	0.37	0.32
NH_2-ETFSD**A**WKLLPE-CO_2H	L22A	$5.0 \pm 0.4 \times 10^{-6}$	$9.0 \pm 0.8 \times 10^{-6}$	1.41	1.54
NH_2-ETFSDL**A**KLLPE-CO_2H	W23A	-	-	-	-
NH_2-ETFSDLW**A**LLPE-CO_2H	K24A	$2.3 \pm 0.2 \times 10^{-7}$	$4.9 \pm 0.4 \times 10^{-7}$	-0.39	-0.15
NH_2-ETFSDLWK**A**LPE-CO_2H	L25A	$7.3 \pm 0.1 \times 10^{-7}$	$6.9 \pm 0.6 \times 10^{-7}$	0.30	0.04
NH_2-ETFSDLWKL**A**PE-CO_2H	L26A	$2.7 \pm 0.1 \times 10^{-5}$	$6.6 \pm 0.1 \times 10^{-5}$	2.39	2.00
NH_2-ETFSDLWKLL**A**E-CO_2H	P27A	$5.1 \pm 0.3 \times 10^{-8}$	$2.4 \pm 0.2 \times 10^{-7}$	-1.26	-0.58
NH_2-ETFSDLWKLLP**A**-CO_2H	E28A	$2.4 \pm 0.2 \times 10^{-7}$	$3.3 \pm 0.1 \times 10^{-7}$	-0.36	-0.39
NH_2-FSDLWKLL-CO_2H	p53[c]	$3.5 \pm 0.4 \times 10^{-5}$	$1.3 \pm 0.2 \times 10^{-4}$	2.55	3.07

a relative to $^{17\text{-}28}$p53; b $^{17\text{-}28}$p53; c $^{19\text{-}26}$p53;

In agreement with previous work,[196,197] the P27A mutation in the $^{17-28}$p53 sequence increases the binding affinity of the peptide 10- and 3-fold for MDM2 and MDMX respectively. The difference in binding between the $^{17-28}$p53 P27A and P27S for MDM2 (10- and 50-fold in comparison to the native $^{17-28}$p53 sequence) gives additional weight to the proposed hydrogen bonding stabilisation imparted by serine. The L22A substituted peptide showed an increase in K_d, which as previously discussed,[194] is due to decreased hydrophobic contact at this position. Similarly, T18A and D21A mutations decrease the affinity of the $^{17-28}$p53 sequence. This is thought to be due to the disruption of hydrogen bonding analogous to the SXXE capping box motif.[198–201] The octapeptide $^{19-26}$p53 was still found to have binding affinity to both MDM-homologues, which is in agreement with previous work.[181,186,187,203]

Table 24- Alanine Scan of PMI Peptide **143**

Sequence		K_d (M)		ΔΔG (kcal/mol)[a]	
		MDM2	MDMX	MDM2	MDMX
NH_2-TSFAEYWNLLSP-CO_2H	PMI **143**	$3.2 \pm 1.1 \times 10^{-9}$	$8.5 \pm 1.7 \times 10^{-9}$	0.00	0.00
NH_2-**A**SFAEYWNLLSP-CO_2H	**144**	$6.2 \pm 0.1 \times 10^{-9}$	$1.6 \pm 0.3 \times 10^{-8}$	0.39	0.35
NH_2-T**A**FAEYWNLLSP-CO_2H	**145**	$2.7 \pm 0.4 \times 10^{-8}$	$3.7 \pm 0.4 \times 10^{-8}$	1.24	0.85
NH_2-TS**A**AEYWNLLSP-CO_2H	**146**	$3.8 \pm 0.2 \times 10^{-5}$	$1.2 \pm 0.1 \times 10^{-4}$	5.46	5.57
NH_2-TSF**A**EYWNLLSP-CO_2H	PMI **143**	$3.2 \pm 1.1 \times 10^{-9}$	$8.5 \pm 1.7 \times 10^{-9}$	0.00	0.00
NH_2-TSFA**A**YWNLLSP-CO_2H	**147**	$2.1 \pm 0.1 \times 10^{-8}$	$6.7 \pm 0.8 \times 10^{-8}$	1.10	1.20
NH_2-TSFAE**A**WNLLSP-CO_2H	**148**	$6.1 \pm 0.7 \times 10^{-7}$	$6.7 \pm 0.8 \times 10^{-7}$	3.06	2.55
NH_2-TSFAEY**A**NLLSP-CO_2H	**149**	$1.6 \pm 0.3 \times 10^{-4}$	$2.3 \pm 0.1 \times 10^{-4}$	6.31	5.94
NH_2-TSFAEYW**A**LLSP-CO_2H	**150**	$4.9 \pm 2.1 \times 10^{-10}$	$2.4 \pm 0.6 \times 10^{-9}$	-1.10	-0.74
NH_2-TSFAEYWN**A**LSP-CO_2H	**151**	$2.4 \pm 0.5 \times 10^{-9}$	$9.0 \pm 2.1 \times 10^{-9}$	-0.17	0.03
NH_2-TSFAEYWNL**A**SP-CO_2H	**152**	$8.9 \pm 0.1 \times 10^{-7}$	$4.3 \pm 0.4 \times 10^{-7}$	3.28	2.28
NH_2-TSFAEYWNLL**A**P-CO_2H	**153**	$3.9 \pm 0.3 \times 10^{-9}$	$1.1 \pm 0.2 \times 10^{-8}$	0.12	0.17
NH_2-TSFAEYWNLLS**A**-CO_2H	**154**	$2.1 \pm 0.5 \times 10^{-9}$	$1.4 \pm 0.3 \times 10^{-8}$	-0.25	0.31
NH_2-FAEYWNLL-CO_2H	**155**	$8.9 \pm 0.7 \times 10^{-6}$	$4.4 \pm 0.5 \times 10^{-5}$	4.62	4.98

a relative to PMI;

After performing the alanine scan on PMI (Table 24), the only significantly deleterious residue detected was from the N8A substitution (**150**). The crystal structures of PMI shows that the N8 residue does not interact with MDM2 or MDMX. By replacing it with alanine, the binding affinity increases 6.5- and 3.5-fold for MDM2 and MDMX

respectively. This is thought to be due to the properties of the asparagine residue itself, which is one of the least commonly found residues in α-helices in globular proteins, and has the poorest helical propensity of any of the proteinogenic residues.[91] Interestingly, the substitution does not create any new energetically significant intermolecular interactions, but stabilises hydrogen bonding in the amide backbone. The truncated octapeptide **155**, corresponding to the $^{19\text{-}26}$p53 peptide, showed a 3-fold greater binding affinity by comparison. This difference appears to be solely due to the favourable L22-Y6 mutation. To date, the PMI N8A peptide has the strongest binding affinities for both MDM-homologues known.[202]

2.3.2 Stapled Peptides

Although peptides can display high binding affinity for MDM2 and its homologues *in vitro*, peptides are not cell penetrable and are easily digested by enzymes making them therapeutically unviable. Stapling, as discussed in Chapter 1, constrains peptides into conformations that replicate the natural secondary structure of the protein they are derived from. This method has been shown to increase bioavailability and efficacy of synthetic peptides.

2.3.2.1 **SAH-p53-8**

The first stapled peptide targeting the p53-hDM2 interaction from Bernal *et al*.[155] was based on the wild type $^{14\text{-}29}$p53 sequence. To design stapled analogues of the $^{14\text{-}29}$p53 sequence, the non-natural amino acids **33** and **156** (Figure 73) were used to replace non-critical residues at a number of positions (**157c** to **160c**, Table 25). The olefinic monomers were spaced 7 residues apart, equivalent to 2 helical turns, ensuring the ring-closing metathesis macrocyclisation between the side chains occurs on the same face of the α-helix.

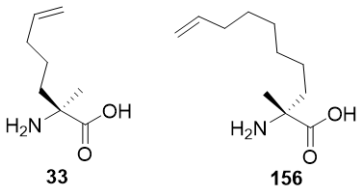

Figure 73- Monomers used by Bernal *et al*.[155]

Table 25- Peptide Library from Bernal *et al*.[155]

Sequence		% Helicity	K_d (nM)	Charge[a]	C. Entry[b]	C. Death[c]
Ac-LSQETFSDLWKLLPEN-NH_2	p53[d]	11	410± 19	-2	-	-
Ac-LSQETFSD**X_1**WKLLPE**X_2**-NH_2	**157c**	25	100 ± 8	-2	-	-
Ac-LSQE**X_1**FSDLWK**X_2**LPEN-NH_2	**158c**	10	400 ± 50	-2	-	-
Ac-LSQ**X_1**TFSDLW**X_2**LLPEN-NH_2	**159c**	12	1200 ± 89	-2	-	-
Ac-LSQETF**X_1**DLWKLL**X_2**EN-NH_2	**160c**	59	0.92 ± 0.11	-2	-	-
Ac-LSQETF**X_1**NLWKLL**X_2**QN-NH_2	**161c**	20	0.82 ± 0.05	0	+	-
Ac-LSQQTF**X_1**NLWRLL**X_2**QN-NH_2	**162c**	14	56 ± 11	1	+	-
Ac-QSQQTF**X_1**NLWKLL**X_2**QN-NH_2	**163c**	36	50 ± 10	1	+	-
Ac-QSQQTF**X_1**NLWRLL**X_2**QN-NH_2	**164c**	85	55 ± 11	1	+	+
Ac-QSQQTA**X_1**NLWRLL**X_2**QN-NH_2	**165c**	39	> 4000	1	+	-
Ac-QSQQTF**X_1**NLWRLL**X_2**QN-NH_2	**164u**	36	100 ± 10	1	+	-

a Charge of peptide at pH 7.4; b Cell Permeability; c Cell Death; d $^{14\text{-}29}$*p53;* ***X_1 156*** *;* ***X_2 33*** *;*

Examining the relative helicity of the peptides by circular dichroism revealed that, after replacing residues for the olefinic monomers and subjecting the peptides to cross-metathesis conditions, the S20 and P27 substitutions (**160c**) induced the greatest helicity. This is in further agreement with other work highlighting the detrimental helix-breaking effect of P27.[196,197,202] This swap also increased the affinity of the peptide almost 3 orders of magnitude and improved the proteolytic stability with respect to the native sequence. When cells were incubated with the peptides however, there was no evidence of cell penetration. This is thought to be due to the negative charge of the peptide at neutral pH, a quality uncommon in potent cell-penetrating peptides.[104,204,205] By replacing the aspartic and glutamic acid residues with the equivalent amide residues asparagine and glutamine (**161c**, **162c**), the peptide charge, and therefore permeability, was modulated favourably. Although the peptides could enter the cells, the apoptotic pathway was not activated. By mutating residues known

to contribute to the degradation of p53 (L14 and K24)[206,207] the peptide **164c** was shown to affect cell viability by restoring the pro-apoptotic p53 pathway by inhibition of hDM2 and hDMX.[155,208]

The peptide **164c** was crystallised with MDM2 by Baek *et al*.[209] and two important binding aspects were revealed. The staple was shown to constrain the peptide such that the extended helical section is extended and now contains L26. This is not observed in any of the unconstrained peptides, which have higher affinity for MDM2, suggesting a degree of flexibility would be more favourable. In addition, the staple was shown to interact favourably with the surface of MDM2, contributing approximately 10% of the contact area of **164c**. It is also thought to shield the tryptophan hydrogen bond to MDM2 from competing solvent interactions (Figure 74).

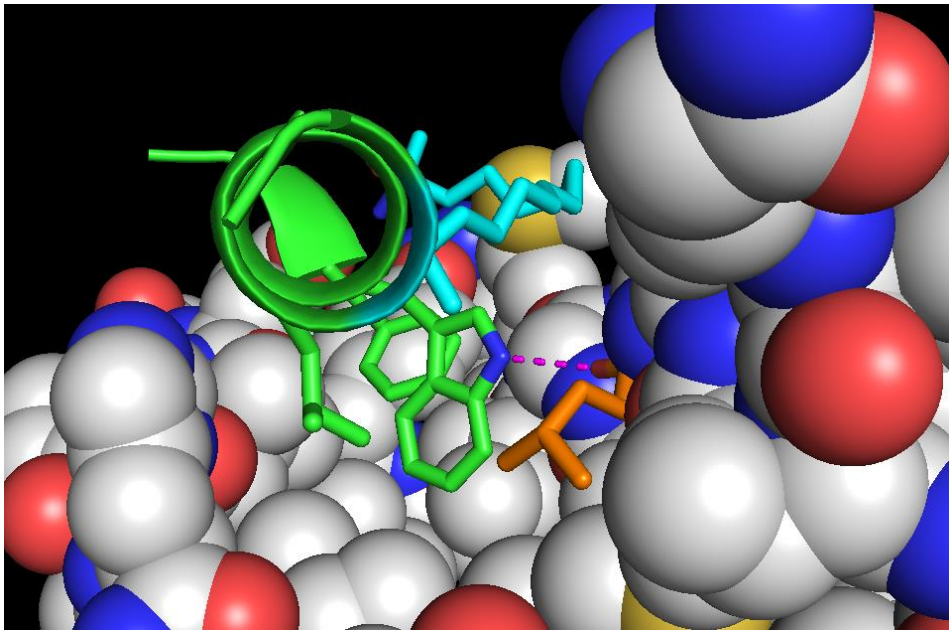

Figure 74- SAH-p53-8 (**164c**, green) bound to MDM2. The hydrocarbon staple (cyan) protecting the W23 indole hydrogen bond (magenta) to Leu54 (orange). PDB code 3V3B, reproduced using PyMol.

2.3.2.2 **ATSP-7041**

With the SAH-p53-8 peptide **164c** as a foundation, Chang *et al*.[210] attempted to refine a stapled version of the pDI peptide **134**. Using the same olefin stapling monomers **33** and **156** (Figure 75) in the optimal position determined by Bernal *et al*.[155] the stapled pDI **167c** exhibited an almost 15- and 3-fold increase in binding affinity to MDM2 and MDMX respectively (Table 26).

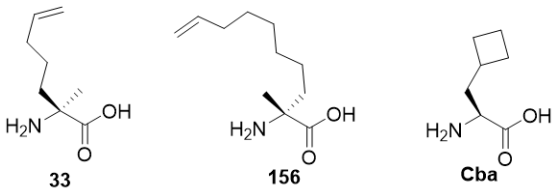

Figure 75- Monomers used by Chang *et al*.[210]

Table 26- Peptide Library from Chang *et al*.[210]

Sequence		K_i (nM)	
		MDM2	MDMX
Ac-LTFEHYWAQLTS-NH_2	pDI **166**[a]	14.6	47.4
Ac-LTF**X$_1$**HYWAQL**X$_2$**S-NH_2	**167c**	1	18.3
Ac-LTF**X$_1$**AYWAQL**X$_2$**S-NH_2	**168c**	4.9	34.3
Ac-LTF**X$_1$**EYWAQL**X$_2$**S-NH_2	**169c**	1.2	8
Ac-LTF**X$_1$**EYWAQ**X$_3$X$_2$**SAA-NH_2	**170c**	0.9	6.8
Ac-LTA**X$_1$**EYWAQ**X$_3$X$_2$**SAA-NH_2	**171c**	536	>1000
Nutlin-3a	**112a**	52.3	>1000
Ac-QSQQTF**X$_1$**NLWRLL**X$_2$**QN-NH_2	**164c**	25.9	105.7

*a pDI **134** N-acetylated and C-amidated; **X$_1$** **156**; **X$_2$** **33**; **X$_3$** **Cba**;*

Further modification showed that a H5E mutation (**169c**) increased the binding affinity to MDMX 6-fold with respect to the unstapled sequence. This may be due to the stabilising effect of the N-terminal TXXE capping box motif.[199] Substitution of L10 for β-cyclobutyl alanine (**Cba**) and extending the α-helix by additional alanine residues at the C-terminus saw the binding affinity for MDM2 increase to the pM range

(ATSP-7041, **170c**). Interestingly, the overall charge of ATSP-7041 is -1, however the peptide was shown to both penetrate cells and reactivate the p53 pathway,[210] showing that it is not necessary to have a neutral/positively charged peptide for *in vitro* activity as suggested by Bernal *et al*.[155]

2.3.2.3 **MTide**

In a similar approach, Brown *et al*.[211] used the more potent PMI peptide **143** as a starting scaffold for a stapled peptide inhibitor of MDM2 and MDMX. Computer simulations of the stapled peptide showed that because of the induced helicity of the staple the P12 residue would not bind optimally and so this was deleted from the sequence (**172**, MTide-01). This sequence had olefin monomers **33** and **156** (Figure 76) substitute the 4 and 11 residues respectively to form the equivalent stapled peptide sMTide-01 **173c**. The position of the stapling residues is identical to the previous p53-based stapled peptides SAH-p53-8 **164c**[155] and ATSP-7041 **170c**.[210] SAH-8 was used as a control, and the measured K_d's for MDM2 and MDMX were similar to reported literature values.[155,208]

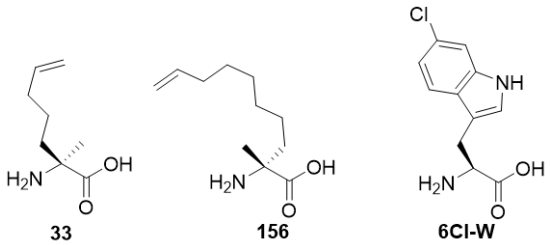

Figure 76- Monomers used by Brown *et al*.[211]

Incorporating the N8A mutation, which has been shown to be beneficial for binding,[202] gave rise to peptides **174** and **175c**. The stapled peptides showed a 3 to 4-fold decrease in K_d for MDMX compared to the unstapled analogues. However when using a T22 assay for cellular p53 activity, **175c** induced the greatest transcription response seen in this assay. This was increased even further with the substitution of W7 with 6-chlorotryptophan residue **6Cl-W**, which has shown to increase binding,[181,182] to give **176c**.

Table 27- p53 Response of Peptide Library from Brown *et al.*[211]

Sequence		T22 (25 μM)
Ac-QSQQTF**X$_1$**NLWRLL**X$_2$**QN-NH$_2$	**164c**	1.34 ± 0.05
Ac-TSFAEYWNLLS-NH$_2$	**172**	1.40 ± 0.01
Ac-TSF**X$_1$**EYWNLL**X$_2$**-NH$_2$	**173c**	2.62 ± 2.51
Ac-TSFAEYWALLS-NH$_2$	**174**	1.23 ± 0.03
Ac-TSF**X$_1$**EYWALL**X$_2$**-NH$_2$	**175c**	48.63 ± 1.85
Ac-TSF**X$_1$**EY**X$_3$**ALL**X$_2$**-NH$_2$	**176c**	82.67 ± 2.90

X$_1$ 156; ***X$_2$ 33***; ***X$_3$ 6Cl-W***;

Table 28- Binding Affinity and IC_{50} values of Peptide Library from Brown *et al.*[211]

	K_d (nM)		IC_{50} (μM)	
Peptide	MDM2	MDMX	MDM2	MDMX
164c	50.21 ± 5.53	14.03 ± 1.85	1.11 ± 0.09	0.26 ± 0.03
172	46.34 ± 6.89	33.16 ± 4.62	1.10 ± 0.10	0.55 ± 0.04
173c	86.99 ± 0.02	118.3 ± 0.04	1.80 ± 0.10	1.57 ± 0.22
174	28.04 ± 1.38	16.33 ± 2.00	0.75 ± 0.02	0.29 ± 0.02
175c	34.35 ± 2.03	45.73 ± 7.65	0.94 ± 0.04	0.66 ± 0.06
176c	6.76 ± 2.11	1360 ± 600	0.32 ± 0.02	3.49 ± 0.63

While the activity of the MTide peptides are still in the low nanomolar range, the phage sequence **143** has a greater affinity. It is known that N-acylation and C-amidation of the PMI peptides weaken the binding by approximately a factor of two,[202] however taking this into account the stapled peptides are still at least 10-fold weaker than the native phage peptide. What is required is a stapling methodology that would ideally match or better the binding affinity of the PMI N8A peptide, while constraining the peptide into the required α-helical secondary structure. This would increase the stability of the peptide to proteolysis and therefore the therapeutic potential.

Chapter 3- Synthesis of Peptides Targeting the p53-MDM2 Interaction

3 Rationale of Stapled Peptide Inhibitor Design

There are a number of possible ways to reactivate p53 activity. One of the most recent examples using peptides is described by Soragni *et al*.[212] Previous work showed that mutated, misfolded p53 tends to aggregate not only other mutated p53 protein, but wild type, active p53 protein also.[213] Analysis of the DNA-binding domain *in silico*, several segments of which are aggregation prone, identified that residues 252-258 (LTIITLE) were the most likely to form an amyloid adhesive segment, or "steric zipper". By taking this sequence and probing the structure, the group were able to confer specificity for the peptide to bind to unfolded p53 and minimise homobinding of the peptide. This new sequence, ReACp53 (LTRITLE) is able to reactivate mutant p53 into a wild-type like active state (Figure 77). This allows the reactivated p53 to enter the nucleus and induce cell death in both *in vitro* and *in vivo* models.

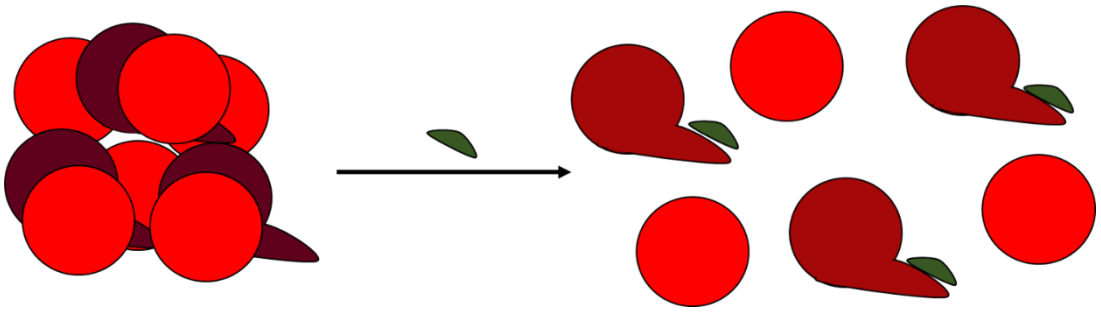

Figure 77- Dispersion and reactivation of wild-type p53 (red spheres) and misfolded mutant p53 (purple/maroon) due to peptide ReCAp53 (green) binding

It was decided that to investigate methods of peptide stapling starting from a known MDM2 inhibitor would be advantageous, given the wealth of information available about the p53-MDM2 protein-protein interaction. According to the recent literature, the peptide PMI N8A is the most potent inhibitor of both MDM2 and MDMX that is synthesised from only proteinogenic amino acids.[202] This was used as the starting scaffold for the library of macrocyclised peptides. Despite the small increase of affinity afforded to the sequence to MDMX, truncation of PMI N8A by removing the helix-breaking proline residue is thought to be beneficial,[211] as it competes conformationally

with the helical induction of the staple. Analysis of the 11-mer sequence (**174**, Figure 78) showed that there were few other residues that could be replaced for stapling monomers without some possible detrimental effect.

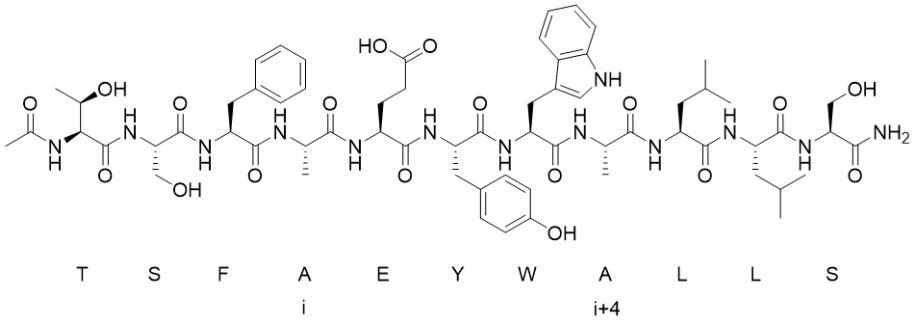

Figure 78- Truncated and Capped PMI N8A Scaffold **174**

Phenylalanine F3, tryptophan W7 and leucine L10 are critical for binding to MDM2 and MDMX, with tyrosine Y6 considered an important hydrophobic residue.[194] Serine S2 and glutamic acid E5 are part of a SXXE N-terminal capping box motif,[198,199,201] threonine T1 is one of the most common N-terminal helix inducing residues[156,200] and there is evidence that serine S11 also stabilises α-helical induction in the sequence.[196,197,202] Considering these factors, over 70% of the residues may contribute to the potency or stability of the sequence. With this in mind, the two alanine residues A4 and A8 have (*i*,*i*+4) spacing, and so are on the same helical face. From the helical wheel projection of peptide **174** (Figure 79) and the crystal structure of PMI N8A bound to MDM2 (Figure 80), it can be seen that the side chains of A4 and A8 are orientated away from the hydrophobic binding pocket. As few other of the residues could be replaced without significantly affecting the conformational stability of the peptide these alanine were selected as the stapling position within the peptide library. This is the first example of an (*i*,*i*+4) stapled peptide targeting the p53 MDM2 interaction.

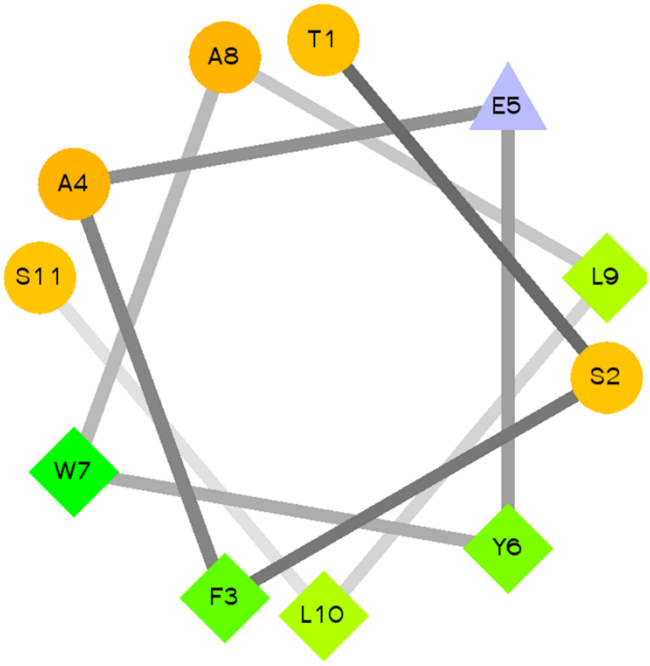

Figure 79- Helical wheel projection of peptide **174**. The alanine residues A4 and A8, to be substituted for cross-linking residues, are seen on the opposite face to the three critical hydrophobic residues F3, W7 and L10.

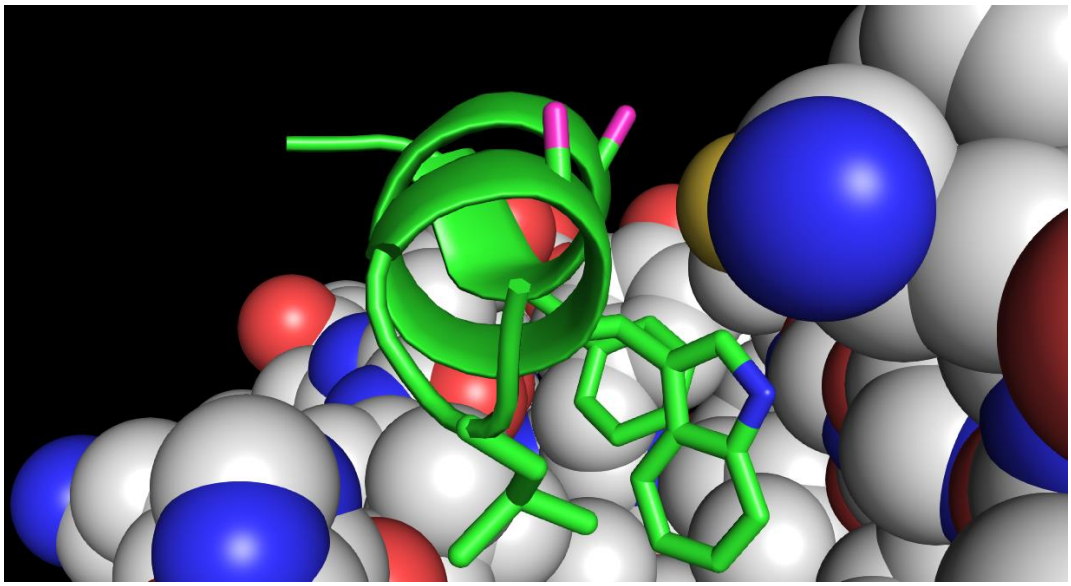

Figure 80- PMI N8A (**143**, Green, with critical residues F3, W7 and L10 shown) bound to MDM2, A4 and A8 Side Chains Highlighted (Magenta). PDB code 3EQS, reproduced using PyMol

3.1 Monomer Synthesis

As previously discussed, linker lengths of around 7-9 atoms are effective for an (*i*,*i*+4) α-helical peptide staple. It was decided to use a CuAAC triazolyl staple as the methodology has not been used in the context of inhibiting the p53 MDM2 interaction. From published investigations, it is evident that moieties within the staple can affect the induced helicity of the peptide. To try and minimise any helical disturbance, the linker was designed such that the triazole has the greatest distance between it and the peptide. This is so that i) the dipole of the triazole will be pointing directly away from the peptide minimising any disruptive electronic effects and ii) the effectiveness of the macrocyclisation would be at a maximum with the azido and alkynyl functional groups equidistant on the side chain residues. This would result in a pseudo-symmetrical staple, with the linker having the same number of atoms on each side of the triazole. This restricted the linker length to either 7 or 9 atoms, as the triazole CH is the centre of pseudo-symmetrical plane. A 9 atom linker length was chosen (Figure 81), as this was thought more to be an optimal length. If moderately too long however, it would allow a degree of flexibility, as opposed to a 7 atom linker potentially constraining the sequence too tightly.

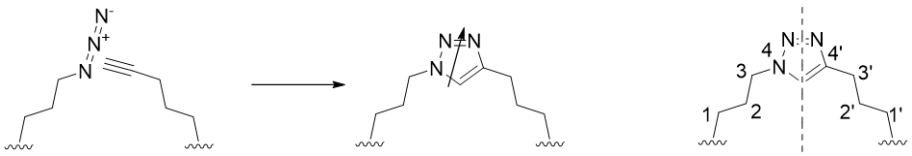

Figure 81- Pseudosymmetrical 9 Atom Triazole Staple

Jacobsen *et al*. showed it was possible to staple a peptide into a 3_{10} helical structure using the synthetic amino acids azido ornithine and propargyl serine.[214] Although a 3_{10}-helix requires a shorter (*i*,*i*+3) substitution to locate the side chains on the same helical face, the overall helical conformation is extended (Figure 82).[65]

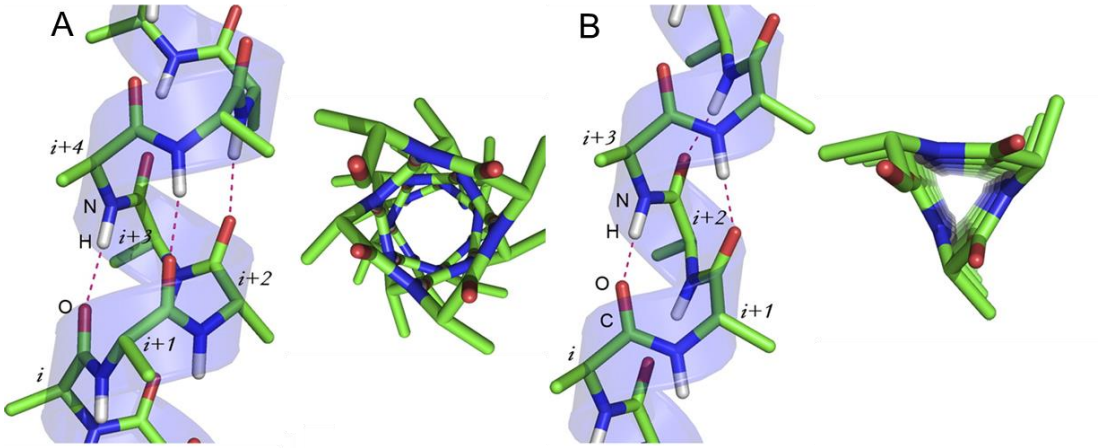

Figure 82- Comparison of **A** α-helix **B** 3_{10} Helix[65]

The introduction of the ether from the serine residue may have some slight effect as there is an additional hydrogen bond acceptor with respect to a hydrocarbon side chain, but is importantly still as chemically stable under biological conditions. These monomers (Figure 83) provide a synthetically simple route to the 9 atom linker desired. To probe any differences that may occur from the regiochemistry of the triazole, the position of the azide and alkyne monomers within the sequence were swapped (eg **179** vs **183**). In addition, both enantiomers of the monomers were incorporated into peptides to investigate the effect of D-amino acids in the helical induction of the staple, as it is important to investigate diastereomerism within the staple, as previously discussed in chapter one. These 8 peptides were compared to their uncyclised sequences and the native alanine substituted peptide **174** for increased helicity which results from the staple. The stability and increased cell permeability of peptoids in comparison to the peptide counterparts has been thoroughly documented.[176,215] With this in mind, incorporation of *N*-substituted glycine stapling monomers may further enhance the desired properties of a stapled peptide. However, using *N*-substituted glycine monomers removes 2 backbone hydrogen bonds, and so there will be an α-helix destabilising effect. There is only one example of a (*i*,*i*+4) CuAAC stapled peptide-peptoid hybrid within the literature from Park *et al.*[216] By combining an alanine scan with a sarcosine (*N*-methyl glycine) scan,[217] residues were replaced within the target sequence at positions that showed the greatest tolerance for both substitutions. As with any macrocyclised peptide, it was shown that the position of the

staple in the peptomer was critical to the effectiveness of the staple. However, there was no direct comparison to the equivalent CuAAC stapled peptide, or consideration of linker length and so this work did not reveal much about the relative efficiency of peptoid monomers as stapling residues. Conversely, the *N*-substituted glycine monomers **187** and **188** are directly comparable in length to the azido ornithine (**177**) and propargyl serine monomers (**178**) used. Also, by swapping the relative positions of **187** and **188** in the sequence the effect of the regiochemistry of the triazole moiety on relative helicity can be compared to both the peptide library and the equivalent sarcosine "native" peptomer **189**.

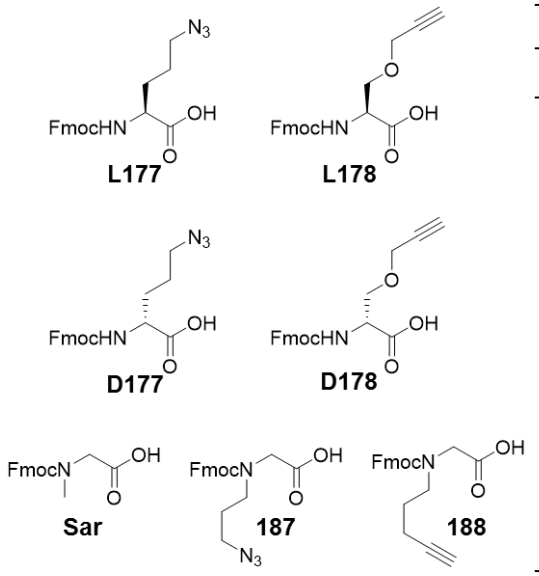

Ac-TSF**X$_1$**EYW**X$_2$**LLS-NH2			
X_1	X_2		
A	A	**174**	Native
L177	**L178**	**179u/c**	1,4-(*S*,*S*)
L177	**D178**	**180u/c**	1,4-(*S*,*R*)
D177	**L178**	**181u/c**	1,4-(*R*,*S*)
D177	**D178**	**182u/c**	1,4-(*R*,*R*)
L178	**L177**	**183u/c**	4,1-(*S*,*S*)
L178	**D177**	**184u/c**	4,1-(*S*,*R*)
D178	**L177**	**185u/c**	4,1-(*R*,*S*)
D178	**D177**	**186u/c**	4,1-(*R*,*R*)
Sar	**Sar**	**189**	N-Native
187	**188**	**190u/c**	1,4-NN
188	**187**	**191u/c**	4,1-NN

Figure 83- Non-natural monomers incorporated into peptide library to form 9-atom staple

3.1.1 Amino Acid Synthesis

The non-proteinogenic monomers **177** and **178** can be synthesised from commercially available amino acids in one- or two-pot processes. Starting from chiral reagents removes any need for chiral induction. The monomers were synthesised based on procedures from Sminia *et al.*[218]

3.1.1.1 Synthesis of Fmoc Azido Ornithine

The synthesis of amino acids containing azide side chains is well documented. Commonly, the corresponding amine or ammonium starting material is converted in one step to the azide via a diazo transfer reagent and metal(II) catalyst. These reagents are highly reactive, and sometimes require *in situ* generation. One of the most frequently used diazo transfer reagents is imidazole-1-sulfonyl azide **192** (Figure 84). This reagent is usually handled as an imidazolium salt, which are stable crystalline solids, making the use of **192** much simpler. The salts of **192** reproduce yields comparable to triflic azide, with the anion having little effect on the efficiency of the diazo transfer. Imidazole-1-sulfonyl azide salts have been shown to have a high functional group tolerance, including those normally found in proteinogenic amino acids.

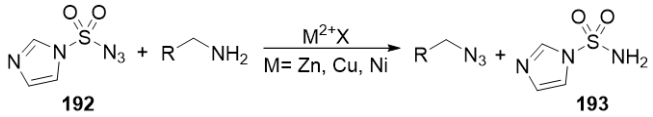

Figure 84- The Diazo Transfer Reaction with Imidazole-1-Sulfonyl Azide **192**

Beginning from commercially available enantiomers of the orthogonally protected amino acid Fmoc-Orn(Boc)-OH **194**, the Boc protecting group was removed using a 20 M solution of trifluoroacetic acid in DCM at room temperature (Scheme 1). After 2 hours stirring the reaction was complete by TLC. The excess TFA can be removed easily *in vacuo*, giving the crude ammonium trifluoroacetate salt **195** quantitatively with no losses from transfer. The salt was resuspended in a mixture of methanol and water. Water was added to help solvate the catalytic copper sulfate and K_2CO_3 base. The catalytic amount of copper(II) used was 5 mol%, but reports suggest that loading can be as low as 1 mol%. At least 3 equivalents of K_2CO_3 must be added to bring the solution to operational pH (9-10), since the free amine acts as the nucleophile in the diazo transfer.

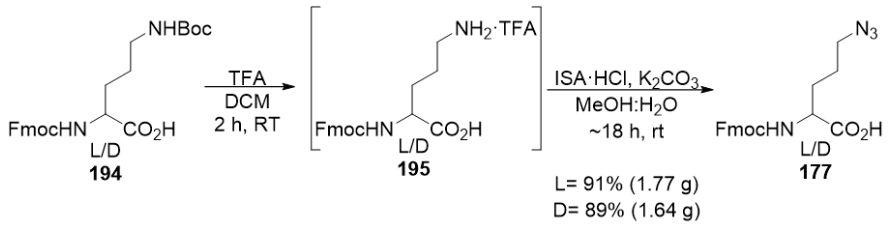

Scheme 1 - Synthesis of Fmoc Azido Ornithine **177**

The transfer proceeds cleanly over 18 hours, with no evidence of Fmoc deprotection. After removing the methanol *in vacuo* the basic solution was washed with toluene to remove the sulphonamide byproduct **193** effectively with little leaching of the azidoornithine product.

3.1.1.2 Synthesis of Fmoc Propargyl Serine

The literature is full of examples of alkylated serine derivatives starting from the commercially available Boc-Ser-OH **196**.[219–221] A number of non-nucleophilic bases have been used to deprotonate the hydroxyl group, with the most commonly used base being sodium hydride in dry DMF (Scheme 2). This base has the advantage that it is both a non-interfering conjugate base and the release of hydrogen acts as an observable indicator of completed alkoxide formation. The reaction temperature was maintained at 0 °C during the deprotonation step to prevent racemisation, the reaction proceeds cleanly with no byproducts. The DMF was removed *in vacuo* to simplify the separation. The crude carboxylate salt was dissolved in dilute aqueous HCl to prevent appreciable Boc deprotection of **197**. The Boc group was removed with a 20 M solution of trifluoroacetic acid in DCM at room temperature. The crude ammonium trifluoroacetate salt was reacted with FmocCl in basic dioxane to give the Fmoc monomer **178**.

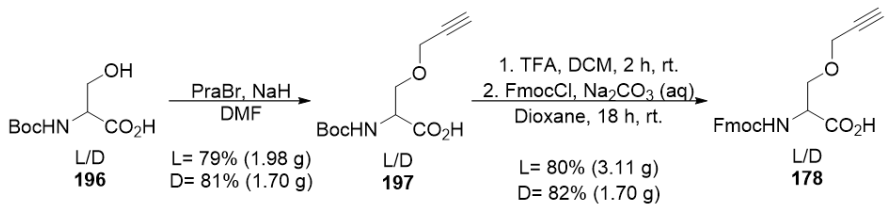

Scheme 2- Synthesis of Fmoc Propargyl Serine **178**

3.1.2 *N*-Substituted Glycine Monomers

The synthesis of *N*-substituted glycine monomers can be accomplished in a number of ways. One common method is the submonomer approach from Zuckermann *et al*.[222] Performed on resin, the monomers are built from the combination of 2 submonomers, an α-haloacetic acid and a primary amine (Figure 85). The submonomer synthesis approach is attractive in that there is minimal protecting group chemistry required, in addition there is a huge variety of primary amines commercially available which allows for installation of non-classic functionality within the sequence, and is compatible with SPPS.[223,224]

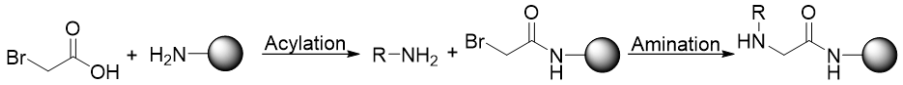

Figure 85- Solid Phase Submonomer Synthesis

A disadvantage of the submonomer approach is the large excess of amine required, typically 20-40 equivalents. While this is not unfeasible for most primary amines, the primary amine required for the submonomer synthesis of the azido monomer was 3-azido propylamine. This molecule falls within the explosive risk parameters of organic azides,[225,226] and so the submonomer synthesis was not considered a viable option.

Currently, there is no synthetic precedent for the synthesis of both the desired *N*-substituted glycine monomers. However, there have already been syntheses of azido peptoid monomers from the Hulme group (Scheme 3).[227] Based upon methodology from Unciti-Broceta *et al*.[228] the synthesis of the desired monomer **187** is accomplished in 5 steps from 1,3-diaminopropane in a 39% overall yield. The amine alkylation is the lowest yielding step (54%), due to disubstitution. A new synthetic methodology was designed, attempting to improve upon these results

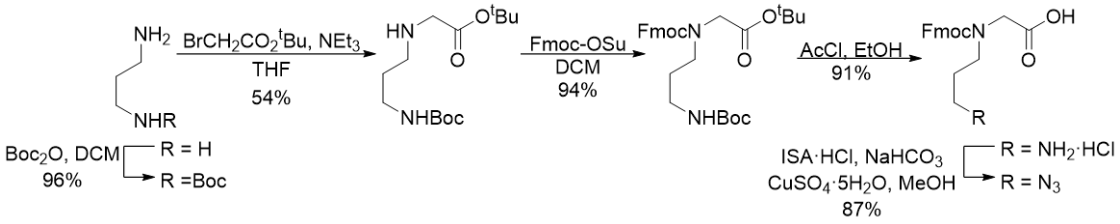

Scheme 3- Hulme Group Synthesis of Azido Monomer **187**[227]

Evaluating the *N*-substituted monomers retrosynthetically, there are two obvious disconnections that can be made. Approach A disconnects the nitrogen side-chain bond, while approach B disconnects the nitrogen α-carbon bond (Figure 86). Both approaches can be achieved with reductive amination and alkylation reactions. A problem with the alkylation approaches is the decreased yield arising from over-alkylation and formation of the tertiary amine product. This could be overcome with increased number of equivalents of amine, however both the alkylations would still require low molecular weight azides. The reductive amination reactions have the advantage of controlled mono-substitution of an amine to the aldehyde moiety, but again require low molecular weight azides. A solution to this is to install the amine function with a side chain containing a leaving group that would allow both the azide and alkyne to be synthesised from a common intermediate. Ideally, this intermediate would be protected with a *tert*-butyl ester to allow for orthogonal deprotection of the acid moiety after the Fmoc group is added.

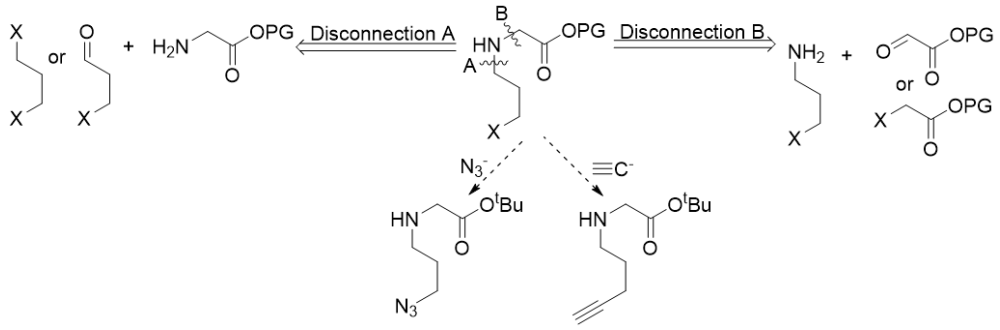

Figure 86- Retrosyntheses of *N*-Substituted Glycine Monomers

Reductive amination approach A would combine a non-commercially available low molecular weight aldehyde and glycine *tert*-butyl ester. The alternative reductive amination approach requires a volatile amine and *tert*-butyl glyoxylate, which is not commercially available and which syntheses of are typically long and poor yielding.[229–231] With these considerations in mind, an alkylation procedure was pursued. In designing an analogous alkylation procedure (Figure 87), approach A requires a dihalopropane and glycine *tert*-butyl ester. While formation of the azetidinyl byproduct is unfavorable, dimerization and oligomerization are feasible side reactions, though this could be controlled by use of a dihalopropane with different nucleofugalities e.g. 3-chloro-1-iodopropane. Approach B requires an α-halo *tert*-butyl acetate and a low molecular weight amine, which has already been deemed problematic. Both approaches also have the drawback of possible dialkylation of the amino group.

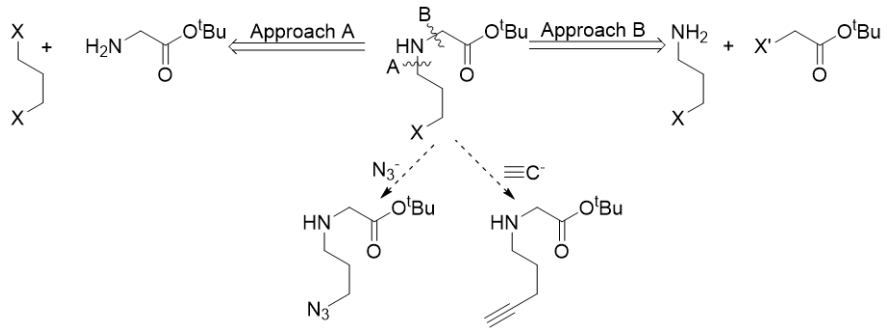

Figure 87- Possible Divergent Amine Alkylation Retrosyntheses

A solution to the dialkylation problem is the use of an amine protecting group. The protecting group must be easy to install, allow the alkylation to proceed, and be removed under mild conditions. The most common amine protecting groups are amides, carbamates and sulfonamides, as all can be synthesised easily from an amine and an acylating agent. The use of an amide protecting group significantly decreases the pK_a of the nitrogen proton (Figure 88), but requires a strong base for deprotonation so reaction times and yields can be hindering and hydrolysis of the amide requires harsh conditions. Carbamate protons have a similar pK_a to amides, but can be removed under milder conditions, as the release of CO_2 is a thermodynamic driving force.

Sulfonamides decrease the pK_a of the nitrogen further and so a milder base can be used, but can require harsh hydrolysis conditions. Trifluoroacetamides can be synthesised in near quantitative yields from the amine starting material, increase the acidity of nitrogen proton equivalent to a sulfonamide, and be removed under mild reaction conditions.

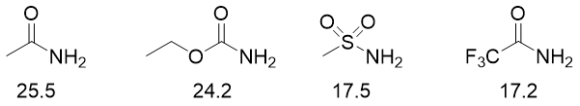

Figure 88- N-H pK_as of Selected Amine Protecting Groups in DMSO[232]

In considering a trifluoroacetamide alkylation methodology, both retrosynthetic disconnections are still feasible (Figure 89). In approach A trifluoroacetyl (Tfac) glycine *tert*-butyl ester is alkylated with a dihalopropane, however using a dihalo reagent there is a risk of dimerization. In approach B, a haloalkyl trifluoroacetamide is alkylated by an α-halo *tert*-butyl ester. This approach has an electron-withdrawing group on the carbon with the leaving group, which is advantageous given the generally poor nucleophilicity of amides. It is also simple to install different reactivities in the trifluoroacetamido alkyl halide and the α-halo *tert*-butyl acetate to prevent polymerisation of the haloalkyl trifluoroacetamide. From there, the formation of the azide and alkyne side chains can be achieved by substitution at the alkyl halide. With these advantages apparent, this approach was pursued.

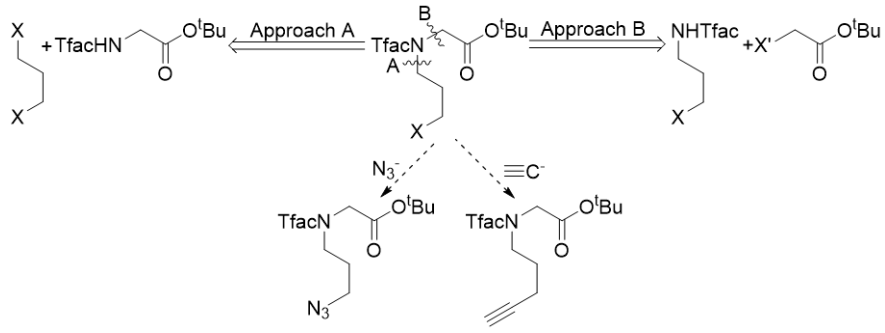

Figure 89- Possible Divergent Trifluoroacetamide Alkylation Retrosyntheses

3.1.2.1 **Synthesis of the Common Intermediate**

Starting from 3-chloropropylamine hydrochloride **198**, the ammonium salt was reacted with trifluoroacetic acid anhydride (TFAA) and a non-nucleophilic base in DCM to give trifluoroacetamide **199** (Scheme 4). Addition of the TFAA last tended to require additional reagent (1.5 - 2.5 eq) for the reaction to go to completion, so the ammonium salt and TFAA was stirred before addition of non-nucleophilic amine base. Addition of 2.2 equivalents of either triethylamine (TEA) or di-isopropylethylamine (DIPEA) worked equally well.

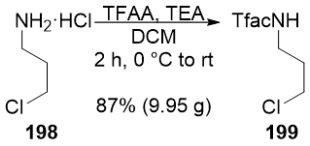

Scheme 4- Synthesis of 3-Chloropropyl Trifluoroacetamide **199**

The alkylation step used commercially available *tert*-butyl bromoacetate to exploit the different leaving group tendencies of the halides. From the literature, a number of bases have been used to alkylate trifluoroacetamides, including metal hydrides,[233,234] potassium *tert*-butoxide,[235] and K_2CO_3.[236] Esiringu *et al*.[232] found that using caesium carbonate (Cs_2CO_3) was very effective, needing only a moderate increase in stoichiometric equivalents with respect to the trifluoroacetamide, if at all, to affect the alkylation. This was attributed to the increased solubility of the base in organic solvents. Interestingly, a catalytic amount of Cs_2CO_3 added to reactions employing K_2CO_3 as the base dramatically accelerated the alkylation. A number of solvents can be used, but DMF and MeCN showed the shortest reaction times. Emulating this strategy, Cs_2CO_3 was stirred with the trifluoroacetamide **199** at 35 °C for 5 minutes before addition of the *tert*-butyl bromoacetate. The reaction proceeded cleanly by TLC in 3 or 4 hours when using DMF or MeCN respectively, with little difference in yield (Scheme 5). As the reaction provided the product **200** efficiently, the reaction mixture can simply be filtered through a silica pad to remove the inorganic salts.

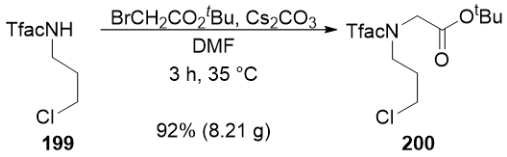

Scheme 5- Alkylation of 3-Chloropropyl Trifluoroacetamide **200**

The alkylation produced a tertiary amide, and so rotamers were observed in the NMR spectra. This was confirmed with a set of variable temperature NMR experiments which ran from 313 K in 10 K increments up to 373 K, which was high enough for signal coalescence to be observable (Figure 90).

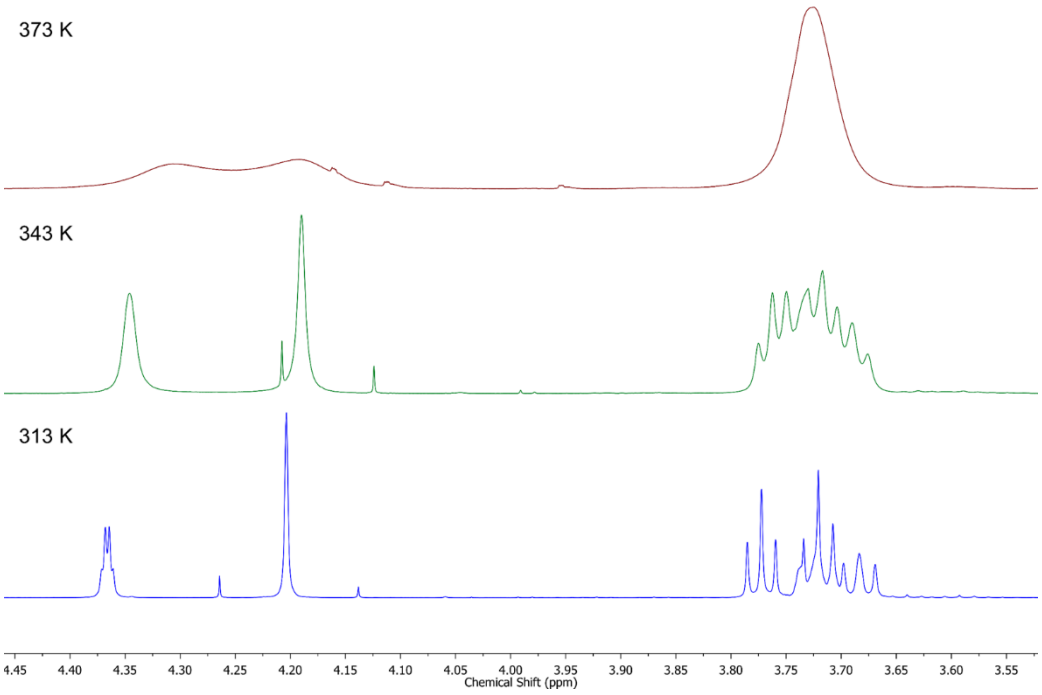

Figure 90- Abstracts of variable temperature ^{1}H experiments (4.45 – 3.50 ppm, *d7*-DMF) showing α-carbon CH_2 rotameric signals (4.35 and 4.20 ppm) and overlapping CH_2Cl and TfacNRC*H*$_2$CH$_2$R' rotameric signals (3.78 – 3.66 ppm). Full series of spectra can be found in Section 5.1.2.1.

In both the ^{1}H NMR and ^{13}C NMR, there is coupling to the fluorine nuclei of the trifluoroacetamide. Studies have shown that there is an observable *trans* coupling in tertiary trifluoroacetamides (~1-2 Hz).[237–239] This allowed the complete assignment of each signal to a specific rotamer of **200** from HSQC and HMBC experiments, which,

along with ^{19}F, showed that the rotameric ratio was 50:50. In the ^{1}H NMR spectrum $^{5}J_{HF}$ couplings are seen, with the complimentary $^{4}J_{CF}$ couplings in the ^{13}C NMR spectrum (Figure 91). The coupling was confirmed with a ^{19}F-decoupled ^{1}H NMR experiment (Figure 92).

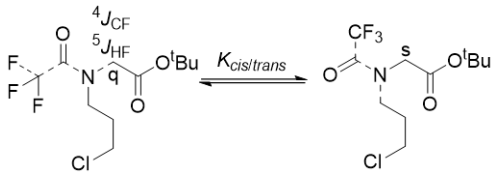

Figure 91- Rotameric ^{19}F Coupling Seen by **200** α-Carbon from *trans* Interaction to CF_3

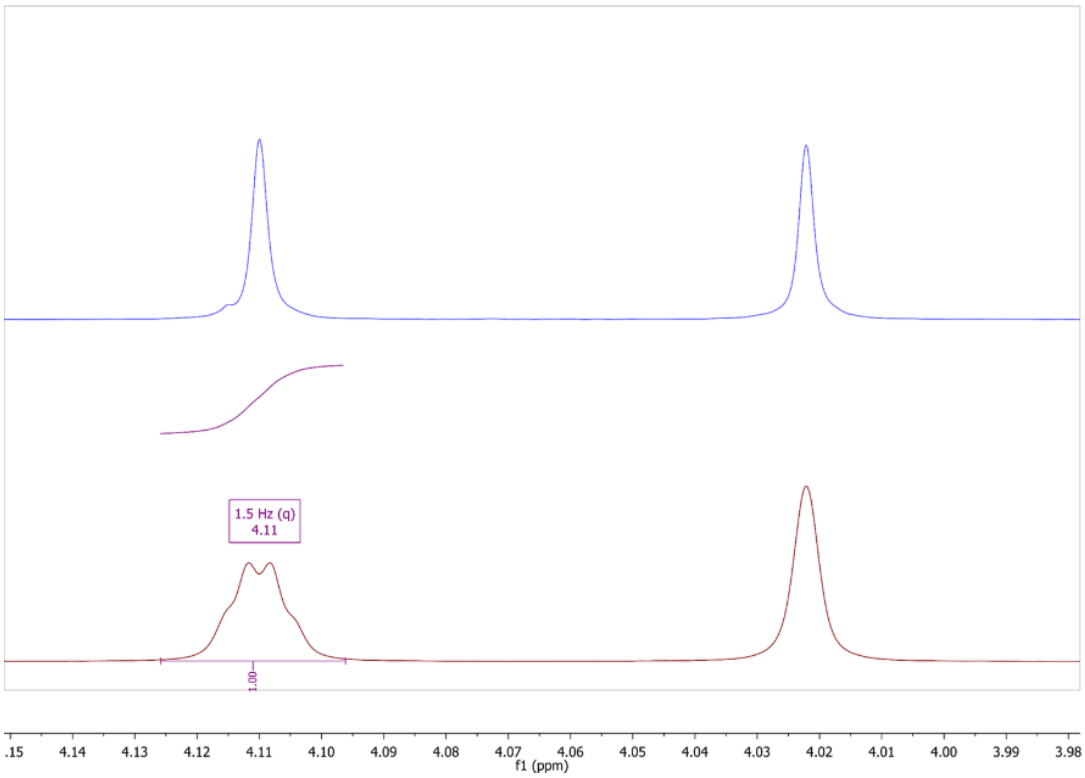

Figure 92- Abstract of NMR spectra (4.15 – 3.98 ppm, $CDCl_3$) comparing ^{1}H (Red) and ^{19}F Decoupled ^{1}H (Blue) spectra, showing α-Carbon ^{1}H Peaks of **200**

Although there are examples of the displacement of alkyl chlorides by azide and alkynyl nucleophiles,[240,241] the decreased reactivity of alkyl chlorides compared to alkyl bromides and iodides tends to result in longer reaction times, greater amounts of nucleophile required, or heating being necessary to affect complete substitution. These

reaction conditions are generally undesirable when using highly reactive azides. The Finkelstein reaction converts less reactive alkyl halides to alkyl iodides using sodium iodide (NaI) in a polar organic solvent.[242] The equilibrium is driven to the products by the insolubility of the sodium halide salt formed compared to the solubility of NaI in the polar solvent (Figure 93).

Figure 93- The Finkelstein Reaction

Classically, the reaction uses acetone as the solvent, however MeCN was used instead. Sodium iodide is still relatively soluble in acetonitrile (24.9 g/ 100 g MeCN vs 50.4 g /100 g acetone) and NaCl is highly insoluble in MeCN (3 mg / 100 g MeCN).[243] Acetonitrile however has a higher boiling point (81-82 °C vs 56-57 °C acetone) which allowed increased reaction temperatures and subsequently shorter reaction times. At 95 °C the reaction of **200** was complete in 5 hours using only 1.25 equivalents of NaI (Scheme 6). The end point was difficult to determine by TLC due to the similar polarity of the alkyl chloride and iodide **201**, but by monitoring the reaction by NMR the upfield shift of the methylene group confirmed the reaction had gone to completion (Figure 94).

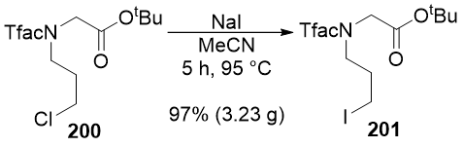

Scheme 6- Finkelstein Reaction of Alkyl Chloride **200**

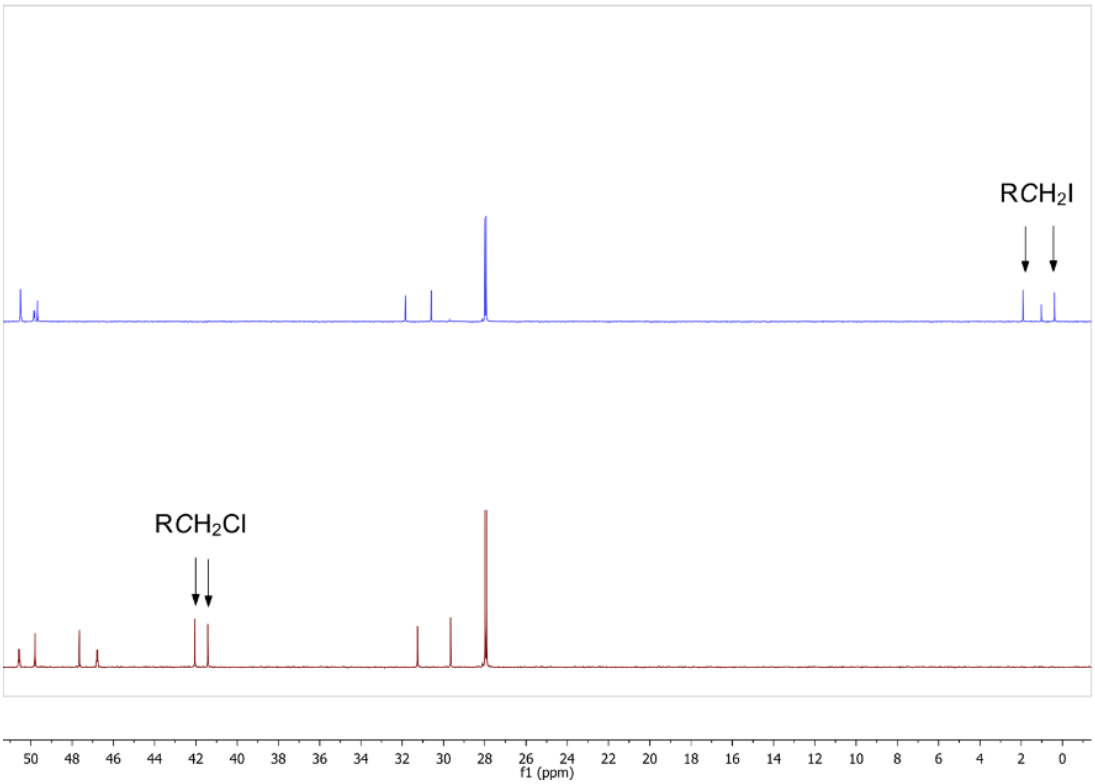

Figure 94- Abstract of ^{13}C Spectra (0 - 50 ppm, $CDCl_3$) of Chloride **200** (Red) and Iodide **201** (Blue), highlighted are the rotomeric RCH_2X Peaks.

The preparation of the common intermediate **201** was achieved in a 79% yield over three steps (Scheme 7). The simple purification procedures made the synthesis amenable to scale up with little variation in yield. With this intermediate in hand, the divergent synthesis of the azido and alkynyl monomers continued.

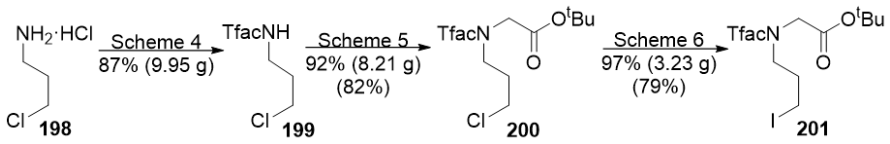

Scheme 7- Synthesis of Iodide **201** from 3-Chloropropylamine Hydrochloride **198**

3.1.2.2 Synthesis of Fmoc *N*-3-Azidopropyl Glycine

Beginning from the common intermediate **201**, the synthesis of the azido monomer **187** required 4 steps (Scheme 8): nucleophilic substitution of the alkyl iodide **201** to

the alkyl azide, hydrolysis of the azido trifluoroacetamide **202**, conversion of the secondary amine **203** to the Fmoc carbamate **204** and finally deprotection of the *tert*-butyl ester to the free acid **187**.

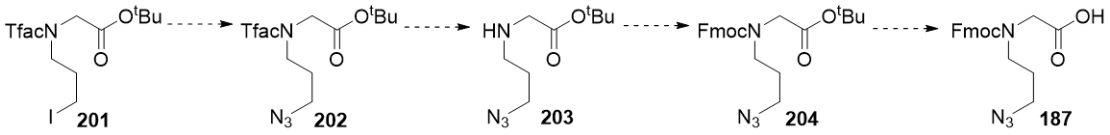

Scheme 8- Proposed Synthesis of Fmoc *N*-Azidoproylglycine **187** from Common Iodide Intermediate **201**

A simple method of azidification of alkyl halides from Alvares *et al*. was used.[244] Dimethyl sulfoxide (DMSO) was shown to dissolve sodium azide sufficiently. The displacement of alkyl bromides was achieved using a 1.2 equivalents of NaN_3 solution (0.5 M in DMSO) at room temperature overnight. Adapting this procedure, a modest increase in equivalents of NaN_3 added in a more concentrated DMSO solution (1 M) gave the corresponding alkyl azide **202** in high yield in 4 hours at room temperature (Scheme 9).

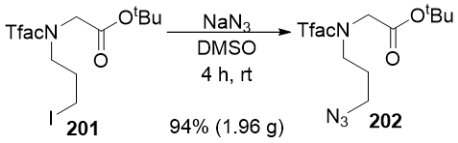

Scheme 9- Azide Displacement of Common Iodide Intermediate **201**

Hydrolysis of the trifluoroacetamide can be affected under extremely mild conditions. Common reaction conditions utilise aqueous hydroxide solutions with a miscible organic co-solvent, or sodium borohydride.[245] However, partial cleavage of the *tert*-butyl ester was seen when hydroxide bases were used, and although the borohydride worked well, another base mediated method was selected instead. Aqueous K_2CO_3 solution in methanol[246,247] gave complete transformation as cleanly as sodium borohydride at room temperature but in longer reaction times (1 h vs ~18 h). With a moderate increase in temperature (40 °C) the reaction was complete in 4 hours (Scheme 10).

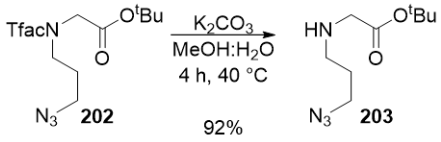

Scheme 10- Hydrolysis of Azido Trifluoroacetamide **202**

The protection of the amine **203** with FmocCl was achieved easily using TEA in MeCN at room temperature in 2 hours (Scheme 11). Similarly to the trifluoroacetamides **200**-**202** the NMR spectra showed rotamers, due to the restricted rotation of the carbamate. The rotameric ratio was 51:49, showing no conformational preference.

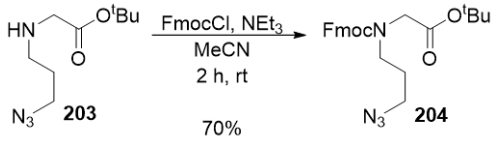

Scheme 11- Fmoc Carbamate **204** Formation

The opportunity to telescope the trifluoroacetamide hydrolysis and Fmoc protection steps was apparent when using the base mediated deprotection of azide **202** (Scheme 12). An excess of K_2CO_3 was used in the hydrolysis step, and so by removing the aqueous methanol *in vacuo*, the crude amine and K_2CO_3 can be used directly in the acylation step. Using the same amount of FmocCl, the reaction was complete in the same time. Following aqueous work up and column chromatography, the carbamate ester **204** was isolated in a similar yield to the non-telescoped route.

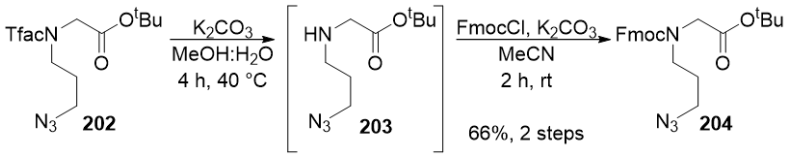

Scheme 12- Telescoped Synthesis of **204**

Finally, the *tert*-butyl ester was deprotected using 20 M TFA in DCM to give the azidopropyl *N*-substituted glycine monomer **187** in high yield (Scheme 13). The rotameric ratio (56:44) suggested a slight preference for one conformation. This preference will be due to the cleavage of the bulky *tert*-butyl ester, allowing a greater amount of rotational freedom, leading to one rotamer being more energetically favourable.

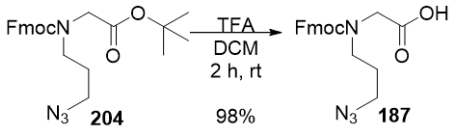

Scheme 13- Acid Deprotection of *tert*-Butyl Ester **204**

Once again, an opportunity to telescope the synthesis was pursued (Scheme 14). Upon completion of the Fmoc protection, the MeCN was removed *in vacuo* and the crude *tert*-butyl ester **204** was redissolved in DCM and filtered through a silica plug to remove the potassium salts. The DCM solution was concentrated and TFA added. After the reaction was complete and the TFA/DCM removed *in vacuo*, the crude monomer was taken up in ethyl acetate and extracted into aqueous sodium bicarbonate. This step separates any excess FmocCl or 9-Fluorenemethanol (FmOH) from the reaction mixture. Acidification of the aqueous layer to pH 3 and extraction with EtOAc allowed the isolation of the desired monomer **187**. In telescoping three steps, a greater overall yield was achieved than that of the separate reactions (77% vs 63%).

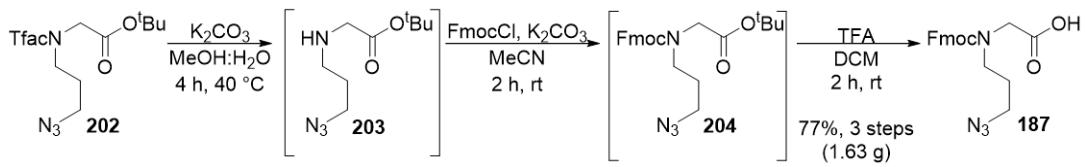

Scheme 14- Telescoped Synthesis of *N*-Substituted Glycine **187**

The azido *N*-substituted glycine monomer **187** was synthesised from the iodide **201** in a 4 step, 2 pot process in 72% yield.

3.1.2.3 **Synthesis of Fmoc *N*-Pentyn-4-yl Glycine**

Beginning from the common iodo intermediate **201**, the synthesis of the alkynyl monomer **188** was visualised as 4 steps (Scheme 15): nucleophilic substitution of the alkyl iodide to the alkyne, hydrolysis of the trifluoroacetamide **205**, conversion of the secondary amine **206** to the Fmoc carbamate **207** and finally deprotection of the *tert*-butyl ester.

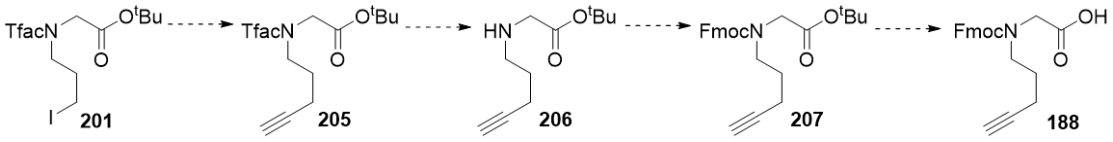

Scheme 15- Proposed Synthesis of Fmoc *N*-Pentyn-4-yl Glycine **188** from Common Iodide Intermediate **201**

Alkylation of the iodide **201** was attempted with lithium acetylide ethylenediamine complex,[248] an easily handled solid. However, even at -78 °C in THF, cleavage of the trifluoroacetamide group was observed (Scheme 16).

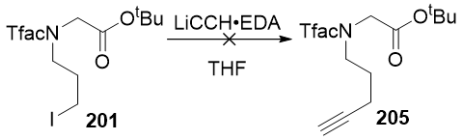

Scheme 16- Unsuccessful Synthesis of Alkyne **205**

To explore solutions to this problem a model system was devised (Scheme 17). The trifluoroacetamide **199** was converted to the corresponding iodide **208**, which would allow favourable alkylation conditions to be explored. Also, successful alkylation of iodide **208** would provide an alternative synthetic route to the desired alkyne monomer.

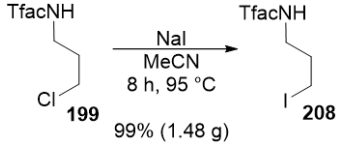

Scheme 17- Finkelstein Reaction of Alkyl Chloride **199**

A number of variables were tested in the model system (Scheme 18). Alternative nucleophiles trimethylsilylacetylene and ethynylmagnesium bromide were used in addition to LiC≡CH·EDA. Deprotonation of TMSC≡CH with NaH as well as BuLi to see if metal coordination has a significant effect. Addition of *N*,*N*′-dimethylpropylene urea (DMPU), a safer alternative to HMPA, to coordinate the metal cations to prevent activation of the trifluoroacetamide was also attempted, yet none of the conditions attempted were successful. Given the mild deprotection conditions that can be used to remove the trifluoroacetyl group, in retrospect these results were not surprising. Following these negative results, an alternative synthesis was planned.

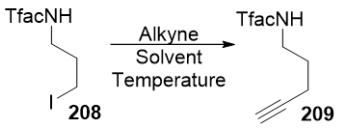

Alkyne	Solvent	Temperature (°C)
LiC≡CH·EDA	THF	0
LiC≡CH·EDA	THF:DMSO[a]	0
LiC≡CH·EDA	THF	-78
LiC≡CH·EDA	THF:DMPU[b]	0
LiC≡CH·EDA	THF:DMPU[b]	-78
HC≡CMgBr	THF	0
HC≡CMgBr	THF:DMPU[b]	0
HC≡CMgBr	THF	-78
HC≡CMgBr	THF:DMPU[b]	-78
TMSC≡CLi[c]	THF:DMPU[b]	-78
TMSC≡CNa[d]	THF:DMPU[b]	-78

a 1:1 v/v; b 4:1 v/v; c TMSCCH + BuLi; d TMSCCH + NaH;

Scheme 18- Attempted Syntheses of Alkyne **209** from Iodide **208**

After the failed divergent synthesis from the alkyl iodide **201**, the original retrosyntheses to the alkyne monomer **188** were reassessed. An alternative synthetic approach involved alkylation of the trifluoroacetylglycine *tert*-butyl ester **210** (Figure 95). This retrosynthesis was not chosen as it was thought that the amide alkylation would proceed better with an electron withdrawing effect of the *tert*-butyl ester next to the leaving group. However, with the azido monomer **187** in hand, this second synthesis of the alkynyl monomer was more attractive than possible alternatives due to the clear parallels with the azido monomer synthesis, and the robust methodology established within.

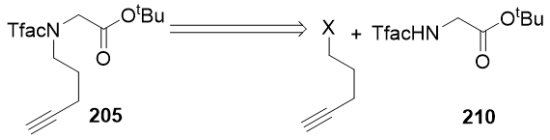

Figure 95- Alternate Retrosynthesis of Trifluoroacetamide **205**

Starting from glycine *tert*-butyl ester hydrochloride **211**, identical conditions previously used furnished the trifluoroacetamide **210** in good yield (Scheme 19).

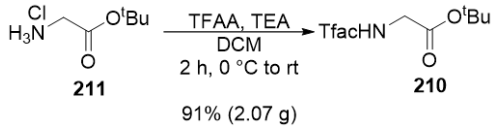

Scheme 19- Trifluoroacetylation of Glycine *tert*-Butyl Ester Hydrochloride **211**

Attempts to alkylate the trifluoroacetamide **210** with commercially available 5-chloropent-1-yne (5-CP) using the conditions previously employed were unsuccessful. This is a result of the comparatively poorer leaving group ability of the chloride nucleofuge, the decreased electrophilicity of the methylene carbon, or more likely a combination of both. A number of conditions were varied, including adding a sub-stoichiometric amount (0.2 eq) of tetrabutylammonium iodide, a phase transfer catalyst thought to increase the solubility of the amide anion in organic media.[249–251] This, in addition to an increase in the temperature (rt to 95 °C), number of equivalents of alkyl chloride (1.2 to 1.5) and Cs_2CO_3 (1.2 to 1.5 eq), afforded the alkyne **205** cleanly in high yield (Scheme 20).

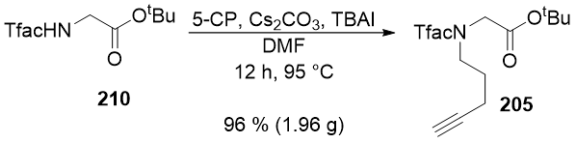

Scheme 20- Alkylation of Trifluoroacetylglycine *tert*-Butyl Ester **210**

Following the antecedent methodology, the 3 step telescoped trifluoroacetamide hydrolysis, Fmoc acylation and *tert*-butyl ester deprotection proceeded cleanly in good

yields comparable to the azide monomer **187** (Scheme 21). Again, following cleavage of the *tert*-butyl ester, the rotameric ratio showed a preference for one conformer (61:39 for **188** vs 52:48 for **207**).

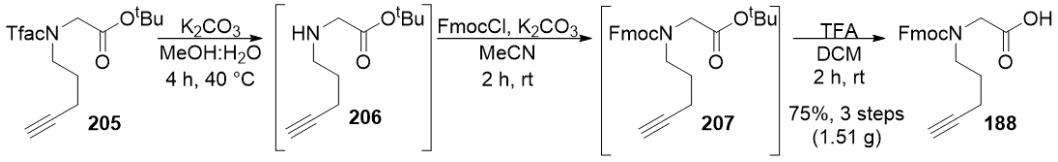

Scheme 21- Telescoped Synthesis of Monomer **188** from Trifluoroacetamide **205**

3.1.3 Summary

Four monomer building blocks were required for the investigation of a (*i*,*i*+4) triazolyl stapled peptide. For incorporation into stapled peptides, both enantiomers of Fmoc Azido Ornithine **177** were synthesised in one step in good yields on gram scale (Scheme 22).

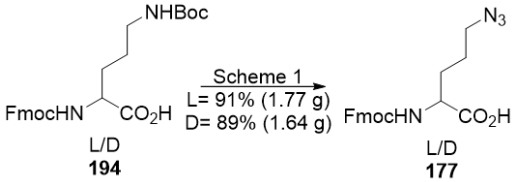

Scheme 22- Complete Synthesis of Enantiomers of Fmoc Azido Ornithine **177**

Beginning from Boc Serine **196**, the enantiomers of Fmoc Propargyl Serine **178** were synthesised in a 3 step, 2 pot process on gram scale in good yields (Scheme 23).

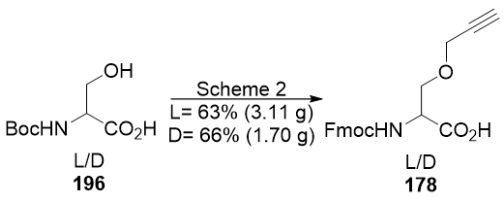

Scheme 23- Complete Synthesis of Enantiomers of Fmoc Propargyl Serine

Two *N*-substituted glycine monomers were synthesised for incorporation into stapled peptomers. The Fmoc *N*-Azidopropyl glycine residue **187** was synthesised successfully from 3-chloropropylamine hydrochloride **198** in 7 steps in a 57% overall yield on gram scale with no column chromatography required (Scheme 24). Although this methodology has an additional two steps compared to the previous synthesis from the Hulme group,[227] the overall yield was improved by 18% (57% vs 39%) while using simpler purification procedures.

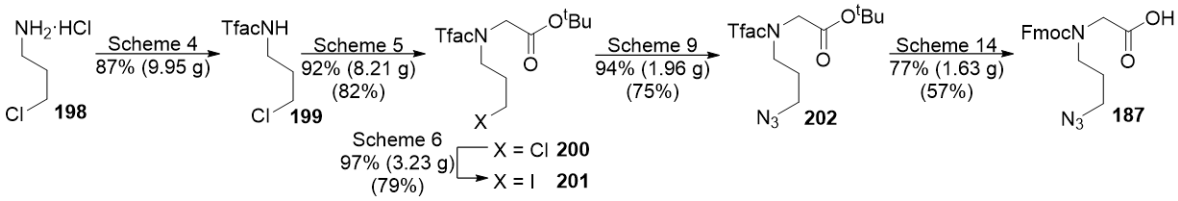

Scheme 24- Complete Synthesis of Fmoc *N*-Azidopropyl Glycine **187**

In a 5 step, 3 pot process, the Fmoc *N*-pentyn-4-yl glycine monomer **188** was synthesised for the first time from commercially available glycine *tert*-butyl ester in a 66% overall yield (Scheme 25). This was also achieved, as with the azido monomer **187**, on gram scale without a single chromatographic purification.

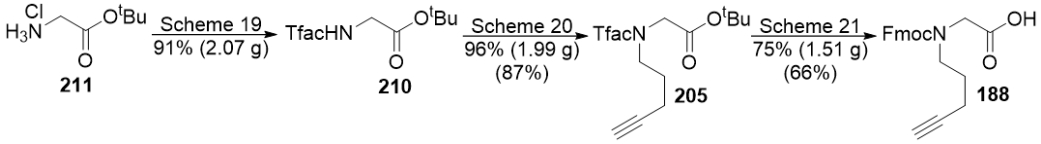

Scheme 25- Complete Synthesis of Fmoc *N*-Pentyn-4-yl Glycine **188**

While a divergent methodology was unsuccessful in this case, the common iodo intermediate **201** could in theory be used to synthesise a number of side-chains from weaker nucleophiles. In addition, the versatility of both established synthetic routes could easily be utilised to produce a range of *N*-substituted glycine monomers from cheap, commercially available starting materials in high yields and purity with minimal purification.

3.2 Peptide Synthesis, Cyclisation and Purification

With the monomers in hand, the peptides were synthesised using established Fmoc solid phase peptide synthesis protocols (Figure 96).[46,48] The methodology uses a base to remove the Fmoc group, freeing the amine group of the polymer for coupling. The free acid monomers are activated by additives to make coupling to the free amine more efficient. To liberate the peptide from the resin and deprotect the side-chains, acid sensitive protecting groups and an acid labile linker are used as these utilise orthogonal conditions to the Fmoc deprotection. A number of reviews and practical guides are available and so the vast number of permutations will not be discussed.[252,253]

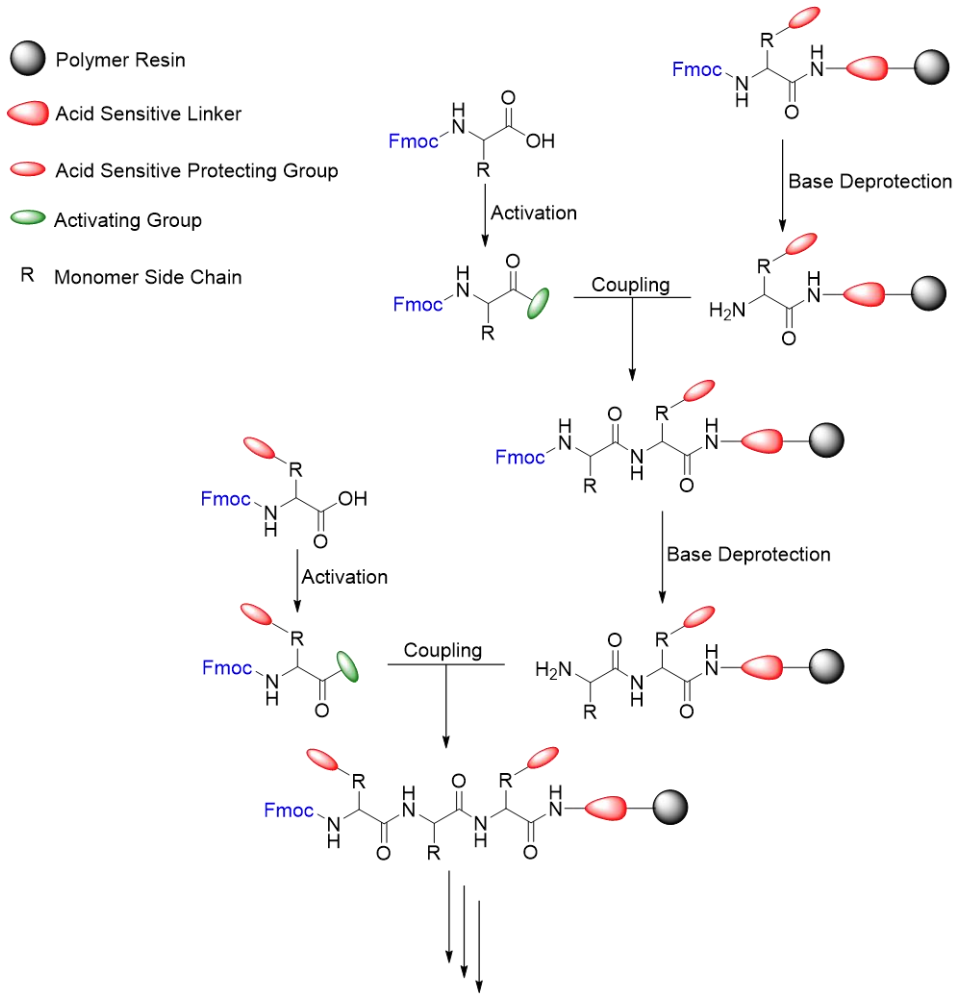

Figure 96- Generic Fmoc Based Protocol for the Synthesis of a Peptide

3.2.1 Peptide Synthesis

The peptides were synthesised manually, using an aminomethyl polystyrene resin with a Rink amide linker.[254] The Rink amide linker was selected as it releases an amidated carboxy terminus upon acidic cleavage of the peptide (Figure 97). The amine handle of the linker was protected with an Fmoc group and so was must be removed before coupling the first amino acid. This deprotection, and the subsequent couplings and Fmoc deprotections of the amino acids were confirmed by the chloranil test for free amines. This colourimetric test gives green/blue beads in the presence of free amines.[255]

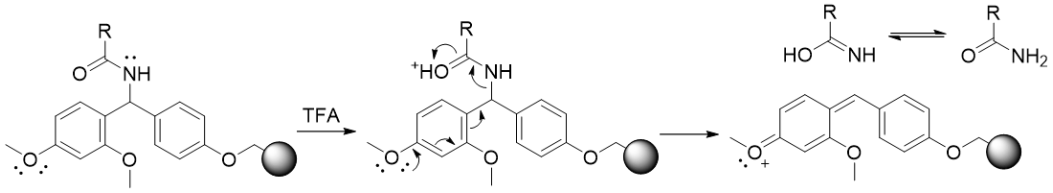

Figure 97- Acidic cleavage of carboxyamidated peptide from Rink linker

The Fmoc monomers were coupled using diisopropylcarbodiimide (DIC) which generates an *O*-acylisourea (Figure 98). After coupling with the free amine of the resin bound peptide, the soluble urea by-product diisopropylurea (DIU) is formed, facilitating solid phase work-up.[256] Ethyl (hydroxyimino)cyanoacetate (Oxyma), a coupling additive, was also used.[257] The addition of Oxyma forms an activated Oxyma-ester which is less reactive than the *O*-acylisourea, but still reactive enough to allow peptide coupling to occur (Figure 98-A). This less reactive Oxyma-ester suppresses racemisation via oxazolone formation (Figure 98-B),[257–260] prevents *N*-acylurea formation (Figure 98-C)[261] and is a safer alternative to other coupling reagents such as hydroxybenzotriazole (HOBt).[257,262,263] After completion of the sequence the peptides were capped using an excess of acetic anhydride (Ac_2O) and DIPEA. This step was also confirmed by the chloranil free amine test.[255]

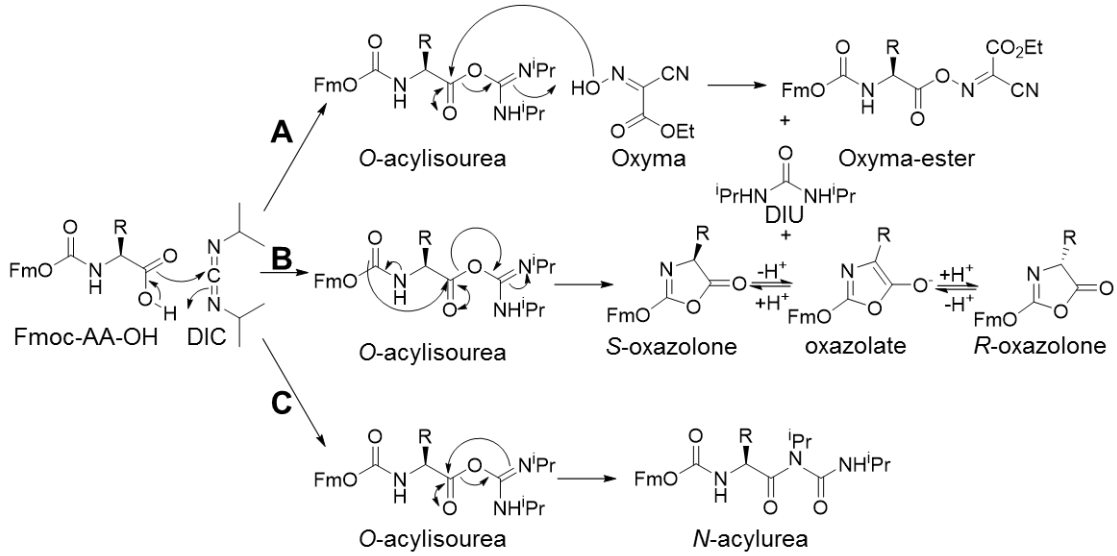

Figure 98- Activation of Fmoc-amino acids with DIC to form the corresponding *O*-acylisourea **A** Reaction with Oxyma to form the activated Oxyma-ester and DIU **B** Reaction with Fmoc carbamate to form *S*-oxazolone and DIU. The *S*-oxazolone can then racemise via the achiral oxazolate **C** *O*-acylisourea undergoes an *O*→*N* shift to form the *N*-acylurea

3.2.2 Peptide Cyclisation

Upon completion of each sequence, the peptide-loaded resin was split in half. The uncyclised peptides were then cleaved from the resin using TFA and triisopropylsilane as a scavenger. The other half was kept to be cyclised on resin. Previous attempts by other groups to cyclise peptides on resin using the CuAAC reaction has proved problematic, and can result in oligomerisation and cyclodimerisation. This is thought to be caused by two main interactions. Firstly, the peptide chains folding over toward the resin and interacting in a β-sheet system, separating the azide and alkyne moieties on the same peptide and putting the reactive groups closer in space to neighbouring chains (Figure 99-A). Secondly, the bicationic dependent catalysis of the CuAAC reaction is thought to be problematic in that by using a typical sub-stoichiometric amount of copper, there may be chelation of the opposing peptide chains to the reactive metal. One way to overcome this problem would be to increase the number of equivalents of copper, however excess copper could cause the peptide to fold in an unwanted way (Figure 99-B).

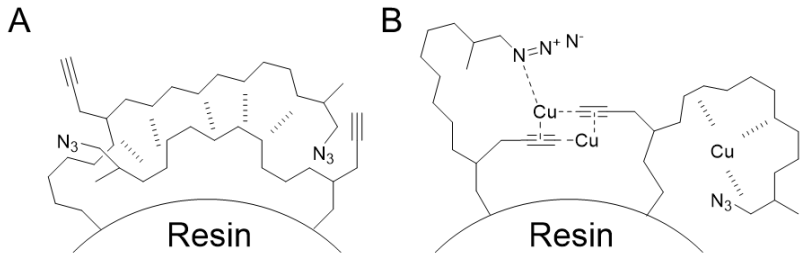

Figure 99- Representations of Detrimental Interactions for On-Resin CuAAC **A** Hydrogen Bonding Between Polymer Chains **B** Copper Coordination

To overcome the first problem, a dual solvent system of 4:1 DCM:TFE was used. This would both swell the resin, separating the peptide chains and due to the trifluoroethanol addition would fold the peptides/peptomers into a helical structure, thereby increasing the chance of cyclisation over cyclodimerisation. The second problem was tackled by using 2 equivalents of tetrakis(acetonitrile)copper(I) tetrafluoroborate, $Cu(MeCN)_4BF_4$, a copper salt with increased solubility in organic solvents and a non-interfering counteranion. This was premixed in the solvent mixture with 2 equivalents of Tris[(1-benzyl-1*H*-1,2,3-triazol-4-yl)methyl]amine, TBTA, a ligand commonly used to protect the Cu(I) centre from redox and to solubilise the cation in organic solvents.[264] The polydentate nature of the TBTA ligand also increases the likelihood of two copper centres being close in space, minimising any unwanted chelating to the peptide backbone (Figure 100).[265] The resin bound peptides were left in this solution at room temperature for 48 h and a test cleavage performed. An observable shift in retention time suggested the reaction was complete (see Figure 103 in Section 3.2.3).

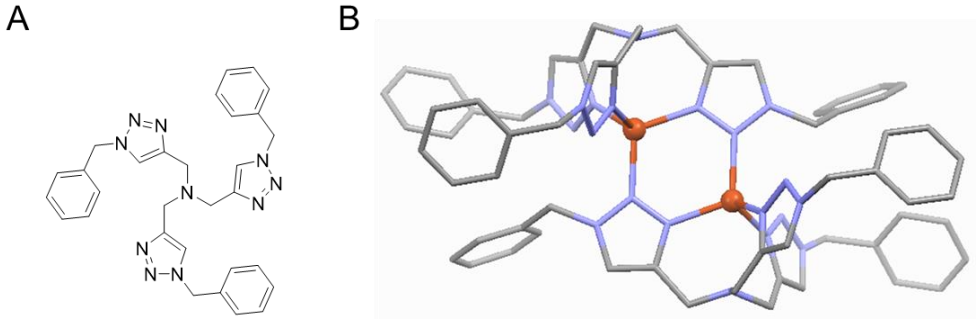

Figure 100- **A** TBTA Ligand **B** Bis-Copper TBTA Complex.[265]

To accelerate the reaction time, microwave heating was used. Microwave heating is now commonly used in peptide synthesis, decreasing reaction times and increasing the purity of the crude peptide.[266] To the on-resin peptides/peptomers $Cu(MeCN)_4BF_4$ and TBTA were added. This was then dissolved in degassed DMSO, a solvent that is able to solubilise metal ions as well as organic compounds, disrupts hydrogen bonding and has a high tanδ value, a ratio that describes the efficiency of microwave heating for solvents.[267] The reaction vial was heated at 80 °C for 0.5 h and was monitored using infra-red spectroscopy. After the 0.5 h reaction time a small amount of resin was washed and then swollen in DCM. The disappearance of the characteristic azide peak at 2096 cm^{-1} (Figure 101) indicated that the reaction had gone to completion. While this is an improvement over the previous reaction conditions, there is still scope for further investigation and enhancement.

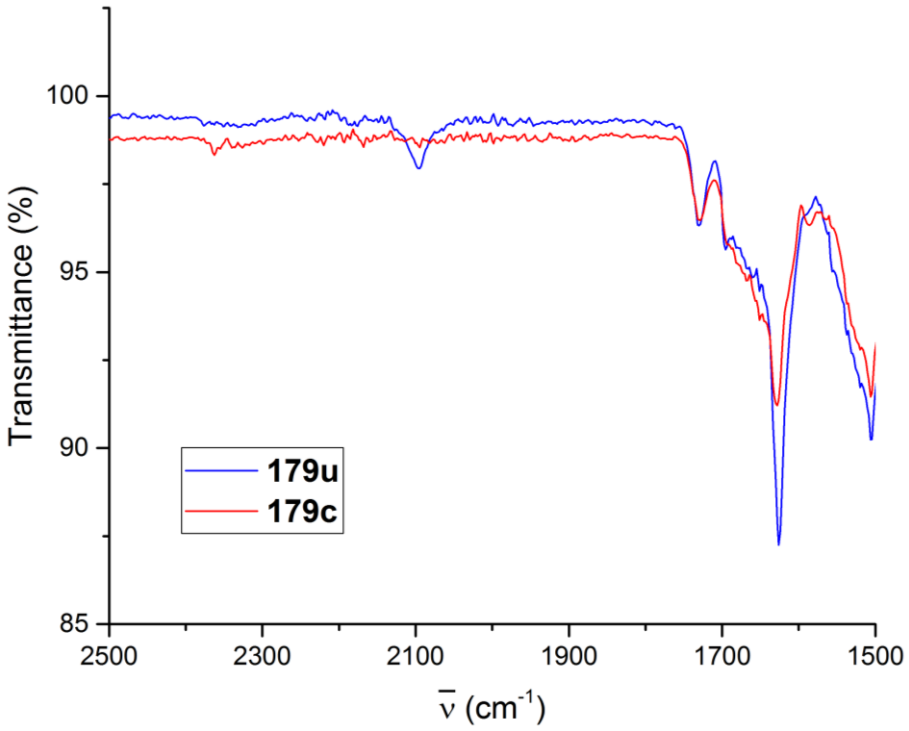

Figure 101- Overlayed IR Spectra Showing Disappearance of Azide Peak after Microwave Assisted On-Bead Cyclisation of peptide **179**

3.2.3 Peptide Purification

Following cleavage from the resin, the uncyclised and cyclised peptides were purified using semi-preparative reverse-phase HPLC. Water and acetonitrile, standard solvent choices for RP-HPLC, with a 0.1% TFA additive were used to elute the peptides from the column. By monitoring both at 220 nm and 280 nm, wavelengths absorbed by amides and aromatic side chains respectively, it was relatively facile to note when the peptides were eluting. The only charged position (at pH 7) in the sequence was the carboxy acid of the glutamic acid residue. This meant that the peptides eluted at a relatively low H_2O:MeCN ratio, approximately 3:2, as the glutamic acid side chain was protonated by the TFA additive making the peptide relatively hydrophobic. After purification, all the isolated peptides were found to be ≥ 90% pure by analytical RP-HPLC. The uncyclised and cyclised peptides were analysed by electrospray ionisation (ESI) mass spectrometry (Table 29). Although there is no change in mass after cyclisation, and therefore no way to tell whether cyclisation has occurred using this method, the presence of dimeric and oligomeric products was able to be discounted. This was possible as there was no evidence of $[2M+X]^+$ (where X = H, Na) peaks present (Figure 102).

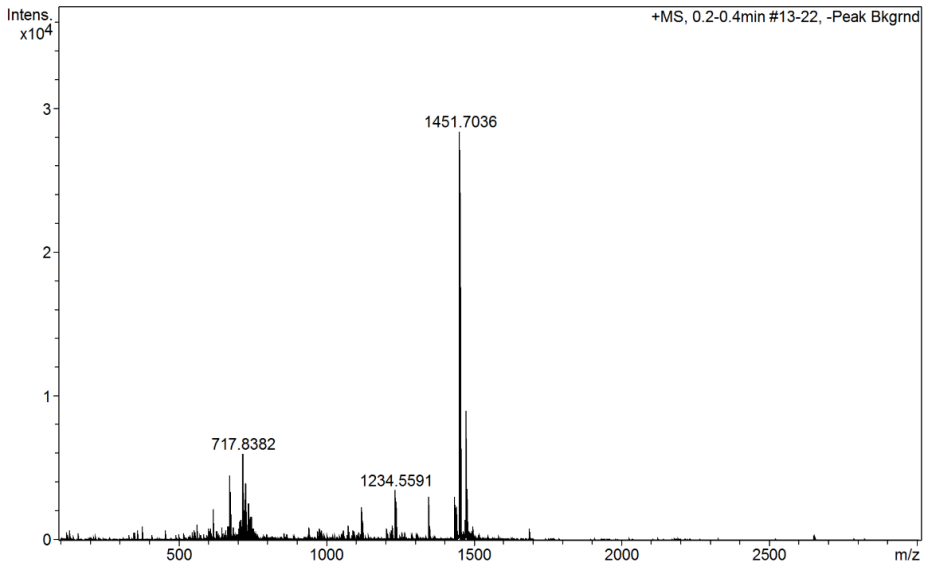

Figure 102- ESI-MS Spectrum of peptide **179c** (1,4-(*S*,*S*)), showing no $[2M+X]^+$ peaks, with 1451.7036 $[M+H]^+$.

Table 29- Elution Times and Observed Ions of Peptide/Peptomer Library

Peptide	Notation	R_t (minute)[a]	Mass (Da)	Theor. Mass (Da)	Ion
174	Native	10	1350.6289	1350.6341	$[M+Na]^+$
179u	1,4-*S*,*S*-u	23[b]	1451.6916	1451.6954	$[M+H]^+$
179c	1,4-*S*,*S*-c	8	1451.7036	1451.6954	$[M+H]^+$
180u	1,4-*S*,*R*-u	18	1473.6828	1473.6773	$[M+Na]^+$
180c	1,4-*S*,*R*-c	7	1451.7029	1451.6954	[M+H]+
181u	1,4-*R*,*S*-u	16	1451.6953	1451.6954	$[M+H]^+$
181c	1,4-*R*,*S*-c	7	1451.6921	1451.6954	$[M+H]^+$
182u	1,4-*R*,*R*-u	16	1473.6769	1473.6773	$[M+Na]^+$
182c	1,4-*R*,*R*-c	7	1451.7002	1451.6954	$[M+H]^+$
183u	4,1-*S*,*S*-u	16	1473.6770	1473.6773	$[M+Na]^+$
183c	4,1-*S*,*S*-c	9	1451.7127	1451.6954	$[M+H]^+$
184u	4,1-*S*,*R*-u	16	1451.7028	1451.6954	$[M+H]^+$
184c	4,1-*S*,*R*-c	8	1451.7075	1451.6954	$[M+H]^+$
185u	4,1-*R*,*S*-u	16	1451.7014	1451.6954	$[M+H]^+$
185c	4,1-*R*,*S*-c	6	1451.7048	1451.6954	$[M+H]^+$
186u	4,1-*R*,*R*-u	16	1473.6824	1473.6773	$[M+Na]^+$
186c	4,1-*R*,*R*-c	7	1451.6974	1451.6954	$[M+H]^+$
189	*N*-Native	5	1350.6389	1350.6341	$[M+Na]^+$
190u	1,4-*N*,*N*-u	14	1471.7047	1471.6981	$[M+H]^+$
190c	1,4-*N*,*N*-c	5	1449.7229	1449.7161	$[M+H]^+$
191u	4,1-*N*,*N*-u	11	1471.7052	1471.6981	$[M+Na]^+$
191c	4,1-*N*,*N*-c	5	1449.7165	1449.7161	$[M+H]^+$

a Isocratic gradient 62:38 (Water + 0.1% TFA:MeCN + 0.1% TFA);
b Isocratic gradient 65:35 (Water + 0.1% TFA:MeCN + 0.1% TFA)

When compared to the native peptide, the uncyclised peptides all had greater elution times with the converse being true for the cyclised peptides (Figure 103). This is consistent with the premise that cyclic peptides are more easily solubilisable in organic media than their uncyclised counterparts.

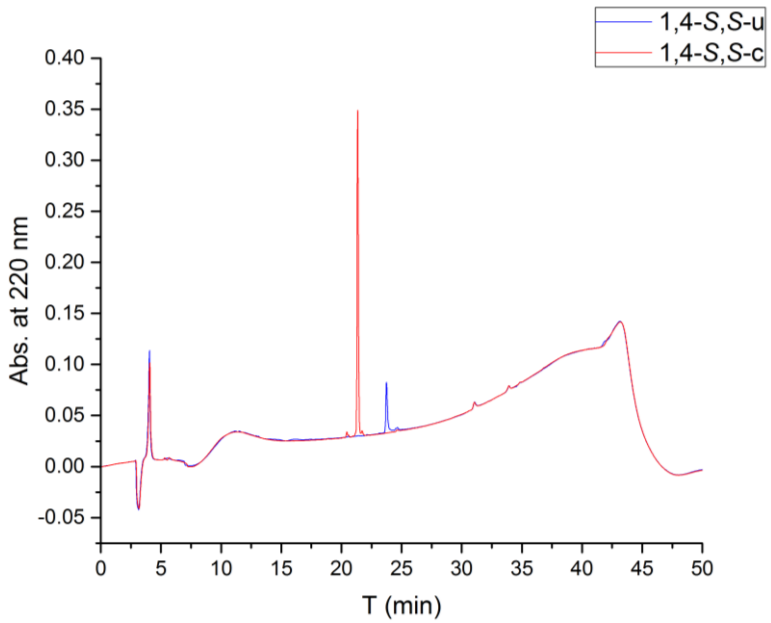

Figure 103- HPLC Spectra of **179u** (Blue) and **179c** (Red).

3.3 Circular Dichroism

After purification, solutions of the peptides (Figure 104) and peptomers (Figure 105) were made up for analysis by circular dichroism. As helical induction from the kosmotropicity of trifluoroethanol levels off after 25% in aqueous solutions,[64] this solvent system was chosen.

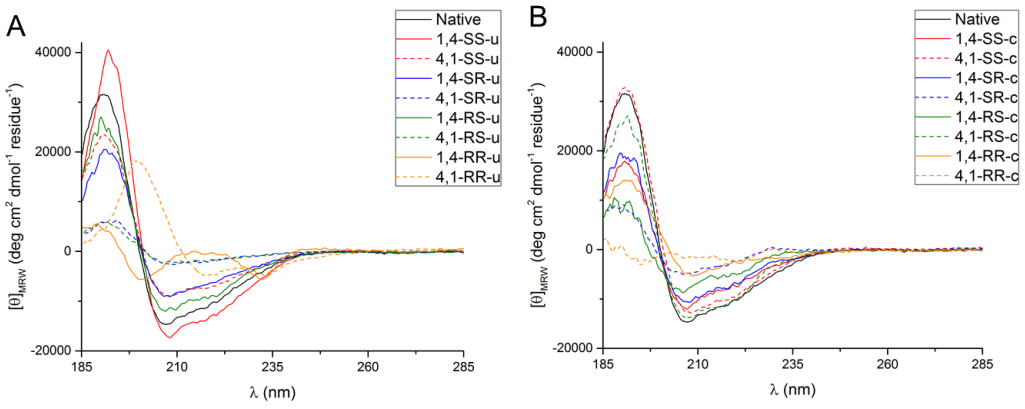

Figure 104- CD Spectra of **A** Native Peptide **174** (Black) and Uncyclised Peptides **179u**-**186u** and **B** Native Peptide **174** (Black) and Cyclised Peptides **179c**-**186c** in 25% TFE in water. Enlarged copies are available in Section **5.3**.

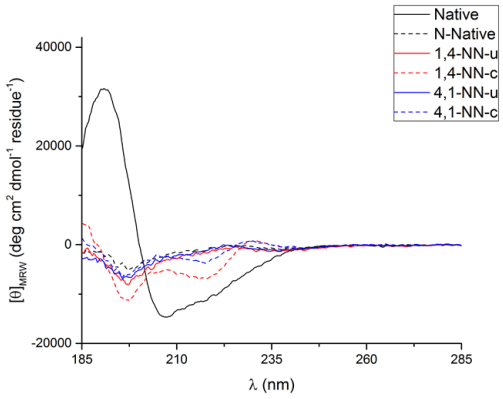

Figure 105- CD Spectra of Native Peptide **174** (Solid Black) and Peptomers **189** (Dashed Black), **190u/c** (red) and **191u/c** (blue) in 25% TFE in water. An enlarged copy is available in Section **5.3**.

To calculate % helicity for each of the peptides/peptomers, a theoretical minimum value at 222 nm must be calculated. This can be calculated from the equation (−44 000 + 250T)(1 − k/n), where T is the temperature that the spectra were recorded at in degrees Celsius, k is a finite length correction (commonly 4.0 for small peptides) and n is the number of amide bonds in the molecules.[45,121] As the peptides/peptomers are N-acetylated and C-amidated, this must be taken into account also, giving an n-value of 12. This gives the theoretical minimum at 222 nm as -25166. This was used to calculate the % helicity of each of the peptides and peptomers from the spectra. These values were compared to the % helicity of the native sequence, and each of the cyclised peptides was compared with the uncyclised counterpart (Table 30).

Table 30- Calculated % Helicity of Peptide/Peptomer Library

Peptide	Notation	$[\theta]_{222}$	$[\theta]_{222}/[\theta]_{Max}$	% Helicity	% H wrt Native	% H wrt u
174	Native	-9243.69	0.367	37	-	-
179u	1,4-*SS*-u	-11766.9	0.468	47	10	-
179c	1,4-*SS*-c	-6266.8	0.249	25	-12	-22
180u	1,4-*SR*-u	-5356.71	0.213	21	-15	-
180c	1,4-*SR*-c	-6123.75	0.243	24	-12	3
181u	1,4-*RS*-u	-8148.33	0.324	32	-4	-
181c	1,4-*RS*-c	-4458.26	0.177	18	-19	-15
182u	1,4-*RR*-u	-710.88	0.028	3	-34	-
182c	1,4-*RR*-c	-2491.73	0.099	10	-27	7
183u	4,1-*SS*-u	-6262.08	0.249	25	-12	-
183c	4,1-*SS*-c	-8376.37	0.333	33	-3	8
184u	4,1-*SR*-u	-1509.63	0.060	6	-31	-
184c	4,1-*SR*-c	-1963.13	0.078	8	-29	2
185u	4,1-*RS*-u	-1574.34	0.063	6	-30	-
185c	4,1-*RS*-c	-9068.38	0.360	36	-1	30
186u	4,1-*RR*-u	-3911.54	0.155	16	-21	-
186c	4,1-*RR*-c	-2196.19	0.087	9	-28	-7
189	*N*-Native	-506.724	0.020	2	-35	-
190u	1,4-(*NN*)-u	-918.208	0.036	4	-33	-
190c	1,4-(*NN*)-c	-4728.12	0.188	19	-18	15
191u	4,1-(*NN*)-u	-126.48	0.005	1	-36	-
191c	4,1-(*NN*)-c	-1834.6	0.073	7	-29	7

Interestingly, the % helicity of the peptides/peptomers follows no observable pattern. Each of the sequences displays a different maximum at 222 nm. The greatest observed increase in helicity with respect to the native sequence **174** was the uncyclised 1,4-(*S*,*S*) peptide **179u**. There is no known research into mutations of the alanine residues within the native sequence, and so it is entirely plausible that some proteinogenic residues may have a similar effect of increasing the α-helicity of the sequence without cyclisation. The greatest increase in helicity after cyclisation was seen in the 4,1-(*R*,*S*) peptide **185**. The uncyclised peptide displayed little helicity (6%), even in helix forming trifluoroethanol. This may be due to the inclusion of a helix breaking d-amino acid. However, the cyclised peptide showed a % helicity comparable to the native sequence (36% and 37% respectively). By comparison, the 1,4-(*R*,*S*) peptide **181** exhibited the second greatest decrease in helicity after cyclisation (32% to 18%). The

greatest decrease in α-helicity after cyclisation was seen in the 1,4-(*S*,*S*) peptide **179** (47% to 25%). Contrasting this, the % helicity of the 4,1-(*S*,*S*) peptide **183** increases following cyclisation (25% to 33%). Analysis of the peptomers **189**, **190u**/**c** and **191u**/**c** clearly show the detriment of removing hydrogen bonding from the sequence, with the N-Native peptomer **189** and uncyclised peptomers exhibiting almost no helicity at all. Nonetheless, the cyclic 1,4-(*N*,*N*) peptomer **190c** displayed an increase in % helicity compared to the uncyclised sequence (4% to 19%). However, looking at the CD spectrum (Figure 105) the graph looks more like the spectrum of a 3_{10}-helix, suggesting a shorter linker may be effective. A number of conclusions can be drawn from the above results:

1. While all the cyclised peptides and peptomers were less helical than the native, the fact that **179u** (1,4-*S*,*S*-u) was shown to be more helical than the native suggests that it may be possible to increase the helicity of the native peptide using a stapling methodology in the (*i*,*i*+4) position selected.

2. Cyclisation did increase the % helicity of some of the peptides with respect to the uncyclised counterparts, but not all. It is possible that an investigation into linker length or asymmetric linkers would show further increases the helicity of the peptides.

3. Although the cyclic peptomers **190c** and **191c** had a greater helicity than the uncyclised counterparts, all the peptomers, including **189** (*N*-Native) were nowhere near as helical as the native peptide sequence, highlighting the devastating effect of knocking out central hydrogen bonding on α-helicity.

4. Importantly, all of the circular dichroism results for every peptide and peptomer were different. While this could be due to the ether moiety in the propargyl serine monomer, it shows that it is critical to screen all permutations available in any stapling methodology to find the most effective pairing.

3.4 Future Work

With the library of peptidyl inhibitors synthesised and purified, a number of further analyses could be performed. These would mostly comprise of *in vitro* experiments. One of the first series of experiments would examine the library's stability toward proteolytic enzymes compared to the native sequence. This would likely be done with chymotrypsin, as opposed to trypsin, as the sequence contains neither a lysine nor arginine residues which are required for recognition by trypsin. Chymotrypsin cleaves peptides at the carboxyl end of bulky, hydrophobic residues such as phenylalanine, tyrosine and tryptophan. As the sequence contains all three of these residues this would be an effective experiment to probe any increased stability toward proteolytic enzymes.

The next experiment would examine the binding affinity of the peptide library to MDM2/MDMX. This could be done using isothermal titration calorimetry (ITC)[268] or surface plasmon resonance (SPR).[269] While SPR requires an immobilised protein target, it lends itself to high-throughput screening which, out of these two techniques, may be better to investigate a library of inhibitors.

Continuing it would be possible to measure cell penetrance and activity using the T22 reporter assay.[270,271] This does not require the peptides to be fluorescently labelled, as it relies on T22 cells transfected with a p53 responsive β-galactosidase reporter, which are then stained. This also avoids attaching a highly hydrophobic fluorescent dye to the peptides, which may have some effect on the ability of the sequence to enter cells. Another similar method would involve probing both cell penetrance and binding with cellular thermal shift assays (CETSAs).[272,273] This relatively new technique relies on the different melting temperatures of the target protein with or without a bound ligand, even in cells. This techniques has already been used to probe the affinity of stapled peptides targeting the p53-MDM2 interaction[274] and avoids the use of fluorescence which, as mentioned, can alter the ability of a peptide to penetrate a cell.

3.5 Summary

For the first time, a peptide targeting the p53 MDM2 interaction has been stapled using the copper alkyne-azide cycloaddition reaction. The staple was in a (*i*,*i*+4) position, which has also not previously been attempted for a p53 MDM2 target. All possible stapling diastereomers were synthesised using non-natural amino acids for cyclisation. In addition, peptomers containing novel *N*-substituted glycine monomers were also synthesised for the first time. The majority of the peptides and peptomers were cyclised on-resin, which was facilitated by microwave heating. Although none of the cyclic peptides or peptomers were more helical than the native target sequence by circular dichroism, increases in helicity with respect to some of the uncyclised peptides suggest that further investigation into this methodology could yield desired results.

Chapter 4- Design of a Bis-Copper (I) Ligand for use in the Copper (I) Alkyne – Azide Cycloaddition Reaction

4 The Copper (I) Alkyne–Azide Cycloaddition (CuAAC) Reaction

The copper (I) alkyne-azide cycloaddition (CuAAC) reaction was first reported in 2002 by the Sharpless and Meldal groups independently.[126,127] The non-catalysed 1,3-dipolar cycloaddition, explored by Huisgen,[124] heats an azide and an alkyne for hours or days to form a mixture of 1,2,3-triazole regioisomers (Figure 106-A). However, with the addition of catalytic amounts of Cu(I), the 1,4-regioisomer is formed selectively under much milder conditions and in shorter times (Figure 106-B).

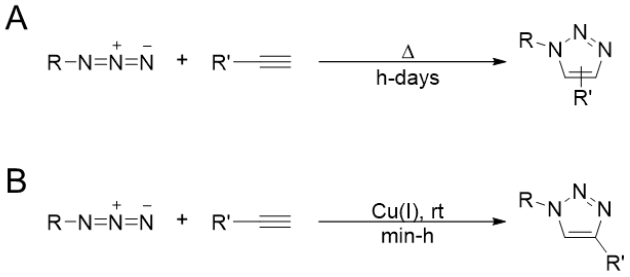

Figure 106- Alkyne-Azide Cycloaddition **A** Huisgen Cycloaddition **B** Copper(I) Catalysed Cycloaddition

While there is still debate about the specifics of the catalytic mechanism, it has been established that the rate of the reaction is second order with respect to the concentration of Cu(I).[139,275] One equivalent is thought to coordinate to the pi orbitals of the alkyne, reducing the pK_a of the methine proton[276] (Figure 107-I). This increase in acidity allows the formation of the copper alkylidine from the second equivalent (Figure 107-II). The dicopper alkylidine is able to coordinate the organoazide, bringing the two reactants in close proximity (Figure 107-III). Rearrangement of the bonds forms the copper triazolide,[277] via some dicopper intermediate[278–280] (Figure 107-IV). This ring is protonated from unreacted alkyne starting material or from solution, regenerating the catalyst (Figure 107-V).

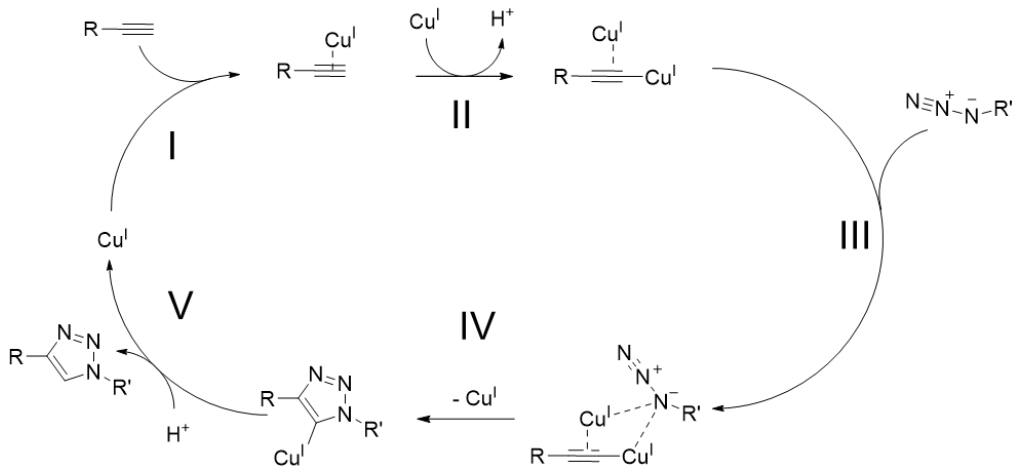

Figure 107- Catalytic Cycle of CuAAC: **I** Cu(I) coordinates to alkyne pi bonds, reducing pK_a of terminal proton **II** formation of copper alkylidine **III** azide coordinates to copper alkylidine **IV** rearrangement to form copper triazolide **V** protonation of copper triazolide and regeneration of catalyst

4.1 Ligands used in CuAAC

The use of Cu(I) presents some problems synthetically. The metal cation has poor solubility in organic media and is easily oxidised to Cu(II).[281,282] The unwanted oxidation can be suppressed by addition of a reducing agent, commonly sodium ascorbate is used.[283] A miscible bisolvent mixture, for example water and *tert*-butanol, helps solvate both the organic reactants and the ionic catalyst, though the reaction can proceed in water alone.[127] Commonly, an organic ligand is added to both solvate the copper cation and help protect the copper centre from oxidation.

4.1.1 Tris-(benzyltriazolylmethyl)amine (TBTA)

One of the first designed ligands discovered that exhibited increased catalytic activity was tris-(benzyltriazolylmethyl)amine (TBTA) from Chan *et al*.[264] (Figure 108-A). When screening a number of soft coordinating ligands, it was found that the oligotriazoles derived from proparylamines showed the greatest enhancement, even under challenging conditions (1 mol% loading of Cu(I) and ligand, no use of reducing agent, no attempt to purge oxygen from solvent). Cyclic voltammetric analysis of a water soluble derivative of TBTA, tris(hydroxypropyltriazolylmethyl)amine (THPTA,

Figure 108-B), exhibited an increase in the redox potential of approximately 300 mV, giving direct evidence that the ligand protects the sensitive Cu(I) centre.

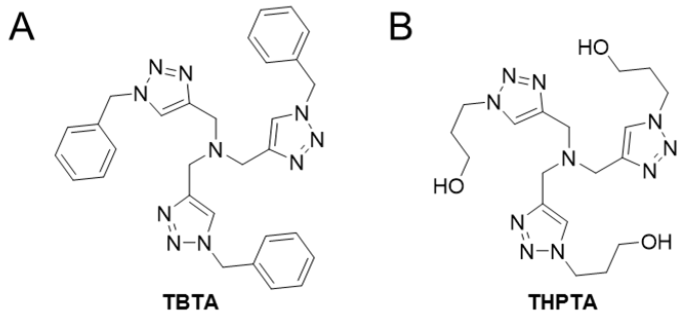

Figure 108- Polytriazole ligands **A** TBTA and **B** THPTA

The synthesis of TBTA uses the CuAAC reaction in a one-step procedure from benzyl azide (BnN_3) and tripropargylamine ($N(Pra)_3$) in an autocatalytic process (Figure 109).

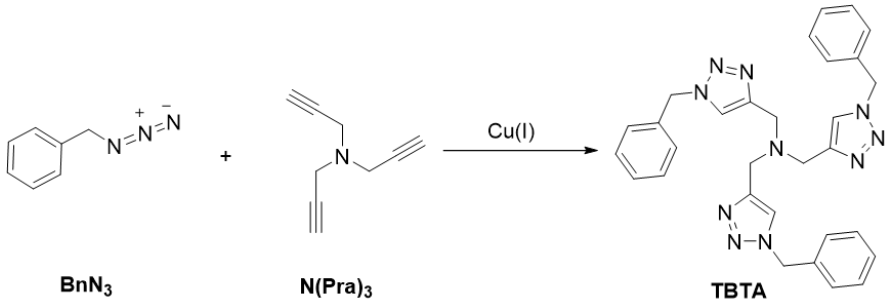

Figure 109- Synthesis of TBTA

Donnelly *et al.*[265] were able to obtain a crystal structure of a bis-Cu(I) bis-TBTA complex (Figure 110). This isolable but oxygen sensitive complex showed that one of the triazolyl moieties of each ligand bridges the two copper cations, with the tertiary amine having no part in complexation in the solid state. The formation of the dimer may be a function of the non-interfering counterion of the copper tetrafluoroborate salt. When the complex was added as a catalyst for an azide-alkyne cycloaddition the reaction proceeded as normal, with no need for an additional reducing agent.

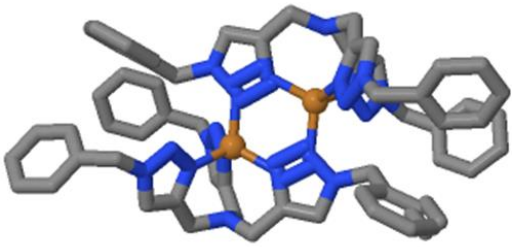

Figure 110- Crystal structure of bis-Cu(I) bis-TBTA complex, CCDC reference code OFILAR.[265]

4.1.2 Tris(*N*[1]-[4-carboxylatobutyl]benzimidazol-2-ylmethyl)amine tripotassium - $(BimC_4A)_3$

In a similar investigation, Rodionov *et al.*[284] looked into the utility of copper ligands primarily based on Tris(2-benzimidazolylmethyl)amine $(BimH)_3$ (TMBA, Figure 111-A). This core is a known ligand of a number of metals, with crystal structure data of copper(I) iodide coordinated to an *N*'-[n]propyl derivative available[285] (Figure 111-B).

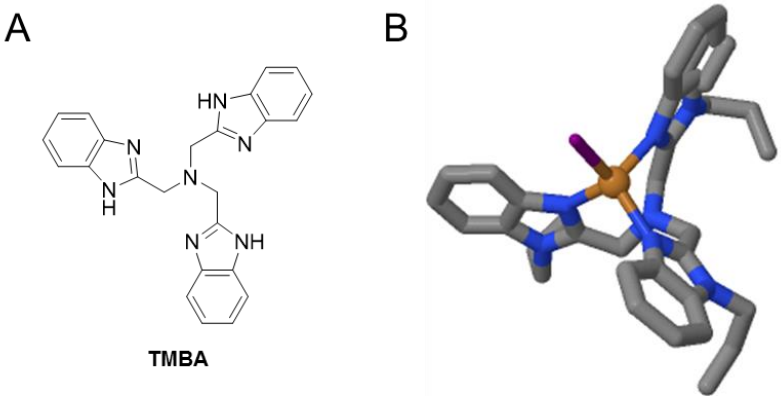

Figure 111- Cu(I) trisbenzimidazole ligands **A** $(BimH)_3$ **B** Crystal structure of Copper [*N*'-propyl tris(2-benzimidazolylmethyl)amine] iodide, CCDC reference code CERRUM.[285]

After using reaction calorimetry to screen a number of alkylated benzimidazole derivatives the ligand Tris(N^1-[4-carboxylatobutyl]benzimidazol-2-ylmethyl)amine tripotassium $(BimC_4A)_3$ was shown to be the most efficient (Figure 112).[284] This ligand was then compared in a low-loading experiment with both $(BimH)_3$ and TBTA. It was shown that even at loadings of 0.01 mol% of Cu(I) and ligand the desired

triazole product was formed in high yield within 24 h. Additionally, the alkyl carboxylate groups are able to solubilise the ligand in aqueous media, simplifying work-up.

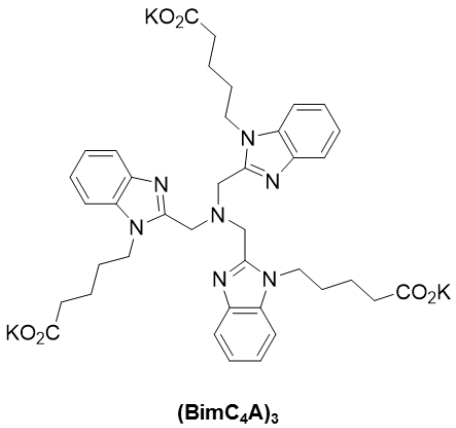

(BimC$_4$A)$_3$

Figure 112- Water soluble Cu(I) ligand tris(N1-[4-carboxylatobutyl]benzimidazol-2-ylmethyl)amine tripotassium - (BimC$_4$A)$_3$[284]

4.2 Ligand Design

With the second order dependence of copper required in the CuAAC reaction[139,275] it follows that a bis-copper chelating ligand, synthesised by somehow tethering together two molecules of TBTA (Figure 113), may affect the reaction beneficially. The close proximity of the two protected copper centres would likely decrease reaction times, given the nature of the copper alkylidine formation.[276] This could result in the reaction requiring lower catalytic loadings, making it possible to use Cu(I) catalysis in bioconjugation reactions where copper toxicity can be an issue.[286,287] The ligand may also provide an air stable bis-copper complex, simplifying reaction procedures.

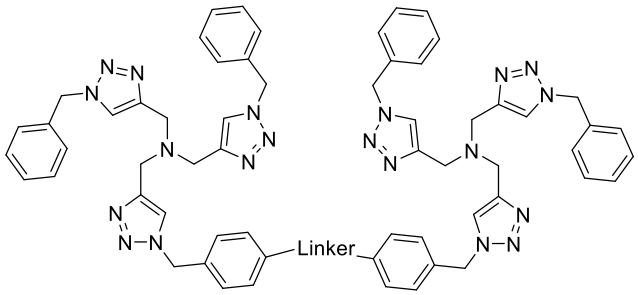

Figure 113- Possible bis-Cu(I) complexes to improve the CuAAC

One of the more obvious solutions to tether the two TBTA molecules is to use a diazide as one of the components in a typical TBTA synthesis.[264] A small library, using both aliphatic and aromatic diazide tethers, would further investigate whether a flexible linker is most efficient, or if there is an optimum rigid arrangement (Figure 114). The bis-TBTA crystal structure shows that the two copper centres are coordinated saturated, therefore the chelating bonds must be broken for the catalysis. Having only one tether would maximise the possibility of the copper centres becoming unsaturated.

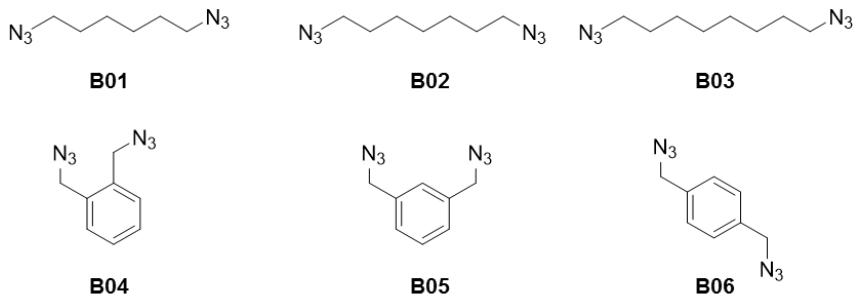

Figure 114- Diazide linkers **B01**-**B06** selected for incorporation into bis-TBTA ligands

To allow for further functionalisation, the benzylic groups of TBTA were replaced with those including a *p*-methyl ester moiety (Figure 115). This may in itself increase the solubility of the highly hydrophobic bis-TBTA ligand. Additionally, it would allow for further functionalisation of the ligand. Transesterification with a PEG group or hydrolysis of the ester to the carboxylate salt could result in increased solubility in aqueous media similar to the $(BimC_4A)_3$ ligand.[284]

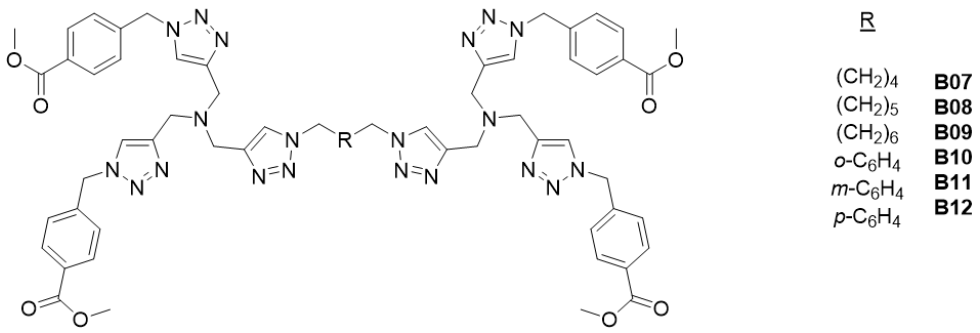

Figure 115- Library of bis Cu(I) ligands **B07**-**B12**

4.3 Ligand Synthesis

A typical TBTA synthesis, as discussed previously, uses 3 equivalents of benzyl azide and one of tripropargylamine.[264] However, synthesis of the ligand required a selectivity in the reaction procedure not required in a TBTA synthesis. Incorporating one equivalent of a diazide tether with four equivalents of 4-(azidomethyl)methyl benzoate **B13** would result in a multitude of products, diminishing the yield of the desired ligand (Figure 116).

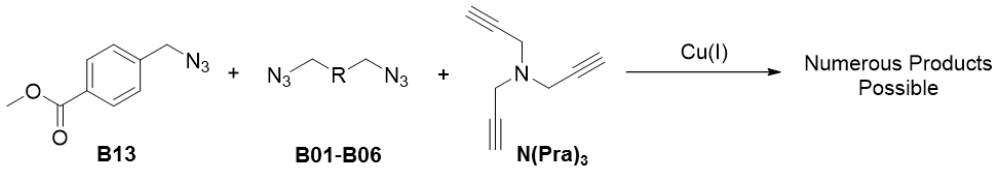

Figure 116- Rejected synthesis of ligand library **B07**-**B12**

Drawing from the literature,[288,289] it was apparent that the ditriazolyl alkyne **B14** could be synthesised from the double reductive amination of propargylamine ($PraNH_2$) and the triazolyl aldehyde **B15** (Figure 117). This would avoid the need to selectively "click" one alkyne with the diazide tether.

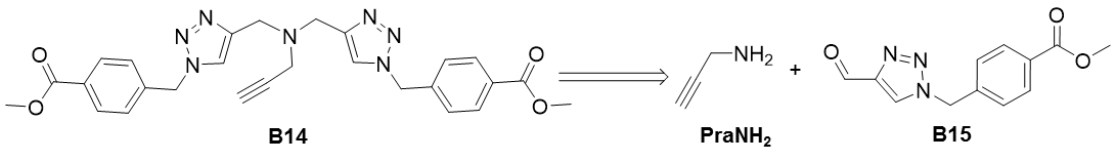

Figure 117- Retrosynthesis of ditriazolyl alkyne **B14**

The triazolyl aldehyde can be synthesised using the CuAAC reaction. This would require the oraganoazide **B13** and propynal (Figure 118). The azide can easily be obtained from the corresponding commercially available bromide 4-(bromomethyl)methyl benzoate (4-(BM)MB). Propynal however is not commercially available and is volatile, so a more accessible, stable alternative was sought. The corresponding alkynyl carboxylic acid and esters would require reduction to the required triazolyl aldehyde **B15**, which is not compatible with the *p*-methyl ester moiety. Propargyl alcohol could be used, but was rejected as the free alcohol would likely be more water soluble and so could present problems during work up. Instead, 3,3-diethoxypropyne (3,3-DEP) was selected. This alkyne is commercially available, and can be easily hydrolysed to the desired triazolyl aldehyde **B15** without hydrolysis of the methyl ester.

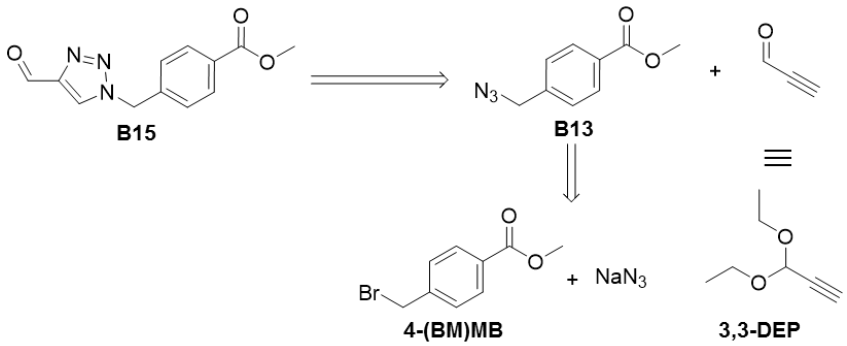

Figure 118- Retrosynthesis of triazolyl aldehyde **B15**

4.3.1 Synthesis of Diazide Tethers

There are a number of ways the six diazide tethers could be synthesised. A modified procedure from Alvares *et al.*[244], which uses sodium azide dissolved in DMSO. The

methodology afforded the 6 diazides **B01**-**B06** from the corresponding dibromides (confirmed by TLC) in excellent yields and in gram quantities (Scheme 26). This methodology did not require heating unlike a number of azide displacements in the literature, which was advantageous as heating could present a risk in low molecular weight diazides, particularly 1,6-diazidohexane **B01**.

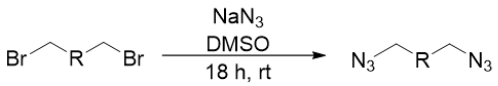

R		Yield (%)
$(CH_2)_4$	**B01**	96
$(CH_2)_5$	**B02**	99
$(CH_2)_6$	**B03**	98
o-C_6H_4	**B04**	99
m-C_6H_4	**B05**	97
p-C_6H_4	**B06**	99

Scheme 26- Synthesis of diazides **B01**-**B06**

4.3.2 Synthesis of Ditriazolyl Alkyne

The desired ditriazolyl alkyne **B14** can be obtained from the double reductive amination of propargylamine and the triazolyl aldehyde **B15**. This methodology avoids the chance of forming an ammonium salt, which could occur during an alkylation approach using propargylamine and bromoester 4-(BM)MB.

4.3.2.1 Synthesis of Triazolyl Aldehyde

Starting from 4-(bromomethyl)methyl benzoate (4-(BM)MB), the previous conditions to obtain the diazides **B01**-**B06** were used (Scheme 27).[244] Fewer equivalents of sodium azide were added to both reduce the explosive risk and to minimise waste, producing the azide **B13** on gram scale in good yield. A shift in retention time (TLC) indicated that the reaction had gone to completion.

Scheme 27- Azidification of bromoester 4-(BM)MB

The copper(I) alkyne-azide cycloaddition with azide **B13** and 3,3-diethoxypropyne (3,3-DEP) was performed with 5 mol% copper(II) sulfate pentahydrate and a 20 mol% excess of sodium ascorbate as the reducing agent (Scheme 28). The reaction was complete after approximately 18 hours at room temperature with quantitative conversion to the triazolyl acetal **B16**.

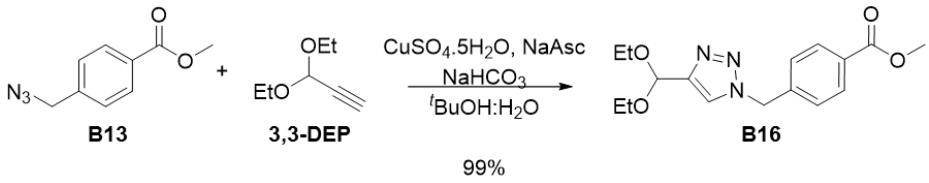

Scheme 28- CuAAC of Azide **B13**

The formation of the triazolyl acetal **B16** was confirmed by ^{1}H NMR (Figure 119). The appearance of the triazole proton E, acetal proton F and the ethyl protons G, H (CH_2) and I (CH_3), plus the shift of the benzylic peak C (4.42 to 5.57 ppm) due to the deshielding effect of the triazole π-electrons proves with high certainty that the desired compound was synthesised. The ethyl CH_2 peaks G and H, instead of appearing as a single quartet, appear as two doublets of quartets (dq). This is because of the diastereotopic nature of these protons and is a common feature of diethyl acetals.[290]

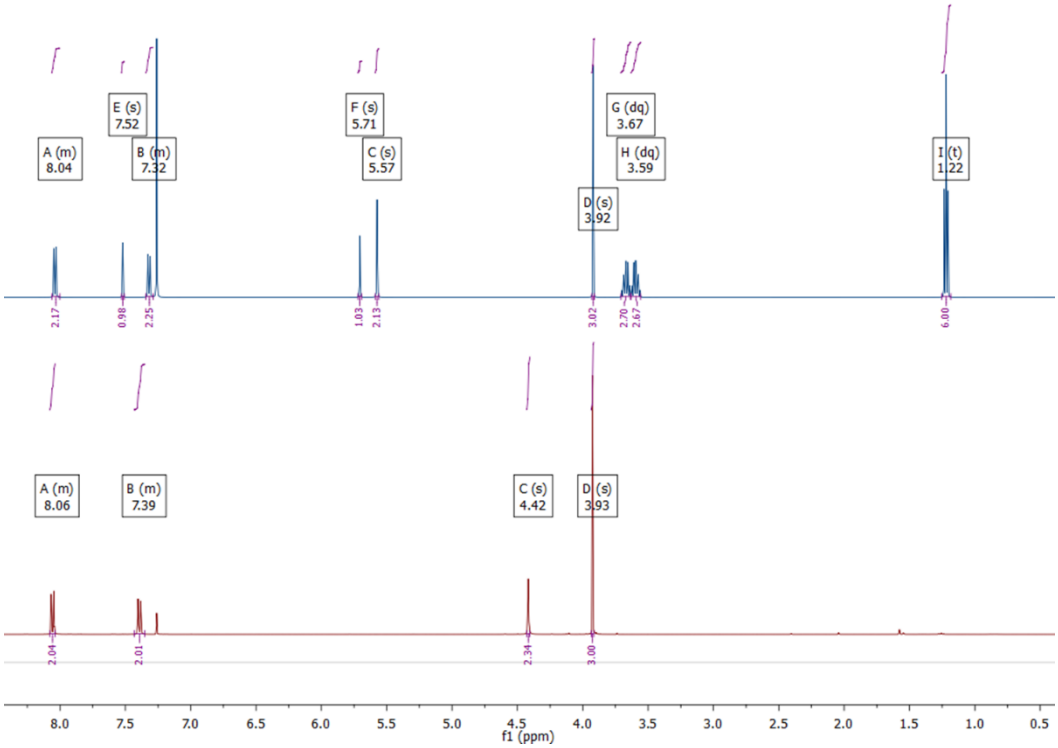

Figure 119- ^{1}H NMR Spectra (8.5 – 0.5 ppm, $CDCl_3$) of azide **B13** (red) and triazolyl acetal **B16** (blue).

Following the methodology described by Wei *et al.*[291] the hydrolysis of the acetal **B16** was achieved (Scheme 29). By stirring the acetal in dry chloroform with a vast excess of TFA (20 eq), the aldehyde was revealed without aqueous acid, thereby preventing any hydrolysis of methyl ester. This "hydrolysis" has been shown to proceed via a hemiacetal trifluoroacetyl ester intermediate **B17**. The reaction was complete in 5 hours at room temperature and afforded the triazolyl aldehyde **B15** in excellent yield.

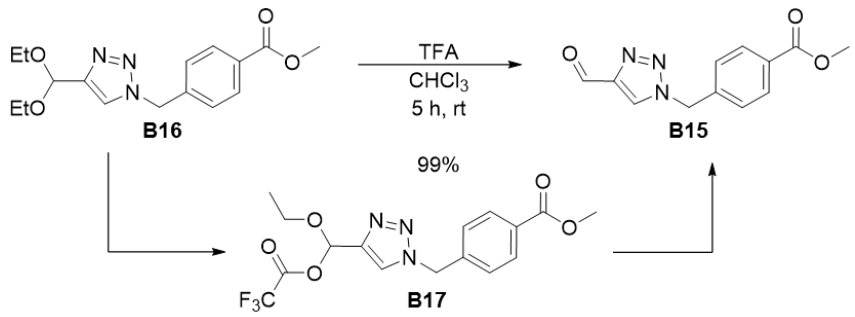

Scheme 29- Deacetalisation of triazolyl acetal **B16**

The formation of the triazolyl aldehyde **B15** was verified by ^{1}H NMR (Figure 120). The disappearance of the ethyl CH_2 (G, H) and CH_3 (I) peaks, and the downfield shifts of the triazole (E) and acetal (F) upon the unmasking of the electron withdrawing aldehyde group all give good evidence that the triazolyl acetal **B16** was hydrolysed.

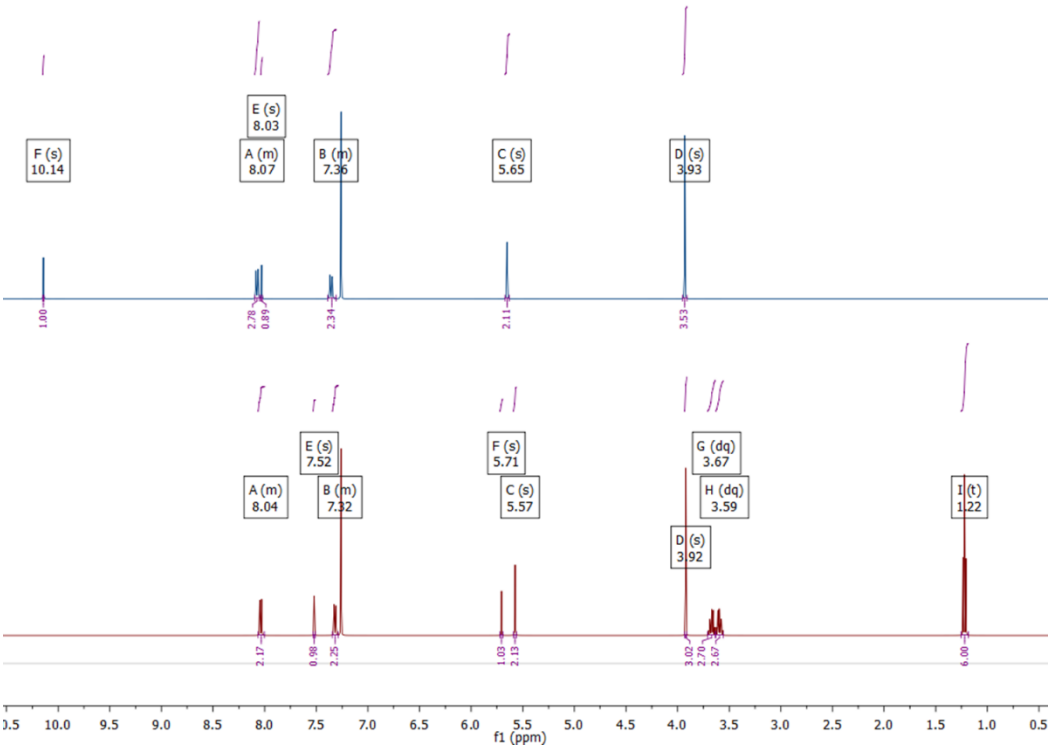

Figure 120- ^{1}H NMR Spectra (10.5 – 0.5 ppm, $CDCl_3$) of triazolyl acetal **B16** (red) and triazolyl aldehyde **B15** (blue).

The triazolyl aldehyde **B15** was synthesised in three steps from commercially available starting material in 96 % overall yield and gram quantities (Scheme 30).

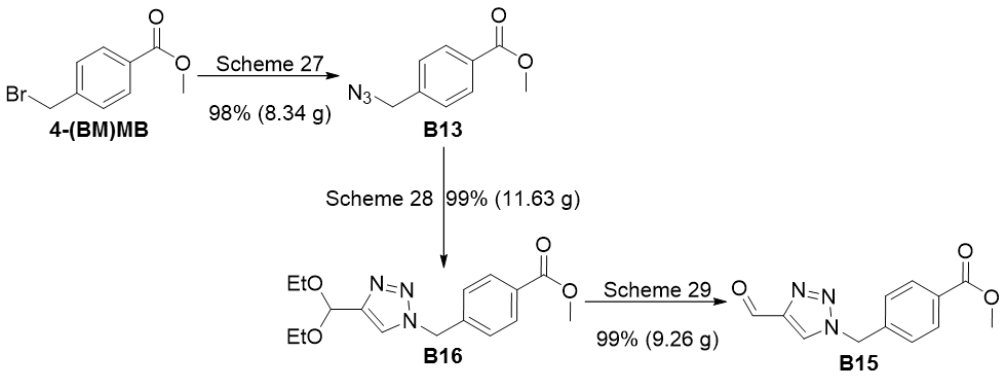

Scheme 30- Complete synthesis of triazolyl aldehyde **B15**

4.3.2.2 **Double Reductive Amination**

With the triazolyl aldehyde **B15** in hand, the double reductive amination with propargylamine could take place. A number of reductants were considered for the transformation. It was decided that sodium triacetoxyborohydride ($NaBH(OAc)_3$, STAB-H) would be the most suitable reductant to use.[292] More common reductants, including the mild sodium borohydride ($NaBH_4$), would reduce the aldehyde before the formation of the imine or iminium intermediates could take place.[293] Alternatively, STAB-H is mild enough to allow the more electrophilic imine and iminium intermediates to form without significant reduction of the aldehyde (Scheme 31).[294] The other milder alternative, sodium cyanoborohydride ($NaBH_3CN$) was rejected due to toxicity issues associated with the reagent.[295]

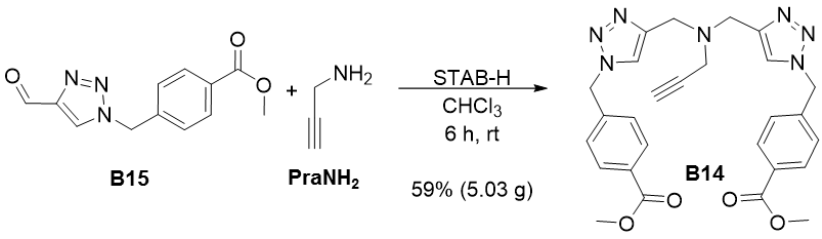

Scheme 31- Double reductive amination of triazolyl aldehyde **B15** and propargylamine

The reaction was complete in 6 hours at room temperature. The ditriazolyl alkyne **B14** was obtained in 59% yield in gram quantity. Assessment of the ^1H NMR spectra

(Figure 121), the appearance of the propargylic CH_2 (J) and CH (K) peaks, with typical doublet and triplet peak splitting of a propargyl $^4J_{HH}$ coupling, suggests that the propargylamine has been incorporated into the product. The shift of the aldehyde peak (F) and the triazole peak (E) upfield (10.14 to 3.84 ppm and 8.03 to 7.53 ppm respectively) shows that the aldehyde has been reduced. As the desired double reductive amination product has a plane of symmetry, no additional new peaks appear, but the peak integrals doubled in comparison to the triazolyl aldehyde **B15**. This evidence confirms that the ditriazolyl alkyne **B14** was formed.

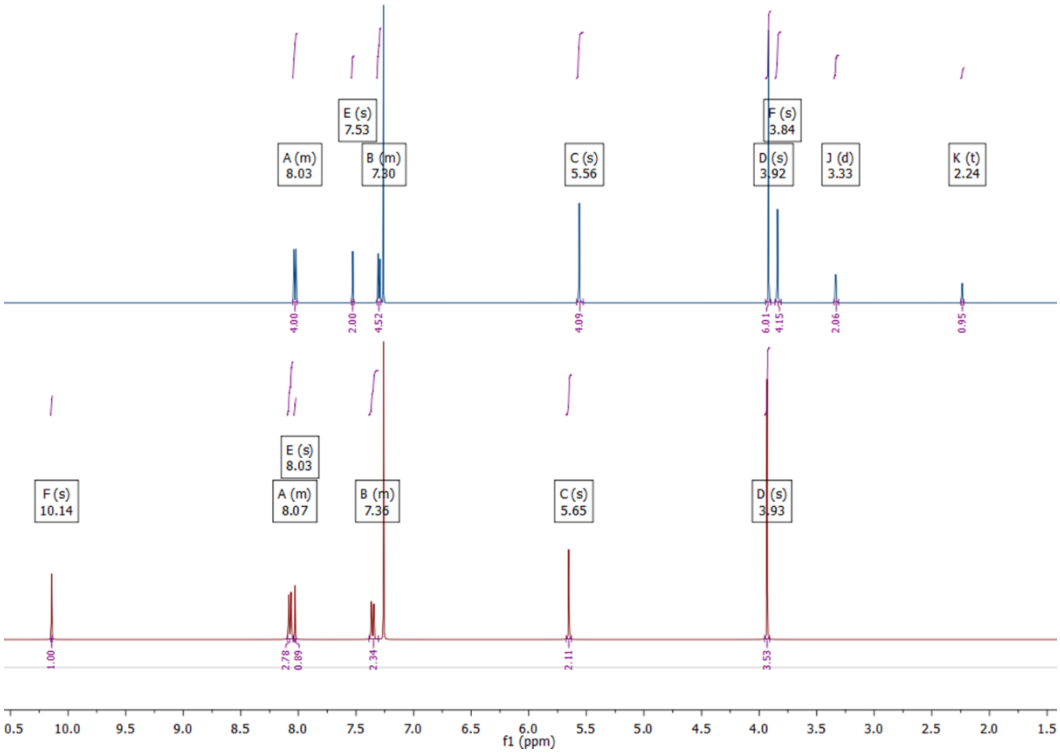

Figure 121- ^{1}H NMR Spectra (10.5 – 1.5 ppm, $CDCl_3$) of triazolyl aldehyde **B15** (red) and ditriazolyl alkyne **B14** (blue).

4.3.3 CuAAC of Bis-TBTA Ligands

After synthesis of the diazides **B01**-**B06** and the ditriazolyl alkyne **B14**, formation of the bis-TBTA ligand library was attempted. As a test substrate, 1,8-diazidooctane **B03** was selected first, as this is the longest and most flexible linker (Scheme 32). After 6

hours under typical CuAAC conditions the bis-TBTA ligand **B09** was isolated in 56% yield.

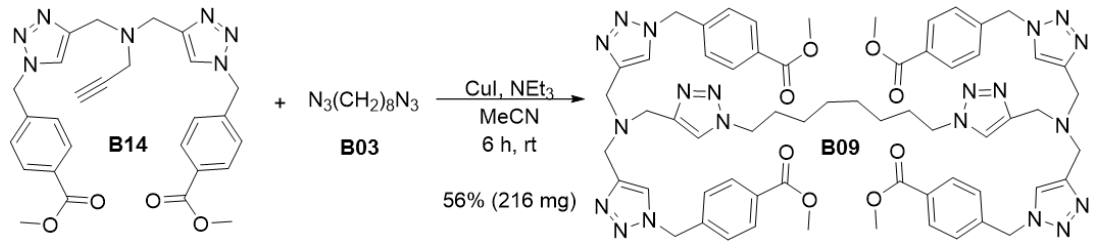

Scheme 32- CuAAC of ditriazolyl alkyne **B14** and diazide **B03**

The ^{1}H NMR spectrum of the isolated product **B09** was compared to the ditriazolyl alkyne starting material **B14** (Figure 122). The transformation of the propargylic CH_2 doublet and CH triplet peaks into downfield singlets (J and K respectively) indicate the formation of the triazole groups. The additional octanyl methylene peaks from the from the diazide linker **B03** (L, M and N) also indicate that the ligand has formed. The N_3CH_2 methylene protons (L) have also moved to a more deshielded position (3.29 to 4.30 ppm, see experimental) also giving evidence of triazole formation. Similar to the ditriazolyl alkyne **B14**, the ligand **B06** has a plane of symmetry. This means that the signals observed are degenerate. Conversely however the mono-CuAAC product would have non-degenerate signals from the octanyl linker, and would therefore be easy to identify. As there are two triazole proton peaks (E and K) in a 2:1 ratio and two triazolylic (analogous to benzylic) proton peaks (F and J) also in a 2:1 ratio, in addition to the degeneracy of the octanyl methylene peaks, it is assured that the desired bis-TBTA ligand **B09** was synthesised.

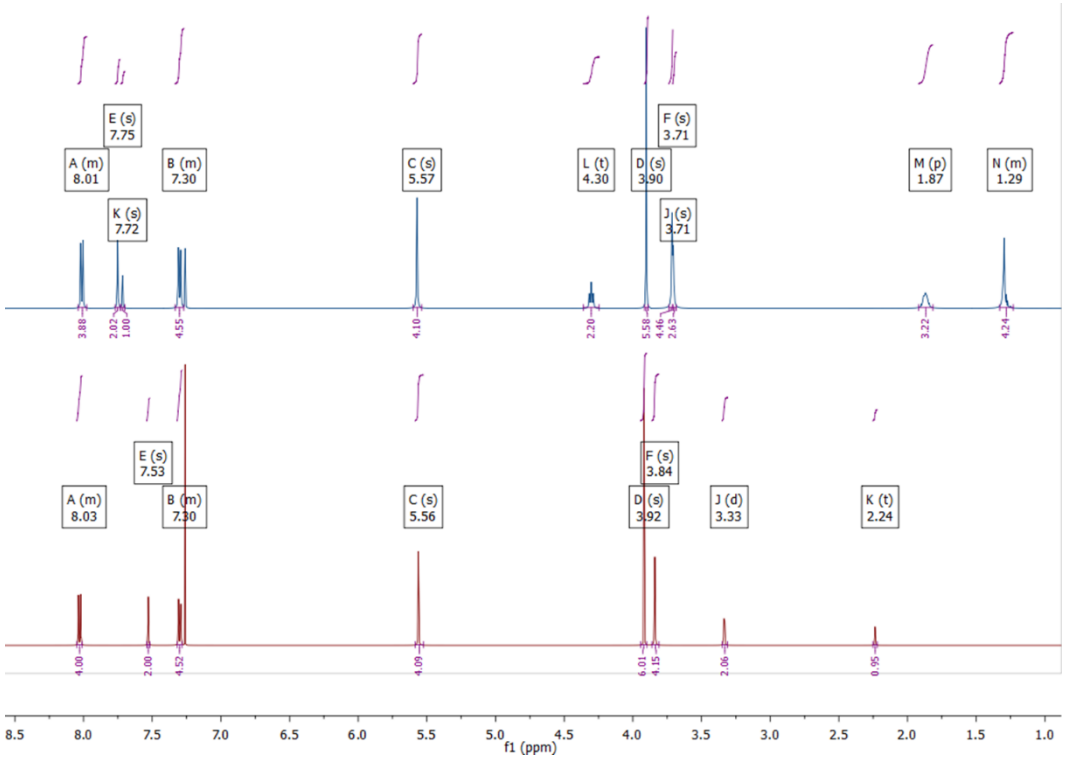

Figure 122- ^{1}H NMR Spectra (8.5 – 1.0 ppm, $CDCl_3$) of ditriazolyl alkyne **B14** (red) and bis-TBTA ligand **B09** (blue).

The next bis-TBTA ligand attempted used 1,4-diazidomethylbenzene **B06** as the tether, employing the same reaction conditions as the 1,8-diazidooctane tether (Scheme 33). After 4 hours the ditriazolyl alkyne **B14** appeared to be consumed (TLC). However, after work up, it became apparent that the bis-TBTA ligand **B12** had not formed in any appreciable amount. A range of reaction conditions were attempted, including altering the copper source and solvent but none were successful (Table 31).

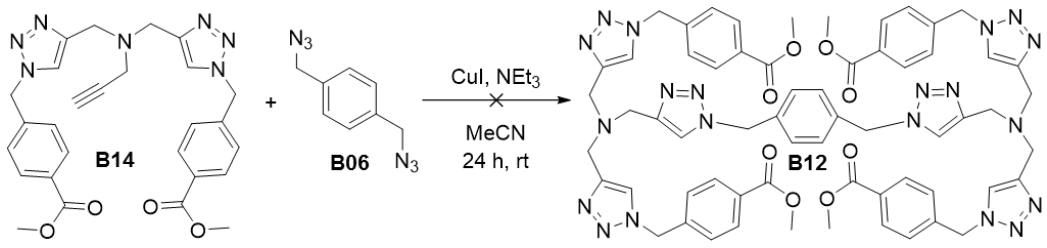

Scheme 33- Failed synthesis of Ligand **B12**

Table 31- Conditions attempted in Synthesis of Ligand **B12**

Cu(I) Source	Amount (mol%)	Solvent	Solvent Ratio	Temp (°C)	Additive	Amount (mol%)
CuI	10	MeCN	-	25	Et_3N	120
CuI	10	MeCN	-	45	Et_3N	120
CuI	10	MeCN	-	25	DIPEA	120
CuI	10	MeCN	-	45	DIPEA	120
CuI	20	MeCN	-	25	Et_3N	120
$CuSO_4$/NaAsc	5/20	$^tBuOH:H_2O$	2:1	25	-	-
$CuSO_4$/NaAsc	5/20	$^tBuOH:H_2O$	2:1	45	-	-
$CuSO_4$/NaAsc	10/20	$^tBuOH:H_2O$	2:1	45	-	-
$CuSO_4$/NaAsc	5/20	$^tBuOH:H_2O$	1:1	45	-	-
$CuSO_4$/NaAsc	10/20	$^tBuOH:H_2O$	2:1	45	$NaHCO_3$	15

To determine whether this poor yield was due to the lack of flexibility in the linker or a function of the tether length, the synthesis of the bis-TBTA ligand **B07** which uses 1,6-diazidohexane **B01** was attempted (Scheme 34). The aliphatic tethers offer a greater degree of flexibility, which would allow the bulky ditriazolyl alkynes to "click" with the shorter tether. However, if the problem was a function of steric bulk and linker length, the shorter tether would not form the bis-TBTA ligand. A number of conditions were attempted (Table 32) however again none gave the desired bis-TBTA ligand **B07**.

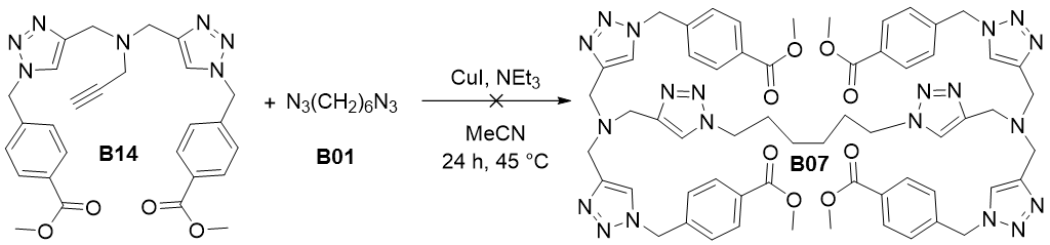

Scheme 34- Failed synthesis of Ligand **B07**

Table 32- Attempted Conditions in synthesis of Ligand **B07**

Cu(I) Source	Amount (mol%)	Solvent	Solvent Ratio	Additive	Amount (mol%)
CuI	10	MeCN	-	Et_3N	120
CuI	10	MeCN	-	DIPEA	120
CuI	20	MeCN	-	Et_3N	120
$CuSO_4$/NaAsc	5/20	$^tBuOH:H_2O$	2:1	-	-
$CuSO_4$/NaAsc	10/20	$^tBuOH:H_2O$	2:1	-	-
$CuSO_4$/NaAsc	10/20	$^tBuOH:H_2O$	2:1	$NaHCO_3$	15

The failure of these reactions highlighted some restriction from either the steric bulk of the ditriazolyl alkyne **B14** or the length of the diazide linkers in yielding the desired products. As such, to obtain the ligands the synthesis route had to be redesigned. However due to time pressures this project was halted in favour of the stapled peptide research.

4.4 Future Work

4.4.1 Alternate Synthesis of Bis-TBTA Ligands

With additional time, the ligand synthesis could have been completed by altering the synthesis sequence to a more stepwise approach. Rather than build the periphery of the ligands and tether them together, the library would be built from the tether out (Figure 123). This would be using similar methodology to that previously attempted. The diazide tethers **B01**-**B06** would form the ditriazolyl diacetals **B18**-**B23** from the cycloaddition of 3,3-diethoxypropyne (3,3-DEP). The acetals could then be hydrolysed to reveal the ditriazolyl dialdehydes **B24**-**B29**.

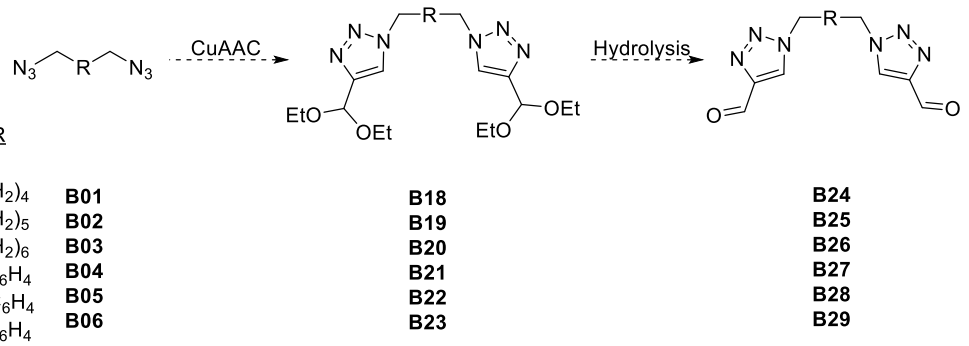

Figure 123- Proposed synthesis of ditriazolyl dialdehydes **B24-B29**

From here, there are a couple of possible routes. In one pathway, the ditriazolyl dialdehydes **B24**-**B29** would undergo reductive amination with dipropargylamine ($NH(Pra)_2$), which is commercially available. This pathway would yield the library of

tetra-alkynes **B30**-**B35**. From here, the CuAAC with azide **B13** would give the complete library of bis-TBTA ligands **B07**-**B12** (Figure 124).

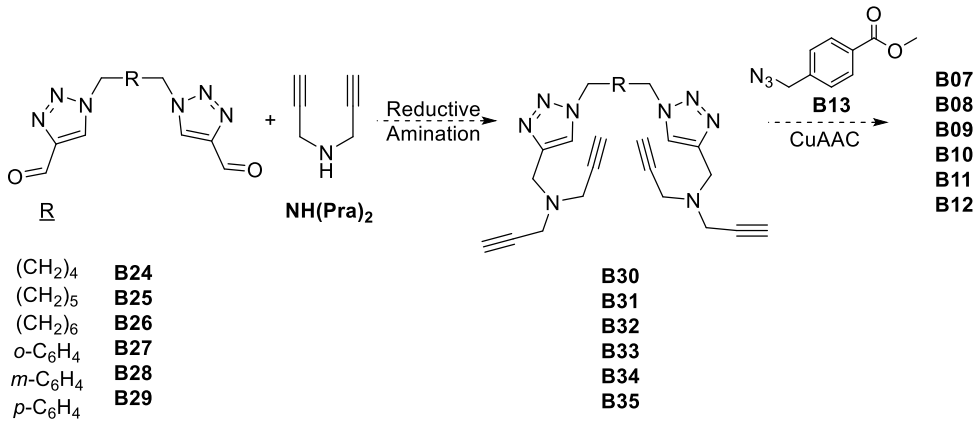

Figure 124- Proposed linear synthesis of ligands **B07**-**B12** from ditriazolyl dialdehydes **B24**-**B29**

In the second route the reductive amination step would be the final step, resulting from the condensation of the ditriazolyl amine **B36**, which is formed from the CuAAC of dipropargylamine ($NH(Pra)_2$) and the azido ester **B13** (Figure 125). This route could present a similar problem to the failed syntheses in that the ditriazolyl amine **B36** is relatively bulky, and so the reaction may not go to completion.

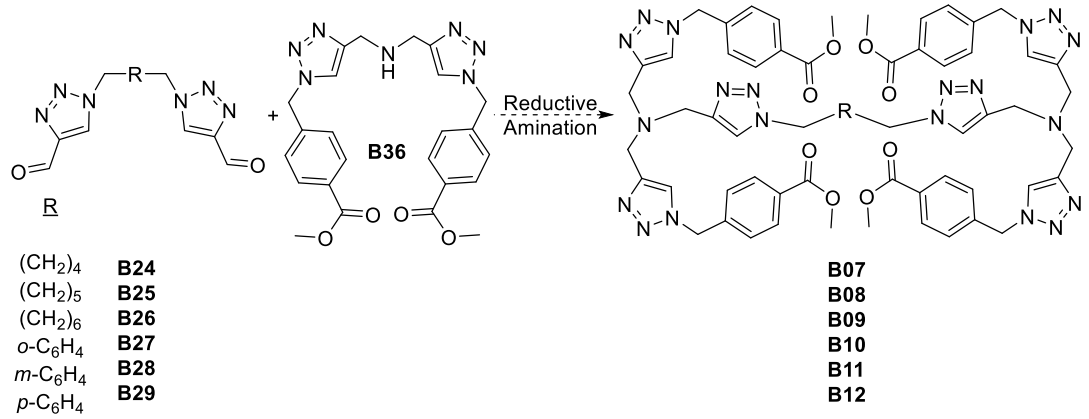

Figure 125- Proposed convergent synthesis of ligands **B07**-**B12** from ditriazolyl dialdehydes **B24**-**B29**

4.4.2 Analysis of Ligands

The utility of the bis-TBTA ligands **B07**-**B12** would be explored by addition to a stereotypical CuAAC reaction, for example benzyl azide and phenylacetylene. Experiments to determine the minimum catalytic loading would be carried out to compare the effectiveness of these new ligands. A direct comparison of the ligands and TBTA would also provide excellent evidence of the increased activity. Crystallisation of the bis-Cu(I) complexes would offer insight into preferred conformations, as it may be possible that rather than forming a bis-Cu(I) monomer, certain tethers would favour dimeric or oligomeric/polymeric structures (Figure 126).

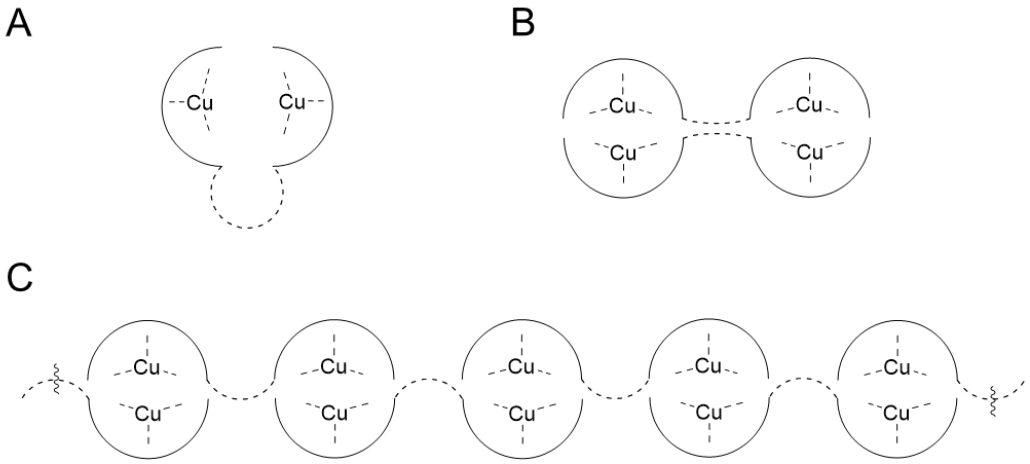

Figure 126- Representations of ligand conformations. Solid curved lines - chelating TBTA moiety; dashed curved lines – linker; **A** monomeric conformation **B** dimeric conformation **C** polymeric conformation

Along with previously discussed ligands, the cyclic voltammetry profile of each of the bis-TBTA library would be valuable to see how well protected both the copper centres are from redox. This, along with experiments probing the "bench stability" of the bis-Cu(I) complexes would reveal the synthetic practicality of the isolated compounds.

4.5 Summary

The synthesis of a small library of novel bis-copper(I) ligands was attempted. While the library was not finished, a new sequence has been proposed for obtaining the complete series. From there, experiments designed to probe the properties and utility of these ligands have been suggested.

Chapter 5- Experimental

5 General Experimental

All non-aqueous reactions were performed in air using oven-dried glassware. All reagents and materials were obtained from commercial suppliers and used without further purification unless otherwise stated. Acetonitrile and dichloromethane were dried and purified by activated alumina column (PPT Glass Contour). Dimethylformamide was purchased over 4 Å molecular sieves (Acros Organics). Triethylamine was distilled over calcium hydride and stored over 4 Å molecular sieves in an inert atmosphere. NMR spectra were obtained on Bruker instruments at the stated frequencies at 300 K unless otherwise stated. Electrospray ionisation mass spectra were obtained on a Bruker MicroToF Focus 2. Electron ionisation mass spectra were obtained on a MAT 900 XP mass spectrometer. Infra-red spectra were obtained neat on a Shimadzu IRAffinity-1S. Optical rotation were measured on an AA Series PolAAr 20 polarimeter with a 1 dm pathlength at 589 nm (sodium D line). Semi-preparative reverse phase HPLC was performed using a Waters 600 (225 µL) system using a Waters 486 tuneable absorbance detector recording at 254 nm equipped with a Phenomonex Luna C18(2), 5 µm, 250 x 21.2 mm column at a flow rate of 21.2 mL minute^{-1}. Analytical reverse phase HPLC analysis using a Waters 600E (100 µL) gradient pump using a Waters 996 PDA equipped with a PhenomenexLuna C18(2), 5 µm, 250 x 4.6 mm column at a flow rate of 1 mL min^{-1}. Microwave heating was accomplished using a Biotage Initiator and SP wave. Circular dichroism spectra were obtained on a JASCO J-810 spectropolarimeter with Peltier variable temperature controller. Melting points were determined on a Gallenkamp Electrothermal melting point apparatus and are uncorrected. Thin Layer Chromatography was performed on Merck 60F_{245} (0.25 mm) aluminium plates and were visualised by ultraviolet light, then either potassium permanganate stain or ninhydrin stain. Flash column chromatography was carried out using Kieselgel 60 silica (Sigma Aldrich).

5.1 Monomer Synthesis

5.1.1 Amino Acid Monomer Synthesis

(2*S*)-5-Azido-2-{[(9*H*-fluoren-9-ylmethoxy)carbonyl]amino}pentanoic acid L177

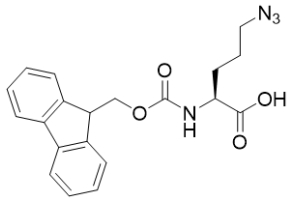

L-Fmoc-Lys(Boc)-OH (2.318 g, 5.10 mmol), was dissolved in DCM (5.1 mL). TFA (7.81 mL, 102 mmol) was added dropwise and the solution was stirred at ambient temperature for 2 h. The solvent was removed *in vacuo* to give the crude TFA salt as a yellow oil. The oil was dissolved in MeOH/H_2O (15 mL, 2:1). K_2CO_3 (1.90 g, 13.8 mmol), copper (II) sulfate pentahydrate (64 mg, 255 μmol) and 1*H*-Imidazole-1-sulfonyl azide·HCl (1.18 g, 5.61 mmol) were added and the pH was adjusted and maintained at pH 9 by addition of K_2CO_3 (sat. aq.). The blue reaction mixture was stirred for 18 h at rt. The solvent was removed *in vacuo*. The residue was re-dissolved in deionised H_2O (100 mL) and washed with toluene (3 x 50 mL). The aqueous layer was acidified to pH 2-3 and extracted with EtOAc (3 x 50 mL). The combined organic layers were washed with brine (3 x 50 mL), dried (Na_2SO_4), filtered and concentrated *in vacuo* to give L-Fmoc-Orn(Azi)-OH as a yellow oil (1.77 g, 91%).

R_f (80:15:5 tol:EtOAc:AcOH) 0.28; **[α]$_D$** -2.4 (c = 1.0 MeOH), lit[144,296] $[\alpha]_D$ -2.3 (c = 1.0 MeOH); **IR** (neat, cm^{-1}) 3337 (N-H), 2091 (N_3), 1728 (C=O ester), 1711 (C=O acid), 1680 (C=O amide), 1531 (N-H amide); **^{1}H NMR** (500 MHz, $CDCl_3$, 323 K) δ 8.96 (1H, br s, COO*H*), 7.78 (2H, d, *J* = 7.5 Hz, FmocAr*H*), 7.60 (2H, s, FmocAr*H*), 7.42 (2H, t, *J* = 7.3 Hz, FmocAr*H*), 7.33 (2H, t, *J* = 7.3 Hz, FmocAr*H*), 5.42 (1H, s, N*H*), 4.75-4.45 (3H, m, FmocCH_2O & C*H*CH_2CH_2), 4.24 (1H, t, *J* = 6.3 Hz, Fmoc*H*), 3.32 (2H, br s, CH_2N_3), 2.15 – 1.50 (m, 4H, CHCH_2C$H_2$$CH_2N_3$); **^{13}C NMR** (126 MHz, $CDCl_3$, 323 K) δ 176.12 (C), 156.25 (C), 143.79 (C), 143.64 (C), 141.40 (2C), 127.78 (2CH), 127.10 (2CH), 124.94 (2CH), 120.01 (CH), 120.00 (CH), 67.26 (CH_2), 53.42

(CH), 50.81 (CH_2), 47.26 (CH), 29.64 (CH_2), 24.83 (CH_2); ***m/z*** (ESI+) 799 ($[2M+K]^+$, 7%), 783 ($[2M+Na]^+$, 18), 419 ($[M+K]^+$, 38), 403 ($[M+Na]^+$, 100), 381 ($[M+H]^+$, 9), 242 (19), 179 (14), 153 (7); **HRMS** (ESI+) $C_{20}H_{20}N_4O_4Na$ ($[M+Na]^+$) requires 403.1377, found 403.1377 (δ 0.0 ppm).

The NMR data is in agreement with the literature[144]

The enantiomer, (2R)-5-Azido-2-{[(9*H*-fluoren-9-ylmethoxy)carbonyl]amino} pentanoic acid **D177**, was synthesised from D-Fmoc-Lys(Boc)-OH (2.287 g, 5.03 mmol) according to the preceding procedure (1.64 g, 86%).

[α]D +2.3 (c = 1.0 MeOH); **IR** (neat, cm^{-1}) 3337 (N-H), 2091 (N_3), 1726 (C=O ester), 1709 (C=O acid), 1680 (C=O amide), 1531 (N-H amide); ***m/z*** (ESI+) 799 ($[2M+K]^+$, 19%), 783 ($[2M+Na]^+$, 24), 419 ($[M+K]^+$, 74), 403 ($[M+Na]^+$, 100), 381 ($[M+H]^+$, 16), 242 (26), 179 (35), 153 (34); **HRMS** (ESI+) $C_{20}H_{20}N_4O_4Na$ ($[M+Na]^+$) requires 403.1377, found 403.1386 (δ 0.9 ppm).

(2*S*)-2-{[(*tert*-Butoxy)carbonyl]amino}-3-(prop-2-yn-1-yloxy) propanoic acid

L197

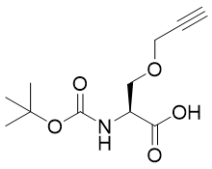

Boc-L-serine (2.10 g, 10.3 mmol) was dissolved in DMF (20 mL), cooled to 0 °C and NaH (902 mg, 22.6 mmol; 60% dispersion in mineral oil) was added. After stirring for 30 min at 0°C propargyl bromide (1.22 ml, 11.3 mmol; 80% solution in toluene) was added dropwise. After stirring at 0 °C for 30 minutes the ice bath was removed and the reaction was stirred for ~18 h at rt. The solvent was removed *in vacuo* and the residue re-dissolved in deionised H_2O (100 mL). The solution was acidified to pH 2-3 and the aqueous layer was extracted with EtOAc (3 x 50 mL). The combined organics were washed with LiBr (2 x 10 mL; 2 M aq) and brine (2 x 25 mL), dried ($MgSO_4$) and

concentrated *in vacuo*. The residue was purified by column chromatography (80:15:5, tol:EtOAc:AcOH) to give Boc-L-Ser(Pra)-OH as a colourless gum (1.98 g, 79%).

R_f (80:15:5 tol:EtOAc:AcOH) 0.24; **$[\alpha]_D$** +0.1 (c = 1.0 MeOH), lit[218] $[\alpha]_D$ +0.10 (c = 1.0 MeOH); **IR** (neat, cm^{-1}) 3290 (N-H), 1705 (C=O), 1506 (N-H amide); **^{1}H NMR** (500 MHz, $CDCl_3$) δ 5.69 and 5.42 (1H, d, *J* = 8.2 Hz, N*H*), 4.51 (1H, dt, *J* = 8.2, 4.7 Hz, NHC*H*RCO_2H), 4.23 (1H, dd, *J* = 16.0, 2.4 Hz, C$H_AH_BC{\equiv}CH$), 4.19 (1H, dd, *J* = 16.0, 2.4 Hz, $CH_AH_BC{\equiv}CH$), 4.02 (1H, dd, *J* = 9.7, 3.1 Hz, $CHCH_CH_DO$), 3.84 (1H, dd, *J* = 9.4, 3.6 Hz, $CHCH_CH_DO$), 2.50 (1H, t, *J* = 2.4 Hz, C≡C*H*), 1.49 (9H, s, $C(CH_3)_3$); **^{13}C NMR** (126 MHz, $CDCl_3$) δ 174.65 (C), 155.78 (C), 80.47 (C), 78.68 (C), 75.37 (CH), 69.37 (CH_2), 58.71 (CH_2), 53.66 (CH), 28.31 ($3CH_3$); ***m/z*** (ESI+) 601 (23%), 585 (45), 569 (27), 320 ($[M+2K-H]^+$, 100), 304 ($[M+Na+K-H]^+$, 84), 288 (13), 282 ($[M+K]^+$, 21), 266 ($[M+Na]^+$, 83), 219 (17), 210 (73), 204 (18), 166 (11); **HRMS** (ESI+) $C_{21}H_{19}NO_5Na$ ($[M+Na]^+$) requires 266.0999, found 266.1015 (δ 1.6 ppm).

The data is in agreement with the literature[297]

The enantiomer, (2*R*)-2-{[(9H-fluoren-9-ylmethoxy)carbonyl]amino}-3-(prop-2-yn-1-yloxy) propanoic acid **D197**, was synthesised from D-Boc-Ser-OH (2.10 g, 10.2 mmol) according to the preceding procedure (1.70 g, 82%).

$[\alpha]_D$ -0.1 (c = 1.0 MeOH); **IR** (neat, cm^{-1}) 3292 (N-H), 1705 (C=O), 1506 (N-H amide); ***m/z*** (ESI+) 601 (28%), 585 (41), 569 (18), 320 ([M+2K-H]+, 100), 304 ($[M+Na+K-H]^+$, 71), 288 (13), 288 (11), 282 ([M+K]+, 14), 266 ([M+Na]+, 57), 219 (17), 210 (50), 204 (15); **HRMS** (ESI+) $C_{11}H_{17}NO_5Na$ ($[M+Na]^+$) requires 266.0999, found 266.1009 (δ 1.0 ppm).

(2*S*)-2-{[(9H-fluoren-9-ylmethoxy)carbonyl]amino}-3-(prop-2-yn-1-yloxy)propanoic acid L178

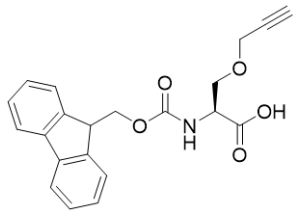

Boc-L-Ser(Pra)-OH (2.59 g, 10.6 mmol) was dissolved in DCM (11 mL). TFA (16.3 mL, 213 mmol) was added dropwise and the solution was stirred at rt for 2 h. The solution was concentrated *in vacuo* to give the crude amine TFA salt as yellow oil. The crude product was dissolved in dioxane (11.5 mL) and Na_2CO_3 (23 mL, 15% w/v) for 15 min at rt. Fmoc-Cl (2.78 g, 10.8 mmol) dissolved in dioxane (11.5 ml) was added over 5 min and the reaction mixture stirred for 18 h. The solvent was removed *in vacuo* and the residue re-dissolved with H_2O (100 ml) and washed with toluene (3 x 50 mL). The aqueous layer was acidified to pH 2-3 and extracted with EtOAc (3 × 50 mL). The combined organic phases were washed with H_2O (3 × 50 mL), brine (3 × 50 mL), dried (Na_2SO_4) and concentrated *in vacuo* to give L-Fmoc-Ser(Pra)-OH **L178** as a colourless gum (3.11 g, 80%).

R_f (80:15:5 tol:EtOAc:AcOH) 0.22; **[α]ᴅ** +6.0 (c = 1.0 MeOH), lit[218] $[\alpha]_D$ +6.2 (c = 1.0 MeOH); **IR** (neat, cm^{-1}) 3404, 3263 (N-H), 1761 (C=O ester), 1714 (C=O acid), 1524 (N-H amide); **^{1}H NMR** (500 MHz, $CDCl_3$) δ 7.80 (2H, d, *J* = 7.5 Hz, FmocAr*H*), 7.64 (2H, t, *J* = 6.0 Hz, FmocAr*H*), 7.43 (2H, t, *J* = 7.4 Hz, FmocAr*H*), 7.35 (2H, t, *J* = 7.4 Hz, FmocAr*H*), 5.67 (1H, d, *J* = 8.3 Hz, N*H*), 4.63 (1H, dt, *J* = 6.9, 2.9 Hz, NHC*H*RCO_2H), 4.49 (1H, dd, *J* = 10.3, 7.3 Hz, FmocCH_AH_BO), 4.42 (1H, dd, *J* = 10.3, 7.3 Hz, FmocCH_AH_BO), 4.28 (1H, t, *J* = 7.0 Hz, Fmoc*H*), 4.23 (2H, m, OCH_2C≡CH), 4.09 (1H, dd, *J* = 9.6, 3.1 Hz, CHCH_AH_BO), 3.87 (1H, dd, *J* = 9.7, 2.7 Hz, $CHCH_AH_BO$), 2.49 (1H, t, *J* = 2.3 Hz, C≡C*H*); **^{13}C NMR** (126 MHz, $CDCl_3$) δ 173.81 (C), 156.18 (C), 143.81 (C), 143.70 (C), 141.34 (2C), 127.77 (2CH), 127.12 (CH), 125.16 (CH), 125.12 (CH), 120.02 (2CH), 78.54 (C), 75.54 (CH), 69.25 (CH_2), 67.37 (CH_2), 58.79 (CH_2), 53.92 (CH), 47.13 (CH); ***m/z*** (ESI+) 878 (9%), 753

([2M+Na]$^+$, 24), 513 (29), 404 ([M+K]$^+$, 14), 388 ([M+Na]$^+$, 100), 366 ([M+H]$^+$, 10), 326 (7), 242 (15), 179 (9); **HRMS** (ESI+) $C_{21}H_{19}NO_5Na$ ([M+Na]$^+$) requires 388.1155, found 388.1172 (δ 1.7 ppm).

The data is in agreement with the literature[218]

The enantiomer, (2*R*)-2-{[(9*H*-fluoren-9-ylmethoxy)carbonyl]amino}-3-(prop-2-yn-1-yloxy) propanoic acid **D178**, was synthesised from D-Boc-Ser(Pra)-OH (1.38 g, 5.68 mmol) according to the preceding procedure (1.70 g, 82%).

[α]$_D$ -5.9 (c = 1.0 MeOH); **IR** (neat, cm^{-1}) 3404, 3263 (N-H), 1761 (C=O ester), 1714 (C=O acid), 1526 (N-H amide); ***m/z*** (ESI+) 975 (6%), 878 (9), 753 ([2M+Na]$^+$, 28), 610 (7), 513 (15), 404 ([M+K]$^+$, 16), 388 ([M+Na]$^+$, 100), 366 ([M+H]$^+$, 11), 326 (18), 270 (17), 248 (15), 179 (11); **HRMS** (ESI+) $C_{21}H_{19}NO_5Na$ ([M+Na]$^+$) requires 388.1155, found 388.1170 (δ 1.5 ppm).

5.1.2 *N*-substituted Glycine Monomer Synthesis

_N_-(3-chloropropyl)-2,2,2-trifluoroacetamide 199

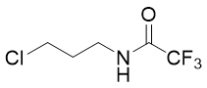

To a solution of 3-chloropropylamine hydrochloride (7.81 g, 60.1 mmol) in DCM (120 mL) was added TFAA (9.32 mL, 66.1 mmol). The solution was allowed to stir at rt for 5-10 minutes until it became homogeneous. The solution was cooled to 0 °C and TEA (18.4 mL, 132 mmol) was added dropwise slowly (gas released). After addition the solution was warmed to rt and allowed to stir for 2 h. The organic layer was washed with hydrochloric acid (3 x 50 mL, 1 M aq). The combined acidic aqueous washes were extracted with additional DCM (2 x 40 mL) and the organic extracts combined. The organic layer was washed with deionised water (3 x 40 mL) and brine (2 x 40

mL). The organic extracts were dried ($MgSO_4$), filtered, and the solvent removed *in vacuo* to give a light yellow oil **199** that solidified on standing (9.95 g, 87%).

R_f (4:1 Hex:EtOAc) 0.26; **Mp**: 30-32 °C; lit[298] Mp = 30 °C; **IR** (neat, cm^{-1}) 3306 (N-H), 1701 (C=O amide), 1152 (C-F); **^{1}H NMR** (500 MHz, $CDCl_3$): δ 6.62 (1H, br s, N*H*), 3.64 (2H, t, *J* = 6.2 Hz, CH_2Cl), 3.59 (2H, q, *J* = 6.5 Hz, CH_2NHR), 2.12 (qn, *J* = 6.7 Hz, 2H, $CH_2CH_2CH_2$); **^{13}C NMR** (126 MHz, $CDCl_3$): δ 157.52 (q, $^2J_{CF}$ = 37.0 Hz, C), 115.75 (q, $^1J_{CF}$ = 287.7 Hz, C), 41.99 (CH_2), 37.67 (CH_2), 31.17 (CH_2); **^{19}F NMR** (471 MHz, $CDCl_3$): δ -75.99 (s, CF_3); ***m/z*** (ESI+, MeCN): 347 (50%), 242 (35), 212 ($[M+Na]^+$ 100); **HRMS** (ESI+, MeCN) $C_5H_7NOClF_3Na$ ($[M+Na]^+$) requires 212.0061, found 212.0063 (δ 0.2 ppm

^{1}H NMR data is in agreement with the literature[299]

tert-butyl 2-[*N*-(3-chloropropyl)-2,2,2-trifluoroacetamido]acetate 200

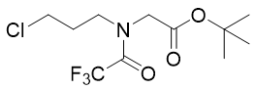

To a solution of *N*-(3-chloropropyl)-2,2,2-trifluoroacetamide **199** (5.57 g, 29.4 mmol) in DMF (29.4 mL) was added Cs_2CO_3 (11.5 g, 35.3 mmol) and the solution warmed to 35 °C. After 5 minutes stirring *tert*-butyl bromoacetate (4.77 mL, 32.3 mmol) was added and the solution left to stir at 35 °C for 3 h. The solvent was removed *in vacuo* and the residue re-dissolved in DCM (10 mL). The solution was passed through a silica plug, which was rinsed with additional DCM (5 x 50 mL). The solvent removed *in vacuo* to yield a light yellow viscous oil **200** (8.21 g, 92%).

R_f (4:1 Hex:EtOAc) 0.39; **IR** (neat, cm^{-1}) 1743 (C=O ester), 1693 (C=O amide), 1138 (C-F); **^{1}H NMR** (500 MHz, $CDCl_3$) δ 4.11 (1H, q, *J* = 1.4 Hz, C$H_2CO_2{}^t$Bu), 4.03* (1H, s, C$H_2CO_2{}^t$Bu), 3.65 (2H, m, $CH_2CH_2NR_2$), 3.61 (2H, t, *J* = 6.2 Hz, ClC$H_2CH_2CH_2NR_2$), 2.18 – 2.08 (2H, m, $CH_2CH_2CH_2$), 1.51 (4.5H, s, C(CH_3)$_3$), 1.50* (4.5H, s, C(CH_3)$_3$); **^{13}C NMR** (126 MHz, $CDCl_3$) δ 166.90 (C), 166.41* (C), 157.49

(q, $^{2}J_{CF}$ = 36.6 Hz, C), 116.31 (q, $^{1}J_{CF}$ = 287.3 Hz, C), 116.13* (q, $^{1}J_{CF}$ = 288.0 Hz, C), 83.33 (C), 82.87* (C), 50.57 (q, $^{4}J_{CF}$ = 3.5 Hz, CH_2), 49.80* (CH_2), 47.65 (CH_2), 46.78* (q, $^{4}J_{CF}$ = 3.0 Hz, CH_2), 42.05 (CH_2), 41.42* (CH_2), 31.26 (CH_2), 29.65* (CH_2), 27.98 ($3CH_3$), 27.91* ($3CH_3$); **^{19}F NMR** (471 MHz, $CDCl_3$) δ -69.17 (s, CF_3), -69.66* (s, CF_3); (*: *trans* rotamer); ***m/z*** (ESI+, MeCN): 629 ($[2M+Na]^+$, 35%), 515 (59), 326 ($[M+Na]^+$ 69), 269 $[M-Cl]^+$ (100), 248 (36), 210 (30); **HRMS** (ESI+, MeCN): $C_{11}H_{17}NO_3ClF_3Na$ ($[M+Na]^+$) requires 326.0741, found 326.0744 (δ 0.3 ppm).

tert-butyl 2-[*N*-(3-iodopropyl)-2,2,2-trifluoroacetamido]acetate 201

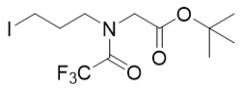

To a solution of *tert*-butyl 2-[*N*-(3-chloropropyl)-2,2,2-trifluoroacetamido]acetate **200** (2.55 g, 8.39 mmol) in MeCN (8.39 mL) was added NaI (1.57 g, 10.5 mmol; dried under high vacuum and heating with a heat gun for 5 mins) and the solution heated to 95 °C under reflux for 8 h. After consumption of the starting material (NMR) the reaction mixture was cooled and the solvent removed *in vacuo*. The residue was re-dissolved in DCM (10 mL) and filtered through a silica pad which was rinsed with additional DCM (5 x 50 mL). The solvent removed *in vacuo* to give a viscous dark yellow orange oil **201** (3.23 g, 97%).

R_f (4:1 Hex:EtOAc) 0.41; **IR** (neat, cm^{-1}) 1743 (C=O ester), 1691 (C=O amide), 1132 (C-F); **^{1}H NMR** (500 MHz, $CDCl_3$) δ 4.11 (1H, q, *J* = 1.3 Hz, $R_2NCH_2CO_2{}^{t}Bu$), 4.02 (1H, s, $CH_2CO_2{}^{t}Bu$), 3.58 (2H, m, $CH_2CH_2NR_2$), 3.20 (1H, t, *J* = 6.9 Hz, ICH_2), 3.18 (1H, t, *J* = 6.8 Hz, ICH_2), 2.18 (1H, qn, *J* = 6.8 Hz, $CH_2CH_2CH_2$), 2.17 (1H, qn, *J* = 6.8 Hz, $CH_2CH_2CH_2$), 1.51 (4.5H, s, $C(CH_3)_3$), 1.50 (4.5H, s, $C(CH_3)_3$); **^{13}C NMR** (126 MHz, $CDCl_3$) δ 166.85 (C), 166.36* (C), 157.50 (q, $^{2}J_{CF}$ = 36.0 Hz, C), 157.43* (q, $^{2}J_{CF}$ = 36.5 Hz, C), 116.29* (q, $^{1}J_{CF}$ = 287.2 Hz, C), 116.11 (q, $^{1}J_{CF}$ = 288.3 Hz, C), 83.37 (C), 82.90* (C), 50.50* (CH_2), 50.49 (q, $^{4}J_{CF}$ = 3.5 Hz, CH_2), 49.84* (q, $^{4}J_{CF}$ = 3.0 Hz, CH_2), 49.68 (CH_2), 31.84* (CH_2), 30.60 (CH_2), 28.00* ($3CH_3$), 27.93 ($3CH_3$), 1.91 (CH_2), 0.38* (CH_2); **^{19}F NMR** (471 MHz, $CDCl_3$) δ -69.07 (CF_3), -69.60* (CF_3); (*: *trans* rotamer); ***m/z*** (ESI+, MeCN): 829 ($[2M+K]^+$, 12%), 813 ($[2M+Na]^+$, 45), 434

([M+K]$^+$, 100), 418 ([M+Na]$^+$, 84), 362 (32), 340 (28), 242 (26), 153 (26); **HRMS** (ESI+, MeCN): $C_{11}H_{17}NO_3F_3INa$ ([M+Na]$^+$) requires 418.0098, found 418.0110 (δ 1.2 ppm).

tert-butyl 2-[*N*-(3-azidopropyl)-2,2,2-trifluoroacetamido]acetate 202

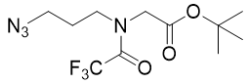

To *tert*-butyl 2-[*N*-(3-iodopropyl)-2,2,2-trifluoroacetamido]acetate **201** (2.66 g, 6.73 mmol) was added NaN_3 solution (13.5 mL; 1 M in DMSO) at rt for 4 h. The solution was then diluted with brine (50 mL) and extracted with EtOAc (3 x 30 mL). The combined organic layers were washed with deionised water (3 x 20 mL) and brine (2 x 20 mL). The organic solution was dried ($MgSO_4$), filtered and the solvent removed *in vacuo* to give a yellow oil **202** (1.96 g, 94%).

R_f (4:1 Hex:EtOAc) 0.34; **IR** (neat, cm^{-1}) 2099 (N_3), 1743 (C=O ester), 1693 (C=O amide), 1140 (C-F); **^{1}H NMR** (500 MHz, $CDCl_3$) δ 4.05 (1H, q, *J* = 1.4 Hz, C*H*$_2$CO$_2$^{t}Bu), 3.96 (1H, s, C*H*$_2$CO$_2$^{t}Bu), 3.56 – 3.48 (2H, m, CH$_2$C*H*$_2$NR$_2$), 3.36 (2H, 2t, *J* = 6.5 Hz, N$_3$C*H*$_2$), 1.86 (2H, m, CH$_2$C*H*$_2$CH$_2$), 1.45 (4.5H, s, C(C*H*$_3$)$_3$), 1.45 (4.5H, s, C(C*H*$_3$)$_3$); **^{13}C NMR** (126 MHz, $CDCl_3$) δ 166.92 (C), 166.39* (C), 157.35 (q, $^2J_{CF}$ = 36.2 Hz, C), 157.31* (q, $^2J_{CF}$ = 36.5 Hz, C), 116.30* (q, $^1J_{CF}$ = 287.2 Hz, C), 116.13 (q, $^1J_{CF}$ = 288.1 Hz, C), 83.21 (C), 82.71* (C), 50.19 (q, $^4J_{CF}$ = 3.4 Hz, CH$_2$), 49.58* (CH$_2$), 48.76 (CH$_2$), 48.35* (CH$_2$), 47.28 (CH$_2$), 46.53* (q, $^4J_{CF}$ = 3.1 Hz, CH$_2$), 27.86* (3CH$_3$), 27.79 (CH$_2$), 27.78 (3CH$_3$), 26.21* (CH$_2$). **^{19}F NMR** (471 MHz, $CDCl_3$) δ -69.27 (C*F*$_3$), -69.74* (C*F*$_3$); (*: *trans* rotamer); ***m/z*** (ESI+, MeCN): 643 ([2M+Na]$^+$, 46%), 638 ([2M+NH$_4$]$^+$, 51), 328 ([M+NH$_4$]$^+$, 100) 255 (35); **HRMS** (ESI+, MeCN): $C_{11}H_{17}N_4O_3F_3Na$ ([M+Na]$^+$) requires 333.1145, found 333.1146 (δ 0.1 ppm).

tert-butyl 2-[(3-azidopropyl)amino]acetate 203

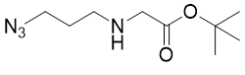

To *tert*-butyl 2-[*N*-(3-azidopropyl)-2,2,2-trifluoroacetamido]acetate **202** (311 mg, 1.00 mmol) in MeOH (1 mL) was added aqueous K_2CO_3 (1 mL; 2.5 M) and the solution was stirred at 40 °C for 4 h. The solvent was removed *in vacuo* and the residue re-dissolved in deionised H_2O (10 mL). The aqueous layer was extracted with EtOAc (3 x 10 mL). The combined organic layers were washed with deionised water (2 x 10 mL) and brine (2 x 10 mL). The solution was dried (Na_2SO_4), filtered and the solvent removed *in vacuo* to give a yellow oil **203** (195 mg, 91%).

R_f (4:1 Hex:EtOAc) 0.08; **IR** (neat, cm^{-1}) 3331 (N-H), 2093 (N_3), 1730 (C=O ester); **^{1}H NMR** (500 MHz, $CDCl_3$) δ 3.41 (2H, t, *J* = 6.7 Hz, N_3CH_2), 3.32 (2H, s, $CH_2CO_2{}^t$Bu), 2.73 (2H, t, *J* = 6.8 Hz, CH_2CH_2NHR), 1.91 (1H, s, N*H*), 1.80 (2H, qn, *J* = 6.8 Hz, $CH_2CH_2CH_2$), 1.50 (9H, s, $C(CH_3)_3$); **^{13}C NMR** (126 MHz, $CDCl_3$) δ 171.56 (C), 81.38 (C), 51.62 (CH_2), 49.42 (CH_2), 46.54 (CH_2), 29.27 (CH_2), 28.13 ($3CH_3$); ***m/z*** (ESI+, MeCN): 441 (17%), 415 (100), 386 (16), 359 (27), 329 (8), 303 (15), 273 (13), 247 (12), 215 ($[M+H]^+$, 26), 159 (70); **HRMS** (ESI+, MeCN): $C_9H_{19}N_4O_2$ ($[M+H]^+$) requires 215.1503, found 215.1514 (δ 1.1 ppm).

tert-butyl 2-[(3-azidopropyl)[(9*H*-fluoren-9-ylmethoxy)carbonyl]amino]acetate 204

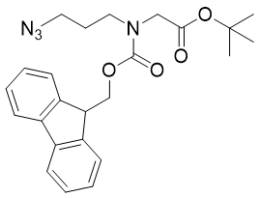

To *tert*-butyl 2-[*N*-(3-azidopropyl)-2,2,2-trifluoroacetamido]acetate **202** (156 mg, 502 μmol) in MeOH (502 μL) was added K_2CO_3 (502 μL; 2.5 M aq) and the solution was stirred at 40 °C for 4 h. The solvent was removed *in vacuo* and the residue re-dissolved in MeCN (1.5 mL). To this FmocCl (156 mg, 602 μmol) was added and the solution stirred at rt for 2 h. The solvent was removed *in vacuo* and the residue dissolved in deionised H_2O (5 mL). The aqueous solution was acidified (0.5 M HCl) and extracted with EtOAc (3 x 5 mL). The combined organic layers were washed with HCl (2 x 5 mL; 0.5 M aq), deionised water (2 x 5 mL) and brine (2 x 5 mL). The combined

organics were dried (Na_2SO_4), filtered and the solvent removed *in vacuo* to give a light yellow oil. This was purified by flash column chromatography (9:1 Hex:EtOAc) to give **204** as a colourless oil (188 mg, 86%).

R_f (4:1 Hex:EtOAc) 0.24; **IR** (neat, cm^{-1}) 2095 (N_3), 1742 (C=O ester), 1701 (C=O carbamate); **^{1}H NMR** (500 MHz, $CDCl_3$) δ 7.79 (2H, d, *J* = 7.5 Hz, FmocAr*H*), 7.61 (2H, d, *J* = 7.4 Hz, FmocAr*H*), 7.43 (2H, t, *J* = 7.3 Hz, FmocAr*H*), 7.35 (1H, t, *J* = 7.3 Hz, FmocAr*H*), 7.33* (1H, t, *J* = 7.6 Hz, FmocAr*H*), 4.62 (1H, d, *J* = 5.5 Hz, FmocCH_2O), 4.43* (1H, d, *J* = 6.9 Hz, FmocCH_2O), 4.27 (0.5H, t, *J* = 5.4 Hz, Fmoc*H*), 4.24* (0.5H, t, *J* = 6.9 Hz, Fmoc*H*), 3.89* (1H, s, C$H_2CO_2{}^t$Bu), 3.85 (1H, s, C$H_2CO_2{}^t$Bu), 3.45* (1H, t, *J* = 6.9 Hz, $CH_2CH_2NR_2$), 3.39* (1H, t, *J* = 6.7 Hz, N_3CH_2), 3.14 (1H, t, *J* = 7.1 Hz, $CH_2CH_2NR_2$), 3.05 (1H, t, *J* = 6.7 Hz, N_3CH_2), 1.88* (1H, qn, *J* = 6.8 Hz, $CH_2CH_2CH_2$), 1.52 (1H, qn, *J* = 6.8 Hz, $CH_2CH_2CH_2$), 1.48* (4.5H, s, C(CH_3)$_3$), 1.47 (4.5H, s, C(CH_3)$_3$); **^{13}C NMR** (126 MHz, $CDCl_3$) δ 168.72* (C), 168.65 (C), 156.26 (C), 156.07* (C), 143.97 (C), 143.93* (C), 141.43 (C), 141.31* (C), 127.73 (CH), 127.71* (CH), 127.17 (CH), 127.10* (CH), 125.08* (CH), 124.70 (CH), 119.99* (CH), 119.92 (CH), 82.10* (C), 81.90 (C), 67.84* (CH_2), 67.04 (CH_2), 50.30 (CH_2), 50.23* (CH_2), 48.96* (CH_2), 48.69 (CH_2), 47.38* (CH), 47.32 (CH), 46.69* (CH_2), 45.92 (CH_2), 28.08 ($3CH_3$), 27.60 (CH_2), 27.52* (CH_2); (*: minor rotamer, 49%); ***m/z*** (ESI+, MeCN): 459 (70%, $[M+Na]^+$), 403 (19), 341 (13), 179 (100); **HRMS** (ESI+, MeCN) $C_{24}H_{28}N_4O_4Na$ ($[M+Na]^+$) requires 459.2003, found 459.2000 (δ 0.3 ppm).

2-[(3-azidopropyl)[(9*H*-fluoren-9-ylmethoxy)carbonyl]amino]acetic acid 187

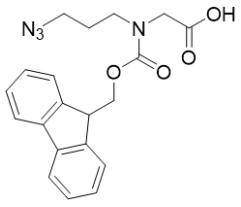

To *tert*-butyl 2-[*N*-(3-azidopropyl)-2,2,2-trifluoroacetamido]acetate **202** (1.72 g, 5.55 mmol) in MeOH (5.5 mL) was added aqueous K_2CO_3 (5.5 mL; 2.5 M aq) and the solution was stirred at 40 °C for 4 h. The solvent was removed *in vacuo* and the residue re-dissolved in MeCN (16.5 mL). To this FmocCl (1.72 g, 6.66 mmol) was added and

the solution stirred at rt for 2 h. The solvent was removed *in vacuo* and the residue dissolved in deionised H_2O (20 mL). The aqueous solution was acidified with HCl (0.5 M aq) and extracted with EtOAc (3 x 20 mL). The combined organic layers were washed with HCl (2 x 20 mL; 0.5 M aq), deionised water (2 x 20 mL) and brine (2 x 20 mL). The combined organics were dried (Na_2SO_4), filtered and the solvent removed in vacuo to give a light yellow oil, which was re-dissolved in DCM (5 mL). TFA (8.50 mL, 111 mmol) was added dropwise and the solution left to stir for 2 h at rt. The solvent was removed in vacuo and the residue re-dissolved in Et_2O (20 mL). The organic layer was extracted with $NaHCO_3$ (5 x 15 mL sat. aq) and the combined aqueous extracts washed with Et_2O (2 x 10 mL). The aqueous solution was acidified and extracted with EtOAc (3 x 20 mL). The combined organic extracts were washed with deionised H_2O (2 x 15 mL) and brine (2 x 20 mL). The solution was dried (Na_2SO_4), filtered and concentrated in vacuo to give **187** as a colourless wax (1.63 g, 77%).

R_f (4:1 Hex:EtOAc) 0.04; **IR** (neat, cm^{-1}) 2093 (N_3), 1714 (C=O acid), 1653 (C=O carbamate); **^{1}H NMR** (601 MHz, $CDCl_3$) δ 7.79 (1.12H, d, *J* = 7.5 Hz, FmocAr*H*), 7.76* (0.88H, d, *J* = 7.6 Hz, FmocAr*H*), 7.60 (1.12H, d, *J* = 7.5 Hz, FmocAr*H*), 7.56* (0.88H, d, *J* = 7.5 Hz, FmocAr*H*), 7.43 (1.12H, t, *J* = 7.5 Hz, FmocAr*H*), 7.40* (0.88H, t, *J* = 7.6 Hz, FmocAr*H*), 7.35 (1.12H, t, *J* = 7.5 Hz, FmocAr*H*), 7.31* (0.88H, t, *J* = 7.5 Hz, FmocAr*H*), 4.65 (1.12H, d, *J* = 5.4 Hz, FmocCH_2O), 4.51* (0.88H, d, *J* = 6.2 Hz, FmocCH_2O), 4.27 (0.56H, t, *J* = 5.5 Hz, Fmoc*H*), 4.22* (0.44H, t, *J* = 6.2 Hz, Fmoc*H*), 3.99 (1.12H, s, CH_2CO_2H), 3.89* (0.88H, s, CH_2CO_2H), 3.41* (0.88H, t, *J* = 6.9 Hz, $CH_2CH_2NR_2$), 3.34* (0.88H, t, *J* = 6.7 Hz, N_3CH_2), 3.14 (1.12H, t, *J* = 7.1 Hz, $CH_2CH_2NR_2$), 3.03 (1.12H, t, *J* = 6.7 Hz, N_3CH_2), 1.82* (0.88H, qn, *J* = 6.9 Hz, $CH_2CH_2CH_2$), 1.51 (1.12H, qn, *J* = 6.9 Hz, $CH_2CH_2CH_2$); **^{13}C NMR** (151 MHz, $CDCl_3$) δ 173.89* (C), 173.79 (C), 156.47 (C), 155.87* (C), 143.80 (2C), 141.44 (C), 141.37* (C), 127.77 (CH), 127.70* (CH), 127.21 (CH), 127.07* (CH), 124.81* (CH), 124.67 (CH), 119.97* (CH), 119.95 (CH), 67.60* (CH_2), 67.23 (CH_2), 49.41 (CH_2), 48.92* (CH_2), 48.85* (CH_2), 48.61 (CH_2), 47.29 (CH), 46.59* (CH_2), 46.06 (CH_2), 27.51 (CH_2), 27.44* (CH_2); (*: minor rotamer, 44%); ***m/z*** (ESI+, MeCN): 403 (100%,

$[M+Na]^+$), 353 (14), 279 (14), 179 (68); **HRMS** (ESI+, MeCN) $C_{20}H_{20}N_4O_4Na$ ($[M+Na]^+$) requires 403.1377, found 403.1382 (δ 0.5 ppm).

N-(3-iodopropyl)-2,2,2-trifluoroacetamide 208

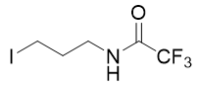

To a solution of *N*-(3-chloropropyl)-2,2,2-trifluoroacetamide **199** (1.01 g, 5.33 mmol) in MeCN (5.3 mL) was added NaI (998 mg, 6.66 mmol, dried under high vacuum and heating with a heat gun for 5 mins) and the solution heated to 95 °C under reflux for 8 h. After consumption of the starting material (TLC) the reaction mixture was cooled and the solvent removed *in vacuo*. The residue was re-dissolved in DCM (10 mL) and filtered through a silica pad which was rinsed with additional DCM (5 x 10 mL). The solvent was removed *in vacuo* to give a light yellow solid (1.48 g, 99%).

R_f (4:1 Hex:EtOAc) 0.30; **Mp**: 57-59 °C; lit[298] Mp = 58 °C; **IR** (neat, cm^{-1}) 3302 (N-H), 1699 (C=O amide), 1169 (C-F); **^{1}H NMR** (500 MHz, $CDCl_3$): δ 6.46 (1H, br s, N*H*), 3.53 (2H, q, *J* = 6.6 Hz, C*H*$_2$NHR), 3.22 (2H, t, *J* = 6.7 Hz, C*H*$_2$I), 2.16 (2H, qn, *J* = 6.7 Hz, $CH_2CH_2CH_2$); **^{13}C NMR** (126 MHz, $CDCl_3$): δ 157.47 (q, $^2J_{CF}$ = 37.7 Hz, C), 115.72 (q, $^1J_{CF}$ = 287.8 Hz, C), 40.62 (CH_2), 31.95 (CH_2), 1.52 (CH_2); **^{19}F NMR** (471 MHz, $CDCl_3$): δ -75.89 (s, C*F*$_3$); **HRMS** (EI+) $C_5H_7NOF_3I$ ($[M]^+$) requires 280.9519, found 280.9522 (δ 0.3 ppm).

tert-butyl 2-(trifluoroacetamido)acetate 210

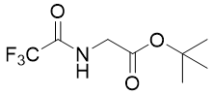

To a solution of glycine *tert*-butyl ester hydrochloride **211** (1.68 g, 10.0 mmol) in DCM (20 mL) was added TFAA (1.55 mL). The solution was allowed to stir at rt for 5-10 minutes until it became homogeneous. The solution was cooled to 0 °C and TEA (3.07 mL) was added dropwise slowly (gas released). After addition the solution was

warmed to rt and allowed to stir for 2 h. The organic layer washed with hydrochloric acid (3 x 10 mL, 1 M aq). The combined acidic aqueous washes were extracted with DCM (2 x 10 mL) and the organic extracts combined. The organic layer was washed with deionised water (3 x 10 mL) and brine (2 x 10 mL). The organic extracts were dried ($MgSO_4$), filtered, and the solvent removed *in vacuo* to give a light yellow oil (2.071 g, 91%).

R_f (4:1 Hex:EtOAc) 0.42; **IR** (neat, cm^{-1}) 3331 (N-H), 1744 (C=O ester), 1710 (C=O amide), 1148 (C-F); **^{1}H NMR** (500 MHz, $CDCl_3$) δ 6.87 (1H, br s, N*H*), 4.05 (dq, *J* = 5.0, 0.7 Hz, 2H, CH_2), 1.53 (9H, s, C(CH_3)$_3$); **^{13}C NMR** (126 MHz, $CDCl_3$) δ 167.32 (C), 157.05 (q, $^2J_{CF}$ = 37.7 Hz, C), 115.64 (q, $^1J_{CF}$ = 287.4 Hz, C), 83.68 (C), 42.04 (CH_2), 27.99 ($3CH_3$); **^{19}F NMR** (471 MHz, $CDCl_3$) δ -75.92 (s, CF_3); ***m/z*** (ESI+): 477 ([2M+Na]$^+$, 100%), 250 [M+Na]$^+$ (91); **HRMS** (ESI+): $C_8H_{12}NO_3F_3Na$ ([M+Na]$^+$) requires 250.0662, found 250.0670 (δ 0.8 ppm).

^{1}H and ^{13}C NMR data are in good agreement with the literature[300]

tert-butyl 2-[*N*-(pent-4-yn-1-yl)-2,2,2-trifluoroacetamido]acetate 205

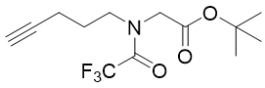

To a solution of *tert*-butyl 2-(trifluoroacetamido)acetate **210** (1.60 g, 7.06 mmol) in DMF (10.6 mL) was added Cs_2CO_3 (3.45 g, 10.6 mmol), and TBAI (652 mg, 1.77 mmol) and the solution stirred for 5 minutes. To the suspension 5-chloropentyne (1.12 mL, 10.6 mmol) was added and the solution was heated to 95 °C and left to stir for 12 h, making sure the solids were well agitated. The solvent was removed *in vacuo* and the residue was re-dissolved in DCM (10 mL) and filtered through a silica pad which was rinsed with additional DCM (5 x 50 mL). The solvent was removed *in vacuo* to yield a dark yellow viscous oil (1.99 g, 96%).

R_f (4:1 Hex:EtOAc) 0.46; **IR** (neat, cm^{-1}) 1744 (C=O ester), 1692 (C=O amide); **^{1}H NMR** (500 MHz, $CDCl_3$) δ 4.10 (1H, q, $^5J_{CF}$ = 1.6 Hz, C*H*$_2$CO$_2$^{t}Bu), 4.02* (s, 1H, C*H*$_2$CO$_2$^{t}Bu), 3.62–3.57 (2H, m, CH$_2$C*H*$_2$NR$_2$), 2.28 (2H, ddt, *J* = 6.7, 2.7 Hz, HC≡C*H*$_2$), 2.03* (0.5H, t, *J* = 2.7 Hz, *H*C≡CH$_2$), 2.01 (0.5H, t, *J* = 2.7 Hz, *H*C≡CH$_2$), 1.86 (p, *J* = 7.0 Hz, 2H, CH$_2$C*H*$_2$CH$_2$), 1.49 (4.5H, s, C(C*H*$_3$)$_3$), 1.49* (4.5H, s, C(C*H*$_3$)$_3$); **^{13}C NMR** (126 MHz, $CDCl_3$) δ 166.96 (C), 166.47* (C), 157.45* (q, $^2J_{CF}$ = 36.5 Hz, C), 157.31 (q, $^2J_{CF}$ = 36.0 Hz, C), 116.35* (q, $^1J_{CF}$ = 287.2 Hz, C), 116.20 (q, $^1J_{CF}$ = 288.2 Hz, C), 83.18 (C), 82.77 (C), 82.71* (C), 82.07* (C), 69.79* (CH$_2$), 69.47 (CH$_2$), 50.15 (q, $^4J_{CF}$ = 3.2 Hz, CH$_2$), 49.50* (CH$_2$), 48.59 (CH$_2$), 47.98* (q, $^4J_{CF}$ = 3.1 Hz, CH$_2$), 27.96* (3CH$_3$), 27.89 (3CH$_3$), 27.04* (CH$_2$), 25.42 (CH$_2$), 15.92 (CH$_2$), 15.74* (CH$_2$); **^{19}F NMR** (471 MHz, $CDCl_3$) δ -69.16, -69.62*; (*: *trans* rotamer); ***m/z*** (ESI+, MeCN) 625 ([2M+K]$^+$, 20%), 609 ([2M+Na]$^+$, 44), 604 ([2M+NH$_4$]$^+$, 21), 332 ([M+K]$^+$, 38), 316 ([M+Na]$^+$, 48), 311 ([M+NH$_4$]$^+$, 100), 238 (21), 102 (5); **HRMS** (ESI+, MeCN) $C_{13}H_{18}NO_3F_3Na$ ([M+Na]$^+$) requires 316.1131, found 316.1141 (δ 1.0 ppm).

tert-butyl 2-[(pent-4-yn-1-yl)amino]acetate 206

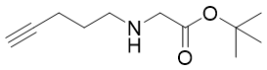

To *tert*-butyl 2-[*N*-(pent-4-yn-1-yl)-2,2,2-trifluoroacetamido]acetate **205** (297 mg, 1.01 mmol) in MeOH (1 mL) was added aqueous K_2CO_3 (1 mL; 2.5 M) at 40 °C for 4 h. The solvent was removed *in vacuo* and the residue re-dissolved in deionised H_2O (10 mL). The aqueous layer was extracted with EtOAc (3 x 10 mL). The combined organic layers were washed with deionised water (2 x 10 mL) and brine (2 x 10 mL). The solution was dried (Na_2SO_4), filtered and the solvent removed *in vacuo* to give a dark yellow oil (179 mg, 90%).

R_f (4:1 Hex:EtOAc) 0.09; **IR** (neat, cm^{-1}) 3296 (N-H), 1730 (C=O ester); **^{1}H NMR** (500 MHz, $CDCl_3$ δ 3.33 (2H, s, RNHC*H*$_2$CO$_2$^{t}Bu), 2.74 (2H, t, *J* = 7.0 Hz, CH$_2$C*H*$_2$NHR), 2.30 (2H, dt, *J* = 7.0, 2.6 Hz, HC≡C*H*$_2$), 1.97 (1H, t, *J* = 2.6 Hz, *H*C≡C), 1.85 (1H, s, N*H*), 1.74 (2H, qn, *J* = 7.0 Hz, CH$_2$C*H*$_2$CH$_2$), 1.49 (9H, s,

C(C*H*$_3$)$_3$); **^{13}C NMR** (126 MHz, $CDCl_3$) δ 171.67 (C), 83.98 (C), 81.24 (C), 68.57 (CH), 51.69 (CH_2), 48.28 (CH_2), 28.72 (CH_2), 28.13 ($3CH_3$), 16.24 (CH_2); ***m/z*** (ESI+, MeCN) 365 (9%), 309 (10), 242 ([M+2Na-H]$^+$, 100), 198 ([M+H]$^+$, 17), 142 (85); **HRMS** (ESI+, MeCN) $C_{11}H_{20}NO_2$ ([M+H]$^+$) requires 198.1489, found 198.1495 (δ 0.6 ppm).

tert-butyl 2-[(pent-4-yn-1-yl)[(9*H*-fluoren-9-ylmethoxy)carbonyl]amino]acetate 207

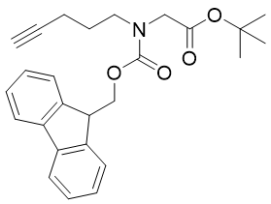

To *tert*-butyl 2-[*N*-(pent-4-yn-1-yl)-2,2,2-trifluoroacetamido]acetate **205** (147 mg, 501 μmol) in MeOH (501 μL) was added K_2CO_3 (501 μL; 2.5 M aq) and the solution was stirred at 40 °C for 4 h. The solvent was removed *in vacuo* and the residue re-dissolved in MeCN (1.5 mL). To this FmocCl (156 mg, 601 μmol) was added and the solution stirred at rt for 2 h. The solvent was removed *in vacuo* and the residue dissolved in deionised H_2O (10 mL). The aqueous solution was acidified with HCl (0.5 M aq) and extracted with EtOAc (3 x 5 mL). The combined organic layers were washed with HCl (2 x 5 mL; 0.5 M aq), deionised H_2O (2 x 5 mL) and brine (2 x 5 mL). The combined organics were dried (Na_2SO_4), filtered and the solvent removed *in vacuo* to give a translucent orange oil. This was purified by flash column chromatography (9:1 Hex:EtOAc) to give an transparent oil (177 mg, 84%).

R_f (4:1 Hex:EtOAc) 0.22; **IR** (neat, cm^{-1}) 1742 (C=O ester), 1701 (C=O carbamate); **^{1}H NMR** (500 MHz, $CDCl_3$) δ 7.79 (2H, d, *J* = 7.5 Hz, FmocAr*H*), 7.62 (2H, t, *J* = 7.5 Hz, , FmocAr*H*), 7.42 (2H, t, *J* = 7.4 Hz, FmocAr*H*), 7.36 – 7.31 (2H, m, FmocAr*H*), 4.55 (1H, d, *J* = 6.0 Hz, FmocC*H*$_2$O), 4.42* (1H, d, *J* = 7.0 Hz, FmocC*H*$_2$O), 4.29 (0.5H, t, *J* = 6.0 Hz, Fmoc*H*), 4.24* (0.5H, t, *J* = 7.0 Hz, Fmoc*H*), 3.92* (1H, s, C*H*$_2$CO$_2$^{t}Bu), 3.90 (1H, s, C*H*$_2$CO$_2$^{t}Bu), 3.48 (1H, t, *J* = 7.1 Hz,

$CH_2CH_2NR_2$), 3.27 (1H, t, *J* = 7.3 Hz, $CH_2CH_2NR_2$), 2.28 (1H, dt, *J* = 7.0, 2.7 Hz, $HC{\equiv}CH_2$), 2.06 (1H, dt, *J* = 7.0, 2.7 Hz, $HC{\equiv}CH_2$), 1.99 (0.5H, t, *J* = 2.6 Hz, $HC{\equiv}CH_2$), 1.96 (0.5H, t, *J* = 2.6 Hz, $HC{\equiv}CH_2$), 1.83 (1H, qn, *J* = 7.1 Hz, $CH_2CH_2CH_2$), 1.57 (1H, d, *J* = 7.1 Hz, $CH_2CH_2CH_2$), 1.48* (4.5H, s, $C(CH_3)_3$), 1.48 (4.5H, s, $C(CH_3)_3$); **^{13}C NMR** (126 MHz, $CDCl_3$) δ 168.80* (C), 168.76 (C), 156.40 (C), 156.05 (C), 144.03 (C), 143.99* (C), 141.40 (C), 141.30* (C), 127.70* (CH), 127.68 (CH), 127.10 (CH), 127.09* (CH), 125.11* (CH), 124.87 (CH), 119.97* (CH), 119.94 (CH), 83.56* (C), 83.34 (C), 81.97* (C), 81.77 (C), 68.97 (CH), 68.88* (CH), 67.78* (CH_2), 67.31 (CH_2), 50.26 (CH_2), 50.15* (CH_2), 48.16* (CH_2), 47.45 (CH_2), 47.39* (CH), 47.31 (CH), 28.09 ($3CH_3$), 26.97 (CH_2), 26.84* (CH_2), 15.92* (CH_2), 15.75 (CH_2); (*: minor rotamer, 48%); ***m/z*** (ESI+, MeCN): 442 (68%, $[M+Na]^+$), 386 (28), 179 (100); **HRMS** (ESI+, MeCN) $C_{26}H_{29}NO_4Na$ ($[M+Na]^+$) requires 442.1989, found 442.1980 (δ 0.9 ppm).

2-[(pent-4-yn-1-yl)[(9*H*-fluoren-9-ylmethoxy)carbonyl]amino]acetic acid 188

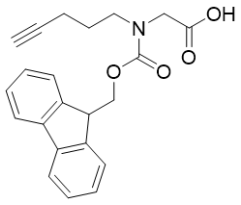

To *tert*-butyl 2-[*N*-(pent-4-yn-1-yl)-2,2,2-trifluoroacetamido]acetate **205** (1.62 g, 5.53 mmol) in MeOH (5.5 mL) was added aqueous K_2CO_3 (5.5 mL; 2.5 M) and the solution was stirred at 40 °C for 4 h. The solvent was removed *in vacuo* and the residue re-dissolved in MeCN (16.5 mL). To this FmocCl (1.72 g, 13.8 mmol) was added and the solution stirred at rt for 2 h. The solvent was removed *in vacuo* and the residue dissolved in deionised H_2O (20 mL). The aqueous solution was acidified with HCl (0.5 M aq) and extracted with EtOAc (3 x 20 mL). The combined organic layers were washed with HCl (2 x 20 mL; 0.5 M aq), deionised H_2O (2 x 20 mL) and brine (2 x 20 mL). The combined organics were dried (Na_2SO_4), filtered and the solvent removed *in vacuo* to give a translucent orange oil, which was re-dissolved in DCM (5 mL). TFA (8.47 mL, 111 mmol) was added dropwise and the solution left to stir for 2 h at rt. The

solvent was removed *in vacuo* and the residue re-dissolved in Et_2O (20 mL). The organic layer was extracted with $NaHCO_3$ (5 x 15 mL) and the combined aqueous extracts washed with Et_2O (2 x 10 mL). The aqueous solution was acidified and extracted with EtOAc (3 x 20 mL). The combined organic extracts were washed with deionised H_2O (2 x 15 mL) and brine (2 x 20 mL). The solution was dried (Na_2SO_4), filtered and concentrated *in vacuo* to give **188** as an orange wax (1.51 g, 75%).

R_f (4:1 Hex:EtOAc) 0.05; **IR** (neat, cm^{-1}) 1726, 1697 (broad C=O); **^{1}H NMR** (601 MHz, $CDCl_3$) δ 7.79 (1.22H, d, *J* = 7.5 Hz, FmocAr*H*), 7.76* (0.78H, d, *J* = 7.5 Hz, FmocAr*H*), 7.61 (1.22H, d, *J* = 7.4 Hz, FmocAr*H*), 7.55* (0.78H, d, *J* = 7.4 Hz, FmocAr*H*), 7.42 (1.22H, t, *J* = 7.5 Hz, FmocAr*H*), 7.39* (0.78H, t, *J* = 7.3 Hz, FmocAr*H*), 7.34 (1.22H, t, *J* = 7.4 Hz, FmocAr*H*), 7.31* (0.78H, t, *J* = 7.4 Hz, FmocAr*H*), 4.59 (1.22H, d, *J* = 5.8 Hz, FmocCH_2O), 4.51* (0.78H, d, *J* = 6.0 Hz, FmocCH_2O), 4.28 (0.61H, t, *J* = 5.7 Hz, Fmoc*H*), 4.22* (0.39H, t, *J* = 5.9 Hz, Fmoc*H*), 4.04 (0.61H, s, CH_2CO_2H), 3.90* (0.39H, s, CH_2CO_2H), 3.44* (0.39H, t, *J* = 7.0 Hz, $CH_2CH_2NR_2$), 3.26 (0.61H, t, *J* = 7.3 Hz, $CH_2CH_2NR_2$), 2.23* (0.39H, dt, *J* = 7.0, 2.6 Hz, HC≡CH_2), 2.04 (0.61H, dt, *J* = 7.0, 2.4 Hz, HC≡CH_2), 1.98 – 1.95 (1H, m, *H*C≡CH_2), 1.77* (0.39H, qn, *J* = 6.8 Hz, $CH_2CH_2CH_2$), 1.54 (0.61H, qn, *J* = 7.0 Hz, $CH_2CH_2CH_2$); **^{13}C NMR** (151 MHz, $CDCl_3$) δ 174.53* (C), 174.28 (C), 156.67 (C), 155.83* (C), 143.82 (C), 141.41 (C), 141.37* (C), 127.75 (CH), 127.69* (CH), 127.15 (CH), 127.06* (CH), 124.80 (CH), 124.77* (CH), 119.97 (CH), 83.37* (C), 83.10 (C), 69.22 (CH), 69.06* (CH), 67.51 (CH_2), 49.47 (CH_2), 48.82* (CH_2), 48.05* (CH_2), 47.63 (CH_2), 47.27 (CH), 26.83 (CH_2), 26.69* (CH_2), 15.77* (CH_2), 15.65 (CH_2); (*: minor rotamer, 39%); ***m/z*** (ESI+) 408 (6%), 386 ($[M+Na]^+$, 100), 282 (4), 179 (52); **HRMS** (ESI+) $C_{22}H_{21}NO_4Na$ ($[M+Na]^+$) requires 386.1363, found 386.1378 (δ 1.5 ppm).

5.1.2.1 Variable Temperature ^{1}H NMR Spectra for *tert*-butyl 2-[*N*-(3-chloropropyl)-2,2,2-trifluoroacetamido]acetate **200**

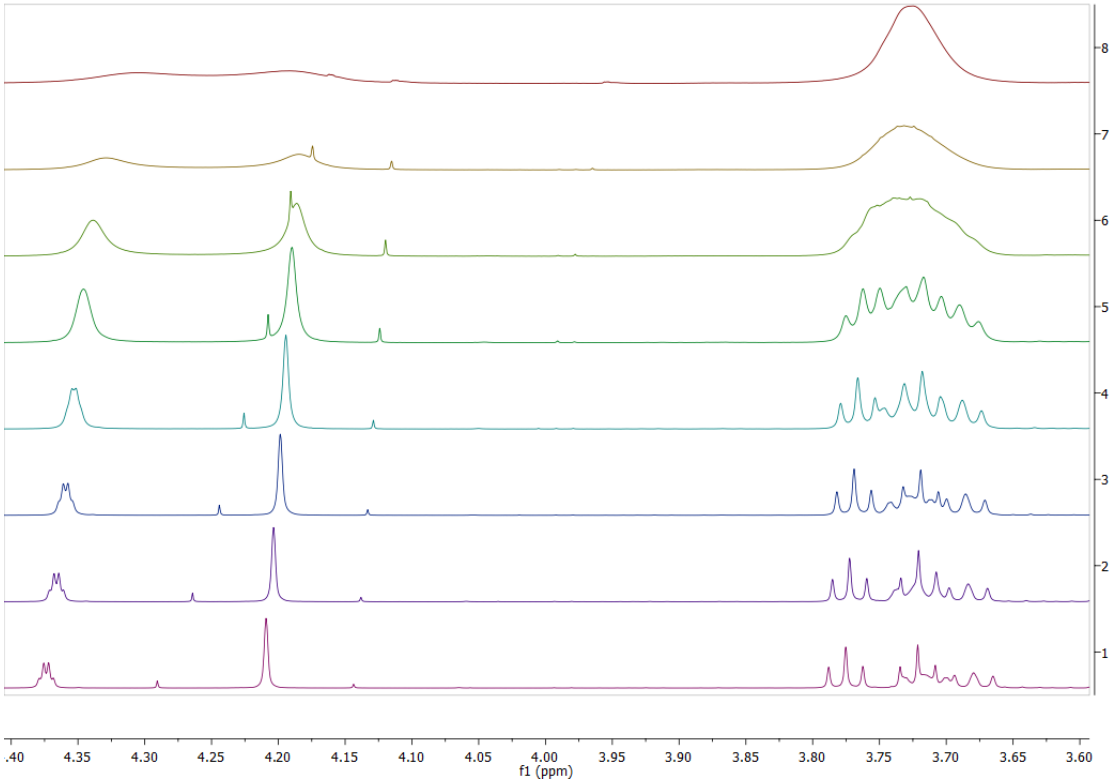

Figure 127- Abstracts of variable temperature ^{1}H experiments (4.40 – 3.60 ppm, *d7*-DMF) showing α-carbon CH_2 rotameric signals (4.35 and 4.20 ppm) and overlapping CH_2Cl and TfacNRC*H*$_2$$CH_2$R' rotameric signals (3.78 – 3.66 ppm) upon heating from 303 K to 373 K (Spectra 1 and 8, respectively) in 10 K increments.

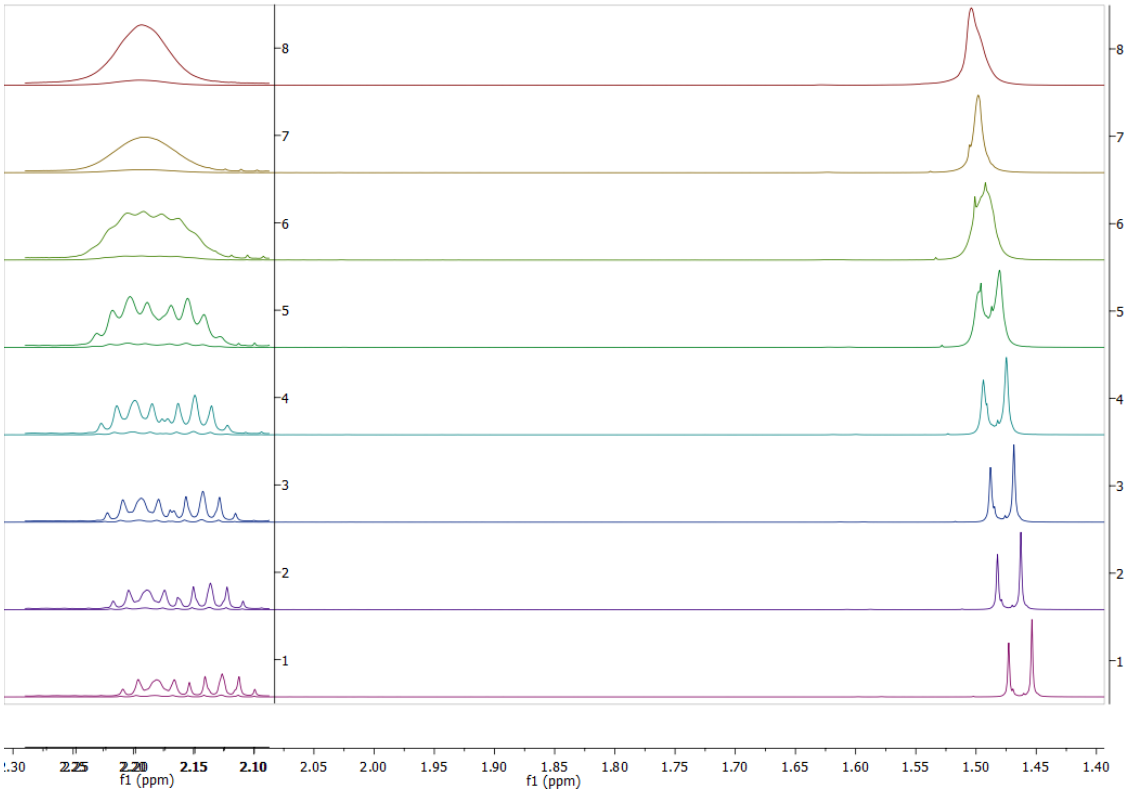

Figure 128- Abstracts of variable temperature ^{1}H experiments (2.30 – 1.40 ppm, *d7*-DMF) showing coalescence of TfacNRCH$_2$C*H*$_2$CH$_2$Cl rotameric signals (2.25 – 2.10 ppm) and CO$_2$CC*H*$_3$ rotameric signals (1.50 – 1.45 ppm) upon heating from 303 K to 373 K (Spectra 1 and 8, respectively) in 10 K increments. Intensity of signals at 2.25 – 2.10 have been increased for clarity.

5.2 Peptide Synthesis

5.2.1 Resin Activation

Polymer bound Fmoc Rink Amide AM (250 mg, 0.69 mmol g^{-1} loading) was swollen in DCM (2 mL) for 2 min and then drained and washed with DCM (2 x 1 mL). Piperidine (2 mL; 20% in DMF) was added to the resin and the mixture stirred at room temperature for 5 min. The solvent was drained and the resin washed with DMF (5 x 2 mL) and DCM (5 x 2 mL). The piperidine addition and wash steps were repeated. The deprotection of the Fmoc protecting group was confirmed by a positive free amine test (*vide infra*).

5.2.2 Coupling Protocol

Resin (173 μmol) with a free amine terminal amino acid was swollen and stirred in DCM (2 mL) for 2 min. Fmoc-AA-OH (518 μmol) and ethyl 2-cyano-2-(hydroxyimino) acetate (Oxyma, 60 mg, 518 μmol) was dissolved in DMF (1.5 mL). To this DIC was added (80 μL, 518 μmol) and the solution was shaken for 2 min. The DCM was drained, the DMF solution was added to the resin and the mixture was stirred at room temperature for 37 min. After this time the solution was drained and the resin washed with DMF (5 x 2 mL), DCM (5 x 2 mL), MeOH (5 x 2 mL) and DCM (5 x 2 mL). The coupling was confirmed by a negative free amine test (*vide infra*).

5.2.3 Fmoc Deprotection

Resin (173 μmol) with an Fmoc-protected terminal amine was swollen and stirred in DCM (2 mL) for 2 min. Piperidine (2 mL; 20% in DMF) was added to the resin and the mixture stirred at room temperature for 5 min. The solvent was drained and the resin washed with DMF (5 x 2 mL) and DCM (5 x 2 mL). The piperidine addition and wash steps were repeated. The deprotection was confirmed by a positive free amine test (*vide infra*).

5.2.4 Test for Free Amines

To a few beads of resin were added 3 drops of each solution (Solution 1: 2% acetaldehyde in DMF [v/v, 100 μL in 5 mL], Solution 2: 2% chloranil in DMF [w/v 100 μg in 5 mL]). The mixture was left at room temperature for 5 min and the beads inspected.

Positive Test – Green/Blue beads (1°/2°) Negative test – No colour change

5.2.5 Capping

The Fmoc deprotection (*vide supra*) was performed 3 times and a positive free amine test confirmed the deprotection step. To the resin was added neat Ac_2O (326 μL 3.45 mmol) and DIPEA (601 μL, 3.45 mmol) in DMF (1 mL) and the mixture was stirred at room temperature for 37 min. After this time the solution was then drained and the resin washed with DMF (5 x 2 mL), DCM (5 x 2 mL), MeOH (5 x 2 mL) and DCM (5 x 2 mL). The coupling was confirmed by a negative free amine test (*vide supra*).

5.2.6 On–Resin CuAAC Reaction

5.2.6.1 On-Resin CuAAC Room Temperature

To the resin (~86.5 μmol) was added a mixture of DCM and TFE (1.5 mL, 4:1). To this, a fresh solution of $Cu(MeCN)_4BF_4$ (63 mg, 173 μmol), and TBTA (106 mg, 173 μmol) in DCM:TFE (2 mL; 4:1) was made and 173 μL was added and the mixture stirred for 48 h. After this time the solution was then drained and the resin washed with DMF (5 x 2 mL), DCM (5 x 2 mL), MeOH (5 x 2 mL) and DCM (5 x 2 mL).

5.2.6.2 On-Resin CuAAC Microwave

To a curved bottom microwave vial resin (~86.5 μmol), $Cu(MeCN)_4BF_4$ (63 mg, 173 μmol) and TBTA (106 mg, 173 μmol) and a stirrer bar were added. This was dissolved in DMSO (2 mL, degassed with N_2 for 5-10 minutes). The vial was then heated in a microwave reactor (80 ℃, 0.5 h). After this time the solution was drained and the resin washed with DMF (5 x 2 mL), DCM (5 x 2 mL), MeOH (5 x 2 mL) and DCM (5 x 2 mL).

5.2.7 Cleavage and Side Chain Deprotection

To the resin was added a solution of TFA:TIS:DCM (90:5:5, 1.5 mL) and the mixture was left for 3 min. The syringe was then sealed with tape and the solution stirred for 3 h. After this time the solution was collected in a vial and the syringe flushed with TFA (2 x 1.5 mL). The TFA was then removed using a N_2 flow. To this vial was added Et_2O (12 mL) and a white solid precipitated. The vial was then spun in a centrifuge (4500 rpm, 2 minutes) and the supernatant liquid poured off. This procedure was repeated twice and the resulting solid dried overnight.

Table 33- Yields and Ions Found of Peptide/Peptomer Library

Peptide	Notation	R_t (minute)[a]	Mass (Da)	Theor. Mass (Da)	Ion	Yield (%)
174	Native	10	1350.6289	1350.6341	$[M+Na]^+$	56
179u	1,4-*S*,*S*-u	23[b]	1451.6916	1451.6954	$[M+H]^+$	23
179c	1,4-*S*,*S*-c	8	1451.7036	1451.6954	$[M+H]^+$	41
180u	1,4-*S*,*R*-u	18	1473.6828	1473.6773	$[M+Na]^+$	33
180c	1,4-*S*,*R*-c	7	1451.7029	1451.6954	[M+H]+	47
181u	1,4-*R*,*S*-u	16	1451.6953	1451.6954	$[M+H]^+$	22
181c	1,4-*R*,*S*-c	7	1451.6921	1451.6954	$[M+H]^+$	31
182u	1,4-*R*,*R*-u	16	1473.6769	1473.6773	$[M+Na]^+$	10
182c	1,4-*R*,*R*-c	7	1451.7002	1451.6954	$[M+H]^+$	26
183u	4,1-*S*,*S*-u	16	1473.6770	1473.6773	$[M+Na]^+$	34
183c	4,1-*S*,*S*-c	9	1451.7127	1451.6954	$[M+H]^+$	41
184u	4,1-*S*,*R*-u	16	1451.7028	1451.6954	$[M+H]^+$	27
184c	4,1-*S*,*R*-c	8	1451.7075	1451.6954	$[M+H]^+$	36
185u	4,1-*R*,*S*-u	16	1451.7014	1451.6954	$[M+H]^+$	28
185c	4,1-*R*,*S*-c	6	1451.7048	1451.6954	$[M+H]^+$	24
186u	4,1-*R*,*R*-u	16	1473.6824	1473.6773	$[M+Na]^+$	19
186c	4,1-*R*,*R*-c	7	1451.6974	1451.6954	$[M+H]^+$	25
189	*N*-Native	5	1350.6389	1350.6341	$[M+Na]^+$	51
190u	1,4-*N*,*N*-u	14	1471.7047	1471.6981	$[M+H]^+$	42
190c	1,4-*N*,*N*-c	5	1449.7229	1449.7161	$[M+H]^+$	45
191u	4,1-*N*,*N*-u	11	1471.7052	1471.6981	$[M+Na]^+$	41
191c	4,1-*N*,*N*-c	5	1449.7165	1449.7161	$[M+H]^+$	46

a Isocratic gradient 62:38 (Water + 0.1% TFA:MeCN + 0.1% TFA);
b Isocratic gradient 65:35 (Water + 0.1% TFA:MeCN + 0.1% TFA)

5.3 Circular Dichroism

Each purified peptide/peptomer was dissolved in TFE (4 mg mL^{-1}). Aliquots of these solutions were diluted with deionised water to produce a 25% TFE aqueous solution (1 mg mL^{-1}). These solutions were pipetted into a cuvette (0.1 cm pathlength, 400 µL). The spectra were recorded at 25℃ with a 1 nm data pitch and 10 nm $minute^{-1}$ scanning speed. Each spectra is the accumulation of 3 scans and smoothed using the Savitzky-Golay method.[301]

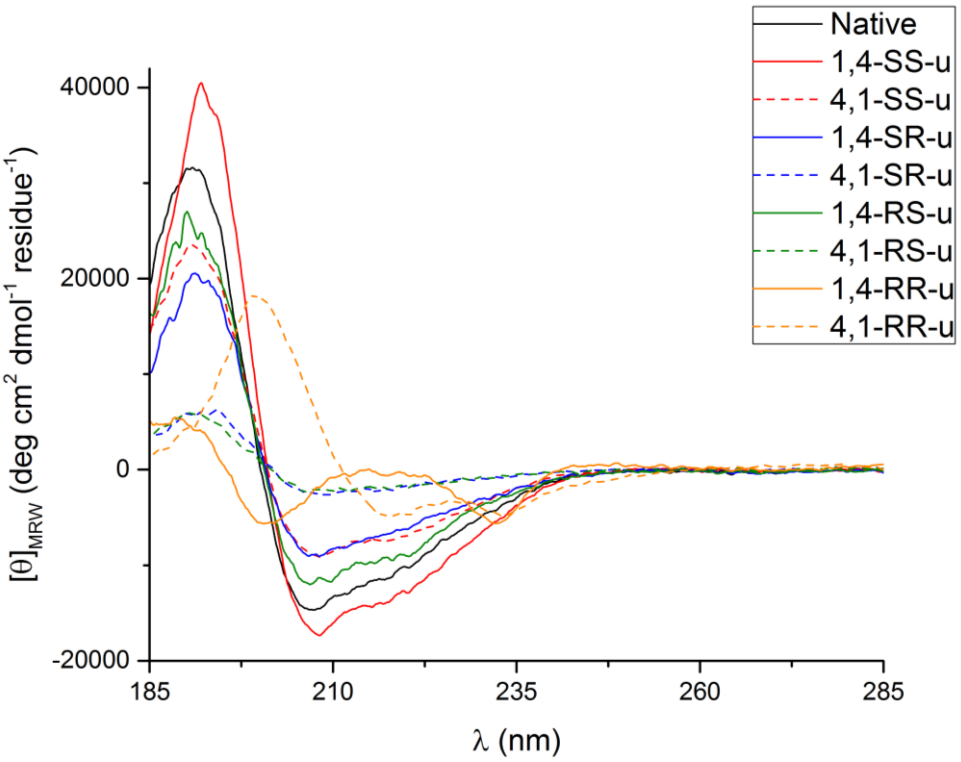

Figure 129- CD Spectra of Native **174** (Black) and Uncyclised Peptides

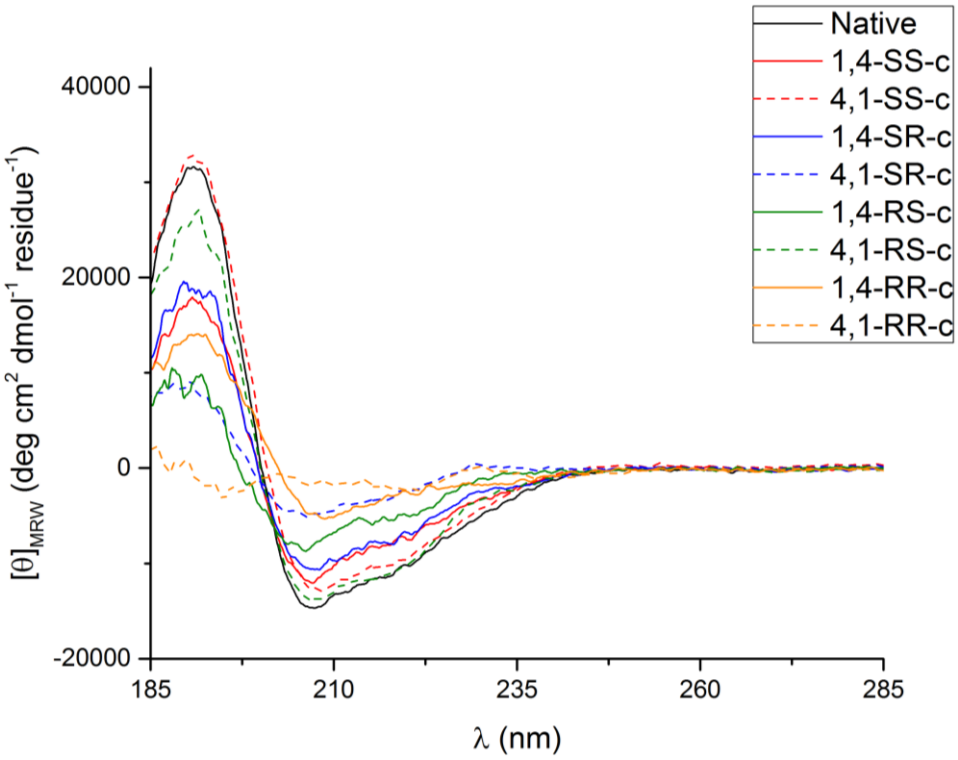

Figure 130- CD Spectra of Native **174** (Black) and Cyclised Peptides

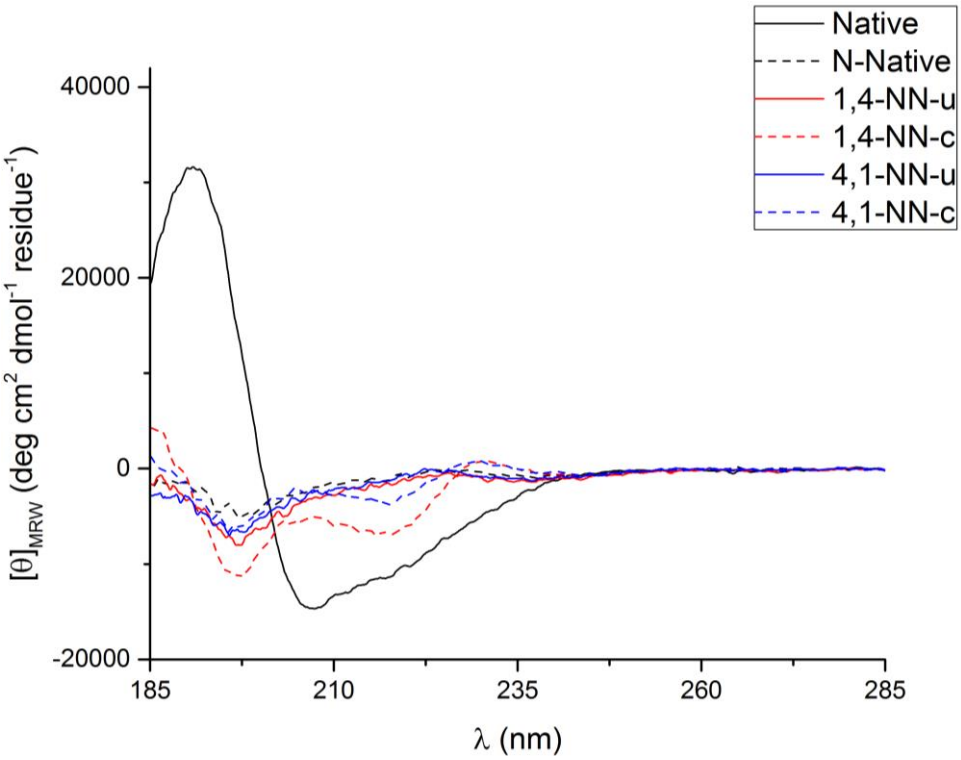

Figure 131- CD Spectra of Native **174** (Black) and Peptomers **189**, **190u/c** (red) and **191u/c** (blue)

5.4 Ligand Synthesis

5.4.1 Diazide Synthesis

Safety in the Handling of Sodium Azide and other Azides:[226]

Sodium azide is toxic and can be absorbed through the skin. It decomposes explosively upon heating to above 275 °C. Sodium azide reacts vigorously with CS_2, bromine, nitric acid, dimethyl sulfate, and a series of heavy metals, including copper and lead. In reaction with water or Brønsted acids the highly toxic and explosive hydrogen azide is released. It has been reported that sodium azide and polymer-bound azide reagents form explosive di- and triazidomethane with CH_2Cl_2 and $CHCl_3$, respectively. Heavy-metal azides that are highly explosive under pressure or shock are formed when solutions of NaN_3 or HN_3 vapors come into contact with heavy metals or their salts. Heavy-metal azides can accumulate under certain circumstances, for example, in metal pipelines and on the metal components of diverse equipment (rotary evaporators, freeze drying equipment, cooling traps, water baths, waste pipes), and thus lead to violent explosions. Some organic and other covalent azides are classified as toxic and highly explosive, and appropriate safety measures must be taken at all times.

All diazides were synthesised under identical conditions from the corresponding dibromides:

To the dibromide (10.1 mmol) was added NaN_3 solution (50.5 mL; 1 M in DMSO) at rt. This was stirred behind a blast shield for 18 h. The solution was then diluted with water (50 mL) and extracted with Et_2O (3 x 30 mL). The combined organic layers were washed with deionised water (3 x 20 mL) and brine (2 x 20 mL). The organic solution was dried ($MgSO_4$), filtered, and the solvent removed *in vacuo* to give a colourless oil.

1,6-diazidohexane B01

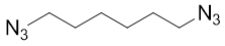

Yield 1.63 g (96%); **R_f** (DCM) 0.72; **^{1}H NMR** (500 MHz, $CDCl_3$) δ 3.36 – 3.25 (4H, t, *J* = 6.9 Hz, N_3CH_2), 1.70 – 1.58 (4H, m, $N_3CH_2CH_2$), 1.48 – 1.39 (4H, m, $N_3CH_2CH_2CH_2$); **^{13}C NMR** (126 MHz, $CDCl_3$) δ 51.32 ($2CH_2$), 28.74 ($2CH_2$), 26.31 ($2CH_2$). The ^{1}H and ^{13}C data were in good agreement with the literature.[302]

1,7-diazidoheptane B02

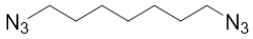

Yield 1.80 g (99%); **R_f** (DCM) 0.69; **^{1}H NMR** (500 MHz, $CDCl_3$) δ 3.33 – 3.26 (4H, t, *J* = 6.9 Hz, N_3CH_2), 1.67 – 1.59 (4H, m, $N_3CH_2CH_2$), 1.46 – 1.34 (6H, m, 3 x CH_2); **^{13}C NMR** (126 MHz, $CDCl_3$) δ 51.41 ($2CH_2$), 28.75 ($2CH_2$), 28.70 (CH_2), 26.59 ($2CH_2$). The ^{1}H datum was in good agreement with the literature.[303,304]

1,8-diazidooctane B03

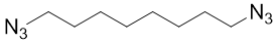

Yield 1.92 g (98%); **R_f** (DCM) 0.63; **^{1}H NMR** (500 MHz, $CDCl_3$) δ 3.33 – 3.25 (4H, t, *J* = 6.9 Hz, N_3CH_2), 1.67 – 1.59 (4H, qn, *J* = 6.9 Hz, $N_3CH_2CH_2$), 1.44 – 1.33 (8H, m, $N_3CH_2CH_2CH_2CH_2$); **^{13}C NMR** (126 MHz, $CDCl_3$) δ 51.45 ($2CH_2$), 29.00 ($2CH_2$), 28.81 ($2CH_2$), 26.62 ($2CH_2$). The ^{1}H and ^{13}C data were in good agreement with the literature.[302]

1,2-bis(azidomethyl)benzene B04

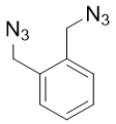

Yield 1.96 g (99%); **R_f** (DCM) 0.68; **^{1}H NMR** (500 MHz, $CDCl_3$) δ 7.44 – 7.38 (4H, m, Ar*H*), 4.46 (4H, s, $N_3C\mathit{H}_2$); **^{13}C NMR** (126 MHz, $CDCl_3$) δ 133.88 (2C), 130.18 (2CH), 129.05 (2CH), 52.28 ($2CH_2$). The ^{1}H and ^{13}C data was in good agreement with the literature.[305,306]

1,3-bis(azidomethyl)benzene B05

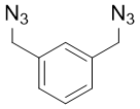

Yield 1.92 g (97%); **R_f** (DCM) 0.67; **^{1}H NMR** (500 MHz, $CDCl_3$) δ 7.47 – 7.42 (1H, m, Ar*H*), 7.35 – 7.30 (3H, m, Ar*H*), 4.40 (4H, s, $N_3C\mathit{H}_2$); **^{13}C NMR** (126 MHz, $CDCl_3$) δ 136.20 (2C), 129.39 (2CH), 128.05 (2CH), 127.83 (2CH), 54.56 ($2CH_2$). The ^{1}H and ^{13}C data were in good agreement with the literature.[302,305]

1,4-bis(azidomethyl)benzene B06

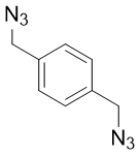

Yield 1.96 g (99%); **R_f** (DCM) 0.68; **^{1}H NMR** (500 MHz, $CDCl_3$) δ 7.37 (4H, s, Ar*H*), 4.39 (4H, s, $N_3C\mathit{H}_2$); **^{13}C NMR** (126 MHz, $CDCl_3$) δ 135.56 (2C), 128.67 (4CH), 54.42 ($2CH_2$). The ^{1}H and ^{13}C data were in good agreement with the literature.[302,305]

5.4.2 Ditriazolyl Alkyne Synthesis

4-(azidomethyl)methyl benzoate B13

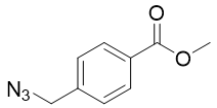

To 4-(bromomethyl)methyl benzoate (10.18 g, 44.5 mmol) was added NaN_3 solution (111 mL; 1 M in DMSO) at rt. This was stirred behind a blast shield for 18 h. The solution was then diluted with brine (250 mL) and extracted with Et_2O (3 x 150 mL). The combined organic layers were washed with deionised water (3 x 75 mL) and brine (2 x 75 mL). The organic solution was dried ($MgSO_4$), filtered, and the solvent removed *in vacuo* to give a colourless oil (8.34 g, 98%). The ^1H data was in good agreement with the literature.[307,308]

R_f (DCM) 0.75; **^1H NMR** (400 MHz, $CDCl_3$) δ 8.10 – 8.06 (2H, m, Ar*H*), 7.48 – 7.36 (2H, m, Ar*H*), 4.44 (2H, s, N_3CH_2), 3.95 (3H, s, CO_2CH_3).

Methyl 4-{[4-(diethoxymethyl)-1*H*-1,2,3-triazol-1-yl]methyl}benzoate B16

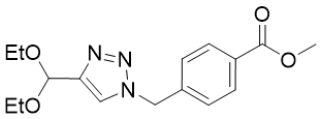

Diethylpropargyl acetal (4.72 g, 36.8 mmol) and 4-(azidomethyl)methyl benzoate (7.74 g, 40.5 mmol) were dissolved in a 1:1 mixture of *t*-BuOH/H_2O (28 mL). To this solution, sodium bicarbonate (464 mg, 5.52 mmol), copper(II) sulfate pentahydrate (459 mg, 1.84 mmol) and sodium ascorbate (1.46 g, 7.36 mmol) were added, and the mixture was stirred at room temperature. After ~18 h, EtOAc (100 mL) was added, and the organic phase was washed with saturated sodium bicarbonate (2 x 50 mL) and brine (2 x 50 mL). The organic layer was dried ($MgSO_4$), filtered, and concentrated *in vacuo* to give a tan crystalline solid (11.63 g, 99%).

^{1}H NMR (400 MHz, $CDCl_3$) δ 8.09 – 8.03 (2H, m, Ar*H*), 7.55 (1H, s, Triazole*H*), 7.34 (2H, d, *J* = 8.5 Hz, Ar*H*), 5.73 (1H, s, $(EtO)_2CH$), 5.60 (2H, s, $ArCH_2$), 3.94 (3H, s, CO_2CH_3), 3.67 (2H, dq, *J* = 9.4, 7.1 Hz, $CH_3CH_AH_BO$), 3.59 (2H, dq, *J* = 9.4, 7.0 Hz, $CH_3CH_AH_BO$), 1.24 (6H, t, *J* = 7.1 Hz, 6H, CH_3CH_2O).

Methyl 4-[(4-formyl-1*H*-1,2,3-triazol-1-yl)methyl]benzoate B15

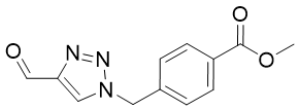

To a solution of methyl 4-{[4-(diethoxymethyl)-1*H*-1,2,3-triazol-1-yl]methyl}benzoate (11.75 g, 36.7 mmol) in $CHCl_3$ (74 mL), TFA (56 mL, 736 mmol) was added. The reaction mixture was stirred vigorously for 5 h at room temperature. Water (75 mL) was added and the aqueous phase washed with $CHCl_3$ (3 x 110 mL). The organic phase was washed with saturated $NaHCO_3$ (2 x 150 mL) and brine (150 mL). The organic layer was dried ($MgSO_4$), filtered, and the solvent were removed *in vacuo* affording a beige solid (8.87 g, 95%).

^{1}H NMR (400 MHz, $CDCl_3$) δ 10.17 (1H, s, C*H*O), 8.12 – 8.07 (2H, m, Ar*H*), 8.05 (1H, s, Triazole*H*), 7.38 (2H, d, *J* = 8.5 Hz, Ar*H*), 5.68 (2H, s, $ArCH_2$), 3.95 (3H, s, CO_2CH_3).

Dimethyl 4,4'-[(prop-2-yn-1-ylimino)bis(methanediyl-1*H*-1,2,3-triazole-4,1-diylmethanediyl)]dibenzoate B14

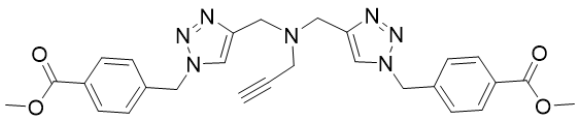

Methyl 4-[(4-formyl-1*H*-1,2,3-triazol-1-yl)methyl]benzoate (8.87 g, 34.9 mmol) and propargylamine (1.06 mL, 16.6 mmol) were stirred in $CHCl_3$ (150 mL). $NaBH(OAc)_3$ (10.56 g, 49.8 mmol) was added in portions. After addition was complete, the reaction was stirred at room temperature for 6 h. Water (95 mL) and H_2SO_4 (4.7 mL) were

added and stirred for ~15 min. The solution was then basified with saturated K_2CO_3 and water (75 mL) was added. The organic phase was separated and the aqueous phase was extracted with $CHCl_3$ (2 x 100 mL). The combined organic extracts were dried (Na_2SO_4), filtered, and the solvent was removed *in vacuo* to give colourless solid (5.03 g, 59%).

R_f (95:5 DCM:MeOH) 0.26; **^{1}H NMR** (500 MHz, $CDCl_3$) δ 8.09 – 8.00 (4H, m, Ar*H*), 7.56 (2H, s, Triazole*H*), 7.33 (4H, d, *J* = 8.3 Hz, Ar*H*), 5.59 (4H, s, ArCH_2), 3.95 (6H, s, CO_2CH_3), 3.87 (4H, s, RNCH_2Triazole), 3.36 (2H, d, *J* = 2.4 Hz, HC≡CCH_2), 2.27 (1H, t, *J* = 2.4 Hz, *H*C≡C); **^{13}C NMR** (126 MHz, $CDCl_3$) δ 166.41 (2C), 145.08 (2C), 139.54 (2C), 130.58 (2C), 130.38 (4CH), 127.80 (4CH), 123.19 (2CH), 78.37 (C), 73.76 (CH), 53.66 ($2CH_2$), 52.29 ($2CH_3$), 47.78 ($2CH_2$), 42.22 (CH_2).

Methyl 4-{[4-({[(1-{8-[4-({bis[(1-{[4-(methoxycarbonyl)phenyl]methyl}-1*H*-1,2,3-triazol-4-yl)methyl]amino}methyl)-1*H*-1,2,3-triazol-1-yl]octyl}-1*H*-1,2,3-triazol-4-yl)methyl][(1-{[4-(methoxycarbonyl)phenyl]methyl}-1*H*-1,2,3-triazol-4-yl)methyl]amino}methyl)-1*H*-1,2,3-triazol-1-yl]methyl}benzoate B09

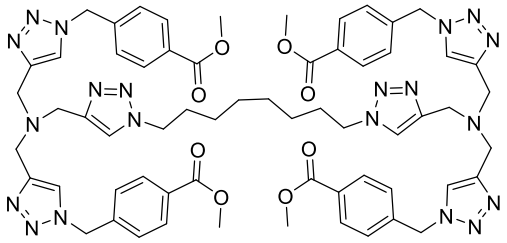

Dimethyl 4,4'-[(prop-2-yn-1-ylimino)bis(methanediyl-1*H*-1,2,3-triazole-4,1-diylmethanediyl)] dibenzoate (160 mg, 312 µmol) and 1,8-diazidooctane (30 mg, 156 µmol) were dissolved in MeCN (6 mL). To this solution copper(I) iodide (3 mg, 15.6 µmol) and NEt_3 (26 µL, 187 µmol) were added, and the mixture was stirred at room temperature for 6 hours. The solvent was removed *in vacuo* and the crude material redissolved in EtOAc (5 mL). The organic phase was washed with water (2 x 3 mL) and brine (2 x 3 mL). The organic layer was dried (Na_2SO_4), filtered, and concentrated *in vacuo* to give a colourless solid (216 mg, 56%).

^{1}H NMR (500 MHz, $CDCl_3$) δ 8.06 – 8.02 (8H, m, Ar*H*), 7.77 (4H, s, (Triazole*H*$CH_2)_2$NR), 7.74 (2H, s, Triazole*H*CH_2NR_2), 7.32 (8H, d, *J* = 8.3 Hz, Ar*H*), 5.59 (8H s, ArC*H*$_2$Triazole), 4.33 (4H, t, *J* = 7.2 Hz, TriazoleC*H*$_2CH_2$), 3.93 (12H, s, CO_2C*H*$_3$), 3.74 (8H, s, (TriazoleC*H*$_2)_2$NR), 3.73 (4H, s, TriazoleC*H*$_2NR_2$), 1.89 (4H, qn, *J* = 7.5 Hz, TriazoleCH_2C*H*$_2$), 1.35–1.27 (8H, m, TriazoleCH_2CH_2C*H*$_2C$*H*$_2$); **^{13}C NMR** (126 MHz, $CDCl_3$) δ 166.42 (4C), 144.46 (4C), 143.55 (2C), 139.64 (4C), 130.50 (4C), 130.35 (8CH), 127.76 (8CH), 124.09 (4CH), 123.69 (2CH), 53.62 ($4CH_2$), 52.26 ($4CH_3$), 50.22 ($2CH_2$), 47.01 ($2CH_2$), 46.96 ($4CH_2$), 30.16 ($2CH_2$), 28.68 ($2CH_2$), 26.30 ($2CH_2$).

Bibliography

(1) Kabsch, W.; Sander, C. *Biopolymers* **1983**, *22* (12), 2577–2637.

(2) Jochim, A. L.; Arora, P. S. *ACS Chem. Biol.* **2010**, *5* (10), 919–923.

(3) Lipinski, C. A.; Lombardo, F.; Dominy, B. W.; Feeney, P. J. *Adv. Drug Deliv. Rev.* **2001**, *46* (1-3), 3–26.

(4) Wells, J. A.; McClendon, C. L. *Nature* **2007**, *450* (7172), 1001–1009.

(5) Morelli, X.; Bourgeas, R.; Roche, P. *Curr. Opin. Chem. Biol.* **2011**, *15* (4), 475–481.

(6) Hopkins, A. L.; Groom, C. R. *Nat. Rev. Drug Discov.* **2002**, *1* (9), 727–730.

(7) Wilson, A. J. *Chem. Soc. Rev.* **2009**, *38* (12), 3289–3300.

(8) Zimm, B. H.; Bragg, J. K. *J. Chem. Phys.* **1959**, *31* (2), 526.

(9) Scholtz, J. M.; Baldwin, R. L. *Annu. Rev. Biophys. Biomol. Struct.* **1992**, *21*, 95–118.

(10) Tyndall, J. D. A.; Fairlie, D. P. *J. Mol. Recognit.* **1999**, *12* (6), 363–370.

(11) Gavathiotis, E.; Suzuki, M.; Davis, M. L.; Pitter, K.; Bird, G. H.; Katz, S. G.; Tu, H.-C.; Kim, H.; Cheng, E. H.-Y.; Tjandra, N.; Walensky, L. D. *Nature* **2008**, *455* (7216), 1076–1081.

(12) Okamoto, T.; Zobel, K.; Fedorova, A.; Quan, C.; Yang, H.; Fairbrother, W. J.; Huang, D. C. S.; Smith, B. J.; Deshayes, K.; Czabotar, P. E. **2012**.

(13) Bird, G. H.; Gavathiotis, E.; LaBelle, J. L.; Katz, S. G.; Walensky, L. D. **2014**.

(14) Walensky, L. D.; Bird, G. H. **2014**.

(15) Chu, Q.; Moellering, R. E.; Hilinski, G. J.; Kim, Y.-W.; Grossmann, T. N.; Yeh, J. T.-H.; Verdine, G. L. *Med. Chem. Commun.* **2014**.

(16) Greenfield, N. J.; Fasman, G. D. *Biochemistry* **1969**, *8* (10), 4108–4116.

(17) Kelly, S. M.; Jess, T. J.; Price, N. C. *Biochim. Biophys. Acta* **2005**, *1751* (2), 119–139.

(18) Bierzynski, A.; Kim, P. S.; Baldwin, R. L. *Proc. Natl. Acad. Sci. U. S. A.* **1982**, *79* (8), 2470–2474.

(19) Shoemaker, K. R.; Kim, P. S.; Brems, D. N.; Marqusee, S.; York, E. J.; Chaiken, I. M.; Stewart, J. M.; Baldwin, R. L. *Proc. Natl. Acad. Sci. U. S. A.* **1985**, *82* (8), 2349–2353.

(20) Scholtz, J. M.; Qian, H.; Robbins, V. H.; Baldwin, R. L. *Biochemistry* **1993**, *32* (37), 9668–9676.

(21) Huyghues-Despointes, B. M.; Scholtz, J. M.; Baldwin, R. L. *Protein Sci.* **1993**, *2* (1), 80–85.

(22) Albert, J. S.; Goodman, M. S.; Hamilton, A. D. *J. Am. Chem. Soc.* **1995**, *117* (3), 1143–1144.

(23) Cheng, R. P.; Wang, W.-R.; Girinath, P.; Yang, P.-A.; Ahmad, R.; Li, J.-H.; Hart, P.; Kokona, B.; Fairman, R.; Kilpatrick, C.; Argiros, A. *Biochemistry* **2012**, *51* (36), 7157–7172.

(24) Ruan, F.; Chen, Y.; Hopkins, P. B. *J. Am. Chem. Soc.* **1990**, *112* (25), 9403–9404.

(25) Ghadiri, M. R.; Choi, C. *J. Am. Chem. Soc.* **1990**, *112* (4), 1630–1632.

(26) Kharenko, O. A.; Ogawa, M. Y. *J. Inorg. Biochem.* **2004**, *98* (11), 1971–1974.

(27) Ma, M. T.; Hoang, H. N.; Scully, C. C. G.; Appleton, T. G.; Fairlie, D. P. *J. Am. Chem. Soc.* **2009**, *131* (12), 4505–4512.

(28) Zaykov, A. N.; Popp, B. V; Ball, Z. T. *Chemistry* **2010**, *16* (22), 6651–6659.

(29) Smith, S. J.; Du, K.; Radford, R. J.; Tezcan, F. A. *Chem. Sci.* **2013**, *4* (9), 3740–3747.

(30) Albert, J. S.; Hamilton, A. D. *Biochemistry* **1995**, *34* (3), 984–990.

(31) Olson, C. A.; Shi, Z.; Kallenbach, N. R. *J. Am. Chem. Soc.* **2001**, *123* (26), 6451–6452.

(32) Tsou, L. K.; Tatko, C. D.; Waters, M. L. *J. Am. Chem. Soc.* **2002**, *124* (50), 14917–14921.

(33) Góngora-Benítez, M.; Tulla-Puche, J.; Albericio, F. *Chem. Rev.* **2014**, *114* (2), 901–926.

(34) Postma, T. M.; Albericio, F. *European J. Org. Chem.* **2014**, *2014* (17), 3519–

3530.

(35) Muppidi, A.; Wang, Z.; Li, X.; Chen, J.; Lin, Q. *Chem. Commun. (Camb).* **2011**, *47* (33), 9396–9398.

(36) Muppidi, A.; Doi, K.; Edwardraja, S.; Drake, E. J.; Gulick, A. M.; Wang, H.-G.; Lin, Q. *J. Am. Chem. Soc.* **2012**, *134* (36), 14734–14737.

(37) Jo, H.; Meinhardt, N.; Wu, Y.; Kulkarni, S.; Hu, X.; Low, K. E.; Davies, P. L.; DeGrado, W. F.; Greenbaum, D. C. *J. Am. Chem. Soc.* **2012**, *134* (42), 17704–17713.

(38) Haney, C. M.; Loch, M. T.; Horne, W. S. *Chem. Commun. (Camb).* **2011**, *47* (39), 10915–10917.

(39) Chi, L.; Sadovski, O.; Woolley, G. A. *Bioconjug. Chem.* **2006**, *17* (3), 670–676.

(40) Madden, M. M.; Muppidi, A.; Li, Z.; Li, X.; Chen, J.; Lin, Q. *Bioorg. Med. Chem. Lett.* **2011**, *21* (5), 1472–1475.

(41) Makwana, K. M.; Mahalakshmi, R. *Org. Lett.* **2015**, *17* (10), 2498–2501.

(42) Mendive-Tapia, L.; Preciado, S.; García, J.; Ramón, R.; Kielland, N.; Albericio, F.; Lavilla, R. *Nat. Commun.* **2015**, *6*, 7160.

(43) Taylor, J. W. *Biopolymers* **2002**, *66* (1), 49–75.

(44) Shepherd, N. E.; Abbenante, G.; Fairlie, D. P. *Angew. Chemie Int. Ed.* **2004**, *43* (20), 2687–2690.

(45) Shepherd, N. E.; Hoang, H. N.; Abbenante, G.; Fairlie, D. P. *J. Am. Chem. Soc.* **2005**, *127* (9), 2974–2983.

(46) Carpino, L. A.; Han, G. Y. *J. Org. Chem.* **1972**, *37* (22), 3404–3409.

(47) Grieco, P.; Gitu, P. M.; Hruby, V. J. *J. Pept. Res.* **2001**, *57* (3), 250–256.

(48) Sheppard, R. *J. Pept. Sci.* **2003**, *9* (9), 545–552.

(49) Fu, G. C.; Grubbs, R. H. *J. Am. Chem. Soc.* **1992**, *114* (13), 5426–5427.

(50) Fu, G. C.; Grubbs, R. H. *J. Am. Chem. Soc.* **1992**, *114* (18), 7324–7325.

(51) Fu, G. C.; Nguyen, S. T.; Grubbs, R. H. *J. Am. Chem. Soc.* **1993**, *115* (21), 9856–9857.

(52) Miller, S. J.; Grubbs, R. H. *J. Am. Chem. Soc.* **1995**, *117* (21), 5855–5856.

(53) Miller, S. J.; Blackwell, H. E.; Grubbs, R. H. *J. Am. Chem. Soc.* **1996**, *118* (40), 9606–9614.

(54) Ravi, A.; Balaram, P. *Tetrahedron* **1984**, *40* (13), 2577–2583.

(55) Toniolo, C.; Crisma, M.; Formaggio, F.; Peggion, C. *Biopolymers* **2001**, *60* (6), 396–419.

(56) Karle, I. L. *Biopolymers* **1996**, *40* (1), 157–180.

(57) Siedler, F.; Quarzago, D.; Rudolph-Böhner, S.; Moroder, L. *Biopolymers* **1994**, *34* (11), 1563–1572.

(58) Blackwell, H. E.; Grubbs, R. H. *Angew. Chemie Int. Ed.* **1998**, *37* (23), 3281–3284.

(59) Blackwell, H. E.; Sadowsky, J. D.; Howard, R. J.; Sampson, J. N.; Chao, J. A.; Steinmetz, W. E.; O'Leary, D. J.; Grubbs, R. H. *J. Org. Chem.* **2001**, *66* (16), 5291–5302.

(60) Karle, I. L.; Flippen-Anderson, J. L.; Uma, K.; Balaram, P. *Proteins* **1990**, *7* (1), 62–73.

(61) Karle, I. L.; Flippen-Anderson, J. L.; Uma, K.; Balaram, P. *Biopolymers* **1993**, *33* (5), 827–837.

(62) Sonnichsen, F. D.; Van Eyk, J. E.; Hodges, R. S.; Sykes, B. D. *Biochemistry* **1992**, *31* (37), 8790–8798.

(63) Dyson, H. J.; Wright, P. E. *Curr. Opin. Struct. Biol.* **1993**, *3* (1), 60–65.

(64) Luo, P.; Baldwin, R. L. *Biochemistry* **1997**, *36* (27), 8413–8421.

(65) Vieira-Pires, R. S.; Morais-Cabral, J. H. *J. Gen. Physiol.* **2010**, *136* (6), 585–592.

(66) Schafmeister, C. E.; Po, J.; Verdine, G. L. *J. Am. Chem. Soc.* **2000**, *122* (24), 5891–5892.

(67) Williams, R. M.; Im, M. N. *J. Am. Chem. Soc.* **1991**, *113* (24), 9276–9286.

(68) Brown, J. E.; Klee, W. A. *Biochemistry* **1971**, *10* (3), 470–476.

(69) Toniolo, C.; Benedetti, E. *Macromolecules* **1991**, *24* (14), 4004–4009.

(70) Walensky, L. D.; Kung, A. L.; Escher, I.; Malia, T. J.; Barbuto, S.; Wright, R.

D.; Wagner, G.; Verdine, G. L.; Korsmeyer, S. J. *Science* **2004**, *305* (5689), 1466–1470.

(71) Wei, M. C.; Zong, W. X.; Cheng, E. H.; Lindsten, T.; Panoutsakopoulou, V.; Ross, A. J.; Roth, K. A.; MacGregor, G. R.; Thompson, C. B.; Korsmeyer, S. J. *Science* **2001**, *292* (5517), 727–730.

(72) Scorrano, L.; Oakes, S. A.; Opferman, J. T.; Cheng, E. H.; Sorcinelli, M. D.; Pozzan, T.; Korsmeyer, S. J. *Science* **2003**, *300* (5616), 135–139.

(73) Danial, N. N.; Korsmeyer, S. J. *Cell* **2004**, *116* (2), 205–219.

(74) Chittenden, T.; Flemington, C.; Houghton, A. B.; Ebb, R. G.; Gallo, G. J.; Elangovan, B.; Chinnadurai, G.; Lutz, R. J. *EMBO J.* **1995**, *14* (22), 5589–5596.

(75) Wang, K.; Yin, X. M.; Chao, D. T.; Milliman, C. L.; Korsmeyer, S. J. *Genes Dev.* **1996**, *10* (22), 2859–2869.

(76) Muchmore, S. W.; Sattler, M.; Liang, H.; Meadows, R. P.; Harlan, J. E.; Yoon, H. S.; Nettesheim, D.; Chang, B. S.; Thompson, C. B.; Wong, S. L.; Ng, S. L.; Fesik, S. W. *Nature* **1996**, *381* (6580), 335–341.

(77) Sattler, M.; Liang, H.; Nettesheim, D.; Meadows, R. P.; Harlan, J. E.; Eberstadt, M.; Yoon, H. S.; Shuker, S. B.; Chang, B. S.; Minn, A. J.; Thompson, C. B.; Fesik, S. W. *Science* **1997**, *275* (5302), 983–986.

(78) Kutchukian, P. S.; Yang, J. S.; Verdine, G. L.; Shakhnovich, E. I. *J. Am. Chem. Soc.* **2009**, *131* (13), 4622–4627.

(79) Yang, J. S.; Chen, W. W.; Skolnick, J.; Shakhnovich, E. I. *Structure* **2007**, *15* (1), 53–63.

(80) Noy, K.; Kalisman, N.; Keasar, C. *BMC Struct. Biol.* **2008**, *8*, 27.

(81) Yang, J. S.; Wallin, S.; Shakhnovich, E. I. *Proc. Natl. Acad. Sci. U. S. A.* **2008**, *105* (3), 895–900.

(82) Schellman, J. A. *C. R. Trav. Lab. Carlsberg. Chim.* **1955**, *29* (14-15), 230–259.

(83) Flory, P. J. *J. Am. Chem. Soc.* **1956**, *78* (20), 5222–5235.

(84) Poland, D. C.; Scheraga, H. A. *Biopolymers* **1965**, *3* (4), 379–399.

(85) Mutter, M. *J. Am. Chem. Soc.* **1977**, *99* (25), 8307–8314.

(86) Kim, Y.-W.; Verdine, G. L. *Bioorg. Med. Chem. Lett.* **2009**, *19* (9), 2533–2536.

(87) Fairman, R.; Anthony-Cahill, S. J.; DeGrado, W. F. *J. Am. Chem. Soc.* **1992**, *114* (13), 5458–5459.

(88) Krause, E.; Bienert, M.; Schmieder, P.; Wenschuh, H. *J. Am. Chem. Soc.* **2000**, *122* (20), 4865–4870.

(89) O'Neil, K.; DeGrado, W. *Science (80-.).* **1990**, *250* (4981), 646–651.

(90) Chakrabartty, A.; Kortemme, T.; Baldwin, R. L. *Protein Sci.* **1994**, *3* (5), 843–852.

(91) Pace, C. N.; Scholtz, J. M. *Biophys. J.* **1998**, *75* (1), 422–427.

(92) Yeo, D. J.; Warriner, S. L.; Wilson, A. J. *Chem. Commun. (Camb).* **2013**, *49* (80), 9131–9133.

(93) Belokon, Y. N.; Tararov, V. I.; Maleev, V. I.; Savel'eva, T. F.; Ryzhov, M. G. *Tetrahedron: Asymmetry* **1998**, *9* (23), 4249–4252.

(94) Belokon, Y. N.; Bespalova, N. B.; Churkina, T. D.; Císarová, I.; Ezernitskaya, M. G.; Harutyunyan, S. R.; Hrdina, R.; Kagan, H. B.; Kocovský, P.; Kochetkov, K. A.; Larionov, O. V; Lyssenko, K. A.; North, M.; Polásek, M.; Peregudov, A. S.; Prisyazhnyuk, V. V; Vyskocil, S. *J. Am. Chem. Soc.* **2003**, *125* (42), 12860–12871.

(95) Pham, T. K.; Yoo, J.; Kim, Y.-W. *Bull. Korean Chem. Soc.* **2013**, *34* (9), 2640–2644.

(96) Fürstner, A.; Langemann, K. *Synthesis (Stuttg).* **1997**, *1997* (07), 792–803.

(97) Kim, Y.-W.; Kutchukian, P. S.; Verdine, G. L. *Org. Lett.* **2010**, *12* (13), 3046–3049.

(98) Shim, S. Y.; Kim, Y.-W.; Verdine, G. L. *Chem. Biol. Drug Des.* **2013**, *82* (6), 635–642.

(99) Tyndall, J. D. A.; Nall, T.; Fairlie, D. P. *Chem. Rev.* **2005**, *105* (3), 973–999.

(100) Yamaguchi, H.; Kodama, H.; Osada, S.; Kato, F.; Jelokhani-Niaraki, M.; Kondo, M. *Biosci. Biotechnol. Biochem.* **2003**, *67* (10), 2269–2272.

(101) Bird, G. H.; Madani, N.; Perry, A. F.; Princiotto, A. M.; Supko, J. G.; He, X.;

Gavathiotis, E.; Sodroski, J. G.; Walensky, L. D. *Proc. Natl. Acad. Sci. U. S. A.* **2010**, *107* (32), 14093–14098.

(102) Hilinski, G. J.; Kim, Y.-W.; Hong, J.; Kutchukian, P. S.; Crenshaw, C. M.; Berkovitch, S. S.; Chang, A.; Ham, S.; Verdine, G. L. **2014**.

(103) Kosuge, M.; Takeuchi, T.; Nakase, I.; Jones, A. T.; Futaki, S. *Bioconjug. Chem.* **2008**, *19* (3), 656–664.

(104) Copolovici, D. M.; Langel, K.; Eriste, E.; Langel, Ü. *ACS Nano* **2014**, *8* (3), 1972–1994.

(105) Brock, R. *Bioconjug. Chem.* **2014**, *25* (5), 863–868.

(106) Avbelj, F.; Luo, P.; Baldwin, R. L. *Proc. Natl. Acad. Sci. U. S. A.* **2000**, *97* (20), 10786–10791.

(107) Vila, J. A.; Ripoll, D. R.; Scheraga, H. A. *Proc. Natl. Acad. Sci. U. S. A.* **2000**, *97* (24), 13075–13079.

(108) Gao, J.; Bosco, D. A.; Powers, E. T.; Kelly, J. W. *Nat. Struct. Mol. Biol.* **2009**, *16* (7), 684–690.

(109) Lifson, S.; Roig, A. *J. Chem. Phys.* **1961**, *34* (6), 1963.

(110) Qian, H.; Schellman, J. A. *J. Phys. Chem.* **1992**, *96* (10), 3987–3994.

(111) Kemp, D. S.; Curran, T. P.; Davis, W. M.; Boyd, J. G.; Muendel, C. *J. Org. Chem.* **1991**, *56* (23), 6672–6682.

(112) Austin, R. E.; Maplestone, R. A.; Sefler, A. M.; Liu, K.; Hruzewicz, W. N.; Liu, C. W.; Cho, H. S.; Wemmer, D. E.; Bartlett, P. A. *J. Am. Chem. Soc.* **1997**, *119* (28), 6461–6472.

(113) Cabezas, E.; Satterthwait, A. C. *J. Am. Chem. Soc.* **1999**, *121* (16), 3862–3875.

(114) Chapman, R. N.; Dimartino, G.; Arora, P. S. *J. Am. Chem. Soc.* **2004**, *126* (39), 12252–12253.

(115) Fukuyama, T.; Jow, C.-K.; Cheung, M. *Tetrahedron Lett.* **1995**, *36* (36), 6373–6374.

(116) Turner, J. J.; Wilschut, N.; Overkleeft, H. S.; Klaffke, W.; van der Marel, G. A.; van Boom, J. H. *Tetrahedron Lett.* **1999**, *40* (38), 7039–7042.

(117) Chen, Y.-H.; Yang, J. T.; Martinez, H. M. *Biochemistry* **1972**, *11* (22), 4120–4131.

(118) Chin, D.-H.; Woody, R. W.; Rohl, C. A.; Baldwin, R. L. *Proc. Natl. Acad. Sci. U. S. A.* **2002**, *99* (24), 15416–15421.

(119) Dimartino, G.; Wang, D.; Chapman, R. N.; Arora, P. S. *Org. Lett.* **2005**, *7* (12), 2389–2392.

(120) Wang, D.; Liao, W.; Arora, P. S. *Angew. Chem. Int. Ed. Engl.* **2005**, *44* (40), 6525–6529.

(121) Wang, D.; Chen, K.; Kulp Iii, J. L.; Arora, P. S. *J. Am. Chem. Soc.* **2006**, *128* (28), 9248–9256.

(122) Douse, C. H.; Maas, S. J.; Thomas, J. C.; Garnett, J. A.; Sun, Y.; Cota, E.; Tate, E. W. *ACS Chem. Biol.* **2014**, *9* (10), 2204–2209.

(123) Huisgen, R. *Angew. Chemie Int. Ed. English* **1963**, *2*, 633–645.

(124) Huisgen, R. *Angew. Chemie Int. Ed. English* **1963**, *2*, 565–598.

(125) Huisgen, R.; Szeimies, G.; Möbius, L. *Chem. Ber.* **1967**, *100* (8), 2494–2507.

(126) Tornøe, C. W.; Christensen, C.; Meldal, M. *J. Org. Chem.* **2002**, *67* (9), 3057–3064.

(127) Rostovtsev, V. V; Green, L. G.; Fokin, V. V; Sharpless, K. B. *Angew. Chem. Int. Ed. Engl.* **2002**, *41* (14), 2596–2599.

(128) Wang, Q.; Chan, T. R.; Hilgraf, R.; Fokin, V. V; Sharpless, K. B.; Finn, M. G. *J. Am. Chem. Soc.* **2003**, *125* (11), 3192–3193.

(129) Cantel, S.; Isaad, A. L. C.; Scrima, M.; Levy, J. J.; DiMarchi, R. D.; Rovero, P.; Halperin, J. A.; D'Ursi, A. M.; Papini, A. M.; Chorev, M. *J. Org. Chem.* **2008**, *73* (15), 5663–5674.

(130) Roice, M.; Johannsen, I.; Meldal, M. *QSAR Comb. Sci.* **2004**, *23* (8), 662–673.

(131) Broadus, A. E.; Mangin, M.; Ikeda, K.; Insogna, K. L.; Weir, E. C.; Burtis, W. J.; Stewart, A. F. *N. Engl. J. Med.* **1988**, *319* (9), 556–563.

(132) Chorev, M.; Roubini, E.; McKee, R. L.; Gibbons, S. W.; Goldman, M. E.; Caulfield, M. P.; Rosenblatt, M. *Biochemistry* **1991**, *30* (24), 5968–5974.

(133) Bisello, A.; Nakamoto, C.; Rosenblatt, M.; Chorev, M. *Biochemistry* **1997**, *36* (11), 3293–3299.

(134) Maretto, S.; Mammi, S.; Bissacco, E.; Peggion, E.; Bisello, A.; Rosenblatt, M.; Chorev, M.; Mierke, D. F. *Biochemistry* **1997**, *36* (11), 3300–3307.

(135) Pelletier, J. C. *Org. Lett.* **2001**, *3* (5), 781–783.

(136) Nyffeler, P. T.; Liang, C.-H.; Koeller, K. M.; Wong, C.-H. *J. Am. Chem. Soc.* **2002**, *124* (36), 10773–10778.

(137) Rijkers, D. T. S.; van Vugt, H. H. R.; Jacobs, H. J. F.; Liskamp, R. M. J. *Tetrahedron Lett.* **2002**, *43* (20), 3657–3660.

(138) Oyelere, A. K.; Chen, P. C.; Yao, L. P.; Boguslavsky, N. *J. Org. Chem.* **2006**, *71* (26), 9791–9796.

(139) Rodionov, V. O.; Fokin, V. V.; Finn, M. G. *Angew. Chemie Int. Ed.* **2005**, *44* (15), 2210–2215.

(140) Punna, S.; Kuzelka, J.; Wang, Q.; Finn, M. G. *Angew. Chem. Int. Ed. Engl.* **2005**, *44* (15), 2215–2220.

(141) Angell, Y.; Burgess, K. *J. Org. Chem.* **2005**, *70* (23), 9595–9598.

(142) Rajan, R.; Awasthi, S. K.; Bhattacharjya, S.; Balaram, P. *Biopolymers* **1997**, *42* (2), 125–128.

(143) Scrima, M.; Le Chevalier-Isaad, A.; Rovero, P.; Papini, A. M.; Chorev, M.; D'Ursi, A. M. *European J. Org. Chem.* **2010**, *2010* (3), 446–457.

(144) Le Chevalier Isaad, A.; Barbetti, F.; Rovero, P.; D'Ursi, A. M.; Chelli, M.; Chorev, M.; Papini, A. M. *European J. Org. Chem.* **2008**, *2008* (31), 5308–5314.

(145) Le Chevalier Isaad, A.; Papini, A. M.; Chorev, M.; Rovero, P. *J. Pept. Sci.* **2009**, *15* (7), 451–454.

(146) Scrima, M.; Grimaldi, M.; Di Marino, S.; Testa, C.; Rovero, P.; Papini, A. M.; Chorev, M.; D'Ursi, A. M. *Biopolymers* **2012**, *98* (6), 535–545.

(147) Fink, A. L. *Enzyme Structure Part L*; Methods in Enzymology; Elsevier, 1986; Vol. 131.

(148) Amodeo, P.; Motta, A.; Picone, D.; Saviano, G.; Tancredi, T.; Temussi, P. A. *J. Magn. Reson.* **1991**, *95* (1), 201–207.

(149) D'Ursi, A.; Albrizio, S.; Tancredi, T.; Temussi, P. A. *J. Biomol. NMR* **1998**, *11* (4), 415–422.

(150) Kawamoto, S. A.; Coleska, A.; Ran, X.; Yi, H.; Yang, C.-Y.; Wang, S. *J. Med. Chem.* **2012**, *55* (3), 1137–1146.

(151) Polakis, P. *Genes & Dev.* **2000**, *14* (15), 1837–1851.

(152) Takemaru, K.-I.; Ohmitsu, M.; Li, F.-Q. *Handb. Exp. Pharmacol.* **2008**, No. 186, 261–284.

(153) Sampietro, J.; Dahlberg, C. L.; Cho, U. S.; Hinds, T. R.; Kimelman, D.; Xu, W. *Mol. Cell* **2006**, *24* (2), 293–300.

(154) Kawamoto, S. A.; Thompson, A. D.; Coleska, A.; Nikolovska-Coleska, Z.; Yi, H.; Wang, S. *Biochemistry* **2009**, *48* (40), 9534–9541.

(155) Bernal, F.; Tyler, A. F.; Korsmeyer, S. J.; Walensky, L. D.; Verdine, G. L. *J. Am. Chem. Soc.* **2007**, *129* (9), 2456–2457.

(156) Rohl, C. A.; Chakrabartty, A.; Baldwin, R. L. *Protein Sci.* **1996**, *5* (12), 2623–2637.

(157) Kruse, J.-P.; Gu, W. *Cell* **2009**, *137* (4), 609–622.

(158) Lane, D. P. *Nature* **1992**, *358* (6381), 15–16.

(159) Picksley, S. M.; Lane, D. P. *Bioessays* **1993**, *15* (10), 689–690.

(160) Tanimura, S.; Ohtsuka, S.; Mitsui, K.; Shirouzu, K.; Yoshimura, A.; Ohtsubo, M. *FEBS Lett.* **1999**, *447* (1), 5–9.

(161) Sharp, D. A.; Kratowicz, S. A.; Sank, M. J.; George, D. L. *J. Biol. Chem.* **1999**, *274* (53), 38189–38196.

(162) Barnard, A.; Miles, J. A.; Burslem, G. M.; Barker, A. M.; Wilson, A. J. *Org. Biomol. Chem.* **2015**, *13* (1), 258–264.

(163) Bell, S.; Klein, C.; Müller, L.; Hansen, S.; Buchner, J. *J. Mol. Biol.* **2002**, *322* (5), 917–927.

(164) Kussie, P. H.; Gorina, S.; Marechal, V.; Elenbaas, B.; Moreau, J.; Levine, A. J.;

Pavletich, N. P. *Science* **1996**, *274* (5289), 948–953.

(165) Popowicz, G. M.; Czarna, A.; Holak, T. A. *Cell Cycle* **2008**, *7* (15), 2441–2443.

(166) A*Star Institute. p53 Domains http://p53.bii.a-star.edu.sg/aboutp53/.

(167) Vassilev, L. T.; Vu, B. T.; Graves, B.; Carvajal, D.; Podlaski, F.; Filipovic, Z.; Kong, N.; Kammlott, U.; Lukacs, C.; Klein, C.; Fotouhi, N.; Liu, E. A. *Science* **2004**, *303* (5659), 844–848.

(168) Vassilev, L. T.; Vu, B. T.; Graves, B.; Carvajal, D.; Podlaski, F.; Filipovic, Z.; Kong, N.; Kammlott, U.; Lukacs, C.; Klein, C.; Fotouhi, N.; Liu, E. A. *Science* **2004**, *303* (5659), 844–848.

(169) Orner, B. P.; Ernst, J. T.; Hamilton, A. D. *J. Am. Chem. Soc.* **2001**, *123* (22), 5382–5383.

(170) Chen, L.; Yin, H.; Farooqi, B.; Sebti, S.; Hamilton, A. D.; Chen, J. *Mol. Cancer Ther.* **2005**, *4* (6), 1019–1025.

(171) Yin, H.; Lee, G.; Park, H. S.; Payne, G. A.; Rodriguez, J. M.; Sebti, S. M.; Hamilton, A. D. *Angew. Chem. Int. Ed. Engl.* **2005**, *44* (18), 2704–2707.

(172) Harbour, J. W. *Arch. Ophthalmol.* **2002**, *120* (10), 1341.

(173) Plante, J.; Campbell, F.; Malkova, B.; Kilner, C.; Warriner, S. L.; Wilson, A. J. *Org. Biomol. Chem.* **2008**, *6* (1), 138–146.

(174) Plante, J. P.; Burnley, T.; Malkova, B.; Webb, M. E.; Warriner, S. L.; Edwards, T. A.; Wilson, A. J. *Chem. Commun. (Camb).* **2009**, No. 34, 5091–5093.

(175) Campbell, F.; Plante, J. P.; Edwards, T. A.; Warriner, S. L.; Wilson, A. J. *Org. Biomol. Chem.* **2010**, *8* (10), 2344–2351.

(176) Kwon, Y.-U.; Kodadek, T. *J. Am. Chem. Soc.* **2007**, *129* (6), 1508–1509.

(177) Miller, S. M.; Simon, R. J.; Ng, S.; Zuckermann, R. N.; Kerr, J. M.; Moos, W. H. *Bioorg. Med. Chem. Lett.* **1994**, *4* (22), 2657–2662.

(178) Hara, T.; Durell, S. R.; Myers, M. C.; Appella, D. H. *J. Am. Chem. Soc.* **2006**, *128* (6), 1995–2004.

(179) Armand, P.; Kirshenbaum, K.; Falicov, A.; Dunbrack, R. L.; Dill, K. A.; Zuckermann, R. N.; Cohen, F. E. *Fold. Des.* **1997**, *2* (6), 369–375.

(180) Wu, C. W.; Kirshenbaum, K.; Sanborn, T. J.; Patch, J. A.; Huang, K.; Dill, K. A.; Zuckermann, R. N.; Barron, A. E. *J. Am. Chem. Soc.* **2003**, *125* (44), 13525–13530.

(181) García-Echeverría, C.; Chène, P.; Blommers, M. J. J.; Furet, P. *J. Med. Chem.* **2000**, *43* (17), 3205–3208.

(182) Chene, P. *Mol. Cancer Res.* **2004**, *2* (1), 20–28.

(183) Böttger, V.; Böttger, A.; Howard, S. F.; Picksley, S. M.; Chène, P.; Garcia-Echeverria, C.; Hochkeppel, H. K.; Lane, D. P. *Oncogene* **1996**, *13* (10), 2141–2147.

(184) Böttger, A.; Böttger, V.; Garcia-Echeverria, C.; Chène, P.; Hochkeppel, H. K.; Sampson, W.; Ang, K.; Howard, S. F.; Picksley, S. M.; Lane, D. P. *J. Mol. Biol.* **1997**, *269* (5), 744–756.

(185) Massova, I.; Kollman, P. A. *J. Am. Chem. Soc.* **1999**, *121* (36), 8133–8143.

(186) Chène, P.; Fuchs, J.; Bohn, J.; García-Echeverría, C.; Furet, P.; Fabbro, D. *J. Mol. Biol.* **2000**, *299* (1), 245–253.

(187) Sakurai, K.; Schubert, C.; Kahne, D. *J. Am. Chem. Soc.* **2006**, *128* (34), 11000–11001.

(188) Hu, B.; Gilkes, D. M.; Chen, J. *Cancer Res.* **2007**, *67* (18), 8810–8817.

(189) Patton, J. T.; Mayo, L. D.; Singhi, A. D.; Gudkov, A. V; Stark, G. R.; Jackson, M. W. *Cancer Res.* **2006**, *66* (6), 3169–3176.

(190) Hu, B.; Gilkes, D. M.; Farooqi, B.; Sebti, S. M.; Chen, J. *J. Biol. Chem.* **2006**, *281* (44), 33030–33035.

(191) Wade, M.; Wong, E. T.; Tang, M.; Stommel, J. M.; Wahl, G. M. *J. Biol. Chem.* **2006**, *281* (44), 33036–33044.

(192) Gu, J.; Kawai, H.; Nie, L.; Kitao, H.; Wiederschain, D.; Jochemsen, A. G.; Parant, J.; Lozano, G.; Yuan, Z.-M. *J. Biol. Chem.* **2002**, *277* (22), 19251–19254.

(193) Linares, L. K.; Hengstermann, A.; Ciechanover, A.; Müller, S.; Scheffner, M. *Proc. Natl. Acad. Sci. U. S. A.* **2003**, *100* (21), 12009–12014.

(194) Phan, J.; Li, Z.; Kasprzak, A.; Li, B.; Sebti, S.; Guida, W.; Schönbrunn, E.;

Chen, J. *J. Biol. Chem.* **2010**, *285* (3), 2174–2183.

(195) Pazgier, M.; Liu, M.; Zou, G.; Yuan, W.; Li, C.; Li, J.; Monbo, J.; Zella, D.; Tarasov, S. G.; Lu, W. *Proc. Natl. Acad. Sci.* **2009**, *106* (12), 4665–4670.

(196) Zondlo, S. C.; Lee, A. E.; Zondlo, N. J. *Biochemistry* **2006**, *45* (39), 11945–11957.

(197) Dastidar, S. G.; Lane, D. P.; Verma, C. S. *J. Am. Chem. Soc.* **2008**, *130* (41), 13514–13515.

(198) Harper, E. T.; Rose, G. D. *Biochemistry* **1993**, *32* (30), 7605–7609.

(199) Seale, J. W.; Srinivasan, R.; Rose, G. D. *Protein Sci.* **1994**, *3* (10), 1741–1745.

(200) Aurora, R.; Rose, G. D. *Protein Sci.* **1998**, *7* (1), 21–38.

(201) Peterson, R. W.; Nicholson, E. M.; Thapar, R.; Klevit, R. E.; Scholtz, J. M. *J. Mol. Biol.* **1999**, *286* (5), 1609–1619.

(202) Li, C.; Pazgier, M.; Li, C.; Yuan, W.; Liu, M.; Wei, G.; Lu, W.-Y.; Lu, W. *J. Mol. Biol.* **2010**, *398* (2), 200–213.

(203) Kallen, J.; Goepfert, A.; Blechschmidt, A.; Izaac, A.; Geiser, M.; Tavares, G.; Ramage, P.; Furet, P.; Masuya, K.; Lisztwan, J. *J. Biol. Chem.* **2009**, *284* (13), 8812–8821.

(204) Milletti, F. *Drug Discov. Today* **2012**, *17* (15-16), 850–860.

(205) Stalmans, S.; Wynendaele, E.; Bracke, N.; Gevaert, B.; D'Hondt, M.; Peremans, K.; Burvenich, C.; De Spiegeleer, B. *PLoS One* **2013**, *8* (8), e71752.

(206) Zhang, Y.; Xiong, Y. *Science* **2001**, *292* (5523), 1910–1915.

(207) Li, M.; Brooks, C. L.; Wu-Baer, F.; Chen, D.; Baer, R.; Gu, W. *Science* **2003**, *302* (5652), 1972–1975.

(208) Bernal, F.; Wade, M.; Godes, M.; Davis, T. N.; Whitehead, D. G.; Kung, A. L.; Wahl, G. M.; Walensky, L. D. *Cancer Cell* **2010**, *18* (5), 411–422.

(209) Baek, S.; Kutchukian, P. S.; Verdine, G. L.; Huber, R.; Holak, T. A.; Lee, K. W.; Popowicz, G. M. *J. Am. Chem. Soc.* **2012**, *134* (1), 103–106.

(210) Chang, Y. S.; Graves, B.; Guerlavais, V.; Tovar, C.; Packman, K.; To, K.-H.; Olson, K. A.; Kesavan, K.; Gangurde, P.; Mukherjee, A.; Baker, T.; Darlak, K.;

Elkin, C.; Filipovic, Z.; Qureshi, F. Z.; Cai, H.; Berry, P.; Feyfant, E.; Shi, X. E.; Horstick, J.; Annis, D. A.; Manning, A. M.; Fotouhi, N.; Nash, H.; Vassilev, L. T.; Sawyer, T. K. *Proc. Natl. Acad. Sci. U. S. A.* **2013**, *110* (36), E3445–E3454.

(211) Brown, C. J.; Quah, S. T.; Jong, J.; Goh, A. M.; Chiam, P. C.; Khoo, K. H.; Choong, M. L.; Lee, M. A.; Yurlova, L.; Zolghadr, K.; Joseph, T. L.; Verma, C. S.; Lane, D. P. *ACS Chem. Biol.* **2013**, *8* (3), 506–512.

(212) Soragni, A.; Janzen, D. M.; Johnson, L. M.; Lindgren, A. G.; Thai-Quynh Nguyen, A.; Tiourin, E.; Soriaga, A. B.; Lu, J.; Jiang, L.; Faull, K. F.; Pellegrini, M.; Memarzadeh, S.; Eisenberg, D. S. *Cancer Cell* **2016**, *29* (1), 90–103.

(213) Xu, J.; Reumers, J.; Couceiro, J. R.; De Smet, F.; Gallardo, R.; Rudyak, S.; Cornelis, A.; Rozenski, J.; Zwolinska, A.; Marine, J.-C.; Lambrechts, D.; Suh, Y.-A.; Rousseau, F.; Schymkowitz, J. *Nat. Chem. Biol.* **2011**, *7* (5), 285–295.

(214) Jacobsen, Ø.; Maekawa, H.; Ge, N.-H.; Görbitz, C. H.; Rongved, P.; Ottersen, O. P.; Amiry-Moghaddam, M.; Klaveness, J. *J. Org. Chem.* **2011**, *76* (5), 1228–1238.

(215) Schwochert, J.; Turner, R.; Thang, M.; Berkeley, R. F.; Ponkey, A. R.; Rodriguez, K. M.; Leung, S. S. F.; Khunte, B.; Goetz, G.; Limberakis, C.; Kalgutkar, A. S.; Eng, H.; Shapiro, M. J.; Mathiowetz, A. M.; Price, D. A.; Liras, S.; Jacobson, M. P.; Lokey, R. S. *Org. Lett.* **2015**.

(216) Park, M.; Wetzler, M.; Jardetzky, T. S.; Barron, A. E. *PLoS One* **2013**, *8* (3), e58874.

(217) Jamieson, A. G.; Boutard, N.; Sabatino, D.; Lubell, W. D. *Chem. Biol. Drug Des.* **2013**, *81* (1), 148–165.

(218) Sminia, T.; Pedersen, D. *Synlett* **2012**, *23* (18), 2643–2646.

(219) Sugano, H.; Miyoshi, M. *J. Org. Chem.* **1976**, *41* (13), 2352–2353.

(220) Glenn, M. P.; Pattenden, L. K.; Reid, R. C.; Tyssen, D. P.; Tyndall, J. D. A.; Birch, C. J.; Fairlie, D. P. *J. Med. Chem.* **2002**, *45* (2), 371–381.

(221) Ballet, S.; Betti, C.; Novoa, A.; Tömböly, C.; Nielsen, C. U.; Helms, H. C.;

Lesniak, A.; Kleczkowska, P.; Chung, N. N.; Lipkowski, A. W.; Brodin, B.; Tourwé, D.; Schiller, P. W. *ACS Med. Chem. Lett.* **2014**, *5* (4), 352–357.

(222) Zuckermann, R. N.; Kerr, J. M.; Kent, S. B. H.; Moos, W. H. *J. Am. Chem. Soc.* **1992**, *114* (26), 10646–10647.

(223) Østergaard, S.; Holm, A. *Mol. Divers.* **1997**, *3* (1), 17–27.

(224) Walewska, A.; Han, T. S.; Zhang, M.-M.; Yoshikami, D.; Bulaj, G.; Rolka, K. *Eur. J. Med. Chem.* **2013**, *65*, 144–150.

(225) Kolb, H. C.; Finn, M. G.; Sharpless, K. B. *Angew. Chem. Int. Ed. Engl.* **2001**, *40* (11), 2004–2021.

(226) Bräse, S.; Gil, C.; Knepper, K.; Zimmermann, V. *Angew. Chem. Int. Ed. Engl.* **2005**, *44* (33), 5188–5240.

(227) Petitjean, N. Peptide and Peptidomimetic Leads for the Inhibition of MDM2-Mediated Ubiquitination of p53, University of Edinburgh, 2013.

(228) Unciti-Broceta, A.; Diezmann, F.; Ou-Yang, C. Y.; Fara, M. A.; Bradley, M. *Bioorg. Med. Chem.* **2009**, *17* (3), 959–966.

(229) Våbenø, J.; Brisander, M.; Lejon, T.; Luthman, K. *J. Org. Chem.* **2002**, *67* (26), 9186–9191.

(230) Yamamoto, Y.; Shirai, T.; Miyaura, N. *Chem. Commun. (Camb).* **2012**, *48* (22), 2803–2805.

(231) Long, K.; Edwards, T. A.; Wilson, A. J. *Bioorg. Med. Chem.* **2013**, *21* (14), 4034–4040.

(232) Esiringu, I.; Gulcan, H. O.; Koyuncu, H.; Reis, Ö.; Sahin, Y. Google Patents 2012.

(233) Prashad, M.; Kathawala, F. G.; Scallen, T. *J. Med. Chem.* **1993**, *36* (10), 1501–1504.

(234) Ohnuma, T.; Nagasaki, M.; Tabe, M.; Ban, Y. *Tetrahedron Lett.* **1983**, *24* (39), 4253–4256.

(235) Dhami, A.; Mahon, M. F.; Lloyd, M. D.; Threadgill, M. D. *Tetrahedron* **2009**, *65* (24), 4751–4765.

(236) Charrier, N.; Demont, E.; Dunsdon, R.; Maile, G.; Naylor, A.; O'Brien, A.; Redshaw, S.; Theobald, P.; Vesey, D.; Walter, D. *Synlett* **2005**, *2005* (20), 3071–3074.

(237) Graham, L. L. *Org. Magn. Reson.* **1972**, *4* (2), 335–342.

(238) Laursen, J. S.; Engel-Andreasen, J.; Fristrup, P.; Harris, P.; Olsen, C. A. *J. Am. Chem. Soc.* **2013**, *135* (7), 2835–2844.

(239) Engel-Andreasen, J.; Wich, K.; Laursen, J. S.; Harris, P.; Olsen, C. A. *J. Org. Chem.* **2015**, *80* (11), 5415–5427.

(240) Schore, N. E.; Knudsen, M. J. *J. Org. Chem.* **1987**, *52* (4), 569–580.

(241) Landi, F.; Johansson, C. M.; Campopiano, D. J.; Hulme, A. N. *Org. Biomol. Chem.* **2010**, *8* (1), 56–59.

(242) Finkelstein, H. *Berichte der Dtsch. Chem. Gesellschaft* **1910**, *43* (2), 1528–1532.

(243) Burgess, J. *Metal Ions in Solution*; Ellis Horwood series in chemical science; Ellis Horwood, 1978.

(244) Alvarez, S. G.; Alvarez, M. T. *Synthesis (Stuttg).* **1997**, *1997* (04), 413–414.

(245) Nordlander, J. E.; Catalane, D. B.; Eberlein, T. H.; Farkas, L. V.; Howe, R. S.; Stevens, R. M.; Tripoulas, N. A.; Stansfield, R. E.; Cox, J. L.; Payne, M. J.; Viehbeck, A. *Tetrahedron Lett.* **1978**, *19* (50), 4987–4990.

(246) Newman, H. *J. Org. Chem.* **1965**, *30* (4), 1287–1288.

(247) Nordlander, J. E.; Payne, M. J.; Balk, M. A.; Gress, J. L.; Harris, F. D.; Lane, J. S.; Lewe, R. F.; Marshall, S. E.; Nagy, D.; Rachlin, D. J. *J. Org. Chem.* **1984**, *49* (1), 133–138.

(248) Beumel, O. F.; Harris, R. F. *J. Org. Chem.* **1963**, *28* (10), 2775–2779.

(249) Landini, D.; Penso, M. *Synth. Commun.* **1988**, *18* (8), 791–800.

(250) Landini, D.; Penso, M. *J. Org. Chem.* **1991**, *56* (1), 420–423.

(251) Miclo, Y.; Garcia, P.; Evanno, Y.; George, P.; Sevrin, M.; Malacria, M.; Gandon, V.; Aubert, C. *Synlett* **2010**, *2010* (15), 2314–2318.

(252) Chan, W. C.; White, P. D. *Fmoc Solid Phase Peptide Synthesis: A Practical*

Approach; 2000; Vol. 222.

(253) Amblard, M.; Fehrentz, J.-A.; Martinez, J.; Subra, G. *Mol. Biotechnol.* **2006**, *33* (3), 239–254.

(254) Rink, H. *Tetrahedron Lett.* **1987**, *28* (33), 3787–3790.

(255) Vázquez, J.; Qushair, G.; Albericio, F. *Methods Enzymol.* **2003**, *369*, 21–35.

(256) Carpino, L. A.; El-Faham, A. *Tetrahedron* **1999**, *55* (22), 6813–6830.

(257) Subirós-Funosas, R.; Prohens, R.; Barbas, R.; El-Faham, A.; Albericio, F. *Chemistry* **2009**, *15* (37), 9394–9403.

(258) Itoh, M. *Bull. Chem. Soc. Jpn.* **1973**, *46* (7), 2219–2221.

(259) Izdebski, J. *Rocz. Chem.* **1975**, *49* (6), 1097–1104.

(260) Izdebski, J. *Pol. J. Chem.* **1979**, *53* (5), 1049–1057.

(261) Bates, H. S.; Jones, J. H.; Witty, M. J. *J. Chem. Soc. Chem. Commun.* **1980**, No. 16, 773.

(262) Subirós-Funosas, R.; El-Faham, A.; Albericio, F. *Biopolymers* **2012**, *98* (2), 89–97.

(263) Subiros-Funosas, R.; Khattab, S. N.; Nieto-Rodriguez, L.; El-Faham, A.; Albericio, F. *ChemInform* **2014**, *45* (44), no – no.

(264) Chan, T. R.; Hilgraf, R.; Sharpless, K. B.; Fokin, V. V. *Org. Lett.* **2004**, *6* (17), 2853–2855.

(265) Donnelly, P. S.; Zanatta, S. D.; Zammit, S. C.; White, J. M.; Williams, S. J. *Chem. Commun. (Camb).* **2008**, No. 21, 2459–2461.

(266) Pedersen, S. L.; Tofteng, A. P.; Malik, L.; Jensen, K. J. *Chem. Soc. Rev.* **2012**, *41* (5), 1826–1844.

(267) Kappe, C. O. *Angew. Chem. Int. Ed. Engl.* **2004**, *43* (46), 6250–6284.

(268) Pierce, M. M.; Raman, C. S.; Nall, B. T. *Methods* **1999**, *19* (2), 213–221.

(269) Madeira, A.; Vikeved, E.; Nilsson, A.; Sjögren, B.; Andrén, P. E.; Svenningsson, P.; Madeira, A.; Vikeved, E.; Nilsson, A.; Sjögren, B.; Andrén, P. E.; Svenningsson, P. In *Current Protocols in Protein Science*; John Wiley & Sons, Inc.: Hoboken, NJ, USA, 2011; pp 19.21.1–19.21.9.

(270) Hupp, T. R.; Sparks, A.; Lane, D. P. *Cell* **1995**, *83* (2), 237–245.

(271) Lu, X.; Burbidge, S. A.; Griffin, S.; Smith, H. M. *Oncogene* **1996**, *13* (2), 413–418.

(272) Martinez Molina, D.; Jafari, R.; Ignatushchenko, M.; Seki, T.; Larsson, E. A.; Dan, C.; Sreekumar, L.; Cao, Y.; Nordlund, P. *Science* **2013**, *341* (6141), 84–87.

(273) Molina, D. M.; Nordlund, P. *http://dx.doi.org/10.1146/annurev-pharmtox-010715-103715* **2016**.

(274) Tan, B. X.; Brown, C. J.; Ferrer, F. J.; Yuen, T. Y.; Quah, S. T.; Chan, B. H.; Jansson, A. E.; Teo, H. L.; Nordlund, P.; Lane, D. P. *Sci. Rep.* **2015**, *5*, 12116.

(275) Ahlquist, M.; Fokin, V. V. *Organometallics* **2007**, *26* (18), 4389–4391.

(276) Himo, F.; Lovell, T.; Hilgraf, R.; Rostovtsev, V. V; Noodleman, L.; Sharpless, K. B.; Fokin, V. V. *J. Am. Chem. Soc.* **2005**, *127* (1), 210–216.

(277) Nolte, C.; Mayer, P.; Straub, B. F. *Angew. Chem. Int. Ed. Engl.* **2007**, *46* (12), 2101–2103.

(278) Straub, B. F. *Chem. Commun.* **2007**, No. 37, 3868.

(279) Worrell, B. T.; Malik, J. A.; Fokin, V. V. *Science* **2013**, *340* (6131), 457–460.

(280) Jin, L.; Tolentino, D. R.; Melaimi, M.; Bertrand, G. *Sci. Adv.* **2015**, *1* (5), e1500304–e1500304.

(281) Simmons, M. G.; Merrill, C. L.; Wilson, L. J.; Bottomley, L. A.; Kadish, K. M. *J. Chem. Soc. Dalt. Trans.* **1980**, No. 10, 1827.

(282) Merrill, C. L.; Wilson, L. J.; Thamann, T. J.; Loehr, T. M.; Ferris, N. S.; Woodruff, W. H. *J. Chem. Soc. Dalt. Trans.* **1984**, No. 10, 2207.

(283) Davies, M. B. *Polyhedron* **1992**, *11* (3), 285–321.

(284) Rodionov, V. O.; Presolski, S. I.; Gardinier, S.; Lim, Y.-H.; Finn, M. G. *J. Am. Chem. Soc.* **2007**, *129* (42), 12696–12704.

(285) Su, C.-Y.; Kang, B.-S.; Wen, T.-B.; Tong, Y.-X.; Yang, X.-P.; Zhang, C.; Liu, H.-Q.; Sun, J. *Polyhedron* **1999**, *18* (11), 1577–1585.

(286) Gaetke, L. *Toxicology* **2003**, *189* (1-2), 147–163.

(287) Agard, N. J.; Prescher, J. A.; Bertozzi, C. R. *J. Am. Chem. Soc.* **2004**, *126* (46), 15046–15047.

(288) Chan, T. R.; Fokin, V. V. *QSAR Comb. Sci.* **2007**, *26* (11-12), 1274–1279.

(289) Lammens, M.; Skey, J.; Wallyn, S.; O'Reilly, R.; Du Prez, F. *Chem. Commun. (Camb).* **2010**, *46* (46), 8719–8721.

(290) Kaplan, F.; Roberts, J. D. *J. Am. Chem. Soc.* **1961**, *83* (22), 4666–4668.

(291) Li, W.; Li, J.; Wu, Y.; Fuller, N.; Markus, M. A. *J. Org. Chem.* **2010**, *75* (4), 1077–1086.

(292) W. Gribble, G. *Chem. Soc. Rev.* **1998**, *27* (6), 395.

(293) Schellenberg, K. A. *J. Org. Chem.* **1963**, *28* (11), 3259–3261.

(294) Abdel-Magid, A. F.; Carson, K. G.; Harris, B. D.; Maryanoff, C. A.; Shah, R. D. *J. Org. Chem.* **1996**, *61* (11), 3849–3862.

(295) Moormann, A. E. *Synth. Commun.* **2006**.

(296) Testa, C.; Scrima, M.; Grimaldi, M.; D'Ursi, A. M.; Dirain, M. L.; Lubin-Germain, N.; Singh, A.; Haskell-Luevano, C.; Chorev, M.; Rovero, P.; Papini, A. M. *J. Med. Chem.* **2014**, *57* (22), 9424–9434.

(297) ten Brink, H. T.; Rijkers, D. T. S.; Liskamp, R. M. J. *J. Org. Chem.* **2006**, *71* (5), 1817–1824.

(298) Gündel, W.-H.; Kramer, W. *Chem. Ber.* **1978**, *111* (7), 2594–2604.

(299) Meng, C. Antiparasitic and Pesticidal Isoxazoline Compounds, 2015.

(300) Zahoor, A. F.; Thies, S.; Kazmaier, U. *Beilstein J. Org. Chem.* **2011**, *7* (1), 1299–1303.

(301) Savitzky, A.; Golay, M. J. E. *Anal. Chem.* **1964**, *36* (8), 1627–1639.

(302) Thomas, J. R.; Liu, X.; Hergenrother, P. J. *J. Am. Chem. Soc.* **2005**, *127* (36), 12434–12435.

(303) Nagao, Y.; Takasu, A. *J. Polym. Sci. Part A Polym. Chem.* **2010**, *48* (19), 4207–4218.

(304) Roe, S.; Gunaratnam, M.; Spiteri, C.; Sharma, P.; Alharthy, R. D.; Neidle, S.; Moses, J. E. *Org. Biomol. Chem.* **2015**, *13* (31), 8500–8504.

(305) Ramírez-López, P.; de la Torre, M. C.; Montenegro, H. E.; Asenjo, M.; Sierra, M. A. *Org. Lett.* **2008**, *10* (16), 3555–3558.

(306) Stengel, I.; Strassert, C. A.; De Cola, L.; Bäuerle, P. *Organometallics* **2014**, *33* (6), 1345–1355.

(307) Lee, C.-H.; Lee, S.; Yoon, H.; Jang, W.-D. *Chemistry* **2011**, *17* (49), 13898–13903.

(308) Rabet, P. T. G.; Fumagalli, G.; Boyd, S.; Greaney, M. F. *Org. Lett.* **2016**, *18* (7), 1646–1649.